Nonequilibrium Thermodynamics and Large Deviations in Open Quantum Systems

Dissertation

der Mathematisch-Naturwissenschaftlichen Fakultät

der Eberhard Karls Universität Tübingen

zur Erlangung des Grades eines

Doktors der Naturwissenschaften

(Dr. rer. nat.)

vorgelegt von

Paulo José Paulino de Souza

aus Varginha/Brasilien

Tübingen

2025

Gedruckt mit Genehmigung der Mathematisch-Naturwissenschaftlichen Fakultät der Eberhard Karls Universität Tübingen.

Tag der mündlichen Qualifikation:	19/05/2025
Dekan:	Prof. Thilo Stehle
1. Berichterstatter:	Assoc. Prof. Federico Carollo
2. Berichterstatter:	Prof. Christian Groß

Abstract

In this thesis, we explore the nonequilibrium thermodynamics of open quantum systems and its applications to quantum devices. Many-body open quantum systems can host exotic phases of matter. A particularly relevant example is the time-crystal phase, in which the time-translation symmetry of the dynamical generator is spontaneously broken. This novel nonequilibrium phase manifests in persistent and stable oscillations of an order parameter of the system. It has gathered significant interest and has shown promising potential applications, for instance in quantum engines and quantum metrology. However, the thermodynamics of these time crystals remains largely unexplored, essentially due to their nonequilibrium nature. This poses serious challenges in evaluating their potential in real-world applications. In particular, systems exhibiting a time-crystal phase are typically described by phenomenological master equations, in which the coupling between the system and its surroundings is simplified by neglecting the influence of external energy sources and the internal interactions among particles within the many-body system. However, it is known that these master equations can violate the laws of thermodynamics if the relevant thermodynamic quantities are not properly defined. To address this open problem, in this thesis, we investigate the thermodynamics of time-crystal phases in our **first** and **third** publications. In our **first work**, we propose a thermodynamic description for nonequilibrium open quantum systems described by phenomenological master equations. Specifically, we consider that Hamiltonian contributions such as laser driving do not count as internal energy terms but rather they represent an input energy source, which allows us to formulate the first law in terms of an energy balance of the persistent nonequilibrium heat currents. Using this idea, we propose a statement of the second law for systems described by phenomenological master equations. We apply these results to

an autonomous quantum engine driven by the time-crystal phase and demonstrate that its efficiency can be properly defined and is supported by a well-defined second law. In our **third publication**, we analyze the thermodynamics of coupled systems, both of which can exhibit a time-crystal phase. To characterize the thermodynamics of the coupled systems, we exploit a collision-model approach, which assumes a specific structure for the environment and the system-environment interaction that leads to phenomenological master equations. Our findings also show that the time-crystal phase can be effectively used for energy storage applications. In our **second publication**, we focus on open quantum systems undergoing an adiabatic evolution, where a parameter of the system is slowly varied. This class of dynamics is relevant in many applications, including Carnot's engine cycles and dissipative quantum computation. The interaction between the system and environment manifests as random jumps, such as photon emissions, which give rise to stochastic trajectories, each one related to a single experimental run. In this regard, it is important to characterize not only the average values of observables related to these quantum jumps, but also their fluctuations. In thermodynamic applications, an important observable is the stochastic heat, where a photon exchanged with the environment represents a discrete amount of heat dissipated or absorbed by the system. The statistics of emissions-related observables can be described through the theory of large deviations, which provides tools to compute asymptotic probability distributions in the limit of long evolution times. This theory captures the statistics of rare events, not explained by the central-limit theorem, and shows how to design systems where typical behavior mirrors the rare behavior of an original system. In our **second work**, we rigorously derive, for the first time, the large-deviation behavior for quantum systems undergoing adiabatic dynamics. Among our results, we show that the time evolution of stochastic observables follows a temporal additive principle, meaning that the total probability distribution is obtained by the composition of the instantaneous ones which all can be described by large deviation theory.

Zusammenfassung

In dieser Arbeit untersuchen wir die Nichtgleichgewichtsthermodynamik offener Quantensysteme und ihre Anwendung in Quantenbauelementen. Vielteilchen-Quantensysteme können exotische Materiephasen beherbergen. Ein besonders relevantes Beispiel ist die Zeitkristallphase, in der die Zeittranslationssymmetrie des dynamischen Generators spontan gebrochen wird. Diese neuartige Nichtgleichgewichtsphase manifestiert sich in anhaltenden und stabilen Oszillationen eines Ordnungsparameters des Systems. Sie wird derzeit mit großem Interesse untersucht und besitzt vielversprechende Anwendungspotenziale, beispielsweise in Quantenmotoren und Quantenmetrologie. Die Thermodynamik dieser Zeitkristalle ist jedoch weitgehend unerforscht, vor allem wegen ihrer Nichtgleichgewichtsnatur. Dies stellt eine erhebliche Herausforderung dar, um ihr Potenzial für reale Anwendungen zu bewerten. Insbesondere werden Systeme, die eine Zeitkristallphase aufweisen, typischerweise durch phänomenologische Mastergleichungen beschrieben, bei denen die Kopplung zwischen dem System und seiner Umgebung stark vereinfacht wird, indem sowohl der Einfluss externer Energiequellen als auch interne Wechselwirkungen zwischen den Teilchen im Vielteilchensystem vernachlässigt werden. Es ist jedoch bekannt, dass solche Mastergleichungen gegen thermodynamische Gesetze verstoßen können, wenn die relevanten thermodynamischen Größen nicht korrekt definiert werden. Um dieses offene Problem zu behandeln, untersuchen wir in dieser Arbeit die Thermodynamik von Zeitkristallphasen in unserer **ersten** und **dritten** Publikation. In unserer **ersten Arbeit** schlagen wir eine thermodynamische Beschreibung für offene Nichtgleichgewichts-Quantensysteme vor, die durch phänomenologische Mastergleichungen beschrieben werden. Insbesondere betrachten wir Hamiltonische Beiträge, wie etwa das Antreiben mittels eines Lasers, nicht als interne Energi-

eterme, sondern als externe Energiequellen, was uns erlaubt, den ersten Hauptsatz durch eine Energiebilanz der Nichtgleichgewichts-Wärmeströme zu formulieren. Auf Basis dieser Idee formulieren wir ebenfalls einen zweiten Hauptsatz für Systeme, die durch phänomenologische Mastergleichungen beschrieben werden. Wir wenden diese Ergebnisse auf einen autonomen Quantenmotor an, der von einer Zeitkristallphase angetrieben wird, und zeigen, dass seine Effizienz eindeutig definiert werden kann und von einem wohldefinierten zweiten Hauptsatz gestützt wird. In unserer **dritten Publikation** analysieren wir die Thermodynamik gekoppelter Systeme, von denen jedes eine Zeitkristallphase aufweisen kann. Um die Thermodynamik dieser gekoppelten Systeme zu charakterisieren, verwenden wir ein Kollisionsmodell, das eine bestimmte Struktur für die Umgebung annimmt. Weiterhin modellieren wir die System-Umgebungs-Wechselwirkung derart, dass diese wiederum zu einer phänomenologischen Mastergleichung führt. Unsere Ergebnisse zeigen, dass die Zeitkristallphase effektiv als Energiespeicherung genutzt werden kann. In unserer **zweiten Publikation** konzentrieren wir uns auf offene Quantensysteme, die einer adiabatischen Entwicklung unterliegen, bei der ein Parameter des Systems langsam verändert wird. Diese Art der Dynamik ist für zahlreiche Anwendungen, wie etwa für den Carnot-Prozess und für dissipative Quantenalgorithmen, relevant. Die Wechselwirkung zwischen System und Umgebung manifestiert sich in Form zufälliger Quantensprünge, wie Photoemissionen, wodurch stochastische Trajektorien entstehen, die jeweils einzelnen experimentellen Durchläufen entsprechen. In diesem Zusammenhang ist es wichtig, nicht nur die Mittelwerte der mit diesen Quantensprüngen verbundenen Observablen zu charakterisieren, sondern auch ihre Fluktuationen. In thermodynamischen Anwendungen ist eine wichtige Observable die stochastische Wärme, wobei ein mit der Umgebung ausgetauschtes Photon eine diskrete Wärmemenge darstellt, die vom System aufgenommen oder abgegeben wird. Die Statistik solcher emissionsbezogenen Observablen kann durch die Theorie der großen Abweichungen beschrieben werden, welche Werkzeuge bietet, um asymptotische Wahrscheinlichkeitsverteilungen bei langen Evolutionszeiten zu berechnen. Diese Theorie erfasst die Statistik seltener Ereignisse, die durch den zentralen Grenzwertsatz nicht erklärt werden können, und zeigt auf, wie Systeme entworfen werden können, deren typ-

isches Verhalten dem seltenen Verhalten des ursprünglichen Systems entspricht. In unserer **zweiten Arbeit** leiten wir erstmals rigoros das Prinzip der großen Abweichung für Quantensysteme unter adiabatischer Dynamik her. Mittels unserer Ergebnisse zeigen wir, dass die zeitliche Entwicklung stochastischer Observablen einem zeitlichen Additivitätsprinzip folgt, was bedeutet, dass die gesamte Wahrscheinlichkeitsverteilung durch Komposition der instantanen Verteilungen beschrieben wird, die alle durch die Theorie der großen Abweichungen charakterisiert werden können.

List of publications and personal contribution

List of publications

1. Paulo J. Paulino, Igor Lesanovsky, and Federico Carollo. *Nonequilibrium thermodynamics and power generation in open quantum optomechanical systems,* Phys. Rev. A **108**, 023516 (2023)

2. Paulo J. Paulino, Igor Lesanovsky, and Federico Carollo. *Large Deviation Full Counting Statistics in Adiabatic Open Quantum Dynamics,* Phys. Rev. Lett. **132**, 260402 (2024)

3. Paulo J. Paulino, Albert Cabot, Gabriele De Chiara, Mauro Antezza, Igor Lesanovsky, and Federico Carollo. *Thermodynamics of coupled time crystals with an application to energy storage*, arXiv:2411.04836 (2024).

Personal contribution of the candidate

No.	Scientific ideas	Data generation	Analysis and interpretation	Paper writing	Status
1	30%	100%	70%	50%	Published
2	70%	100%	80%	70%	Published
3	70%	95%	80%	80%	Preprint

Acknowledgements

I would like to express my gratitude to my supervisors, Federico Carollo and Igor Lesanovsky, for their exceptional guidance, patience, and support during my PhD years. A special acknowledgement goes to Federico for our insightful discussions, his remarkable positivity, and the enthusiasm about physics and life. I would also like to extend my sincere thanks to W. Martins, A. Cabot, J. Cesar, F. Carnazza, M. Svendsen, M. Nairn, F. Headley, G. Perfetto, J. Wilkinson, C. Nill, M. Cech (thanks for helping me with the German abstract), M. Boneberb, M. Magoni, F. Gerbino, and G. Cemin (who was also a fantastic flatmate), S. Vidal, A. B. Barreto, P. Solanki, C. De Fazio, R. Mattes, and S. Euchner, M. Eissler, and A. Thaqi for their help and friendship. I am grateful to the entire AG Lesanovsky group for creating such a wonderful and collaborative environment. A special thanks to I. Estiry and A. Lorösch for their assistance with the bureaucratic matters. To friends in Tübingen, Peter, Annika, Bernardo, Przemysław, Yaro, Illia, Younghee, Chiara, Alba, Andoni, and many others, thank you for the nice time we spent together. I also want to thank my friends and family in Brazil for all their support at a distance. A small note of appreciation for a few places that were truly meaningful during my time in Tübingen, McFit, Blauer Salon, and Ammerschlag. Finally, I am thankful to my wife, Ana Flávia, for her love and patience in enduring our long-distance relationship, as well as to my parents and my sister for their unconditional support.

In Memoriam, Fabio Marques Martins.

Contents

Chapter 1

Introduction

1.1 Thermodynamics

Thermodynamics was developed starting from a phenomenological understanding of heat engines and gave a meaning to concepts like heat, temperature, and work. In particular, it led to the formulation of two fundamental principles, or axioms, known as the first and second laws of thermodynamics [1]. The first law deals with the conservation of energy and it distinguishes between two different manifestations of energy, heat and work. Heat was associated with thermal energy, while work with mechanical energy. The second law, on the other hand, establishes how heat flows between two regions at different temperatures, imposing that heat must always flow from a hot to a cold region [2]. As an immediate consequence, these two laws set theoretical bounds to the efficiency of heat engines and rule out the existence of perpetual motion machines.

Given the nature of these two statements, thermodynamics has a different character compared to other physical theories, as it does not require a specific physical system nor does it introduce new fundamental laws [1, 3]. For example, Maxwell's electromagnetism introduces a set of fundamental equations governing the motion of charged particles interacting with an electromagnet field [4]. Thermodynamics, on the other hand, tells whether physical processes are allowed and imposes bounds on them, according to the first and second laws [1].

Thermodynamics deals with macroscopic concepts, such as as pressure and volume, and it was initially formulated for the specific scenario of systems in thermal

equilibrium with their surroundings. These macroscopic quantities were later connected to the behavior of an ensemble of microscopic particles, by the kinetic theory of gases [5, 6], which describes dilute gases as ensembles of particles. In particular, it defines that the internal energy of the particles is related to temperature of the gas and pressure corresponds to the momentum of the particles transferred to the walls of the recipient containing the gas. These ideas were generalized by Boltzmann, Ehrenfest, Maxwell, and Gibbs into what is now known as statistical mechanics [7]. Statistical mechanics defines that each configuration also referred to as a microstate, of a many-particle system, is associated with a probability of being observed. These probabilities are then combined into statistical ensembles. For example, when the temperature of the system is fixed, each configuration of the system is weighted according to the Boltzmann factor. The normalization of the reweighed probability is the partition function, which provides all the thermodynamic quantities associated with the system, *e.g.* internal energy and heat capacity [6]. When considering the number of particles in these ensembles approaching infinity, which is referred to as the thermodynamic limit, the statistical ensembles recover the results predicted by the laws of thermodynamics.

Many results in thermodynamics, such as the analysis of Carnot's cycle, which sets an upper bound for the efficiency of heat engines, are only valid in equilibrium conditions. Therefore, the *improper* application of the laws of thermodynamics conceived and derived for equilibrium settings to nonequilibrium scenarios can lead to apparent inconsistencies [8].

Phenomena like Brownian motion, where a particle suspended in a liquid exhibits random motion, are also described by statistical mechanics. This branch of the theory concerns stochastic processes, which describe sequences of random events occurring in a physical system [6, 9]. Many physical processes exhibit the so-called memorylessness property, or Markovianity, where realizations of the noise are not correlated in time. This property is connected to the emergence of irreversibility in systems undergoing a stochastic process [10], which can be interpreted as a production of entropy, thereby linking stochastic processes with thermodynamics. In the context of stochastic processes, thermodynamic observables assume a probabilistic character. Significant effort has been devoted to characterizing the thermodynamics of these observables, such as

fluctuation theorems, which predict that the second law can be violated in individual realizations of the stochastic process, with a probability that decreases exponentially with the system size [11]. In addition to that, stochastic processes are connected to information theory, initially developed in engineering and telecommunications, which further relates thermodynamic entropy to a measure of information about the state of the system [12]. In this context, it can be shown that Markovian stochastic processes obey a version of the second law [3, 13], unifying thermodynamics, stochastic processes, and information theory. Using the informational interpretation of entropy, the problem of Maxwell's demon [14], an apparent violation of the second law, was resolved. In this thought experiment, a demon measures the velocity of the particles within a gas in thermal equilibrium and separates them into two regions based on their outcomes, creating hot and cold regions. However, information theory says that the demon acquired information about the particles, which needs to be erased requiring an entropic cost. This is known as the Landauer principle [15–17].

Quantum thermodynamics aims to extend thermodynamic concepts to open quantum systems, which are quantum systems interacting with an external environment, integrating fields such as stochastic quantum dynamics and quantum information [2, 18, 19]. Like classical thermodynamics, quantum thermodynamics aims to establish general principles governing energy and entropy, independent of a specific system. However, quantum mechanics introduces novel nonequilibrium properties connected to quantum resources such as entanglement, which need to be considered when defining thermodynamic quantities [20–23]. In particular, since it is not straightforward to define thermodynamic principles for quantum systems, many challenges emerge when describing applications of thermodynamics to quantum technologies. In particular, it is not clear how to define the energy costs and efficiencies of quantum devices and identifying which quantum resources can improve their performance [24]. For instance, quantum engines with efficiencies surpassing Carnot's limit can be designed using squeezed reservoirs [25–27]. In metrology, entanglement and other quantum resources can enhance measurement sensitivity [28]. Quantum batteries, as a further example, make use of resources such as coherence to increase energy storage compared to their classical counterparts [29–31]. Nonetheless, many proposed applications

neglect the energetic cost of producing quantum resources and the nonequilibrium states enabling these advantages [32].

1.2 Time crystals

Symmetries have a fundamental role in physical systems, as they are directly linked to conservation laws according to the Noether's theorem [33]. Also, they are relevant when investigating phase transitions between different states of matter. For example, when water solidifies, the continuous spatial symmetry of the liquid phase is broken as the system exhibits a crystalline structure with discrete translational symmetry [34]. Symmetry breaking phenomena also appears in quantum systems. A quantum many-body system governed by a Hamiltonian with continuous spatial translation symmetry can spontaneously form a crystalline structure in its ground state, exhibiting a discrete symmetry instead, analogous to the phase transition between ice and liquid water. This emergent ordering is regarded as a spontaneous symmetry breaking, where the ground state of the system does not preserve the full symmetry of the underlying Hamiltonian [34].

Recently, a question emerged on whether a phenomenon analogous to spatial crystalline structures could occur in the time-translational symmetry of a quantum system [35]. Initially, it was hypothesized that a many-body quantum system could spontaneously break the time-translational symmetry in the ground state of its Hamiltonian, leading to a periodic temporal self-organization. However, this scenario was subsequently ruled out by a series of no-go theorems, which demonstrated that spontaneous time-translation symmetry breaking cannot occur in ground states or under equilibrium conditions [36–38].

The time-crystal phase was later investigated in settings not encompassed by the no-go theorems. It has been shown that time-translation symmetry breaking in quantum systems can arise as an emergent many-body effect in nonequilibrium settings [39–41]. In particular, a manifestation of this symmetry breaking occurs in *time-independent* open quantum systems, which posses a continuous time-translational symmetry, and is known as a continuous time crystal [39]. In this scenario, the state of the

system breaks the continuous time-translational symmetry of the dynamical generator. This emerging phenomena is due to the competition between coherent energy input and environmental dissipation, causing the many-body system to exhibit stable, long-lived oscillatory behavior rather than relaxing to a stationary state. This symmetry breaking in open quantum systems has been explored theoretically in many settings [39, 42–54]. Also, continuous time crystals were experimentally investigated in several setups [55–61].

Furthermore, technological applications of time crystals have been proposed in the fields of quantum sensing [62–65] and quantum thermodynamics, such as in nonequilibrium quantum engines [54, 66] and energy storage devices [67, 68]. To properly evaluate the potential of this phase of matter, there is a need for a consistent thermodynamic framework that accounts for its inherent nonequilibrium nature [13, 21]. In particular, time crystals cannot appear in equilibrium, therefore they are described by master equations featuring nonequilibrium dynamics, which are modelled from phenomenological arguments. These master equations, referred to as local master equations, can be derived by assuming that terms describing external energy sources or interactions between particles within the quantum system do not affect the coupling between the Hamiltonian of the bare quantum system and its surrounding environment [21, 69–72]. While this approach has been successfully employed to model and interpret several experiments [73–77], it can lead to thermodynamic inconsistencies if the relevant quantities are not properly defined [13, 21]. However, a consistent description of systems governed by local master equations can be achieved, for instance, by interpreting their interactions with the environment through a collision-model framework [22, 78–84]. In particular, this framework provides a microscopic model for environments that describe local master equations, enabling consistent thermodynamics for such open quantum systems.

In one part of this thesis, we focus on characterizing the nonequilibrium thermodynamics of time crystals and exploring their applications. In our **first work**, we demonstrate how to define the second law of thermodynamics for open quantum dynamics described by local master equations [54]. Our thermodynamic description is based on separating, in the system Hamiltonian, the bare-energy contributions of the system

from those related to external driving. This decomposition allows for the formulation of a natural energetic balance in terms of persistent nonequilibrium dissipated heat currents. Using our derivations, we show that it is possible to design a quantum engine driven by time-translational symmetry breaking with finite efficiency. Moreover, in our **third work**, we characterize the thermodynamics of coupled time crystals using a collision-model framework and demonstrate their potential for efficient energy storage [67].

1.3 Large deviations

The dynamics of open quantum systems follows a stochastic process, where each experimental realization of the system corresponds to a random quantum trajectory [18, 85–88]. In other words, a quantum trajectory is the evolution of a pure state, which is affected by a noise that acts at random times, promoting a quantum jump. For example, inside an optical cavity the state of the light field changes abruptly whenever a photon leaks out through imperfect mirrors, each photon loss corresponds to a quantum jump in the state of the system [89–93]. These quantum jumps can be associated with thermodynamic quantities [94]. For example, a photon emitted or absorbed by the environment in a quantum trajectory corresponds to a discrete amount of heat dissipated or absorbed by the system. This provides a probabilistic perspective on thermodynamic quantities in open quantum systems [94–99]. Understanding the statistics of these stochastic observables is relevant for thermodynamics and applications, such as quantum heat engines [19, 100].

The full statistics of observables associated with quantum jumps can be described by large deviations theory [101–103]. This theory describes how probability distributions associated with stochastic observables decay exponentially and how they concentrate around a typical value [101]. Additionally, it addresses rare events that are generally not well predicted by Gaussian fluctuations in the central-limit theorem and provides insights into system behavior during such occurrences [101, 104]. Another important result of large deviations in open quantum systems is the quantum Doob transform, which is a method to make the rare behavior of a system typical [102, 105].

In particular, this method is useful to tailor the statistics of emissions of quantum systems, making them more or less active, and even creating intermittency [106, 107]. In open quantum systems, finding large deviation statistics requires solving an eigenvalue problem, similar to determining the stationary state of an open quantum system [108]. Techniques like tensor networks can also be applied for this task [109, 110].

In our **second publication**, we show how the large deviations theory applies to evaluate stochastic observables in adiabatic open quantum dynamics. In this case, the parameters of the system are slowly varied, such that the state of the system follows the instantaneous stationary state manifold of the generator of the dynamics [111, 112]. In particular, adiabatic, or quasi-static, processes in open quantum systems are related to reversible cycles in thermodynamics, enabling the construction of engines that operate at maximum efficiency [1]. Following our adiabatic theorem for large deviations theory, we described the quantum Doob transform in these settings and showed that the time-history of stochastic observables can also be described using the large deviations framework.

1.4 Structure of this thesis

The goal of this thesis is to present the theoretical background supporting our three publications. To this end, we review in Chapter 2 the standard derivation of a master equation that describes the Markovian dynamics of the state of a system interacting with an environment. In this chapter, we also focus on the thermodynamic description of a quantum system in thermal equilibrium with its surroundings. Additionally, we introduce an alternative approach that phenomenologically describes processes occurring in open quantum systems, which leads to local master equations. While these equations are useful for interpreting experiments, they can potentially violate the laws of thermodynamics. Chapter 3 addresses this issue by using the collision model approach to ensure consistency with thermodynamic principles of local master equations. Further in the chapter, we explore time crystals, which were investigated in the **first and third publications**. We use a minimal model to illustrate how this phase of matter can manifest in open quantum systems. Furthermore, we provide a consistent char-

acterization of their thermodynamic behavior within the collision-model framework. Chapter 4 focuses on the theoretical foundation of our **second publication**. It introduces the theory of large deviations and explains how the dynamics of open quantum systems can be mapped onto stochastic processes. The chapter concludes by describing how quantum jump trajectories can be analyzed using the large deviations theory. Finally, the last chapter connects the theoretical background to the results of our work, summarizing the contributions we have made to the field and highlighting their significance in the broader context of quantum thermodynamics. In the **appendix**, we report the full publications.

Chapter 2

Methods: Open quantum systems

In this chapter, we review the fundamental concepts in the theory of open quantum systems which are of relevance for this thesis. To this end, we derive the Markovian master equation for the dynamics of a quantum system weakly-coupled to a thermal environment and discuss the different assumptions in the derivation and their consequences [113–115]. We then show how the resulting master equation leads to thermal equilibrium between the system and its environment, which is relevant to describe the thermodynamic quantities in open quantum systems [13, 116].

Furthermore, we dedicate a section to local master equations, which come from phenomenological modelling of dissipation effects of a quantum system [13]. These master equations feature nonequilibrium stationary states, which can result in violations of the thermodynamic laws formulated for a quantum system weakly-coupled to its environment [21]. In the following chapters, we will exploit the local master equations in many applications and provide a proper description of their thermodynamics.

2.1 Markovian master equation

The time evolution of a closed quantum system follows a unitary dynamics described by Schrödinger or Heisenberg equations and it preserves the purity of the state [117]. When a quantum system interacts with a much larger system, referred to as the environment [see Fig. 2.1 for a pictorial representation], directly applying the Schrödinger equation to describe their combined dynamics becomes impractical. This

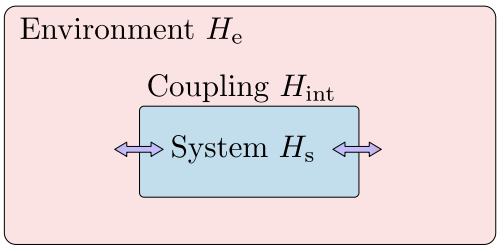

Figure 2.1: **Sketch of an open quantum system.** A quantum system, described by the Hamiltonian H_s is surrounded by an environment, described by H_e and they interact according to H_{int} [113].

is due to the exponential growth of the Hilbert space with system size, making the computational cost of describing large quantum systems prohibitive. However, one is typically only interested in the reduced dynamics of the system, which can be obtained by tracing out the environment's degrees of freedom. An important regime where the dynamics of the reduced state of the system can be computed is the so-called weak-coupling limit [81, 113, 114, 118]. In this limit, we assume that the coupling between the system and the environment is weak, the environment is significantly larger than the system, and information transferred from the system to the environment is instantly lost. As a result, the dynamics of the system is described by a master equation that contains the unitary part arising from the Hamiltonian of the system and a non-unitary part that emerges from the coupling with the environment. In the following, we derive this master equation closely following Ref. [113], but analogous derivations can also be found, for instance, in Refs. [81, 114, 115, 118].

We begin the derivation of the master equation by considering the Hamiltonian H, which includes the Hamiltonian of the system, H_s, the Hamiltonian of the environment, H_e, and the Hamiltonian describing their interaction, H_{int},

$$H = H_s + H_e + H_{int} \,. \tag{2.1}$$

Next, we use the interaction picture [117], defined in relation to the Hamiltonian $H_0 = H_s + H_e$, where the joint density matrix of the system and environment evolves

according to the von Neumann equation

$$\frac{\mathrm{d}\rho(t)}{\mathrm{dt}} = -i[H_{\mathrm{int}}(t), \rho(t)] \,, \tag{2.2}$$

where $H_{\mathrm{int}}(t) = e^{itH_0} H_{\mathrm{int}} e^{-itH_0}$. The formal solution of this differential equation can be written as

$$\rho(t) = \rho(0) - i \int_0^t [H_{\mathrm{int}}(t'), \rho(t')] \mathrm{d}t' \,. \tag{2.3}$$

where we consider the initial time to be $t = 0$. Thus, we substitute Eq. (2.3) in Eq. (2.2) and we trace out the environment degrees of freedom, leading to the differential equation

$$\frac{\mathrm{d}\rho_{\mathrm{s}}(t)}{\mathrm{d}t} = \frac{\mathrm{dTr_e}[\rho(t)]}{\mathrm{d}t} = -\int_0^t \mathrm{Tr_e}\{[H_{\mathrm{int}}(t), [H_{\mathrm{int}}(t'), \rho(t')]]\} \mathrm{d}t' \,, \tag{2.4}$$

where $\mathrm{Tr_e}$ indicates a partial trace over the degrees of freedom of the environment. Also, without loss of generality we consider that $\mathrm{Tr_e}[H_{\mathrm{int}}(t)\rho(0)] = 0$ [81, 115]. We note that Eq. (2.4) is still exact and this process of substituting Eq. (2.2) in Eq. (2.3) could be repeated to reconstruct an infinite series for the full evolution. However, in the weak-coupling limit, the interaction between the system and the environment is small and can be treated as a perturbation to the Hamiltonian $H_0 = H_{\mathrm{s}} + H_{\mathrm{e}}$.

Born-Markov approximations

The derivation of a Markovian master equation for a system weakly-coupled to a large environment requires two approximations. The first assumes that the bath is significantly larger than the system, such that the coupling to the system has a negligible effect on the state of the bath, while still influencing the dynamics of the system [113, 115]. Using this idea, we consider that the state of the system and the environment at all times can be written as the product state

$$\rho(t) \approx \rho_{\mathrm{s}}(t) \otimes \rho_{\mathrm{e}} \,, \tag{2.5}$$

where ρ_{e} is the state of the environment, which remains time-independent [115, 119, 120]. This is known as the *Born* approximation. Now, we consider the *Markov* approx-

imation, which consists of replacing $\rho_s(t')$ to $\rho_s(t)$ inside the integral of Eq. (2.4), such that the reduced state of the system only depends on the present state and not on past times. Therefore, we find

$$\frac{d\rho_s(t)}{dt} = -\int_0^t \mathrm{Tr}_e\{[H_{int}(t),[H_{int}(t'),\rho_s(t)\otimes\rho_e]]\}dt' \,. \tag{2.6}$$

This approximation is well justified when considering that the relaxation time τ_{se} by which the state of the system changes due to the coupling with the environment is much slower than the time scale whereby the correlation functions of the environment decay τ_e, *i.e.* $\tau_{se} \gg \tau_e$. This assumption implies that information dissipates inside the environment much faster than the dynamics induced by the environment in the system. Hence, the integral in Eq. (2.6) is different than zero only when $t' \approx t$. Under this condition, we substitute $t' \to t - s$ in the integral in Eq. (2.4) and use that the limit of integration is from zero to infinity,

$$\frac{d\rho_s(t)}{dt} = -\int_0^\infty \mathrm{Tr}_e\{[H_{int}(t),[H_{int}(t-s),\rho_s(t)\otimes\rho_e]]\}ds \,. \tag{2.7}$$

This equation is the so-called Redfield master equation [121], which is Markovian, trace-preserving, but the dynamics it generates is, in general, not completely positive [113, 122]. Therefore, there can appear nonphysical negative probabilities in the state of the system.

Secular approximation

To ensure a completely positive dynamics, it is necessary to consider a further approximation, referred to as the secular approximation (or rotating wave) [113, 123]. The idea is to find a regime where the terms that do not preserve complete positivity do not contribute to the dynamics. To apply the secular approximation, we first consider the interaction Hamiltonian in the *Schrödinger picture* to have the form

$$H_{int} = g\sum_\mu A_\mu \otimes B_\mu \,, \tag{2.8}$$

where A_μ and B_μ are operators of the system and the bath, respectively. Also, g gives the scale of the interaction between system and environment and it is given in units of frequency ($\hbar = 1$). We now consider the Hamiltonian of the system in its diagonal basis

$$H_\mathrm{s} = \sum_j \epsilon_j |\epsilon_j\rangle\langle\epsilon_j| \,, \tag{2.9}$$

where ϵ_j is the energy associated with the eigenstate $|\epsilon_j\rangle$. Then, we represent the operator A_μ in the eigenbasis of the Hamiltonian of the system as $A_\mu = \sum_\omega A_\mu(\omega)$, with

$$A_\mu(\omega) = \sum_{\epsilon_j - \epsilon_i = \omega} P(\epsilon_i) A_\mu P(\epsilon_j) \,, \tag{2.10}$$

where $P(\epsilon_j) = |\epsilon_j\rangle\langle\epsilon_j|$ is a projector in the eigenstae $|\epsilon_j\rangle$. The sum iterates over all pairs of eingestates, $|\epsilon_i\rangle$ and $|\epsilon_j\rangle$, of the Hamiltonian H_s, which have energy difference ω. The operators of the system in this representation become eigenoperators of the Hamiltonian of the system [113], as illustrated by the commutation relations

$$[H_\mathrm{s}, A_\mu(\omega)] = -\omega A_\mu(\omega) \,, \quad [H_\mathrm{s}, A_\mu^\dagger(\omega)] = \omega A_\mu^\dagger(\omega) \,. \tag{2.11}$$

Moreover, from the commutation relations in Eq. (2.11), the operators A_μ in the interaction picture become

$$e^{iH_\mathrm{s}t} A_\mu(\omega) e^{-iH_\mathrm{s}t} = e^{-i\omega t} A_\mu(\omega) \,, \quad e^{iH_\mathrm{s}t} A_\mu^\dagger(\omega) e^{-iH_\mathrm{s}t} = e^{i\omega t} A_\mu^\dagger(\omega) \,. \tag{2.12}$$

With this, we note that $A_\mu^\dagger(\omega) = A_\mu(-\omega)$ and that $[H_\mathrm{s}, A_\nu^\dagger(\omega) A_\mu(\omega)] = 0$, whereby the interaction Hamiltonian in the interaction picture becomes

$$H_\mathrm{int}(t) = g \sum_{\mu,\omega} e^{-i\omega t} A_\mu(\omega) \otimes B_\mu(t) \,. \tag{2.13}$$

Here, we define the operators of the environment in the interaction picture as $B_\mu(t) = e^{iH_\mathrm{e}t} B_\mu e^{-iH_\mathrm{e}t}$. Moreover, we substitute the expression of $H_\mathrm{int}(t)$ in Eq. (2.7), which gives

the differential equation for the reduced state of the system

$$\frac{\mathrm{d}\rho_{\mathrm{s}}(t)}{\mathrm{d}t} = g^2 \sum_{\omega,\omega',\mu,\nu} e^{i(\omega'-\omega)t} \Gamma_{\mu\nu}(\omega) \left[A_\nu(\omega)\rho_{\mathrm{s}}(t)A_\mu^\dagger(\omega') - A_\mu^\dagger(\omega')A_\nu(\omega)\rho_{\mathrm{s}}(t) \right] , \tag{2.14}$$

where we define the Fourier transform of the bath operators corresponding the environment correlation functions

$$\Gamma_{\mu\nu}(\omega) = \int_0^\infty \mathrm{d}t' e^{i\omega t'} \langle B_\mu^\dagger(t) B_\nu(t-t') \rangle . \tag{2.15}$$

In this derivation of the master equation, we consider that the bath is always in equilibrium, such that $[H_{\mathrm{e}}, \rho_{\mathrm{e}}(t)] = 0$. Also, we note that $\Gamma_{\mu\nu}(\omega)$ has dimension of time. Moreover, we can write the correlation function as

$$\begin{aligned} \langle B_\mu^\dagger(t) B_\nu(t-t') \rangle &= \mathrm{Tr}\{ e^{iH_{\mathrm{e}}t} B_\mu^\dagger e^{-iH_{\mathrm{e}}t} e^{iH_{\mathrm{e}}(t-t')} B_\nu e^{-iH_{\mathrm{e}}(t-t')} \rho_{\mathrm{e}} \} \\ &= \langle B_\mu^\dagger(t') B_\nu(0) \rangle . \end{aligned} \tag{2.16}$$

Here, we use that the state of the bath is time-invariant $\rho_{\mathrm{e}}(t) = e^{iH_{\mathrm{e}}t}\rho_{\mathrm{e}}(0)e^{-iH_{\mathrm{e}}t} = \rho_{\mathrm{e}}(0)$. This shows that under the *Born* and *Markov* assumptions, the correlation functions are not dependent on time t and the only time-dependency in the master equations is confined in the complex exponentials [115].

Next, we apply the rotating wave approximation, which consists of neglecting the off-diagonal terms with respect to the frequencies within the master equations, *i.e.* the nonzero complex exponentials with $\omega \neq \omega'$. For the Markov approximation, we consider that the correlation functions of the environment decay much faster than the relaxation time of the system. Therefore, we consider that terms with $\omega - \omega' \neq 0$ oscillate rapidly in comparison with the terms $\omega - \omega' = 0$, therefore averaging out and not contributing to the dynamics [113]. In particular, this approximation is valid as long as $\min_{\omega' \neq \omega}\{\omega' - \omega\} \ll \tau_{\mathrm{e}}^{-1}$. This regime is especially relevant for optical systems, where the frequencies associated with the system are much larger than the decay rates induced in the system by the environment [113]. The master equation after this

approximation is expressed as

$$\frac{\mathrm{d}\rho_{\mathrm{s}}(t)}{\mathrm{d}t} = g^2 \sum_{\omega,\alpha,\beta} \Gamma_{\mu\nu}(\omega) \left[A_\nu(\omega)\rho_{\mathrm{s}}(t)A_\mu^\dagger(\omega) - A_\mu^\dagger(\omega)A_\nu(\omega)\rho_{\mathrm{s}}(t) \right] . \tag{2.17}$$

To make a further simplification and find the final form of the Lindblad master equation, we decompose the Fourier transform of the correlation function according to

$$\Gamma_{\mu\nu}(\omega) = \frac{1}{2}\gamma_{\mu\nu}(\omega) + iS_{\mu\nu}(\omega) , \tag{2.18}$$

where $S_{\mu\nu}(\omega) = [\Gamma_{\mu\nu}(\omega) - \Gamma_{\nu\mu}^*(\omega)]/2i$ is a Hermitian matrix and

$$\gamma_{\mu\nu}(\omega) = \Gamma_{\mu\nu}(\omega) + \Gamma_{\nu\mu}^*(\omega) = \int_{-\infty}^{\infty} \mathrm{d}t' e^{i\omega t'} \langle B_\mu^\dagger(t')B_\nu(0)\rangle , \tag{2.19}$$

is positive.

Now, we can write the master equation in the laboratory frame using the so-called standard form

$$\frac{\mathrm{d}\rho_{\mathrm{s}}(t)}{\mathrm{d}t} = -i[H_{\mathrm{s}} + H_{\mathrm{LS}}, \rho_{\mathrm{s}}(t)] + \mathcal{D}[\rho_{\mathrm{s}}(t)] , \tag{2.20}$$

where

$$H_{\mathrm{LS}} = \sum_{\omega,\alpha,\beta} S_{\alpha\beta}(\omega)A_\alpha^\dagger(\omega)A_\beta(\omega) \tag{2.21}$$

is referred to as the Lamb shift Hamiltonian and it accounts for the changes in the energy levels of the system due to the coupling to the environment [124]. This term is often ignored since it commutes with the Hamiltonian of the system [113]. Additionally, the dissipator $\mathcal{D}$ describes the non-unitary dynamics induced in the system due to its coupling with the environment and it is expressed as

$$\mathcal{D}[\rho_{\mathrm{s}}(t)] = g^2 \sum_{\omega,\mu,\nu} \gamma_{\mu\nu}(\omega) \left[A_\nu(\omega)\rho_{\mathrm{s}}(t)A_\mu^\dagger(\omega) - \frac{1}{2}\{A_\mu^\dagger(\omega)A_\nu(\omega), \rho_{\mathrm{s}}(t)\} \right] . \tag{2.22}$$

Here $\{A, B\} = AB + BA$ is the anti-commutator. The Eq. (2.20), when derived from the set of approximations formerly described, is referred to as *global master equation*, since it considers the complete system Hamiltonian, rather than assuming that the environment couples locally to individual constituents of the system Hamiltonian [125].

Stationary state

When the environment is in a thermal state at an inverse temperature β, one would physically expect to observe a thermalization process, such that the system, in the long-time dynamics, also features a thermal state with the same inverse temperature β [6]. Here, we use the properties of the master equation describing a system weakly coupled to its surroundings to show that thermalization indeed occurs in these cases [113, 115].

We first consider that the environment is in a thermal state with inverse temperature β

$$\rho_{\rm e}^{\rm th} = \frac{e^{-\beta H_{\rm e}}}{{\rm Tr}\{e^{-\beta H_{\rm e}}\}} \, . \tag{2.23}$$

The correlation functions, in this case, can be written as

$$\langle B_\nu^\dagger(t) B_\mu(0)\rangle = \langle B_\mu(0) B_\nu^\dagger(t+i\beta)\rangle \, , \quad \langle B_\nu^\dagger(t) B_\mu(0)\rangle = \langle B_\mu(-t-i\beta) B_\nu^\dagger(0)\rangle \, . \tag{2.24}$$

These relations are known as Kubo-Martin-Schwinger condition [113, 115], where the inverse temperature is regarded as an imaginary time. The important result of these relations is the emergence of *detailed balance* between conjugate transitions induced by the environment

$$\gamma_{\mu\nu}(-\omega) = e^{-\beta\omega}\gamma_{\nu\mu}(\omega) \, . \tag{2.25}$$

The proof of this relation is given in detail in Ref. [115]. This condition shows that transitions related to a negative Bohr frequency, ω, are exponentially suppressed in comparison to the conjugated transition with a positive Bohr frequency. In other words, a system interacting with a thermal environment is more likely to dissipate excitations into the environment than to absorb them [115].

To show the consequence of the emergence of detailed balance in the master equation we derive in this section, we consider that the stationary state of the system has a Gibbs form

$$\rho_{\rm s}^{\rm th} = \frac{e^{-\beta H_{\rm s}}}{{\rm Tr}\{e^{-\beta H_{\rm s}}\}} \, . \tag{2.26}$$

To demonstrate that $\rho_{\rm s}^{\rm th}$ is the stationary state of the Lindblad equation, Eq. (2.20), we first use that it commutes with the Hamiltonian of the system, $[\rho_{\rm s}^{\rm th}, H_{\rm s}] = 0$. Then, we

consider the relation

$$e^{Y}Xe^{-Y} = \sum_{n=0}^{\infty} \frac{[Y,X]_n}{n!}\,, \tag{2.27}$$

where $[Y,X]_n = [Y,[Y,X]_{n-1}]$ and $[Y,X]_0 = X$ [117]. Using this identity, we find that

$$[H_s, A_\mu(\omega)]_n = (-\omega)^n A_\mu(\omega)\,, \quad [H_s, A_\mu^\dagger(\omega)]_n = (\omega)^n A_\mu^\dagger(\omega)\,. \tag{2.28}$$

Now, we substitute the stationary-state ansatz (2.23) into the master equation (2.22) and apply the relations above to obtain

$$\mathcal{D}[\rho_s^{\text{th}}] = g^2 \sum_{\omega,\mu,\nu} \gamma_{\mu\nu}(\omega) \left[e^{-\beta\omega} A_\nu(\omega) A_\mu^\dagger(\omega) - A_\mu^\dagger(\omega) A_\nu(\omega)\right] \rho_s^{\text{th}}\,. \tag{2.29}$$

Furthermore, we separate the sum in the above equation into a part with positive ω and into a part where ω is negative

$$\begin{aligned}\mathcal{D}[\rho_s^{\text{th}}] = {} & g^2 \sum_{\omega>0} \sum_{\mu,\nu} \gamma_{\mu\nu}(\omega) \left[e^{-\beta\omega} A_\nu(\omega) A_\mu^\dagger(\omega) - A_\mu^\dagger(\omega) A_\nu(\omega)\right] \rho_s^{\text{th}} \\ & + g^2 \sum_{-\omega>0} \sum_{\mu,\nu} \gamma_{\mu\nu}(-\omega) \left[e^{\beta\omega} A_\nu(-\omega) A_\mu^\dagger(-\omega) - A_\mu^\dagger(-\omega) A_\nu(-\omega)\right] \rho_s^{\text{th}}\,.\end{aligned} \tag{2.30}$$

Using that $A_\mu(-\omega) = A_\mu^\dagger(\omega)$ and the detailed balance condition, $\gamma_{\mu\nu}(-\omega) = e^{-\beta\omega}\gamma_{\nu\mu}(\omega)$, we obtain

$$\begin{aligned}\mathcal{D}[\rho_s^{\text{th}}] = {} & g^2 \sum_{\omega>0} \sum_{\mu,\nu} \gamma_{\mu\nu}(\omega) \left[e^{-\beta\omega} A_\nu(\omega) A_\mu^\dagger(\omega) - A_\mu^\dagger(\omega) A_\nu(\omega)\right] \rho_s^{\text{th}} \\ & + g^2 \sum_{\omega<0} \sum_{\mu,\nu} \gamma_{\mu\nu}(\omega) \left[A_\nu^\dagger(\omega) A_\mu(\omega) - e^{-\beta\omega} A_\mu(\omega) A_\nu^\dagger(\omega)\right] \rho_s^{\text{th}} \\ & = 0\,.\end{aligned} \tag{2.31}$$

This result shows that the Gibbs state, $\rho_s^{\text{th}} = e^{-\beta H_s}/\text{Tr}[e^{-\beta H_s}]$ is the stationary state of the master equation derived in this section [113, 115].

2.2 Quantum thermodynamics in adiabatic equilibrium settings

The goal of this section is to characterize the thermodynamics of an open quantum system, whose dynamics is given by a master equation derived from first principles, as we show in the previous section [13, 126, 127]. In this case, jump operators describing the coupling between system and environment obey the detailed balance condition, Eq. (2.25), and they are eigenoperators of the Hamiltonian of the system [6, 13, 113]. These features of the master equation lead the system to a stationary state given by a Gibbs state $\rho_{\rm s}^{\rm th} = e^{-\beta H_{\rm s}}/Z$. Here, β is the inverse temperature of the environment and $Z = {\rm Tr}[e^{-\beta H_{\rm s}}]$ is the thermodynamic partition function. We also consider an adiabatic, or quasi-static, change in a parameter of the Hamiltonian $H_{\rm s}(t)$, such that the system remains in the instantaneous equilibrium Gibbs state at all times, *i.e.* $\dot{\rho}_{\rm s}^{\rm th}(t) = \mathcal{L}(t)[\rho_{\rm s}^{\rm th}(t)] = 0$. In this way, the Lindbladian acquires also a time-dependency $\mathcal{L} \to \mathcal{L}(t)$. Since the variation of a parameter of the system is done adiabatically, the derivation of the master equation in the previous section remains valid for each time-interval [128].

The first law

The first law of thermodynamics for a quantum system with Hamiltonian $H_{\rm s}(t)$ undergoing this class of dissipative dynamics is expressed in terms of the derivative of the internal energy $U(t) = {\rm Tr}[H(t)\rho(t)]$

$$\dot{U}(t) = {\rm Tr}[\dot{H}_{\rm s}(t)\rho(t)] + {\rm Tr}[H_{\rm s}(t)\dot{\rho}(t)]\,, \tag{2.32}$$

where we define the dissipated heat to the environment $\dot{Q}(t) \equiv {\rm Tr}[H_{\rm s}(t)\dot{\rho}(t)]$ and the work input in the system $\dot{W}(t) \equiv {\rm Tr}[\dot{H}_{\rm s}(t)\rho(t)]$ [13]. Here, Eq. (2.32) is a statement of energy conservation and it distinguishes work from heat.

The second law

To define the second law of thermodynamics, we consider the von Neumann entropy, given by $S(t) = -\mathrm{Tr}[\rho(t)\ln\rho(t)]$, which is the extension of the Gibbs entropy for quantum systems [6]. The time derivative of the entropy is $\dot{S}(t) = -\mathrm{Tr}[\dot{\rho}(t)\ln\rho(t)]$. As defined above, we consider that the open quantum system follows an isothermal adiabatic dynamics, such that it features an instantaneous Gibbs state during the whole dynamics. Thus, the time derivative of the entropy becomes

$$\dot{S}(t) = \beta\mathrm{Tr}[H_{\mathrm{s}}(t)\dot{\rho}(t)] = \beta\dot{Q}(t)\,. \tag{2.33}$$

Here, the variation of the entropy of the system is directly connected to the exchanged heat with the environment [13]. Moreover, the external work contribution can be expressed as $\dot{W}(t) = -\beta^{-1}\dot{F}(t)$, with $F(t)$ being the free energy, defined as $F(t) = -\beta^{-1}\ln Z(t)$, where $Z(t) = \mathrm{Tr}[e^{-\beta H_{\mathrm{s}}(t)}]$ is the partition function. Here, we use that the Boltzmann constant is $k = 1$. Therefore, the first law can be expressed as

$$\dot{F}(t) = \dot{U}(t) - \beta^{-1}\dot{S}(t)\,. \tag{2.34}$$

The free energy quantifies the energy available for performing work, showing that this is given by the internal energy deducted by the thermal energy within the system. The latter form of energy cannot be transformed into work [129,130]. This equation is in accordance with the standard thermodynamics for classical and equilibrium systems [6]. We note that the idea of free energy assumes a more general definition in quantum systems. In finite quantum systems, the maximum amount of extractable work is referred to as ergotropy and accommodates quantum resources, such as entanglement [131]. In particular, this quantity is relevant in energy storage applications using finite quantum systems [132].

A relevant scenario for quantum thermodynamics is when a quantum system is weakly-coupled simultaneously to a hot and a cold environment, at inverse temperatures β_{h} and β_{c}, respectively. In this case, the system goes to a nonequilibrium state where there can be persistent energy currents flowing from the hot bath to the cold one.

This setting is relevant, for instance, in devising quantum engines [116, 133, 134] and to investigate the transport of particles or energy in open quantum systems [135, 136]. The master equation describing this scenario is given by

$$\dot{\rho}_{\rm s}(t) = -i[H_{\rm s}(t), \rho_{\rm s}(t)] + \mathcal{D}^{\rm h}(t)[\rho_{\rm s}(t)] + \mathcal{D}^{\rm c}(t)[\rho_{\rm s}(t)]\,, \tag{2.35}$$

where $\mathcal{D}^{\rm h}(t)$ $(\mathcal{D}^{\rm c}(t))$ is the dissipator defined in Eq. (2.22) for the hot (cold) environment. We can formulate the second law in terms of the entropy production [2], which we define as

$$\dot{\Sigma}(t) \equiv \dot{S}(t) + \sum_{\alpha} \beta_{\alpha} \dot{Q}_{\alpha}(t)\,, \tag{2.36}$$

where $\dot{Q}_{\alpha}(t)$ is the heat dissipated to the environment α. To show that this quantity is positive, following the second law of thermodynamics, we can invoke Spohn's theorem [21, 54, 116, 137]. This theorem states that for any superoperator $\mathcal{D}^{\alpha}(t)$ of Lindblad form, given by Eq. (2.22), the following inequality holds

$$-{\rm Tr}\{\mathcal{D}^{\alpha}(t)[\rho(t)](\ln \rho(t) - \ln \rho^{\alpha}_{\rm ss}(t))\} \geq 0\,, \tag{2.37}$$

where $\rho^{\alpha}_{\rm ss}(t)$, is the steady-state of the dissipator, *i.e.* $\mathcal{D}^{\alpha}(t)[\rho^{\alpha}_{\rm ss}(t)] = 0$. When the superoperator $\mathcal{D}^{\alpha}(t)$ has a thermal steady state, $\rho^{\alpha}_{\rm ss}(t) = e^{-\beta_{\alpha} H_{\rm s}(t)}/{\rm Tr}[e^{-\beta_{\alpha} H_{\rm s}(t)}]$, we find that $-{\rm Tr}\{\mathcal{D}^{\alpha}(t)[\rho(t)] \ln \rho(t)\} + \beta_{\alpha} \dot{Q}_{\alpha}(t) \geq 0$, where $\dot{Q}_{\alpha}(t)$ is the heat dissipated to the environment α. The sum of the contributions from all heat baths reads

$$\dot{\Sigma}(t) = \dot{S}(t) + \beta_{\rm h} \dot{Q}_{\rm h}(t) + \beta_{\rm c} \dot{Q}_{\rm c}(t) \geq 0\,. \tag{2.38}$$

The entropy production rate is thus non-negative, as requested by the second law of thermodynamics [2]. Here, we note that the entropy production rate is valid beyond the stationary state and it is in accordance with the result for irreversible processes in classical thermodynamics [1]. Moreover, when the time-dependent dynamics stops and the system goes to the stationary state, we have that $\dot{S} = 0$ and Eq. (2.38) recovers the Clausius inequality, $\beta_{\rm h} \dot{Q}_{\rm h} + \beta_{\rm c} \dot{Q}_{\rm c} \geq 0$ [13].

In summary, the reduced dynamics of a quantum system coupled to an environ-

ment derived from first principles and employing the Born, Markov, and secular approximations, can be described by a Markovian master equation. This master equation yields a stationary state of the Gibbs form, implying that the system naturally evolves toward thermal equilibrium with its surroundings. This property follows directly from two features of the master equation, which are the detailed balance condition that appears in the jump operators and the fact that the jump operators are eigenoperators of the Hamiltonian of the system H_s. In this section, we highlight the importance of having a dissipator featuring a Gibbs stationary state when defining thermodynamic quantities, especially in connecting changes in the entropy of the system with the dissipated heat. When a dissipator fails to satisfy these conditions, its stationary state may not be a Gibbs state, and the thermodynamic quantities in the second law must be revised to avoid inconsistencies [21].

2.3 Local master equations

The dynamics of a quantum system weakly-coupled to its environment can be described by the global master equation, as described by Sec. 2.1. This task, however, requires the diagonalization of the Hamiltonian of the system, which can be computationally expensive for large systems given the exponential growth of the Hilbert space with the system size. In this section, we will introduce local master equations, which are derived using phenomenological arguments, based on a separation of time scales within the quantum system, to describe its coupling with the surrounding environment [118]. Our aim is not to derive the master equation explicitly, as it follows directly from the methods outlined earlier in this chapter. Rather, we want to demonstrate that, under certain conditions, the influence of external energy sources can be neglected when analyzing the dynamics of a system coupled to its surroundings.

We consider a simple example to illustrate this technique and show its consequences for the thermodynamic description of the system. The model we choose is a driven qubit, whose Hamiltonian is given by

$$H = \frac{\omega}{2}\sigma_z + \frac{\Omega}{2}(\sigma_- e^{-i\omega t} + \sigma_+ e^{i\omega t}) \,, \tag{2.39}$$

where ω is the bare frequency of the qubit and Ω is the Rabi frequency of an external laser, which promotes coherent transitions between the ground and the excited states of the qubit. To provide a microscopic model of the environment, we consider that the system interacts with a collection of harmonic oscillators, given by the Hamiltonian $H_{\rm e} = \sum_j \omega_j a_j^\dagger a_j$, where ω_j is the frequency of the j-th system and $a_j^\dagger(a_j)$ are creation (annihilation) operators [118]. Also, the system interacts with the environment according to the Hamiltonian

$$H_{\rm int} = \sum_j g_j(a_j^\dagger \sigma_- + a_j \sigma_+) \,, \tag{2.40}$$

where g_j is the strength of this interaction. We also consider that the harmonic oscillators are in a thermal state.

Since the Hamiltonian of the system is time-dependent, due to the laser driving, we need to perform further calculations to evaluate the operators of the system in the interaction picture. To this end, we use the time-evolution of operators evaluated in the Heisenberg picture [117, 118]. Hence, we find the system of equations

$$\begin{aligned} \dot{\sigma}_- &= -i\omega\sigma_- - i\frac{\Omega}{2}e^{-i\omega t}\sigma_z \,, \\ \dot{\sigma}_+ &= i\omega\sigma_+ + i\frac{\Omega}{2}e^{i\omega t}\sigma_z \,, \\ \dot{\sigma}_z &= i\Omega e^{-i\omega t}\sigma_+ - i\Omega e^{i\omega t}\sigma_- \,. \end{aligned} \tag{2.41}$$

To proceed, we define the new variables

$$\tilde{\sigma}_x = \sigma_+ e^{-i\omega t} + \sigma_- e^{i\omega t} \,, \quad i\tilde{\sigma}_y = \sigma_+ e^{-i\omega t} - \sigma_- e^{i\omega t} \,. \tag{2.42}$$

whose equations of motion are

$$\dot{\tilde{\sigma}}_x = 0 \,, \quad \dot{\tilde{\sigma}}_y = \Omega\sigma_z \,, \quad \dot{\tilde{\sigma}}_x = -\Omega\tilde{\sigma}_y \,. \tag{2.43}$$

Using these new equations, we find that $\ddot{\sigma}_z = -\Omega^2\sigma_z$. Also, the full solution of the

dynamics of the operators in the interaction picture is

$$\begin{aligned}\sigma_-(t) &= e^{-i\omega t}\left[\sigma_- + \frac{\sigma_+ - \sigma_-}{2}(1-\cos\Omega t) - \sigma_z\frac{i}{2}\sin\Omega t\right] ,\\ \sigma_+(t) &= e^{i\omega t}\left[\sigma_+ - \frac{\sigma_+ - \sigma_-}{2}(1-\cos\Omega t) + \sigma_z\frac{i}{2}\sin\Omega t\right] .\end{aligned} \tag{2.44}$$

In particular, these time-dependent operators will enter in Eq. (2.13), introducing two additional frequencies within the system. Therefore, when considering the terms containing Ω, we find, as shown in Ref. [118], rates that are proportional to $\gamma(\omega)$ and $\gamma(\omega \pm \Omega)$, where $\gamma(\omega) \propto \omega^3 n_\beta(\omega)$, for $n_\beta(\omega) = [e^{\beta\omega} - 1]^{-1}$ being the Bose–Einstein occupation number [113, 118]. See Ref. [138] for the full derivation of the global master equation for this system. Now, we remark on the importance of the time scales within the system when describing its coupling to the environment. In quantum optics experiments, one usually finds $\omega \approx 10^{15} s^{-1}$, while the Rabi frequency is around $10^{10} s^{-1}$ [139]. Therefore, it is usually justified to assume that external lasers do not significantly change the coupling of the bare quantum system to the surrounding environment, as demonstrated in several experiments [73–77]. In the model presented here, the local master equation describing the dynamics of the driven-dissipative qubit reads

$$\dot{\rho} = -\frac{i}{2}\left[\omega\sigma_z + i\Omega(\sigma_- e^{-i\omega t} + \sigma_+ e^{i\omega t}), \rho\right] + \gamma[\sigma_-\rho\sigma_+ - \frac{1}{2}\{\sigma_+\sigma_-, \rho\}] , \tag{2.45}$$

where we assumed that the environment is effectively at zero temperature, $n_\beta(\omega) = 0$, since ω is very large.

Until now, we argued that local master equations can indeed provide an accurate method to model experiments. However, in the local master equations, the jump operators are not eigenoperators of the Hamiltonian in Eq. (2.39). This results in a stationary state that deviates from a Gibbs structure and may exhibit quantum coherence between eigenstates of the Hamiltonian. Therefore, the application of Spohn's theorem, as it was introduced in Sec. 2.2, does not yield an entropy production rate containing the heat flow to the environment and the entropy variation, as in Eq. (2.38). Thus, Eq. (2.38), in principle, cannot be applied to local master equations, since it may

not be valid in such scenarios [21]. However, as we will show in the next section, it is possible to reconcile local master equations with the second law of thermodynamics using the collision-model framework [22,80,81]. In our **third work**, we use this framework to describe the thermodynamics of time crystals and to characterize this phase of matter in energy storage applications. In addition to that, in our **first work**, we provide another approach to describe the thermodynamics of local master equations in a consistent way using the standard Spohn's theorem, but considering that Hamiltonian terms describing external energy input, such as input energy from laser driving, do not contribute to the internal energy of the system.

To provide a general summary of the phenomenological approach for describing open quantum systems, we consider a many-body quantum system whose Hamiltonian is given in the form

$$H = \sum_j H_j^{\text{bare}}(\omega_j) + \sum_j H_j^{\text{driving}}(\Omega_j) + \sum_{j \neq k} H_{jk}^{\text{int}}(g_{jk}) \,, \tag{2.46}$$

where H_j^{bare} describes the bare Hamiltonian of a subsystem j. Also, $H_j^{\text{driving}}(\Omega_j)$ describes an external driving in the j-th subsystem, and the interaction between subsystems j and k is given by $H_{jk}(g_{jk})$. Here, the symbols in parenthesis indicate the frequency associated with each operator. Therefore, as long as $\omega_j \gg \{\Omega_j, g_{jk}\} \; \forall \; j,k$, we can disregard H_j^{driving} and H_{jk}^{int} in the derivation of the master equation and describe the coupling between the system and the environment using local master equations. These time scales are usually found in quantum optical setups, as reported in several experiments. However, in systems featuring ultrastrong coupling, such as in circuit cavity electrodynamics [140] or in Rydberg atoms [141], the global description of the master equation becomes relevant.

Properties of the Lindblad equation

The master equation derived in the previous section is a linear differential equation

$$\dot{\rho}(t) = \mathcal{L}[\rho(t)] \,, \tag{2.47}$$

where $\mathcal{L}$ is referred to as the Lindblad generator, which is a linear map, or superoperator, acting on the density matrix of the system $\rho(t)$. This equation exhibits the semigroup property, meaning its solution can be divided into segments over different time intervals. To show how this property works, we consider a density matrix, such that $\rho(t) = \mathcal{W}_t[\rho(0)]$ and $\mathcal{W}_t$ is a superoperator, which represents the formal solutions of the Lindblad master equation. The semigroup property, for time-independent generators, is defined by $\mathcal{W}_{t_j}\mathcal{W}_{t_k} = \mathcal{W}_{t_j+t_k}$. This means that the solution of the equation from time 0 to t_k, can be split into two solutions, each governed by structurally identical maps. To ensure a physical evolution, the dynamics should be completely positive and trace preserving (CPTP), such that the eigenvalues of ρ represent probabilities for all times. The Lindblad theorem [142] states that the generator of any quantum CPTP dynamics with the semigroup property can be expressed as

$$\mathcal{L}[\rho(t)] = -i[H, \rho(t)] + \sum_k \gamma_k \left[L_k \rho(t) L_k^\dagger - \frac{1}{2}\{L_k^\dagger L_k, \rho(t)\} \right] . \tag{2.48}$$

Here, H must be a Hermitian operator, L_k are arbitrary operators, and $\gamma_k \geq 0$.

We now describe the spectral properties of the dynamical generator $\mathcal{L}$. The solution of the dynamics is given by

$$\rho(t) = e^{t\mathcal{L}}[\rho(0)] . \tag{2.49}$$

The Lindblad superoperator $\mathcal{L}$ is in general non-Hermitian, such that it can be expressed using a basis, consisting of distinct left, ℓ_i and right, r_i eigenmatrices associated with an eigenvalue λ_i

$$\mathcal{L}[r_i] = \lambda_i r_i, \quad \mathcal{L}^*[\ell_i] = \lambda_i \ell_i , \tag{2.50}$$

where $\mathcal{L}^*$ is the dual of $\mathcal{L}$ [90, 113]. Given the CPTP property of $\mathcal{L}$, its eigenvalues can be ordered such that $\mathrm{Re}[\lambda_0] > \mathrm{Re}[\lambda_1] > \cdots$, with $\lambda_0 = 0$. Here, the fact that the dominant eigenvalue λ_0 is zero reflects the trace-preservation property of $\mathcal{L}$ while the negativity of the real parts of all other eigenvalues is a manifestation of complete positivity, thereby ensuring a valid physical evolution [143]. Due to these spectral properties, the dominant right eigenmatrix, r_0, corresponds to the stationary state of the dynamics, $\rho_{\mathrm{ss}} = r_0$, since we can choose the normalization $\mathrm{Tr}[r_0] = 1$. Additionally, the

left eigenmatrix associated with the dominant eigenvalue is *always* the identity, $\ell_0 = \mathrm{I}$, which follows from the trace preservation property of the Lindbladian. Also, the right eigenmatrices associated with the eigenvalues with negative real parts are traceless. Using these properties, we can decompose any density matrix in the eigenbasis of the Lindbladian

$$\rho(t) = \rho_{\mathrm{ss}} + \sum_j e^{\lambda_j t} \mathrm{Tr}[\ell_j \rho(0)] r_j \,, \tag{2.51}$$

where we consider that λ_0 is non-degenerated. From this decomposition and the ordering of the eigenvalues, one can straightforwardly observe that all projections of the density matrix outside of the dominant subspaces exponentially decay, which in the long-time limit reads $\lim_{t\to\infty} \rho(t) = \rho_{\mathrm{ss}} = r_0$.

The spectral properties of the Lindblad superoperator can be used to understand many phenomena in open quantum systems. For example, it can be used to explain the Mpemba effect in open quantum systems, where states with higher thermodynamic free energy reach equilibrium faster than those closer to equilibrium [144–146]. Dissipative phase transitions manifest when the spectrum of $\mathcal{L}$ exhibits a gap closing [53, 143] and metastability phenomena can also be explained by analyzing the eigenvalues of $\mathcal{L}$ [147, 148]. In the derivation of the master equation, we assumed time-independent dynamics, but in our **second work**, we consider open quantum systems undergoing adiabatic dynamics, where parameters of the system are slowly changed. In this case, this spectral decomposition can be done in the instantaneous eigenbasis of the Lindbladian [92, 128].

Chapter 3

Methods: Collision models

Local master equations are a versatile approach to describe the open quantum system dynamics in many experimental setups. However, the fact that they can lead to nonequilibrium states can pose difficulties in using them in thermodynamic applications [21, 54, 116, 137]. Nevertheless, a consistent description of systems governed by local master equations can be achieved by interpreting their interaction with the environment using a collision model [22, 78–81]. In brief, the collision-model framework describes the environment as composed of a set of ancillary systems that individually interact with the system through unitary dynamics. By evaluating the energy and information exchanged between the system and ancillae, it is possible to devise a consistent characterization of thermodynamic quantities associated with local master equations. In particular, the requirement of an energetic cost to induce interactions between each ancilla and the system establishes a thermodynamic price for generating nonequilibrium dynamics, which leads to a consistent thermodynamic formulation of local master equations [22]. In the following, we provide the details of this method and we show how to define a consistent thermodynamic description of any local master equation.

3.1 From collision models to master equations

Within the collision-model framework, the environment is composed of a set of ancillary units [79–81, 83, 84]. The joint dynamics of the system and environment is

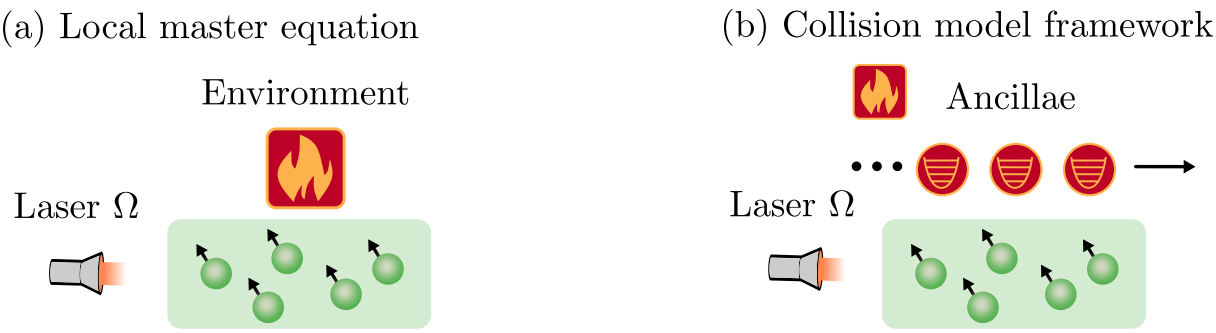

Figure 3.1: **Collision model framework** (a) An ensemble of atoms is externally driven by a laser, while it is in contact with a heat bath. (b) A collision model representation of (a), where the environment is replaced by a stream of ancillae units that collides with the atomic ensemble.

initially considered in discrete time, such that in each time interval, the system interacts with a single ancilla. After each interaction, the degrees of freedom of the ancilla are traced out, and the process is repeated over and over again [see Fig. 3.1 for a pictorial representation of a collision model]. We represent the system plus a set of k ancillae through the Hamiltonian

$$H = H_{\rm s} + \sum_{j=1}^{k} \left(H_{{\rm int}_j} + H_{e_j} \right) , \tag{3.1}$$

where $H_{{\rm e}_j}$ is the bare Hamiltonian of the j-th ancilla and $H_{{\rm int}_j}$ is the interacting term between the system and the ancilla. To make our discussion concrete, we consider that the ancillary system is given by harmonic oscillators, whose j-th element is represented by the bare Hamiltonian

$$H_{{\rm e}_j} = \omega a_j^\dagger a_j \, . \tag{3.2}$$

To ensure a Markovian environment, we assume that the ancillae are initially in a product state, $\rho_{\rm se} = \rho_{\rm s}(0) \otimes (\otimes_{j=1}^{k} \rho_{{\rm e}_j}(0))$, where $\otimes_{j=1}^{k}$ denotes that the ancillary system is in a product state, $\rho_{{\rm e}_j}$ is the density matrix of the j-th auxiliary system, and k is the total number of ancillary units. Note that this assumption is equivalent to the Born approximation made in Sec. 2.1, since the ancillary system is initially uncorrelated to the system and the system always sees the same environment [81]. Also, we consider that all ancillae start in a thermal state, satisfying ${\rm Tr}[\rho_{{\rm e}_j} a_j^\dagger a_j] = n_\beta(\omega) = [e^{\beta\omega} - 1]^{-1}$, where $n_\beta(\omega)$ is the bosonic occupation number of the j-th ancilla. The interaction Hamilto-

nian is given by

$$H_{\text{int}_j}(t) = g_j(t) \sum_{\mu} A_\mu \otimes B_\mu^j \,, \tag{3.3}$$

where A_μ is an operator of the system, B_μ^j an operator of j-th ancilla, and $g_j(t) = \sqrt{\gamma/\delta t}\theta(t,j)$ gives the rate at which the system interacts with each ancilla, where γ is a constant in units of frequency and δt gives the time of the interaction. Here, $\theta(t,j)$ is defined as $\theta(t,j) = 1$, for $j\delta t < t < (j+1)\delta t$ and 0 otherwise. The function $\theta(t,j)$ plays an important role within the collision model framework since it implies that it is necessary to exchange work to facilitate the interaction between system and ancilla, given its time-dependency [22, 84].

The evolution during the collision with the j-th ancilla is implemented by a unitary evolution,

$$V_j = e^{-iH_j\delta t} \,, \tag{3.4}$$

where $H_j = H_{\text{s}} + H_{\text{e}_j} + H_{\text{int}_j}$ and δt is the collision time, which goes from $t = j\delta t$ to $t = (j+1)\delta t$. After this interaction, we trace out the degrees of freedom of the ancilla j. After repeating this procedure k times, each time with a different ancilla, the reduced density matrix of the system can be expressed as

$$\rho_{\text{s}}(k\delta t) = \text{Tr}_{\text{e}_1,\text{e}_2\cdots\text{e}_k}\left[V_k V_{k-1}\cdots V_1\left(\rho_{\text{s}}(0)\otimes(\bigotimes_{j=1}^{k}\rho_{\text{e}_j}(0))\right)V_1^\dagger\cdots V_{k-1}^\dagger V_k^\dagger\right] \,.$$

Our goal is to take the limit of vanishing collision time, which is necessary to establish a connection with Lindblad master equations. For this purpose, we expand the unitary dynamics in powers of δt and keep terms up to the second order, obtaining

$$V_j \approx \text{I} - i\delta t H_j - \frac{(\delta t)^2}{2}H_j^2 \,. \tag{3.5}$$

Using this expansion, we calculate the density matrix of the system after k collisions

$$\begin{aligned}\rho_{\text{s}}(k\delta t) = {} & \rho_{\text{s}}\left[(k-1)\delta t\right] - i\delta t\text{Tr}_{\text{e}_k}\left\{\left[H_{\text{s}},\rho_{\text{s}}\left[(k-1)\delta t\right]\otimes\rho_{\text{e}_k}\right]\right\} \\ & + \left[g_k(t)\delta t\right]^2\text{Tr}_{\text{e}_k}\left\{H_{\text{int}_k}\left(\rho_{\text{s}}\left[(k-1)\delta t\right]\otimes\rho_{\text{e}_k}\right)H_{\text{int}_k}\right\} \\ & - \frac{\left[g_k(t)\delta t\right]^2}{2}\text{Tr}_{\text{e}_k}\left\{H_{\text{int}_k}^2\rho_{\text{s}}\left[(k-1)\delta t\right]\otimes\rho_{\text{e}_k} + \rho_{\text{s}}\left[(k-1)\delta t\right]\otimes\rho_{\text{e}_k}H_{\text{int}_k}^2\right\} \,.\end{aligned}$$

To find this expression, we used that the ancillae are in a thermal state, therefore $[H_{e_k}, \rho_{e_k}] = 0$ [79]. We consider that $\mathrm{Tr}_{e_k}\{H_{\mathrm{int}_k}[\rho_s(k\delta t - 1) \otimes \rho_{e_k}]\} = 0$, which was also used in the microscopic derivation of Sec. 2.1. Then, we write the state of the system after tracing out the ancilla, as

$$\frac{\Delta\rho_s(k\delta t)}{\delta t} = -i[H_s, \rho_s[(k-1)\delta t] + \delta t g_k^2(t)\mathrm{Tr}_{e_k}\left\{H_{\mathrm{int}_k}\left(\rho_s[(k-1)\delta t]\otimes\rho_{e_k}\right)H_{\mathrm{int}_k} - \frac{1}{2}\{H_{\mathrm{int}_k}^2, \rho_s[(k-1)\delta t]\otimes\rho_{e_k}\}\right\},$$

where $\Delta\rho_s(k\delta t) = \rho_s(k\delta t) - \rho_s\left[(k-1)\delta t\right]$. After substituting the interacting Hamiltonian, Eq. (3.3), we obtain

$$\frac{\Delta\rho_s(k\delta t)}{\delta t} = -i[H_s, \rho_s[(k-1)\delta t] + \delta t g_k^2(t)\sum_{\mu,\nu}\Gamma_{\mu\nu}\left[A_\mu\rho_s\left[(k-1)\delta t\right]A_\nu^\dagger - \frac{1}{2}\left\{A_\nu^\dagger A_\mu, \rho_s\left[(k-1)\delta t\right]\right\}\right],$$

where $\{\Gamma_{\mu\nu}\}$ is the set of correlation functions of the environment, which for the collision model framework, takes the form of

$$\Gamma_{\mu\nu} = \mathrm{Tr}_{e_j}\{(B_\nu^j)^\dagger B_\mu^j \rho_{e_j}\}\,. \tag{3.6}$$

Note that a similar object appeared in the derivation of the master equation from the microscopic model, Eq. (2.15). However, a key difference is that we do not need to express the operators $A_s^{(\alpha)}$ in the eigenbasis of H_s. For instance, in spin systems, the jump operators are associated with $\sigma_\pm$, whereas in cavity modes, they correspond to the creation ($a^\dagger$) and annihilation (a) operators. This distinction arises from the discrete nature of collision models, where the environment does not feature a continuum of modes coupling to all possible transitions within the eigenbasis of the system's Hamiltonian. In the collision-model framework, we explicitly specify which transitions between energy levels couples to the environment [81]. Another difference in collision models is the absence of the secular approximation. Since collision models implement a composition of completely positive maps, they ensure a positive dynamics from the beginning [79, 81].

The last step for finding the Lindblad master equation is to go to the continuous limit, which is done by considering $\lim_{k\to\infty,\delta t\to 0} k\delta t = t$. This completes the derivation of a Lindblad master equation from a collision model framework.

Driven-dissipative qubit

To make these ideas concrete, we conclude this section by considering the collision model description of a driven-dissipative qubit, which is the same model introduced in Sec. 2.3. As in Eq. (2.39), the Hamiltonian of the driven qubit is

$$H = \frac{\omega}{2}\sigma_z + \frac{\Omega}{2}(\sigma_- e^{-i\omega t} + \sigma_+ e^{i\omega t}) \,. \tag{3.7}$$

Then, we assume an environment composed of a set of harmonic oscillators, described by the Hamiltonian

$$H_{\mathrm{e}_j} = \omega a_j^\dagger a_j \,, \tag{3.8}$$

where $a_j(a_j^\dagger)$ is the creation(annihilation) bosonic operators of the j-th ancilla and ω is its frequency. In addition to that, we consider the interaction Hamiltonian between the system and ancilla to be

$$H_{\mathrm{int}_j} = g_j(t)\left(\sigma_+ a_j + \sigma_- a_j^\dagger\right) \,, \tag{3.9}$$

where the interaction strength is given by

$$g_j(t) = \sqrt{\frac{\gamma}{\delta t}}\theta(t,j) \,. \tag{3.10}$$

Here, we remark that our choice of the interaction Hamiltonian implies that the collision model dynamics implement transitions within the eigenbasis of the bare Hamiltonian of the ancilla, given by $H_{\mathrm{bare}} = \omega\sigma_z/2$. We note that this procedure will yield the same result of deriving the global master equation for bare Hamiltonian H_{bare} as described in Sec. 2.1.

The remaining part is to find the correlation functions of the environment, which

are

$$\Gamma_{a^\dagger a} = \mathrm{Tr}_{\mathrm{e}_j}\{a^\dagger a \rho_{\mathrm{e}_j}\} = n_\beta(\omega), \quad \Gamma_{aa^\dagger} = \mathrm{Tr}_{\mathrm{e}_j}\{aa^\dagger \rho_{\mathrm{e}_j}\} = 1 + n_\beta(\omega)\,, \tag{3.11}$$

where we considered that the ancillae are in a thermal state, with the bosonic occupation number $n_\beta(\omega) = [e^{\beta\omega} - 1]^{-1}$, as previously defined. Also, given this property of the ancillae states, we have $\Gamma_{aa} = \Gamma_{a^\dagger a^\dagger} = 0$. The choice of ω for the bare frequency of the ancilla ensures that the collision model dynamics matches the one predicted by local master equations derived from phenomenological arguments, as described in Sec. 2.1, when considering the limit of $\Omega \to 0$. We note that for the collision model, the master equation is valid even when Ω is not small, contrary to the phenomenological approach.

Therefore, by applying the framework of the collision model dynamics, we find the master equation of the driven-dissipative qubit, with $n_\beta(\omega) \to 0$ and in the laboratory frame, reads

$$\dot{\rho} = -i\left[\frac{\omega}{2}\sigma_z + \frac{\Omega}{2}(\sigma_- e^{-i\omega t} + \sigma_+ e^{i\omega t}), \rho\right] + \gamma[\sigma_-\rho\sigma_+ - \frac{1}{2}\{\sigma_+\sigma_-, \rho\}]\,, \tag{3.12}$$

which is the same master equation, Eq. (2.39), found by considering the phenomenological arguments presented in Sec. 2.3.

3.2 The first law of thermodynamics for collision models

In the previous section, we showed that a system interacting with an array of ancillae exhibits Markovian open quantum dynamics described by a local master equation. Defining thermodynamic quantities for the collision model requires computing the exchange of energy between the system and ancilla or evaluating the information loss after tracing out the degrees of freedom of the ancilla.

To illustrate how thermodynamics is defined from a collision model, we begin by describing the variation of the density matrix after a collision

$$\Delta\rho_{\mathrm{se}_j}(j\delta t) = V_j\left[\rho_{\mathrm{s}}((j-1)\delta t) \otimes \rho_{\mathrm{e}_j}\right] V_j^\dagger - \rho_{\mathrm{s}}((j-1)\delta t) \otimes \rho_{\mathrm{e}_j}\,, \tag{3.13}$$

where ρ_{e_j} is the density matrix of the j-th ancilla before the collision. As defined in the previous section, Eq. (3.4), the unitary evolution of the system and the ancillae is given by $V_j = e^{-iH_j\delta t}$, where $H_j = H_s + H_{e_j} + H_{int_j}$.

The heat dissipated by the system after a collision is defined as the negative of the ancilla's energy variation

$$\Delta Q(j\delta t) = -\mathrm{Tr}_{e_j}\{H_{e_j}\Delta\rho_{se_j}(j\delta t)\}\,. \tag{3.14}$$

Similarly, the variation of the internal energy of the system after a collision is defined as

$$\Delta U(j\delta t) = \mathrm{Tr}_{e_j}\{H_s\Delta\rho_{se_j}(j\delta t)\} \tag{3.15}$$

where $\Delta U(j\delta t)$ is the internal energy variation of the system after the collision. We find the first law of thermodynamics by considering that the work input in the system can be computed as the difference between the variation of the internal energy of the system and the total dissipated heat

$$\dot{W} = \lim_{\delta t\to 0}\frac{1}{\delta t}\Delta W_{env} = \dot{U} - \dot{Q} \tag{3.16}$$

where $\dot{A} = \lim_{\delta t\to 0}\Delta A/\delta t$ and ΔW_{env} is the work required to turn on the interaction between the system and the ancillae. In particular, the external work rate, $\dot{W}$, arises even for systems with *time-independent* Hamiltonians. This result follows from the microscopic model, *i.e.* ancillary system and their collision with the system, and it resolves all issues in the thermodynamics of local master equations, including abnormal heat flows and negative entropy production rates [22, 84, 149].

3.3 The second law of thermodynamics for collision models

In this section, we derive the second law of thermodynamics within the collision-model framework [2, 22, 84, 150]. For this purpose, we define the states, $\rho'_{se_j} \equiv V_j\left(\rho_s\otimes\rho_{e_j}\right)V_j^\dagger$, $\rho'_{s_j} \equiv \mathrm{Tr}_{e_j}[\rho_{se_j}]$, and $\rho'_{e_j} \equiv \mathrm{Tr}_s[\rho'_{se_j}]$. Now, considering the informa-

tion loss when tracing out the ancillae's degrees of freedom, we express the entropy production as

$$\Sigma = \mathcal{I}_{\mathrm{e}_j}(\mathrm{s}_j : \mathrm{e}_j) + S(\rho'_{\mathrm{e}_j} || \rho_{\mathrm{e}_j}) \geq 0, \tag{3.17}$$

where $\mathcal{I}_{\mathrm{e}_j}(\mathrm{s}_j : \mathrm{e}_j) = S(\rho'_{\mathrm{s}_j}) + S(\rho'_{\mathrm{e}_j}) - S(\rho'_{\mathrm{se}_j})$ denotes the mutual information between the system and the ancilla after the j-th collision [2]. $S(A||B) = \mathrm{Tr}[A \ln A - A \ln B]$ is the is the relative entropy between the states A and B and $S(A)$ is the von Neumann entropy of the state A. The two terms on the right-hand side of Eq. (3.17) can be interpreted as follows: The first term represents the mutual information between the system and the ancilla, quantifying the amount of information lost by the system when the ancilla is traced out. The second term measures how far the state of the ancilla deviates from equilibrium due to its interaction with the system [2, 151]. The non-negativity of the entropy production follows directly from the non-negativity of both mutual information and relative entropy [2, 12]. To proceed with our definitions, we rewrite the entropy production above as

$$\Sigma = \Delta S - \Phi_j, \tag{3.18}$$

where Φ_j, is the entropy flux from the system to the environment during the j-th collision, with

$$\Phi_j = \mathrm{Tr}\{(\rho'_{\mathrm{e}_j} - \rho_{\mathrm{e}_j}) \ln \rho_{\mathrm{e}_j}\}. \tag{3.19}$$

ΔS is the variation of the von Neumann entropy of the system. When dividing the above equation by δt and taking the limit of δt to zero, we go to the continuous-time limit. Hence, $\dot{\Sigma} = \dot{S} - \dot{\Phi}$. Here, we focus on collision models, whose set of ancillae units are initially in a thermal state, given by $\rho_{\mathrm{e}_j} = e^{-\beta H_{\mathrm{e}_j}} / Z_{\mathrm{e}_j}$, with Z_{e_j} as the partition function of the j-th ancilla. In this scenario, the entropy flux reduces to

$$\dot{\Phi}(t) = -\beta \lim_{\delta t \to 0} \frac{1}{\delta t} \mathrm{Tr}\{(\rho'_{\mathrm{e}_j} - \rho_{\mathrm{e}_j}) \omega a_j^\dagger a_j\} = \beta \dot{Q}(t). \tag{3.20}$$

This result shows that when the ancillae are in a thermal state, the entropy flux to the environment is proportional to the heat current flowing between the system and the bath [2, 150]. Given the structure of entropy production defined for collision models, which is composed only of positive quantities, it follows that $\dot{\Sigma} \geq 0$ [2].

3.4 Example: Time crystals

In this thesis, we investigated the time-crystal phase in our **first** [54] and **third** [67] works. Therefore, we provide a theoretical background of this phase of matter by analyzing a minimal model exhibiting a time-crystal phase. Here, we discuss the spectral signature of this phase and the mean-field approach to its dynamics. Finally, we characterize its thermodynamics using a collision-model framework. In particular, we extend the ideas present in this section to coupled boundary time crystals in our **third work** [67].

For an open quantum system governed by a time-independent Lindblad generator $\mathcal{L}$, the density matrix is expected to converge to a stationary state, ρ_{ss}, satisfying $\mathcal{L}[\rho_{\text{ss}}] = 0$, as discussed in Sec. 2.1. Since the generator $\mathcal{L}$ is time-independent, it is time-translation invariant and commutes with the time-translation operator $e^{t\mathcal{L}}$, also referred to as the propagator. The time-translational symmetry of the system follows from the invariance of its stationary state under the application of the propagator, *i.e.* $e^{t\mathcal{L}}[\rho_{\text{ss}}] = \rho_{\text{ss}}$. In this context, the spontaneous breaking of the time-translation symmetry of the generator gives rise to the time crystal phase. In this phase, the state of the system exhibits persistent oscillations instead of settling into a stationary state. We denote the state of the system in the time-crystal phase as $\rho^{\text{tc}}(t)$, assuming a periodic oscillation with period T, such that $\rho^{\text{tc}}(t+T) = \rho^{\text{tc}}(t)$. Applying the time-translation operator to this state results in $e^{t'\mathcal{L}}[\rho^{\text{tc}}(t)] = \rho^{\text{tc}}(t+t')$, which is not equal to $\rho^{\text{tc}}(t)$ for $t, t' \neq T$. Thus, in the time-crystal phase, the state of the system breaks the continuous time-translational symmetry of the generator $\mathcal{L}$.

3.4.1 The boundary time crystal

A paradigmatic model exhibiting time-translational symmetry breaking is the boundary time crystal [39], which consists of a driven-dissipative atomic ensemble composed by N atoms. The bare Hamiltonian describing the atoms is given by

$$H_{\text{at}} = \frac{\omega_{\text{at}}}{\sqrt{2}} S_z \,, \tag{3.21}$$

where ω_{at} is the energy splitting of the atomic ensemble. Here, $S_\alpha = 1/\sqrt{2}\sum_{m=1}^{N}\sigma_{\alpha,m}$ is a collective operator representing the atomic ensemble, where $\sigma_{\alpha,m}$ denotes the Pauli matrix in the α direction ($\alpha = x, y, z$) for the m-th atom. The atoms are collectively driven by an external laser that is modeled by the Hamiltonian

$$H_{\text{las}} = \frac{\Omega}{\sqrt{2}}(S_- e^{i\omega_{\text{las}}t} + S_+ e^{-i\omega_{\text{las}}t}) \,, \tag{3.22}$$

where $S_\pm = S_x \pm iS_y$, ω_{las} is the laser frequency and Ω is the Rabi frequency. The Hamiltonian of the full system in the frame rotating with the laser frequency becomes

$$H_{\text{s}}^{\text{rot}} = \frac{\Omega}{\sqrt{2}}S_x + \frac{\delta}{\sqrt{2}}S_z \,. \tag{3.23}$$

Here $\delta = \omega_{\text{at}} - \omega_{\text{las}}$ is the detuning between the laser frequency and the energy splitting ω_{at}. The atomic ensemble undergoes collective coupling to a thermal bath with inverse temperature β. The driven-dissipative dynamics is then governed by the master equation $\dot{\rho} = \mathcal{L}[\rho]$, where

$$\mathcal{L}[\rho] = -i[H_{\text{s}}^{\text{rot}}, \rho] + \sum_\alpha \left[L_\alpha \rho L_\alpha^\dagger - \frac{1}{2}\left\{ L_\alpha^\dagger L_\alpha, \rho \right\} \right] . \tag{3.24}$$

The jump operators that describe the dissipative processes are

$$L_+^{(j)} = \sqrt{\frac{\kappa n_\beta(\omega_{\text{at}})}{N}} S_+^{(j)}, \quad L_-^{(j)} = \sqrt{\frac{\kappa(1 + n_\beta(\omega_{\text{at}}))}{N}} S_-^{(j)}, \tag{3.25}$$

where $n_\beta(\omega_{\text{at}}) = (e^{\beta\omega_{\text{at}}} - 1)^{-1}$ is the occupation number of the environment degrees of freedom and β is the inverse temperature. Here, the parameter κ encodes the strength of the coupling between the system and the environment. Since the coupling between the system and the environment remains unaffected by the laser, this model is described by a local master equation. Note that the same arguments used in Sec. 2.3 could be applied here to argue that the local master equation approach is valid, as long as $\omega_{\text{at}} \gg \Omega$. In this case, however, the model does not include local atomic decay [152] or any spatial properties related to the arrangement of the atoms [153]. Despite its simplicity, this model has been shown to successfully describe experiments exhibit-

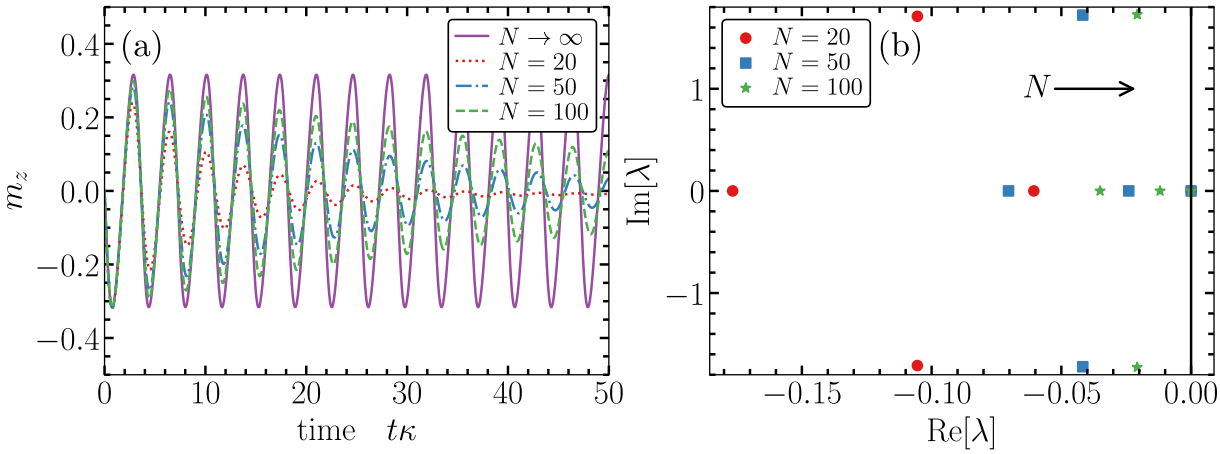

Figure 3.2: **Finite-size boundary time crystal** (a) Magnetization in the z direction as a function of time, $t\kappa$, for different system sizes, as indicated in the legend. The asymptotic behavior for $N \to \infty$ is exactly described by the mean-field solution. (b) The first four eigenvalues of the Lindblad generator are ordered with descending real parts. Here, we observe that the real part of the first pair of imaginary eigenvalues approaches zero as the system size increases, as indicated by the legend and the arrow. Parameters $\Omega = 2\kappa$ and $\delta = 0$.

ing time-crystal phases [56]. Nonetheless, this master equation can be derived from a collision model following the same procedure of Sec. 3.1.

To describe the dynamics of the system, we define the average values $m_\alpha = \langle S_\alpha / N \rangle$. In Fig. 3.2(a) we show the behavior of the magnetization, m_z, of the boundary time crystal for different system sizes, where we observe that the lifetime of the oscillations increases with N, being stable in the thermodynamic limit, $N \to \infty$. Moreover, in finite systems, signatures of the emergence of the time-crystal phase can be identified by analyzing the spectrum of the Lindblad generator. In Fig. 3.2(b), we plot the first eigenvalues of the Lindblad generator $\mathcal{L}$, given in Eq. (3.24) with $n_\beta(\omega) \to 0$, for different systems size. This plot shows that there is the dominant eigenvalue with both real and imaginary parts equal to zero, independently of the system size, while the real part of other eigenvalues approaches zero as N increases [39, 90]. We observe that the imaginary part of the eigenvalues is independent of N and corresponds to the oscillation frequency of the state of the system [154, 155]. The relation between the oscillation frequency and the imaginary part of the eigenvalues comes from the spectral decomposition of the density matrix given in Eq. (2.51).

In the thermodynamic limit, $N \to \infty$, the average dynamics of the system is exactly

described by the mean-field equations [156, 157]

$$\begin{aligned} \dot{m}_x &= \kappa\sqrt{2}m_x m_z \,, \\ \dot{m}_y &= \kappa\sqrt{2}m_y m_z - \Omega m_z \,, \\ \dot{m}_z &= -\kappa\sqrt{2}(m_x^2 + m_y^2) + \Omega m_y \,. \end{aligned} \tag{3.26}$$

Here, we consider $\delta = 0$ and we note that the temperature does not appear in the mean-field dynamics [67, 150]. In Fig. 3.3(a), we show the phase diagram of the boundary time crystal. To distinguish between the two phases, we use the time-averaged magnetization as the order parameter, expressed as

$$\bar{m}_z = \frac{1}{\tau}\int_0^\tau m_z(t)\mathrm{d}t \,. \tag{3.27}$$

The point wherein the time-translational symmetry is broken can be found by analyzing the stationary solutions of the coupled system of differential equations for the magnetization. They are given by

$$m_x^{\mathrm{s}} = 0 \,, \quad m_y^{\mathrm{s}} = \frac{1}{\sqrt{2}}\frac{\Omega}{\kappa} \,, \quad m_z^{\mathrm{s}} = \frac{\pm 1}{\sqrt{2}}\sqrt{1 - \frac{\Omega^2}{\kappa^2}} \,. \tag{3.28}$$

Here we note that the magnetization in the z direction has two solutions, but only the negative-valued one is stable [154]. When $\Omega > \kappa$, the stationary solutions become unphysical, *i.e.* the magnetization becomes imaginary, which corresponds to a breakdown of the stationary phase and the emergence of the time-crystal one.

It is noteworthy that this set of equations conserves two quantities [39, 154]. The first conserved quantity is the norm of the vector $\vec{m} = [m_x, m_y, m_z]$, which emerges in the thermodynamic limit, meaning that angular momentum is conserved throughout the dynamics [154]. The other conserved quantity is given by $c(t) = m_x(t)/[m_y(t) - \Omega/(\sqrt{2}\kappa)]$, whose effect can be observed in the behavior of the system in the time-crystal phase. Due to the conservation of $c(t)$, the time-crystal phase lacks sufficient dynamical freedom to exhibit transient periods, which constrain its dynamics to closed periodic orbits [39, 154, 158], as Fig. 3.3(b) shows. In this regime, each solution can be accessed through different initial conditions. In our **third publication**, we extended

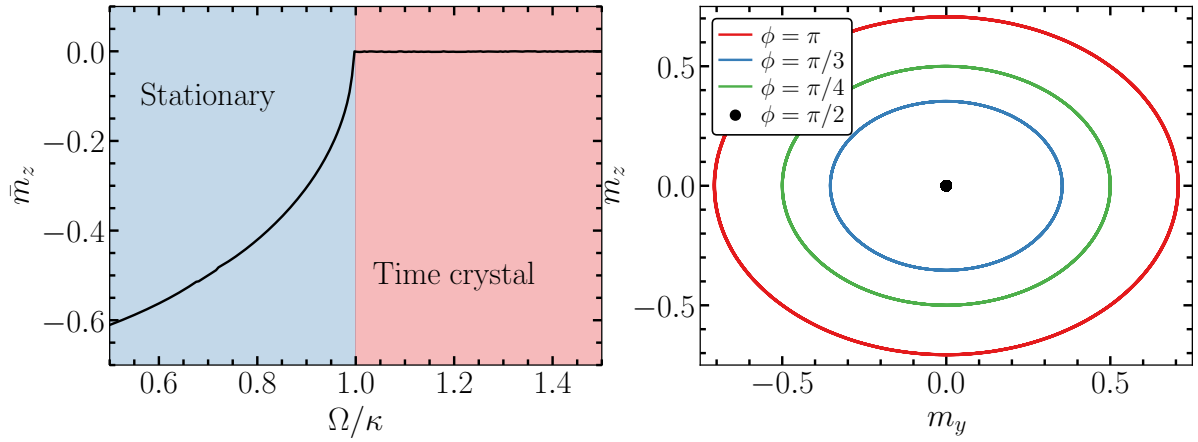

Figure 3.3: **Mean-field analysis of the boundary time crystal** (a) Time-averaged magnetization in the z direction for different values of Ω and κ. The phase transition between the stationary and the time-crystal phase is well separated by the line where $\Omega = \kappa$. We consider the time-window to be $\tau\kappa = 10^3$. (b) Different time crystal solutions are accessed by changing the initial condition. For this, we use $m_x(0) = 0$ and $m_y(0) = \sin(\phi)/\sqrt{2}$, and $m_z(0) = -\cos(\phi)/\sqrt{2}$. For different initial conditions we vary ϕ, as indicated in the legend. Note that the time crystal solution has a vanishing amplitude for $\phi = \pi/2$.

this analysis to a system composed of two coupled boundary time crystals. Concerning the dynamics of the coupled systems, we show that it exhibits a rich phase diagram, including time crystals and quasi-periodic solutions.

3.4.2 Quantum thermodynamics of time crystals

In this section, we aim to provide a thermodynamic description of the boundary time crystal using the collision-model approach [150]. In particular, this is closely related to our **third** publication [67], where we describe the thermodynamics of two coupled time crystals.

The boundary time crystal is described by a local master equation, such that we model the environment as a set of harmonic oscillators within the collision-model approach [22, 78–81]. As described in Sec. 3.1, the dynamics of the system coupled to the environment is governed by the joint unitary time evolution of the system and the ancillae. The ancillary system is described by the bare Hamiltonian $H_\mathrm{e} = \sum_j H_{\mathrm{e}_j}$, where $H_{\mathrm{e}_j} = \omega_\mathrm{at} a_j^\dagger a_j$ is the bare Hamiltonian of the ancilla corresponding to the j-th collision, ω_at is its bare frequency, and it is the same as the atomic bare frequency defined in

Eq. (3.21). Additionally, a_j ($a_j^\dagger$) are the bosonic annihilation (creation) operators. The Hamiltonian describing the j-th ancilla interacting with the atomic ensemble is

$$H_{\mathrm{se}_j}(t) = \sqrt{\frac{\kappa}{N\delta t}}\theta(t,j)\left(a_j^\dagger S_- + a_j S_+\right), \tag{3.29}$$

where $\theta(t,j)$, as defined in Eq. (3.3), is $\theta(t,j) = 1$ for $j\delta t < t < (j+1)\delta t$ and 0 otherwise. To ensure a completely positive Markovian dynamics for the system, we use the *ancillae* initially in a product state, with each ancilla being in the thermal state $\rho_{\mathrm{e}_j} = e^{-\beta H_{\mathrm{e}_j}}/\mathrm{Tr}[e^{-\beta H_{\mathrm{e}_j}}]$, with β being the temperature of the environment.

To find the expression for the thermodynamic quantities, as described in Sec. 3.2, we consider the thermodynamic behavior of the atomic ensemble in the laboratory frame. In this frame, the heat exchanged with the j-th environment is given by [67,150]

$$\dot{Q} = -\frac{\kappa\omega_{\mathrm{at}}}{N}\left\langle S_x^2 + S_y^2 + \sqrt{2}(2n_\beta(\omega_{\mathrm{at}})+1)S_z\right\rangle, \tag{3.30}$$

The heat currents are characterized by a dominant part, proportional to N, and another contribution dependent on the temperature (through $n_\beta(\omega_{\mathrm{at}})$) that is intensive with N. This follows from the factorization $\langle S_\alpha S_\beta/N^2\rangle = m_\alpha m_\beta + \mathcal{O}(N^{-1})$, where $\mathcal{O}(N^{-1})$ denotes a contribution of order N^{-1}, which is suppressed in the thermodynamic limit [150]. Therefore, in this limit, the heat exchanged (per atom) with the environment becomes

$$\dot{q} = -\kappa\omega_{\mathrm{at}}\left[m_x^2 + m_y^2\right], \tag{3.31}$$

where we denote $\lim_{N\to\infty}\dot{Q}/N = \dot{q}$.

Noteworthy, the dissipated heat $\dot{q}$ does not depend on the temperature of environment since the latter does not appear in the mean-field dynamics [150]. Moreover, the heat is always negative, indicating that energy is dissipated and consistently flows from the system to the environment. The time-average of $\dot{q}(t)$ during a long time-window, reduces the first law, Eq. (3.16), to

$$\bar{w} = -\bar{\dot{q}}, \tag{3.32}$$

where $\bar{\dot{a}} = \lim_{t\to\infty} t^{-1} \int_0^t \dot{a}(t')\mathrm{d}t'$. In deriving this expression, we use the fact that the internal energy rescaled by $1/N$ does not grow indefinitely with time, such that $t^{-1} \int_0^t \dot{u}\mathrm{d}t' = t^{-1}(u_t - u_0)$ goes to zero for large times t. The first law of thermodynamics presented in Eq. (3.32) shows that all work input is converted into dissipated heat averaged over a sufficiently large time window. Moreover, this analysis demonstrates how to relate the aforementioned thermodynamic quantities to system observables, such as magnetization, which are experimentally accessible [150]. In our **third work**, we used this result to characterize time crystals in applications related to energy storage. As a remark, the second law of thermodynamics in the boundary time crystal is discussed in detail in Refs. [67, 150].

Chapter 4

Methods: Quantum jump trajectories

The goal of this chapter is to establish the theoretical foundation supporting the results of our **second work** [111]. To achieve this, we begin with a concise and intuitive overview of large deviations theory, following Refs. [101,102,111]. Later in this chapter, we discuss the concept of quantum jump trajectories, which provides a stochastic description of open quantum systems [87,159]. Next, we explore the application of large deviations theory to the stochastic dynamics of open quantum systems and introduce the quantum Doob transform, which is a method for tailoring the statistical behavior of open quantum systems [102].

4.1 Fundamental concepts of large deviations

The theory of large deviations characterizes the asymptotic exponential decay of the probability distribution describing an observable defined over a stochastic process [160]. The description of these probability distributions goes beyond the central-limit theory, providing information about rare events that can occur, although exponentially unlikely. Furthermore, large deviations theory provides tools to investigate dynamical phase transitions, the mechanisms by which rare events occur [102], as well as how to engineer systems whose typical behavior mirrors rare events [105].

To introduce the concepts of large deviations relevant to this thesis, we consider a quantum system that emits photons to a detector at random times [118]. The total number of photons emitted by the system up to time t is a random variable, defined

as $K(t)$ and referred to as activity. Considering that the statistics of emission follows a Poisson process, the probability distribution of observing m emissions during a time interval from 0 to t is given by

$$P(K(t) = m) = \frac{(\gamma t)^m}{m!} e^{-\gamma t} , \tag{4.1}$$

where γ is the characteristic frequency whereby the atom emits photons.

Large deviation theory is concerned with the probability distribution of the process when a parameter of the system, *e.g.*, the total number of particles, approaches infinity. Here, we consider time to be this parameter, which motivates us to define the normalized activity $k(t) = K(t)/t$, which is the emission rate of the atom. The probability distribution describing the statistics of $K(t)$ can be expressed as

$$P(K(t) = t\kappa) = \frac{(\gamma t)^{\kappa t}}{(\kappa t)!} e^{-\gamma t} . \tag{4.2}$$

By considering Stirling's approximation for the factorial and that $x^y = e^{y \ln x}$, we can rewrite this probability as

$$P(K(t) = t\kappa) \approx e^{-\gamma t} e^{\kappa t \log \gamma t} e^{-\kappa t \log \kappa t + \kappa t} . \tag{4.3}$$

We can now factorize t and write the exponential as

$$P(K(t) = t\kappa) \approx e^{-tI(\kappa)} , \tag{4.4}$$

where $I(\kappa) = \kappa \log(\kappa/\gamma) - (\kappa - \gamma)$. Here, we define $I(\kappa)$ as the *rate function*, which describes the large deviation probability distribution of the stochastic observable $\kappa(t)$ for $t \gg 1$. In particular, when the probability distribution of a stochastic observable K can be written as in Eq. (4.4), it is said that the observable K obeys the so-called large deviation principle with rate function $I(\kappa)$. We make two important remarks about the rate function. The first one concerns the concentration of probability around the minimum of $I(\kappa)$, which, in this case, occurs at $\kappa = \gamma$. Note that $I(\kappa = \gamma) = 0$ and the probability distribution is exponentially smaller for other values of κ. This re-

sult corresponds to the law of large numbers, which states that a stochastic observable converges to its average value as the number of stochastic realizations approaches infinity [101]. The second remark concerns the central-limit theorem. We note that when the time-averaged stochastic variable κ is close to its average value, we can expand the logarithm, such that $\log \frac{\kappa}{\gamma} \approx (\frac{\kappa}{\gamma} - 1)$, and, therefore,

$$I(\kappa \approx \gamma) \approx \frac{(\kappa - \gamma)^2}{2\gamma} \,. \tag{4.5}$$

This result shows that when we expand the rate function for values around the average, we find the central-limit theorem, where the time-averaged activity converges to a Gaussian distribution. Nonetheless, for κ far from the average value, the rate function $I(\kappa)$ predicts correctly the *rare* behavior of the system.

In the example we used above, it is possible to find the rate function by directly evaluating the probability distribution of the stochastic process. However, such information is rarely available, requiring alternative methods to estimate this quantity.

4.2 The scaled cumulant generating function

The scaled cumulant generating function is a mathematical object that provides an alternative method to compute the asymptotic probability distribution of stochastic observables, such as time-integrated noise or currents [19, 101].

To introduce this object, let us consider the sum of a binary random variable, x, which assumes the values 0 with probability q and 1 with probability $1 - q$. Now, we define K as the sum of its realizations, $K = \sum_{i=1}^{N} x_i$. We also note that the realizations of the random variable x are statistically independent. The scaled cumulant generating function is defined as

$$\theta_s = \lim_{N\to\infty} \frac{1}{N} \log Z_s \,, \tag{4.6}$$

where $Z_s = \mathbb{E}[e^{-sK}]$ is the moment generating function and it corresponds to a Laplace transform of the probability distribution associated with $P(K)$. Here, s is the conjugate field of the observable K. To evaluate θ_s, we first consider the moment-generating

function

$$Z_s = \mathbb{E}[e^{-sK}] = \sum_k e^{-sK} P(K) \,, \tag{4.7}$$

where the sum is over all possible configurations of K. To compute this quantity, we assume that the variables x are independent and substitute K in the exponent

$$\begin{aligned} Z_s &= \sum_{\{x_1, x_2, \cdots x_N\}} P(\{x_1, x_2, \cdots, x_N\}) e^{-s(x_1+x_2+\cdots+x_N)} \\ &= \sum_{x_1}\sum_{x_2}\cdots\sum_{x_N} P(x_1)P(x_2)\cdots P(x_N) e^{-s(x_1+x_2+\cdots+x_N)} \\ &= \Big[\sum_x P(x) e^{-sx}\Big]^N \end{aligned} \tag{4.8}$$

Using the definition of the random variable x and its probability distribution, we obtain $Z_s = [q + (1-q)e^{-s}]^N$. Therefore, the scaled cumulant generating function is given by

$$\theta_s = \log\left[q + (1-q)e^{-s}\right] \,. \tag{4.9}$$

The derivatives of θ_s yield the cumulants of the probability distribution $P(K)$

$$\langle \kappa \rangle = -\frac{\partial \theta_s}{\partial s}\Big|_{s=0}, \quad \mathrm{Var}(\kappa) = \frac{\partial^2 \theta_s}{\partial s^2}\Big|_{s=0} \,, \tag{4.10}$$

where $\kappa = K/N$ is the simple mean. In summary, the cumulant of order n can be found by taking the n-th derivative of θ_s evaluated at $s = 0$. In our example, we find the cumulants

$$\langle \kappa \rangle = 1 - q, \quad \mathrm{Var}(\kappa) = q(1-q) \,. \tag{4.11}$$

In summary, using this simple example we show how to evaluate the scaled cumulant generating function and how it contains all information about the probability distribution $P(K)$.

Gärtner-Ellis theorem

The remaining task is to find the rate function using the scaled cumulant generating function, which follows from the Gärtner-Ellis theorem [101]. To show how the relation between the scaled cumulant generating function and the rate function works, we use

as an example the stochastic processes defined by the sum of random variables defined in Sec. 4.2. To this end, we introduce the tilted probability distribution for K

$$P_s(K) = \frac{e^{-sK}}{Z_s} P(K) \, . \tag{4.12}$$

The probability distribution $P_s(K)$ fixes the parameter s and weights the probability to observe the configuration K according to the exponential factor e^{-sK}. The average value of κ, for $N \gg 1$, calculated using $P_s(K)$, is

$$\langle \kappa \rangle_s = \sum_K P_s(K)\kappa = -\partial_s \theta_s \, . \tag{4.13}$$

This extends to all cumulant of $P_s(K)$ [160–162]. Assuming that θ_s is well-defined and analytic, we can write the tilted probability in the limit of $N \gg 1$, according to Eq. (4.6), as

$$\frac{P_s(K)}{P(K)} \approx e^{-sK - N\theta_s} \, . \tag{4.14}$$

In this limit, the tilted probability distribution $P_s(K)$ will be concentrated around the mean value $K^*/N = \kappa^*$, which follows from the central-limit theorem and gives $P_s(K^* = N\kappa^*) \approx 1$. Hence, from Eq. (4.12) and considering the large deviation principle $P(K = N\kappa) \approx e^{-NI(\kappa)}$, we find that the rate function can be expressed as

$$I(k^*) \approx -s^*\kappa^* - \theta_{s^*} \, , \tag{4.15}$$

where $k^* = -\partial\theta_s/\partial s\big|_{s=s^*}$. Conversely, this procedure can be rigorously defined in terms of the Legendre transform [163] of the scaled cumulant generating function with respect to s,

$$I(k) = \sup_{s \in \mathbb{R}} \{-sk - \theta_s\} \, . \tag{4.16}$$

This derivation is possible when θ_s is a convex and differentiable function. Equation (4.16) follows from the Gärtner-Ellis theorem [101]. We remark that θ_s has the same mathematical interpretation as the free energy density in statistical mechanics, where s plays the role of the inverse temperature β [6]. Although the scaled cumulant generating function is assumed to be convex, this does not necessarily hold for the rate

function. As a result, the rate function obtained via the Gärtner-Ellis theorem corresponds to the convex envelope of the exact rate function [see Ref. [101] for examples and more mathematical details].

As an example of the Gärtner-Ellis theorem, we use the results from our previous example of random bits to derive the rate function associated with the observable K. In this case, the Legendre transform in Eq. (4.16) takes the form

$$\frac{\partial}{\partial s}\left[-s\kappa-\theta_s\right]=-\kappa+\frac{(1-q)e^{-s}}{q+(1-q)e^{-s}}=0\,. \tag{4.17}$$

After inverting s, we find that

$$s^*=-\log\left[\frac{\kappa q}{(1-q)(1-\kappa)}\right]\,. \tag{4.18}$$

Now, we substitute s^* in Eq. (4.15) and we obtain the rate function

$$I(\kappa)=\kappa\log\left[\frac{\kappa}{1-q}\right]-(\kappa-1)\log\left[\frac{1-\kappa}{q}\right]\,. \tag{4.19}$$

This example concludes the theoretical background on the large deviation theory necessary to support the results in this thesis.

4.3 Quantum jump trajectories

In this section, we consider the time evolution of a quantum system undergoing continuous measurement. In particular, the continuous monitoring introduces randomness into the time-evolution of the system, which is captured by the so-called stochastic Schrödinger equation. This equation describes how the *pure* state of the system evolves conditioned on the outcomes of the measurement process. A paradigmatic example where this formalism is particularly relevant is quantum cavity electrodynamics experiments. In such systems, a single electromagnetic mode confined in a cavity is continuously monitored via an external detector that measures the leakage of photons, which happens at random times. The continuous time-evolution of the state of the system, abruptly modified when the light mode loses a photon, is regarded as a

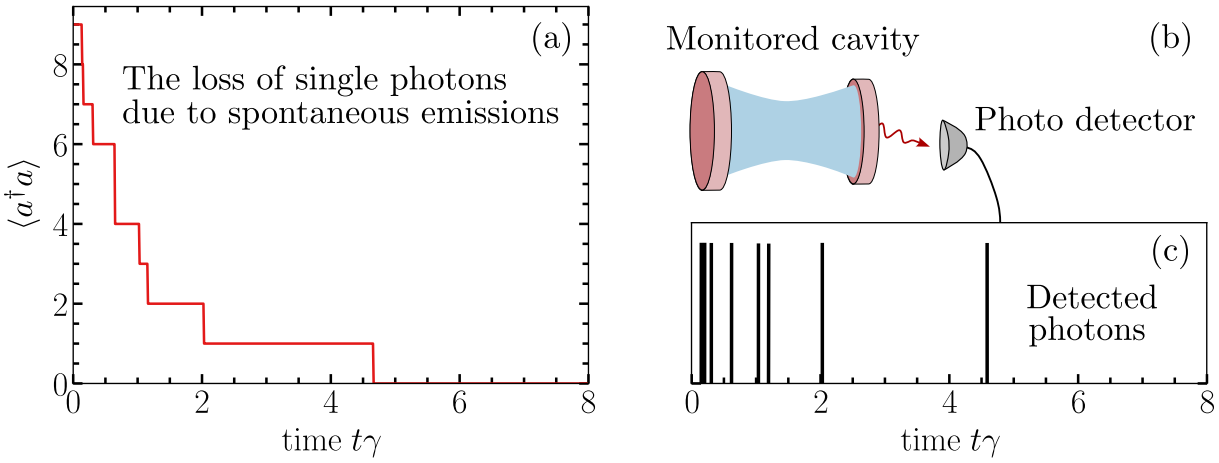

Figure 4.1: **Stochastic trajectory of the number of photons inside an optical cavity.** (a) A single quantum jump trajectory showing the number of photons inside a cavity changing in time. The cavity is modelled as a harmonic oscillator with Hamiltonian $H = \omega a^\dagger a$ and jump operator $J = \sqrt{\gamma} a$ [118]. (b) The experimental sketch of the system, where a photo-detector is placed behind an imperfect mirror through which photons are lost. (c) The readout of the detector, where each click corresponds to a detected photon. Parameters: $\omega = \gamma$.

quantum jump trajectory [87, 89] [see the schematic in Fig. 4.1].

To introduce the quantum jump trajectories formalism, we consider an optical cavity under continuous monitoring. We assume that the monitoring is performed by a set of measurements with an infinitesimal small duration, denoted by $\mathrm{d}t$, and we consider a perfect detector, meaning that all emissions are detected [see Refs [152, 164] for discussions with imperfect detection schemes]. The effect on the system due to the monitoring apparatus can be modelled by a set of positive operator-valued measures (POVM) [12]. In this context, when a photon is detected, the change in the state of the system can be described by the POVM operator

$$M_1(\mathrm{d}t) = J\sqrt{\mathrm{d}t}\,, \tag{4.20}$$

where J in the example of the cavity mode is proportional to an annihilation operator [see Fig. 4.1(b)-(c)]. Now, when the quantum system is coupled to an external detector, the absence of detection after a time interval $\mathrm{d}t$ implies that the system has evolved according to the von Neumann equation under the influence of the external measurement apparatus. This evolution conditioned to no-detection can be described by the

operator $M_0(\mathrm{d}t)$,

$$M_0(\mathrm{d}t) = \mathrm{I} - \left(\frac{J^\dagger J}{2} + iH\right)\mathrm{d}t\,, \tag{4.21}$$

where $J^\dagger J$ is a hermitian operator modelling the effect of the detector in the time-evolution of the system [87]. This term emerges naturally when we impose the condition $\sum_i M_i^\dagger(\mathrm{d}t)M_i(\mathrm{d}t) = \mathrm{I}$, up to the first order in $\mathrm{d}t$, which is necessary to ensure probability conservation. After an interval $\mathrm{d}t$, the density matrix of the system under continuous monitoring is given by

$$\rho(t+\mathrm{d}t) = \sum_i M_i(\mathrm{d}t)\rho(t)M_i^\dagger(\mathrm{d}t), \tag{4.22}$$

Using Eq. (4.22), the density matrix at time $t+\mathrm{d}t$ will be given by

$$\begin{aligned}\rho(t+\mathrm{d}t) &= \left[\mathrm{I} - \left(\frac{J^\dagger J}{2} + iH\right)\mathrm{d}t\right]\rho(t)\left[\mathrm{I} - \left(\frac{J^\dagger J}{2} - iH\right)\mathrm{d}t\right] + J\rho(t)J^\dagger\mathrm{d}t \\ &\approx \rho(t) - \left\{i\,[H,\rho] - J\rho(t)J^\dagger + \frac{1}{2}(J^\dagger J\rho(t) + \rho(t)J^\dagger J\right\}\mathrm{d}t\,.\end{aligned} \tag{4.23}$$

In this way, when considering a *closed* quantum system under continuous monitoring, the resulting dynamics is given by a Lindblad master equation [85–87].

Furthermore, let us now evaluate the probabilities of the outcomes of two POMV operators. We first consider M_0, therefore we have

$$p_0(t) = \mathrm{Tr}\{M_0(\mathrm{d}t)\rho(t)M_0^\dagger(\mathrm{d}t)\} = 1 - \mathrm{Tr}\{J\rho(t)J^\dagger\}\mathrm{d}t\,. \tag{4.24}$$

Since the total probability must be conserved, this implies that $p_1(t) = \mathrm{Tr}\{J\rho(t)J^\dagger\}\mathrm{d}t$, such that for almost all times, the system is evolved by $M_0(\mathrm{d}t)$. For modelling the continuous measurement scheme as a stochastic process, we can construct a noise that represents the action of the operators $M_0(\mathrm{d}t)$ and $M_1(\mathrm{d}t)$. The first consideration is, either the system is evolved by the operator $M_1(\mathrm{d}t)$ or by $M_0(\mathrm{d}t)$, such that $\mathrm{d}n(t) = 1, 0$ is a stochastic increment that has the properties

$$[\mathrm{d}n(t)]^2 = \mathrm{d}n(t), \quad \mathbb{E}[\mathrm{d}n(t)] = \mathrm{d}t\mathrm{Tr}[J\rho(t)J^\dagger]\,. \tag{4.25}$$

To separate the dynamics into two regimes, when $\mathrm{d}n(t) = 0$, the system evolves according to M_0

$$\begin{aligned} |\psi(t+\mathrm{d}t)\rangle &= \frac{M_0(\mathrm{d}t)|\psi(t)\rangle}{\sqrt{\mathrm{Tr}\{|\psi(t)\rangle\langle\psi(t)|M_0^\dagger(\mathrm{d}t)M_0(\mathrm{d}t)\}}} \\ &\approx \left[\mathrm{I} - \mathrm{d}t\left(iH + \frac{1}{2}J^\dagger J - \frac{1}{2}\mathrm{Tr}\{|\psi(t)\rangle\langle\psi(t)|J^\dagger J\}\right)\right]\psi(t)\,. \end{aligned} \tag{4.26}$$

Here, we consider a first-order expansion in the denominator and $|\psi(t)\rangle$ as the pure state vector at time t. Additionally, when $\mathrm{d}n = 1$, a photon is emitted and the state of the system changes according to $M_1(\mathrm{d}t)$

$$|\psi(t+\mathrm{d}t)\rangle = \frac{M_1(\mathrm{d}t)|\psi(t)\rangle}{\sqrt{\mathrm{Tr}\{|\psi(t)\rangle\langle\psi(t)|M_1^\dagger(\mathrm{d}t)M_1(\mathrm{d}t)\}}} = \frac{J|\psi(t)\rangle}{\sqrt{\mathrm{Tr}\{|\psi(t)\rangle\langle\psi(t)|J^\dagger J\}}}\,. \tag{4.27}$$

In this case, $M_1(\mathrm{d}t)$ dominates the dynamics, due to the discontinuous change in the pure state, the quantum jump. Therefore, a quantum jump trajectory is described as a continuous evolution interrupted by quantum jumps occurring at random intervals [85, 86].

We can follow the same reasoning for the matrix representation of the state $\psi(t) = |\psi(t)\rangle\langle\psi(t)|$ and after some algebra, as done in the Refs. [87, 103], it is possible to write the stochastic equation for the pure state as

$$\mathrm{d}\psi(t) = \mathcal{B}[\psi(t)]\mathrm{d}t + \left(\frac{\mathcal{J}[\psi(t)]}{\mathrm{Tr}\,\{\mathcal{J}[\psi(t)]\}} - \psi(t)\right)\mathrm{d}n(t)\,, \tag{4.28}$$

where we define

$$\mathcal{B}[\psi(t)] = -i\tilde{H}\psi(t) + i\psi(t)\tilde{H}^\dagger - \psi(t)\mathrm{Tr}[-i\tilde{H}\psi(t) + i\psi(t)\tilde{H}^\dagger]\,, \tag{4.29}$$

and

$$\tilde{H} = H - \frac{i}{2}J^\dagger J\,, \tag{4.30}$$

is the effective non-Hermitian Hamiltonian governing the continuous evolution, and $\mathcal{J}[\rho(t)] = J\rho(t)J^\dagger$ represents the quantum jump process.

This equation is known as the *Stochastic Schrödinger equation*. When considering the

average of the ensemble of pure state trajectories, we find $\rho(t) = \mathbb{E}[\psi(t)]$ [87].

4.4 Thermodynamics of quantum jump trajectories

In this section, we demonstrate the application of the large deviation framework to characterize the statistical properties of emission-related observables in quantum jump trajectories [102].

We begin by defining the time-integrated observable

$$A(t) = \int_0^t \mathrm{d}n(t') \,, \tag{4.31}$$

where $\mathrm{d}n(t')$ is a Poisson increment associated with a quantum jump at time t', as defined in Eq. (4.25). To calculate the scaled cumulant generating function of this observable, we first introduce the moment generating function $Z_s(t) = \mathbb{E}[\mathcal{A}(t)]$, where $\mathcal{A}(t) = e^{-sA(t)}$. We use that $Z_s(t) = \mathrm{Tr}[\varrho_s(t)]$, where $\varrho_s(t)$ is a biased density matrix. As shown in Ref. [102], the biased density matrix $\varrho_s(t)$ evolves according to the tilted Lindblad generator

$$\dot{\varrho}_s(t) = \mathcal{L}_s[\varrho_s(t)] = -i\left[\tilde{H}\varrho_s(t) - \varrho_s(t)\tilde{H}^\dagger\right] + e^{-s}J\varrho_s(t)J^\dagger \,, \tag{4.32}$$

where $\tilde{H}$ is the effective Hamiltonian defined in Eq. (4.30). The tilted generator provides a positive dynamics, but it does not preserve the trace of the density matrix ϱ_s. This can be verified by considering that $\mathcal{L}_s^*[\mathrm{I}] = (e^{-s} - 1)J^\dagger J \neq 0$ [105]. Therefore, $\mathcal{L}_s$ does not generate a physical evolution. However, its spectrum contains all information about the statistics of the observable A. To show how to obtain the statistics of A from the spectrum of the tilted generator, we consider that $\mathcal{L}_s$ can be decomposed in a dual basis [similarly to what we show in Sec. 2.1], with $\mathcal{L}_s[r_s^j] = \lambda_s^j r_s^j$ and $\mathcal{L}_s^*[\ell_s^j] = \lambda_s^j \ell_s^j$, where λ_s^j is the eigenvalue associated with the right and left eigenmatrices r_s^j and ℓ_s^j, respectively. Also, we have that $\mathrm{Tr}[r_s^i \ell_s^j] = \delta_{ij}$ and the normalization $\mathrm{Tr}[r_s^0] = 1$ [102]. Additionally, we find that the eigenvelues of $\mathcal{L}_s$ can be ordered such that $\mathrm{Re}[\lambda_s^0] \geq \mathrm{Re}[\lambda_s^1] \geq \cdots \geq \mathrm{Re}[\lambda_s^N]$. We note that for a completely positive and trace preserve dynamics, $\lambda_s^0 = 0$, but here λ_s^0 is a real number.

Using these properties, we can expand the tilted density matrix in the eigenbasis of $\mathcal{L}_s$

$$\varrho_s(t) = r_s^0 e^{\lambda_s^0 t} + \sum_j e^{\lambda_s^j t} \mathrm{Tr}[\ell_s^j \varrho_s(0)] r_s^j \,. \tag{4.33}$$

Now we factorize the dominant term $e^{\lambda_s^0 t}$, which leads to

$$\varrho_s(t) = e^{\lambda_s^0 t} \left(r_s^0 + \sum_j e^{(\lambda_s^j - \lambda_s^0)t} \mathrm{Tr}[\ell_s^j \varrho_s(0)] r_s^j \right) \,. \tag{4.34}$$

Now, we use the ordering property of the eigenvalues λ_s^s and we observe that for $t \to \infty$ the projection of $\varrho_s(t)$ in the dominant eigenbasis with eigenvalue λ_s^0 exponentially suppresses all the other projections. Such results allow us to identify that the tilted density matrix is well approximated $\varrho_s(t \gg 1) \approx e^{\lambda_s^0 t} r_s^0$. Therefore, the moment-generating function associated with the probability distribution of the observable A becomes

$$Z_s(t) = \mathrm{Tr}[\varrho_s(t)] \approx e^{\lambda_s^0 t} \,. \tag{4.35}$$

Finally, the scaled cumulant generating function is obtained as

$$\theta_s = \lim_{t \to \infty} \frac{1}{t} \ln Z_s(t) = \lambda_s^0 \,. \tag{4.36}$$

This method provides a systematic approach to obtain the full probability distribution governing the statistics of emission-related observables in quantum jump trajectories. In our **second work** [111], we generalized this result to open quantum systems undergoing adiabatic dynamics. In particular, we show that at each time interval observables rate can be described by the instantaneous scaled cumulant generating function.

4.5 Example: Meta-stable 3-level system

To make these ideas more concrete, we consider an example in which the above formalism can be applied to explain an actual experiment exhibiting intermittence in the statistic of the number of jumps [106, 107]. In this example, we have a three-level

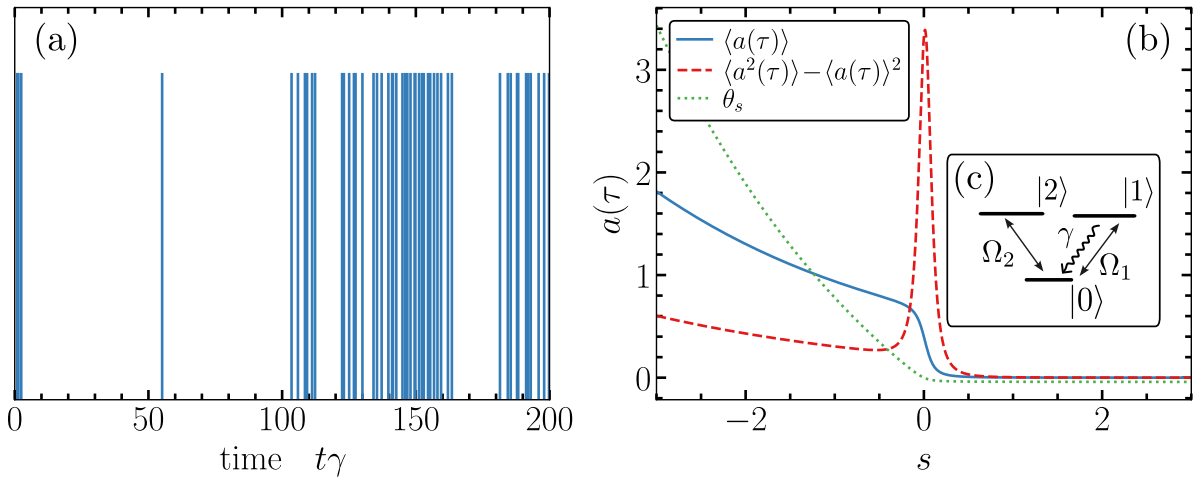

Figure 4.2: **Metastable three-level system** (a) A single quantum jump trajectory for the three-level system, where the vertical lines represent a quantum jump. (b) Large deviation statistics of the time-averaged number of jumps of the three-level system. We show the average values of $a(t)$, its scaled variance and the scaled cumulant generating function θ_s as a function of s. (c) Sketch of the three-level system. Parameter $\Omega_2 = 10\Omega_1$ and $\kappa = \Omega_1/4$.

system, with basis states $|0\rangle, |1\rangle, |2\rangle$, and Hamiltonian

$$H = \Omega_1(|0\rangle\langle 1| + |1\rangle\langle 0|) + \Omega_2(|0\rangle\langle 2| + |2\rangle\langle 0|)\,. \tag{4.37}$$

In this system, two lasers drive two different transitions, with Rabi frequency given by Ω_1 and Ω_2. Additionally, the system is subject to decay from state $|1\rangle$ to $|0\rangle$, described by the jump operator $J = \sqrt{\gamma}|0\rangle\langle 1|$ [see Fig. 4.2(c) for a pictorial representation of the model]. As our stochastic observable, we consider the dynamical activity associated with the decay transition from state 1 and 0

$$A(t) = \int_0^t \mathrm{d}n(t')\,. \tag{4.38}$$

The typical behavior of the quantum jump trajectories of the system features coexistence between an active phase (frequent emissions) and an inactive one (no emissions) [102, 106, 107, 165], as we depict in Fig. 4.2(a). This behavior can be explained by analyzing the statistics of rare trajectories. In Fig. 4.2(b) we show the behavior of the time-averaged number of jumps, $a(t) = t^{-1}A(t)$ and its scaled variance for rare trajectories, $-\partial_s\theta_s$ and $\partial_s^2\theta_s$, respectively, which can be accessed considering Eq. (4.13). For

$s > 0$, the system enters an inactive phase, where quantum jumps are nearly absent, whereas for $s < 0$, the system goes to a highly active phase. We observe that around $s = 0$, fluctuations grow, while the average activity exhibits a rapid transition between a highly active and an inactive phase. This characteristic indicates that around $s = 0$, the system exhibits a coexistence of both active and inactive phases.

4.6 Quantum Doob transform

The rate function gives the probability of observing rare events beyond the central-limit theorem. As an example, the blinking system of the previous example could have an ensemble of quantum jump trajectories whose time-average number of emissions deviates from the typical value by a factor of two [105]. However, these rare events are exponentially unlikely to be observed, which makes it challenging to sample their stochastic trajectories. In this section, we describe the quantum Doob transform, which provides a transformed Lindblad generator, whose typical behavior mirrors the rare behavior of the original dynamics [102, 105, 166]. This can be used for investigating the structure of the generator of the dynamics that reproduces the rare behavior of the original system and for sampling their rare trajectories.

To illustrate this transform, we first consider an open quantum system described by a Lindblad master equation with Hamiltonian H and jump operator J. We then define the stochastic observable $A = \int_0^t \mathrm{d}n_{t'}$, which represents the number of quantum jumps occurring between times 0 and t. The tilted probability distribution associanted to the observable A with bias s, defined in Sec. 4.2, is given by

$$P_s(A) = \frac{e^{-sA} P(A)}{Z_s} \,. \tag{4.39}$$

As we commented in Sec. 4.2, the cumulants of the stochastic observable computed using the tilted probability distribution can be tuned by changing the value of bias s, for instance $\langle A \rangle_s = -\partial_s \theta_s$ [102, 105]. In this respect, the tilted Lindblad

$$\mathcal{L}_s[\varrho_s(t)] = -i\,[H, \varrho_s(t)] + \left[e^{-s} J \varrho_s(t) J^\dagger - \frac{1}{2}\{J^\dagger J, \varrho_s(t)\} \right] , \tag{4.40}$$

generates the ensemble of quantum jump trajectories whose statistics is given by derivatives of θ_s [102, 105]. However, $\mathcal{L}_s$ is a non-trace-preserving map, such that the average over the ensemble of quantum trajectories does not recover a physical density matrix. To make this generator trace-preserving, we apply a generalized rotation in $\mathcal{L}_s$

$$\tilde{\mathcal{L}}[\circ] = G\mathcal{L}_s[G^{-1} \circ G^{-1}]G - x \circ \ , \tag{4.41}$$

where $\circ$ indicates a state, x a number, and G is a Hermitian matrix. The dual of this generator is

$$\tilde{\mathcal{L}}^*[\circ] = G^{-1}\mathcal{L}_s^*[G \circ G]G^{-1} - x \circ \ . \tag{4.42}$$

To find the expression of G and x, we act the dual generator in the identity matrix to obtain

$$G^{-1}\mathcal{L}_s^*[G^2]G^{-1} - x = 0 \, . \tag{4.43}$$

This leads to the eigenvalue equation $\mathcal{L}_s^*[G^2] = xG^2$. Therefore, by choosing G^2 to be the dominant left eigenmatrix of the tilted generator, ℓ_s^0, we find that x is the scaled cumulant generating function, θ_s. The dynamics that generate the emission statistics of trajectories for $s \neq 0$ is given by the Doob-transformed master equation

$$\dot{\rho}(t) = \tilde{\mathcal{L}}[\rho(t)] = (\ell_s^0)^{1/2}\mathcal{L}_s[(\ell_s^0)^{-1/2}\rho(t)(\ell_s^0)^{-1/2}](\ell_s^0)^{1/2} - \theta_s\rho(t) \, . \tag{4.44}$$

The Doob-transformed Lindblad generator can be rewritten, as done in Ref. [105], in terms of a transformed Hamiltonian

$$\tilde{H} = \frac{1}{2}(\ell_s^0)^{1/2}\left(H - \frac{i}{2}J^\dagger J\right)(\ell_s^0)^{-1/2} + \text{H.c.} \tag{4.45}$$

and the jump operator

$$\tilde{J} = e^{-s/2}(\ell_s^0)^{1/2}J(\ell_s^0)^{-1/2} \, . \tag{4.46}$$

The statistics of the number of jumps generated by $\tilde{\mathcal{L}}$, corresponds to the statistics predicted by the derivatives of θ_s.

The idea of the quantum Doob transform, which makes rare events typical, also exists in classical stochastic processes [167, 168] and it can be applied to chaotic

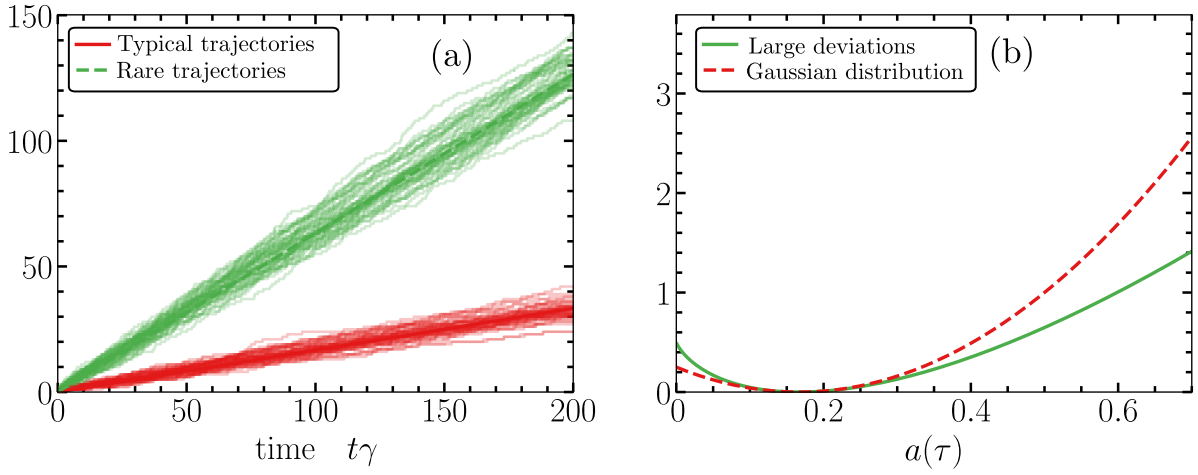

Figure 4.3: **Large deviation statistics** (a) Stochastic trajectories for the number of emissions of the driven-dissipative two-level system. The number of emissions follows a modified Poisson process, where red curves depict typical trajectories, while the green curve represents rare behavior beyond Gaussian fluctuations. The straight lines correspond to the average values. The rare trajectories were sampled with the Doob transform for $s = -4$. (b) The large deviation probability distribution and the Gaussian approximation for the time-averaged number of jumps $a(\tau)$. Parameters: $\gamma = 4\Omega$.

maps [166]. In our **second work**, we show that the quantum Doob transform also applies to open quantum systems undergoing an adiabatic evolution. Additionally, our results provide a way to tailor the statistics of the time history of emission-related observables during an adiabatic time evolution.

Example: Driven-dissipative two-level system

To give an example of a physical process for the quantum Doob transform, let us consider a two-level system described by the Hamiltonian

$$H = \Omega\sigma_x \,, \tag{4.47}$$

where σ_x is the Pauli matrix. This system is subjected to random emissions at rate γ, which is captured by the jump operator $J = \sqrt{\gamma}\sigma_-$. The number of emission during the time evolution is given by the stochastic observable $A(\tau) = \int_0^\tau \mathrm{d}n(t)$. When $\gamma = 4\Omega$, the scaled cumulant generating function associated with the observable $a(\tau) = \tau^{-1}A(\tau)$ is given by $\theta_s = 2\Omega(e^{-s/3} - 1)$, which corresponds to a Conway-Maxwell-

Poisson distribution [102]. In this case, the simple mean of emissions of rare trajectories is $\langle a(\tau)\rangle_s = 2\Omega e^{-s/3}/3$, while the scaled variance is $\mathrm{Var}(a(\tau))_s = 2\Omega e^{-s/3}/9$ [102]. For this system, the cumulants characterizing the statistics of rare trajectories differ from those of typical trajectories only by an overall factor of $e^{-s/3}$.

In Fig. 4.3(a), we plot stochastic trajectories of the number of emissions as a function of time. The red trajectories of the total number of emissions follow the typical behavior. On the other hand, in green, we plot rare trajectories associated with $s = -4$, which we sampled using the quantum Doob transform. In Fig. 4.3(b), we show a comparison between the Gaussian approximation and the rate function for this stochastic process, which is given by

$$I(a) = 3\left[a\log\left(\frac{a}{a_0}\right) - (a - a_0)\right], \tag{4.48}$$

where $a_0 = 2\Omega/3$ is the simple mean of the emissions found in the typical behavior of the system. We observe that around $a \approx a_0$, the Gaussian probability distribution is close to the rate function. However, the rare bahavior of the system beyond the Gaussian fluctuations cannot be accurately described by the law of large numbers, and large deviation tools are required.

Chapter 5

Results and conclusions

Thermodynamics describes the behavior of quantities such as energy and entropy, which are fundamental to characterize engines and other devices. When applied to classical settings, thermodynamics provides tools to describe even systems featuring nonequilibrium properties. Conversely, the simplest quantum system, such as a driven dissipative qubit, breaks fundamental rules of thermodynamics when they are not properly defined in accordance with quantum mechanics. The immediate consequence is the lack of understanding of whether a quantum system can be used as a quantum engine or a quantum battery. In this thesis, we aim to consistently define the nonequilibrium thermodynamics of quantum systems operating as quantum devices. We report our full publications in the appendix.

First publication

In our **first work** [54], we investigate the quantum thermodynamics of the time-crystal phase and its exploitation as a resource for quantum engines. In particular, we built upon the ideas in Ref. [66]. In our work, we consider a quantum engine composed of an ensemble of atoms inside an optical cavity, where one of its mirrors is coupled to a classical harmonic oscillator. The work output consists of periodic motion generated in the harmonic oscillator by the time crystal phase. Experiments realizing time crystals are quantitatively very well captured by phenomenological models, which encode non-thermal dissipative dynamics and do not belong to the set of dynamics stemming

from a weak system-bath coupling. As such, a standard thermodynamic interpretation of these experiments can lead to thermodynamic inconsistencies, such as violations of the second law of thermodynamics, which make it challenging to provide a sound description of their energy fluxes and their efficiency. In our contribution, we present a consistent thermodynamic description of quantum engines driven by the time crystal phase. Our approach does not rely on a collision-model framework, but it is based on separating, in the system Hamiltonian, the bare-energy contributions of the atoms and the cavity from those related to external driving. This decomposition allows for the formulation of a very natural energetic balance in terms of persistent nonequilibrium dissipated heat currents. To investigate the second law of thermodynamics, we apply the standard Spohn's theorem using this energy separation within the system. This allowed us to define a measure of efficiency, supported by a well-defined second law, for quantum engines driven by time-translation symmetry breaking. We show that in these systems, it is possible to devise a quantum engine that operates in the time-crystal phase with finite efficiency.

One possible follow-up of this work is to consider the mechanical mode as an actual quantum system [169]. In this regime, we expect the development of quantum correlations between the cavity, atoms, and the mechanical mode, which could be harnessed for microscopic quantum engines and metrology applications. Additionally, it would be interesting to investigate whether our thermodynamic description of local master equation could be extended to quantum jump trajectories and other results of nonequilibrium thermodynamics, such as the thermodynamic uncertainty relations [170, 171] and fluctuation theorems [11, 71, 172].

Second publication

The time crystal phase that we investigate in the **first and third publications** manifests in the thermodynamic limit and can be accurately described using a mean-field approach. However, in a few-body system, it is necessary to use strategies beyond mean-field to characterize the system. In this respect, for investigating open quantum systems, in our **second work** we consider that single experimental realizations are described by stochastic trajectories, where the state of the system evolves continually and

it is affected by quantum jumps, such as photon emissions. In these stochastic trajectories, dissipated heat and entropy production are stochastic observables whose probability distributions are fully characterized by the large deviations theory. In our **second work** [111], we focus on an open quantum system undergoing an adiabatic evolution, which here refers to time-dependent processes where a parameter of a system varies slowly, such that the system is always in its instantaneous stationary state [112, 173]. This class of dynamics is important, for instance, in the context of the engine cycle, given that Carnot's efficiency can only be achieved in adiabatic processes [1]. In our work, we show that when open quantum systems are slowly driven, the large deviation objects, such as the scaled cumulant generating function associated with jump-related observables, obey an adiabatic theorem. Through our adiabatic theorem, we demonstrate that emission-related observables (like the net number of emitted photons) obey a temporal additive principle, which says that the rate of such observables is fully characterized independently at each time interval. Therefore, it is possible to calculate the probability of any time history of these observables in adiabatic dynamics. We also extended the quantum Doob transform to adiabatic dynamics, *i.e.*, we demonstrated how to map an arbitrary rare time history of an observable onto the typical time history of an engineered system. In particular, our analysis provides the full statistics of thermodynamic quantities for an open quantum system undergoing adiabatic dynamics.

A possible continuation of this work is to describe the thermodynamics of the quantum Doob transform. This transform provides a Lindblad master equation with modified Hamiltonian and jump operators. In this regard, it is not clear whether the Doob-transformed system obeys the standard laws of thermodynamics or if it is necessary to provide corrections to them. Once the thermodynamics of Doob-transformed master equations is established, a possible direction for further investigation would be the design of quantum devices, such as quantum engines or sensors, based on rare trajectories.

Third publication

In our **third work** [67], we explored the time-crystal phase for energy storage. To this end, we consider two driven-dissipative atomic ensembles and we use the collision model approach to characterize their thermodynamic behavior. The main finding of this work is a measure of energy-storing efficiency for driven-dissipative systems described by local master equations. Using these results, we show that the time-crystal phase can store energy, in some cases, even more efficiently than the stationary phase. In addition to that, we analyzed the dynamics of the coupled time crystal beyond the mean field, which was done by evaluating the fluctuations around the average values [49, 154, 174]. In our findings, we show that the coupled atomic ensemble can feature entanglement and other types of quantum correlations during the time-crystal phase.

Further investigation concerning the results of this publication would be related to considering a network of coupled macroscopic dissipative spins, with a particular focus on the emergence of non-stationary phases in such systems. In this context, we could investigate transport applications, and try to answer whether information propagates faster in the time crystal phase in comparison to the stationary one [175]. Also, it would be interesting to analyze synchronization effects in these networks [176, 177].

Appendix: publications

First publication

Nonequilibrium thermodynamics and power generation in open quantum optomechanical systems

Paulo J. Paulino [1,*] Igor Lesanovsky [1,2] and Federico Carollo [1]

[1]*Institut für Theoretische Physik, Eberhard Karls Universität Tübingen, Auf der Morgenstelle 14, 72076 Tübingen, Germany*

[2]*School of Physics and Astronomy and Centre for the Mathematics and Theoretical Physics of Quantum Non-Equilibrium Systems, University of Nottingham, Nottingham NG7 2RD, United Kingdom*

(Received 16 January 2023; revised 24 July 2023; accepted 26 July 2023; published 21 August 2023)

Cavity optomechanical systems are a paradigmatic setting for the conversion of electromagnetic energy into mechanical work. Experiments with atoms coupled to cavity modes are realized in nonequilibrium conditions, described by phenomenological models encoding nonthermal dissipative dynamics and falling outside the framework of weak system-bath couplings. This fact makes their interpretation as quantum engines, e.g., the derivation of a well-defined efficiency, quite challenging. Here, we present a consistent thermodynamic description of open quantum cavity-atom systems. Our approach takes advantage of their nonequilibrium nature and arrives at an energetic balance which is fully interpretable in terms of persistent dissipated heat currents. The interaction between atoms and cavity modes can further give rise to nonequilibrium phase transitions and emergent behavior and allows us to assess the impact of collective many-body phenomena on the engine operation. To enable this, we define two thermodynamic limits, one related to a weak optomechanical coupling and one related to a strong optomechanical coupling. We illustrate our ideas by focusing on a time-crystal engine and discuss power generation, energy-conversion efficiency, and the emergence of metastable behavior in these limits.

DOI: 10.1103/PhysRevA.108.023516

I. INTRODUCTION

The application of thermodynamics to quantum systems [1–6] allows us to conceive quantum heat engines, which perform ideal cycles between thermal equilibrium states [7–9]. In many experiments of interest, however, quantum systems are realized under genuine out-of-equilibrium conditions, for example, in the case of experiments with cold atoms in optomechanical cavities [10–20] [see the sketch in Fig. 1(a)]. These systems absorb energy from an external source, e.g., a laser, which prevents them from equilibrating with their surrounding and gives rise to persistent energy currents. This aspect motivates the development of alternative nonequilibrium quantum-engine cycles [21,22], with driving protocols that are not described by thermal dynamics [23,24]. It further poses the problem of devising theoretical approaches [25–32] providing a *consistent* thermodynamic understanding of established experimental models [19,33–35]. These open challenges do not solely concern quantum systems and are of much broader relevance, as indicated by recent efforts to characterize work in active matter [36–43].

In this paper, we focus on paradigmatic open quantum optomechanical systems which can nowadays be realized and efficiently controlled in experiments [10–19,44–48]. These setups are promising for the conversion of electromagnetic energy into mechanical work in both equilibrium [49,50] and nonequilibrium conditions [51–54]. For these systems, we develop a thermodynamic description which characterizes the power transferred by the cavity to the mechanical oscillator [see Fig. 1(b)] as well as the efficiency of this energy conversion. Our approach allows us to formulate an energy balance in terms of the persistent nonequilibrium heat currents [see Fig. 1(b)]. To investigate the impact of phase transitions and collective behavior on the performance of nonequilibrium engines, we consider two different thermodynamic limits [55–60] [see Fig. 1(c)]. One features a weak optomechanical coupling, ensuing from a finite density of atoms in the cavity [59], and is characterized by finite power and zero efficiency. The other one features a strong optomechanical coupling due to an infinite density of atoms. In this case, the delivered mechanical power is extensive in the "size" of the system and the efficiency is finite.

We illustrate our ideas by exploiting a time-crystal [61–65] engine, which is a manifestation of a nonequilibrium many-body quantum engine [59,66,67]. Our results also apply to generic optomechanical settings [19,46] and related spin-boson models, such as Rydberg-atom systems with interacting electronic and vibrational degrees of freedom [68,69] and superconducting-qubit systems [70].

II. THE MODEL

We consider the setup in Fig. 1(a), which shows an ensemble of N atoms loaded into a cavity. The atoms are described by two-level systems with ground state $|g\rangle$, excited state $|e\rangle$, and bare Hamiltonian $H_{\rm at} = \hbar\omega_{\rm at}\sum_{k=1}^{N} n^{(k)}$, where $n = |e\rangle\langle e|$. The bare-cavity Hamiltonian is $H_{\rm cav} = \hbar\omega_{\rm cav} a^\dagger a$, with a and $a^\dagger$ being the cavity-mode operators. The atoms and the cavity

*paulo.paulino.souza96@gmail.com

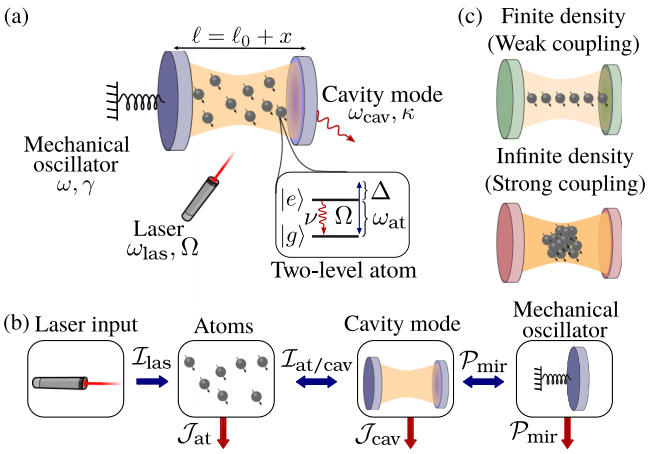

FIG. 1. Nonequilibrium cavity-atom optomechanical engine. (a) Atoms in a cavity are driven by a laser with Rabi frequency Ω and detuning Δ. One of the cavity mirrors can move, allowing for oscillations of the cavity length ℓ from its equilibrium position ℓ_0. (b) The laser provides energy which flows through the cavity to the mirror. Atom and photon losses at rates ν and κ, respectively, determine energy dissipation. The mechanical power delivered by the engine equals the power the mirror dissipates due to friction. (c) Two possible thermodynamic limits for the system. The first features a finite density of atoms and results in a weak optomechanical coupling. The second features an infinite density of atoms, giving rise to a strong optomechanical coupling.

mode interact through a Tavis-Cummings term [71–73],

$$H_{\rm int} = \frac{\hbar g}{\sqrt{N}}(aS_+ + a^\dagger S_-), \tag{1}$$

where $S_- = \sum_{k=1}^N \sigma_-^{(k)}$, with $\sigma_- = |g\rangle\langle e|$, and $S_+ = S_-^\dagger$. The atoms are further driven by a laser which, in combination with the bare-atom energy, is described by the Hamiltonian (in the interaction picture)

$$H_{\rm las} = \hbar\Omega(S_- + S_+) - \hbar\Delta \sum_{k=1}^N n^{(k)}, \tag{2}$$

where Ω is the Rabi frequency and $\Delta = \omega_{\rm las} - \omega_{\rm at}$ is the detuning of the laser frequency from the atom transition frequency [see Fig. 1(a)].

The dynamics of the system state ρ_t is governed by the master equation [74] (in the interaction picture)

$$\dot\rho_t = \mathcal{L}[\rho_t] := -\frac{i}{\hbar}[H, \rho_t] + \mathcal{D}_{\rm at}[\rho_t] + \mathcal{D}_{\rm cav}[\rho_t], \tag{3}$$

with Hamiltonian $H = H_{\rm las} + H_{\rm int} - \hbar\delta a^\dagger a$ and $\delta = \omega_{\rm las} - \omega_{\rm cav}$. The dissipators $\mathcal{D}_{\rm at/cav}$ account for irreversible effects due to a coupling of the atoms and the light field to thermal reservoirs at inverse temperature β. For the atoms, we have the dissipator

$$\mathcal{D}_{\rm at}[\rho] = \nu \sum_{k=1}^N \left(\sigma_-^{(k)}\rho\sigma_+^{(k)} - \frac{1}{2}\{n^{(k)}, \rho\}\right) + \nu e^{-\beta\hbar\omega_{\rm at}} \sum_{k=1}^N \left(\sigma_+^{(k)}\rho\sigma_-^{(k)} - \frac{1}{2}\{1 - n^{(k)}, \rho\}\right),$$

while for the light field the dissipator reads

$$\mathcal{D}_{\rm cav}[\rho] = \kappa\left(a\rho a^\dagger - \frac{1}{2}\{a^\dagger a, \rho\}\right) + \kappa e^{-\beta\hbar\omega_{\rm cav}}\left(a^\dagger\rho a - \frac{1}{2}\{aa^\dagger, \rho\}\right).$$

Both encode the spontaneous atom (photon) decay at rate ν (κ) and atom (photon) excitation at rate $\nu e^{-\beta\omega_{\rm at}}$ ($\kappa e^{-\beta\omega_{\rm cav}}$). The latter excitation process is often irrelevant in experiments since $\beta\hbar\omega_{\rm cav/at} \gg 1$ [19].

The cavity further features a movable mirror [see Fig. 1(a)], with mass m, frequency ω, and damping rate γ. For our purposes, we can consider it to be a classical object whose deviation x_t from its equilibrium position ℓ_0 evolves through the equation [75,76]

$$m\ddot x_t + \gamma\dot x_t + m\omega^2 x_t = f_t. \tag{4}$$

Here, $f_t = \hbar G\langle a^\dagger a\rangle_t$, with $G = \omega_{\rm cav}^0/\ell_0$, is the radiation-pressure force on the mirror in the linear-coupling regime, $|x_t|/\ell_0 \ll 1$, with $\omega_{\rm cav} \approx \omega_{\rm cav}^0(1 - x_t/\ell_0)$ [46,77].

This system can be interpreted as an engine [see Fig. 1(b)], or, more precisely, as an optomechanical energy converter. The atoms and light field represent the engine many-body *working fluid*. They absorb electromagnetic energy from the external driving and convert it into mechanical work which is delivered to the mirror to sustain its motion. The output power can be estimated as the heat dissipated by the mirror due to friction, thereby modeling a "dissipative load" [78].

III. NONEQUILIBRIUM THERMODYNAMICS

The mirror "state" (solely specified by instantaneous position x_t and velocity $\dot x_t$) and the state of the cavity-atom system ρ_t are in product form. Equation (3) provides the reduced quantum-system dynamics, parametrically depending on x_t via the cavity frequency $\omega_{\rm cav}$. Similarly, Eq. (4) provides the reduced mirror dynamics. This dynamical decoupling suggests that, also from a thermodynamic viewpoint, the cavity-atom system and the mirror can be regarded as uncorrelated. The mirror dynamics can be accounted for, e.g., within the framework of stochastic thermodynamics [76]. The challenge is, however, to consistently characterize the cavity-atom quantum engine.

The master equation [see Eq. (3)] is "local" [26] as it is obtained by a weak coupling of the system with a thermal bath [74] which, however, solely considers the bare-system Hamiltonians $H_{\rm at/cav}$. This can be seen by the fact that $\mathcal{D}_{\rm at/cav}$ do not implement transitions between eigenstates of the full Hamiltonian H but rather of $H_{\rm at/cav}$. A thermodynamic approach considering as the internal energy the expectation of a total system Hamiltonian would thus run into inconsistencies [26,27,33] since it generically predicts negative entropy production for local master equations [79]. A textbook approach [1–6] considering the total Hamiltonian H and deriving a "global" master equation would not show any inconsistency. However, here, we are interested in providing a consistent description of the experimentally relevant [16,19] local master equation (3).

A. The first laws

Our approach takes inspiration from the separation, done in the framework of stochastic thermodynamics [75,76], between conservative forces [see the harmonic force in Eq. (4)] and nonconservative external ones [see the force f_t in Eq. (4)]. This entails the definition of two internal energies, one for the atoms and one for the light field, through the bare energies and the identification of the remainder of the Hamiltonian, e.g., the laser driving, as an external driving contribution.

We thus start by defining the atom internal energy as $u_t^{\rm at} := \langle H_{\rm at}\rangle_t$. Then, considering the generator $\mathcal{L}^*$, which is the dual of the generator $\mathcal{L}$ acting on observables, we find

$$\begin{aligned}\dot{u}_t^{\rm at} &= {\rm Tr}(H_{\rm at}\mathcal{L}[\rho_t]) = \langle \mathcal{L}^*[H_{\rm at}]\rangle_t \\ &= \frac{i}{\hbar}\langle [H, H_{\rm at}]\rangle_t + \langle \mathcal{D}^*_{\rm at}[H_{\rm at}]\rangle_t + \langle \mathcal{D}^*_{\rm cav}[H_{\rm at}]\rangle_t \\ &= \frac{i}{\hbar}\langle [H_{\rm las}, H_{\rm at}]\rangle_t + \frac{i}{\hbar}\langle [H_{\rm int}, H_{\rm at}]\rangle_t + \langle \mathcal{D}^*_{\rm at}[H_{\rm at}]\rangle_t, \end{aligned} \tag{5}$$

where the dissipators $\mathcal{D}^*_{\rm at/cav}$ are the dual dissipators for $\mathcal{D}_{\rm at/cav}$ in the Heisenberg picture. For the last equality, we used the fact that $\mathcal{D}^*_{\rm cav}$ acts nontrivially only on light-field operators. From the last line in Eq. (5), we can already identify the physical meaning of the different terms. The first term describes how the internal energy of the atoms varies due to the laser driving. The second describes the energy flows from the atoms to the light field, while the last term, which comes from the dissipator, describes the heat power exchanged by the atoms with their environment.

Instead of looking at the instantaneous currents, we want to take an average over a time window τ. The latter could be a period of the engine cycle or, in general, just a long time window. Time averaging Eq. (5), we find

$$\frac{1}{\tau}\int_0^\tau dt\, \dot{u}_t^{\rm at} = \frac{u_\tau^{\rm at} - u_0^{\rm at}}{\tau} = \mathcal{I}_{\rm las} - \mathcal{I}_{\rm at} - \mathcal{J}_{\rm at}. \tag{6}$$

Here, we have defined

$$\begin{aligned}\mathcal{I}_{\rm las} &= \frac{i}{\hbar\tau}\int_0^\tau dt\, \langle [H_{\rm las}, H_{\rm at}]\rangle_t, \\ \mathcal{I}_{\rm at} &= -\frac{i}{\hbar\tau}\int_0^\tau dt\, \langle [H_{\rm int}, H_{\rm at}]\rangle_t, \\ \mathcal{J}_{\rm at} &= -\frac{1}{\tau}\int_0^\tau dt\, \langle \mathcal{D}^*_{\rm at}[H_{\rm at}]\rangle_t. \end{aligned} \tag{7}$$

The term $\mathcal{I}_{\rm las}$ represents the time-averaged input power that the atoms receive from the laser, and the term $\mathcal{I}_{\rm at}$ is, instead, the average power exchanged between the atoms and the light field (in this convention it is positive when flowing from the atoms to the light field). The third term, $\mathcal{J}_{\rm at}$, is the average heat power dissipated by the atoms into the environment (this quantity is also positive when energy is leaving the atoms). Assuming that the integration time τ is large and the internal energy does not grow indefinitely with time, we have $\frac{u_\tau^{\rm at} - u_0^{\rm at}}{\tau} \to 0$, so from the above relation we can write

$$\mathcal{I}_{\rm las} = \mathcal{I}_{\rm at} + \mathcal{J}_{\rm at}. \tag{8}$$

The internal energy of the light field is defined as $u_t^{\rm cav} := \langle H_{\rm cav}\rangle_t$. By taking the time derivative and following a procedure analogous to the one exploited in Eq. (5), we find

$$\dot{u}_t^{\rm cav} = \frac{i}{\hbar}\langle [H_{\rm int}, H_{\rm cav}]\rangle_t - f_t v_t + \langle \mathcal{D}^*_{\rm cav}[H_{\rm cav}]\rangle_t, \tag{9}$$

with $v_t := \dot{x}_t$ being the mirror velocity. Taking the time average over τ, the power absorbed by the light field due to the coupling with the atoms, $\mathcal{I}_{\rm cav} = i/(\hbar\tau)\int_0^\tau dt\, \langle [H_{\rm int}, H_{\rm cav}]\rangle_t$, is

$$\mathcal{I}_{\rm cav} = \mathcal{P}_{\rm mir} + \mathcal{J}_{\rm cav}, \tag{10}$$

where

$$\mathcal{P}_{\rm mir} = \frac{1}{\tau}\int_0^\tau dt\, f_t v_t, \quad \mathcal{J}_{\rm cav} = -\frac{1}{\tau}\int_0^\tau dt\, \langle \mathcal{D}^*_{\rm cav}[H_{\rm cav}]\rangle_t. \tag{11}$$

The first term above is the average heat power exchanged by the light field and the environment, while $\mathcal{P}_{\rm mir}$ is the power delivered by the cavity-atom system to the mirror. Exploiting the mirror internal energy $u_t^{\rm mir} = (m v_t^2 + m\omega^2 x_t^2)/2$ [75,76] and Eq. (4), we also find the relation

$$\mathcal{P}_{\rm mir} = \gamma/\tau \int_0^\tau dt\, v_t^2, \tag{12}$$

i.e., the power delivered by the cavity-atom system to the mirror is equal, over a long time window, to the power dissipated by the mirror due to friction [see Figs. 1(a) and 1(b)].

In order to find the total input power, we observe that the quantity $\mathcal{I}_{\rm cav} - \mathcal{I}_{\rm at}$ can be written as

$$\mathcal{I}_{\rm cav} - \mathcal{I}_{\rm at} = \frac{1}{\tau}\int_0^\tau dt\, \frac{i}{\hbar}\langle [H_{\rm int}, H_{\rm at} + H_{\rm cav}]\rangle_t.$$

This quantity can be different from zero whenever the atoms and the light field are not on resonance, in which case it represents an "imbalance" between the power delivered by the atoms and the power absorbed by the light field. We consider this imbalance, which comes from the interaction Hamiltonian and is due to energy gain or energy loss associated with the exchange of excitations, to be an additional input-power contribution. The rationale is that, in typical cavity-atom experiments, interactions between the atoms and the cavity field need to be "facilitated" by means of an additional laser driving, for instance, through stimulated Raman emissions [80]. In this sense, the imbalance term $\mathcal{I}_{\rm cav} - \mathcal{I}_{\rm at}$ is analogous, in spirit, to the term $\mathcal{I}_{\rm las}$. The total input is thus $\mathcal{I}_{\rm in} = \mathcal{I}_{\rm las} + \mathcal{I}_{\rm cav} - \mathcal{I}_{\rm at}$, which combining Eqs. (8)–(10), can be written as

$$\mathcal{I}_{\rm in} = \mathcal{J}_{\rm cav} + \mathcal{J}_{\rm at} + \mathcal{P}_{\rm mir}. \tag{13}$$

For the sake of simplicity, we have considered here a nonfluctuating mirror dynamics, which effectively accounts for a zero-temperature bath for the mirror. Similar results could be obtained for finite temperatures for the mirror. For the regimes investigated here, the power delivered by the engine would still be proportional to the square of the average mirror velocity (see, e.g., considerations in Ref. [59]).

B. The second law

In order to formulate a consistent efficiency for the optomechanical engine, we first need to show that the heat powers obey the inequality $\mathcal{J}_{\rm at} + \mathcal{J}_{\rm cav} \geqslant 0$. This is achieved by proving a suitable second law of thermodynamics through

a modification of Spohn's theorem [31,79,81]. To this end, we define the map $\mathcal{D} = \mathcal{D}_{\rm at} + \mathcal{D}_{\rm cav}$, whose stationary state is the thermal state $\rho^\beta \propto e^{-\beta(H_{\rm at}+H_{\rm cav})}$. Next, we consider the von Neumann entropy of the quantum state ρ_t, $S(\rho_t) = -{\rm Tr}[\rho_t \ln \rho_t]$ and define the entropy production as

$$\sigma_t = \dot{S}(\rho_t) - \beta {\rm Tr}\{\mathcal{D}[\rho_t](H_{\rm at} + H_{\rm cav})\}. \tag{14}$$

In the above equation, the first and second terms are the entropy and heat variations, respectively, and we further note that $\dot{S}(\rho_t) = -{\rm Tr}\{\mathcal{D}[\rho_t]\ln\rho_t\}$. The task is now to show that the entropy production is always positive. We proceed by defining the relative entropy $S(\rho_t||\rho^\beta) = {\rm Tr}[\rho_t(\ln\rho_t - \ln\rho^\beta)]$, which can only decrease under the action of a completely positive trace-preserving map [82]. Thus,

$$\frac{d}{du} S(e^{u\mathcal{D}}[\rho_t]||e^{u\mathcal{D}}[\rho^\beta])|_{u=0} \leqslant 0. \tag{15}$$

Since $e^{u\mathcal{D}}[\rho^\beta] = \rho^\beta$, the derivative of the relative entropy evaluated in $u = 0$ becomes

$$\begin{aligned}\frac{d}{du} S(e^{u\mathcal{D}}[\rho_t]||e^{u\mathcal{D}}[\rho^\beta])|_{u=0} \\ = -\dot{S}(\rho_t) + \beta {\rm Tr}\{\mathcal{D}[\rho_t](H_{\rm at} + H_{\rm cav})\}.\end{aligned} \tag{16}$$

The nonpositivity of the above quantity then implies the nonnegativity of the entropy production.

Averaging the entropy production over a long time window τ, we find

$$\frac{1}{\tau}\int_0^\tau dt\, \sigma_t = \frac{S(\rho_\tau) - S(\rho_0)}{\tau} + \beta(\mathcal{J}_{\rm at} + \mathcal{J}_{\rm cav}) \geqslant 0. \tag{17}$$

Now, assuming that $S(\rho_t)$ does not grow indefinitely with time, the above implies $\mathcal{J}_{\rm at} + \mathcal{J}_{\rm cav} \geqslant 0$, which is the inequality that we need. Before using this inequality to discuss the efficiency of the engine, we make an important remark on the above derivation. The main ingredient that we have exploited is that the reduced dynamics of the quantum state obeys the Lindblad equation (3), which only parametrically depends on the instantaneous position of the mirror x_t. The reduced dynamics of the quantum system assumes this form since the state of the mirror, fully specified by x_t and $\dot{x}_t$, and the quantum state are in product form. The product structure of the quantum-classical state also remains generically when considering single trajectories of stochastic dynamical equations for the mirror. However, when the mirror is promoted to a quantum degree of freedom, the derivation above requires appropriate modifications, given the emergence of intrinsic quantum correlations among all subsystems.

C. Efficiency

We are now able to obtain a thermodynamically consistent efficiency η of the energy conversion occurring in our optomechanical setup. The input power is equal, at long times, to the total power dissipated by the optomechanical system, i.e., $\mathcal{I}_{\rm in} = \mathcal{P}_{\rm mir} + \mathcal{J}_{\rm cav} + \mathcal{J}_{\rm at}$. Thus,

$$\eta = \frac{\mathcal{P}_{\rm mir}}{\mathcal{P}_{\rm mir} + \mathcal{J}_{\rm cav} + \mathcal{J}_{\rm at}} \leqslant 1. \tag{18}$$

The efficiency is bounded by 1 since both $\mathcal{P}_{\rm mir}$ and $\mathcal{J}_{\rm at} + \mathcal{J}_{\rm cav}$ are positive, as shown in the previous section. Considering the total input power, Eq. (13), we can express $\mathcal{I}_{\rm in}$ as in the denominator of Eq. (18) and identify a well-defined efficiency formulated in terms of the persistent heat currents.

IV. TIME-CRYSTAL ENGINE

As an application of the general theory that we have developed, we analyze power and efficiency for the recently introduced time-crystal engine [59].

For Markovian open quantum systems described by a time-independent Lindblad generator $\mathcal{L}$, one generically expects the density matrix of the system to converge for long times to a stationary state ρ_∞ such that $\mathcal{L}[\rho_\infty] = 0$. The generator $\mathcal{L}$ is time translation invariant due to its time independence and further commutes with the "time-translation operator" (propagator) $e^{t\mathcal{L}}$. Whenever the system approaches a steady state, one has $e^{t\mathcal{L}}[\rho_\infty] = \rho_\infty$, showing that ρ_∞ is *time translation symmetric* and thus obeys the same symmetry as the generator (see also, e.g., the discussion in Ref. [65]). The emergence of time-translation symmetry breaking, and thus of the so-called time-crystal phase, occurs when the state of the system approaches a limit cycle rather than a stationary state. By denoting with $\rho_t^{\rm lc}$ the state inside such an asymptotic limit cycle and assuming that the latter has period T, we find that $\rho_{t+T}^{\rm lc} = \rho_t^{\rm lc}$. In such a case, we have $e^{t'\mathcal{L}}[\rho_t^{\rm lc}] = \rho_{t+t'}^{\rm lc} \neq \rho_t^{\rm lc}$ whenever $t, t' \neq T$. This shows that, despite the fact that the generator $\mathcal{L}$ is time translation symmetric, the asymptotic state of the system breaks such symmetry. In this case, the system features persistent oscillations and is said to enter a time-crystal phase. We note that signatures of the emergence of a time-crystal phase can be seen in the spectrum of the (finite-system) generator $\mathcal{L}$ [63].

We now proceed by discussing how time-translation symmetry breaking can be used as a power-generation mechanism in our setup [59]. In the regime in which the system approaches a stationary state, we find that the radiation-pressure force f_t becomes time independent for long times since it approaches its stationary value associated with the stationary state. In this case, the mirror is subject to a static force, and thus, its velocity converges to zero, leading to zero power production. On the other hand, in the time-crystal phase of the model, the state of the system features persistent oscillations so that the radiation-pressure force f_t remains asymptotically time dependent. As a consequence, the mirror is subject to a time-dependent force and thus never comes to rest and always sustains a finite velocity [16,19,63,80,83,84]. In the time-crystal regime, the mirror thus continuously dissipates power which must be provided by the time-crystal quantum engine. We note that, in the regime in which the Lindblad generator is time independent, the engine is clearly in contact with a single bath at fixed temperature. As such, the optomechanical engine in this setup does not function as a heat engine but rather as a nonequilibrium isothermal one [76].

A. Mean-field treatment

Since time-crystalline phases emerge only in the thermodynamic limit, we consider the system in the thermodynamic large-N limit, in which the quantum dynamics is exactly captured by a mean-field treatment [65]. That is, the rescaled

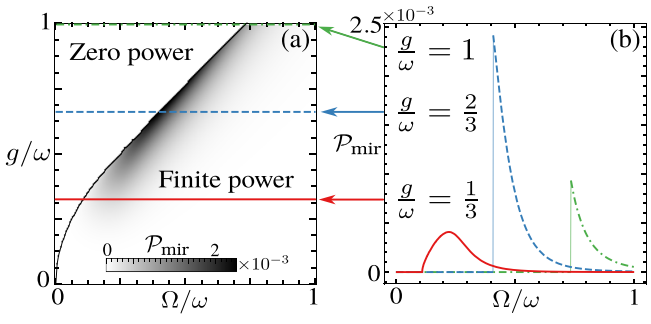

FIG. 2. Mechanical power output of the time-crystal quantum engine. (a) Power as a function of Ω and g, given in units of $\gamma(\Lambda\omega)^2$, with $\Lambda=\hbar GN/(m\omega^2)$. Note that, in our scaling limits, Λ remains finite for all N. The parameter γ is instead proportional to N in the infinite-density limit in which the optomechanical engine thus delivers extensive power output. The stationary phase (zero power) and the time-crystal phase (finite power) are separated by a critical line. (b) Three sections across (a) for different values of g. The solid line refers to $g/\omega=1/3$, the dashed line refers to $g/\omega=2/3$, and the dot-dashed line is associated with $g/\omega=1$. The atoms are all initialized in the ground state and the light field in the vacuum. The parameters used are $\kappa=\gamma/m=\omega$.

operators $\alpha=a/\sqrt{N}$, $s_\pm=S_\pm/N$, and $s_z=S_z/N$, with $S_z=\sum_{k=1}^{N}(2n^{(k)}-1)$, converge, with $N\to\infty$, to scalar quantities evolving through nonlinear equations [65,85,86]. For concreteness, we consider the case $\omega_{\rm at}-\omega_{\rm cav}^0=\Delta=\nu=0$ and $\beta\to\infty$, for which the equations are given by

$$\begin{aligned}\dot{s}_z&=-2[i\Omega s_+ + ig\alpha s_+ + \text{c.c.}],\\ \dot{s}_+&=-i\big(\Omega+g\alpha^\dagger\big)s_z,\\ \dot{\alpha}&=-\frac{\kappa}{2}\alpha+i[Gx\alpha-gs_-].\end{aligned}\tag{19}$$

As shown below (see also Figs. 2 and 3), for large Ω/g ratios the system state approaches indeed long-lived limit-cycle solutions [62,63,87]. In these cases, the radiation-pressure force is time dependent, and the mirror thus moves against friction, so that the cavity-atom engine delivers power [see $\mathcal{P}_{\rm mir}$ in Eq. (11)] even without a time-dependent driving protocol [59]. In order to characterize the performance of the engine, we need to analyze the time evolution of the mirror and the dissipated power $\mathcal{P}_{\rm mir}$ in the thermodynamic limit. However, the force f_t is extensive in N, $f_t\approx\hbar GN|\alpha_t|^2$, and this can give rise to an unphysical diverging displacement of the mirror. To arrive at a well-defined mirror dynamics [see Eq. (4)], in the thermodynamic limit, we identify below two suitable scaling regimes which are associated with two different physical scenarios.

B. Finite-density (weak-coupling) limit

First, we consider the regime in which, ideally, all atoms are located in the minima of an optical lattice inside the cavity [see sketch in Fig. 1(c)]. The cavity length is thus proportional to the number of atoms [16,59], i.e., $\ell_0=N/D_0$, with D_0 being the linear density. The optomechanical coupling constant is here $G=\omega_{\rm cav}^0 D_0/N$ and thus vanishes in the large-N limit. This scenario is associated with a weak optomechanical coupling [see Fig. 1(c)]. Looking at Eq. (19), this implies that the quantum-system dynamics does not depend on any of the mirror parameters. Still, the mirror dynamics is driven by the light-field intensity through the force $f_t=\hbar\omega_{\rm cav}^0 D_0|\alpha_t|^2$, which, in this regime, becomes independent of N.

In Fig. 2(a), we show the power delivered by the engine to the mirror. We observe a parameter region in which the delivered power $\mathcal{P}_{\rm mir}$ is zero. This occurs when the quantum system approaches a stationary state, the radiation-pressure force is a stationary value, and the mirror comes to rest, as is expected for static driving. Nonetheless, even with static driving, for certain parameters the quantum system can spontaneously enter a state of sustained oscillations, determining a time-dependent force on the mirror and thus a finite power $\mathcal{P}_{\rm mir}$ [see Fig. 2(b)]. In this regime the optomechanical setup operates as a time-crystal quantum engine [59]. However, in the finite-density limit $\mathcal{P}_{\rm mir}$ is intensive in N, while $\mathcal{J}_{\rm cav}\propto N$, so that the engine efficiency is zero.

C. Infinite-density (strong-coupling) limit

We now introduce a regime in which the cavity-atom engine operates with finite efficiency. We consider the limit $N\to\infty$ while keeping ℓ_0 finite, which leads to an infinite density of atoms in the cavity [see the sketch in Fig. 1(c)] and to a finite G. We dub this limit the "strong" optomechanical coupling regime since the force f_t remains proportional to N. To have a physically meaningful mirror dynamics [see Eq. (4)], we rescale the mass and the friction parameter as $m=N\tilde{m}$ and $\gamma=N\tilde{\gamma}$, respectively. This means relating the size of the mirror to the number of atoms, which is natural when the "mirror" is a vibrational degree of freedom of the atom ensemble [11–13,20] or when the cavity hosts a cloud of atoms, as illustrated in Fig. 1(c). In this way, the mirror velocity remains finite, while the power is extensive in N, since $\gamma\propto N$. This gives the efficiency (at lowest order in Λ/ℓ_0)

$$\eta\approx\frac{\gamma}{\kappa m}\frac{\Lambda}{\ell_0}\frac{\int_0^{\omega\tau}d[\omega t]V_{\omega t}^2}{\int_0^{\omega\tau}d[\omega t]|\alpha_{\omega t}|^2}.\tag{20}$$

Here, $\Lambda=\hbar GN/(m\omega^2)$ is the characteristic length scale of x, while $V_{\omega t}$ is the dimensionless velocity at the dimensionless time ωt, such that $v_t=\Lambda\omega V_{\omega t}$. The complete expression of the efficiency, including finite temperature and finite atom decay, is given in Appendix A.

In this infinite-density limit, the dynamics of the quantum system is influenced by the motion of the mirror [see Eq. (19)]. For a timescale of the order of $(G\Lambda)^{-1}$, this back-action is irrelevant, and the cavity-atom system can host a (metastable) time-crystal phase [see Figs. 3(a) and 3(b) and Appendixes B and C]. Thereafter, back-action effects become non-negligible and drive the system towards a stationary state, where no power can be generated anymore.

Even if it appears as a metastable phase, we can characterize the time-crystal engine in the long prestationary regime. The average power is the same as that shown in Fig. 2, albeit now being extensive with N. The efficiency is reported in Figs. 3(c) and 3(d). It also signals the transition from the stationary to the (metastable) time-crystal phase, where the

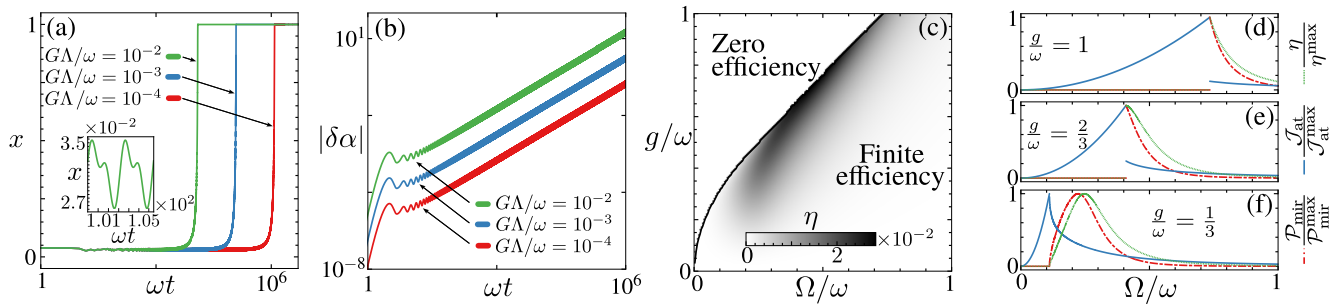

FIG. 3. Metastable time-crystal engine and efficiency in the infinite-density limit. (a) Mirror position x in units of Λ as a function of time for $\Omega = g = \omega$. The plot shows an emergent metastable regime in which the mirror features oscillations (see inset), unveiling that the quantum system is in a time-crystal phase. The smaller $G\Lambda/\omega$ (see arrows in the plot) is, the longer the metastable regime lasts before the system ends up in the stationary state. (b) Growth of the fluctuation $\delta\alpha$, associated with the light-field expectation α, due to the back-action of the dynamics of the mirror on the time evolution of the quantum system. The different lines refer to different values of $G\Lambda/\omega$, as indicated by the arrows in the plot. (c) Efficiency (in the metastable regime) in units of $\gamma\Lambda/(\kappa m\ell_0)$, obtained from Eq. (20). (d)–(f) Normalized power, light-field dissipation, and efficiency as a function of Ω for different values of g. The unspecified parameters are $\kappa = \gamma/m = \omega$.

system generates mechanical power. In Fig. 3(d), we see that for large g/ω the maximal power delivered by the engine occurs close to the transition line, where a maximal efficiency is also reached.

V. DISCUSSION

We characterized the nonequilibrium thermodynamics of phenomenological cavity-atom models. Contrary to other thermodynamic frameworks, our approach does not require the introduction of a repeated-interaction scheme [27–29]. It also does not consider as internal energy the expectation value of the total Hamiltonian [4,31,79]. We note that this is also what one would expected in the case of weak cavity-atom coupling, i.e., $\omega_{\rm at/cav} \gg |\Omega|, |g|$. Instead, it relies on separating, within the system Hamiltonian, the bare-energy contributions from those related to external driving. This allows us to interpret dynamical contributions such as the laser driving as external power sources, which is closer, in spirit, to the physics of experiments with driven-dissipative quantum systems. Importantly, our identification of the different thermodynamic contributions leads to heat currents which are supported by the second law of thermodynamics. This leads to a well-defined energy-conversion efficiency. For concreteness, we illustrated our ideas considering a time-crystal engine [59]. However, our approach may also be applied more generally to cavity-only open quantum systems and to different manifestations of collective behavior hosted by them [12,60,88–93].

ACKNOWLEDGMENTS

We are grateful to A. Cabot and S. Marcantoni for useful discussions. We acknowledge funding from the Deutsche Forschungsgemeinschaft (DFG, German Research Foundation) under Project No. 435696605 and through the Research Unit FOR 5413/1, Grant No. 465199066. This project has also received funding from the European Union's Horizon Europe research and innovation program under Grant Agreement No. 101046968 (BRISQ). F.C. is indebted to the Baden-Württemberg Stiftung for the financial support for this research project through the Eliteprogramme for Postdocs.

APPENDIX A: DETAILS OF THE TWO THERMODYNAMIC LIMITS

We provide here details of the discussion reported in the main text concerning the two thermodynamic limits. We start deriving the quantities of interest, considering a finite number of atoms N. However, we already introduce the mean-field approximation since the latter becomes exact in the limit $N \to \infty$.

The time evolution of the relevant quantum operators is thus described by the mean-field equations reported in the main text. Through these operators we can write the heat currents as (derived for finite temperature)

$$\mathcal{J}_{\rm cav} = \frac{\hbar\kappa}{\tau}\int_0^\tau dt\,\omega_{\rm cav}\langle a^\dagger a - e^{-\beta\hbar\omega_{\rm cav}}(1 + a^\dagger a)\rangle,$$
$$\mathcal{J}_{\rm at} = \frac{\hbar\omega_{\rm at}\nu}{\tau}\int_0^\tau dt\sum_{k=1}^{N}[(1 + e^{-\beta\hbar\omega_{\rm at}})\langle n^{(k)}\rangle - e^{-\beta\hbar\omega_{\rm at}}]. \tag{A1}$$

To derive the mechanical output power, we need to look at the dynamics of the mirror, described by the second-order differential equation reported in the main text. The solution to this equation is given by $x_t = \Lambda X_{\omega t}$, with $\Lambda = \frac{\hbar GN}{m\omega^2}$ and

$$X_{\omega t} = \int_0^{\omega t} d[\omega s]\,|\alpha_{\omega s}|^2 e^{-\frac{\gamma_0}{\omega}(\omega t - \omega s)}\frac{\omega}{\Sigma}\sin\left[\frac{\Sigma}{\omega}(\omega t - \omega s)\right]. \tag{A2}$$

Here, $\gamma_0 = \gamma/(2m)$, and we consider the dimensionless time ωt. Moreover, with a slight abuse of notation, we denote by $\alpha_{\omega t}$ the light-field operator at the dimensionless time ωt. Furthermore, by taking the derivative, we find the velocity of

the mirror as $v_t = \Lambda\omega V_{\omega t}$, with

$$V_{\omega t} = \int_0^{\omega t} d[\omega s]\,|\alpha_{\omega s}|^2 e^{-\frac{\gamma_0}{\omega}(\omega t-\omega s)} \times\left(\cos\left[\frac{\Sigma}{\omega}(\omega t-\omega s)\right]-\frac{\gamma_0}{\Sigma}\sin\left[\frac{\Sigma}{\omega}(\omega t-\omega s)\right]\right). \tag{A3}$$

Here, $V_{\omega t}$ is the dimensionless velocity at the dimensionless time ωt. We note that $\dot{X}_{\omega t} = V_{\omega t}$ and $\dot{V}_{\omega t} = -X_{\omega t} - 2\gamma_0/\omega V_{\omega t} + |\alpha_{\omega t}|^2$, which is a dimensionless system of equations. Solving this combined with the mean-field equations, it is possible to compute the average mechanical output power as

$$\mathcal{P}_{\rm mirr} = \frac{\gamma}{\tau}\int_0^\tau dt\, v_t^2 = \gamma(\Lambda\omega)^2\left[\frac{1}{\omega\tau}\int_0^{\omega\tau} d[\omega t]V_{\omega t}^2\right].$$

1. Finite-density limit

We start by considering the finite-density limit. In this situation we have $G = \omega_{\rm cav}^0 D_0/N$, which thus tends to zero in the large-N limit. This means that the mean-field equations become independent of x_t and that the quantum system does not feel the back-action due to the motion of the mirror.

In the finite-density limit, we find that $\Lambda = \hbar\omega_{\rm cav}^0 D_0/(m\omega^2)$ and that the power $\mathcal{P}_{\rm mirr}$ remains finite. However, as shown by Eqs. (A1), the heat fluxes are extensive with N, so the efficiency in this regime vanishes.

2. Infinite-density limit

In the infinite-density limit, the length of the cavity ℓ_0 remains independent of N. This means that G is finite in the thermodynamic limit. To have a well-defined dynamics for x_t we thus rescale the mass of the mirror, $m = N\tilde{m}$, as well as the friction parameter, $\gamma = N\tilde{\gamma}$. We note that Eqs. (A2) and (A3) remain valid and also that $\Lambda = \hbar G/(\tilde{m}\omega^2)$ does depend on N. The average mechanical power delivered by the optomechanical engine is now extensive since

$$\mathcal{P}_{\rm mirr} = N\tilde{\gamma}(\Lambda\omega)^2\left[\frac{1}{\omega\tau}\int_0^{\omega\tau} d[\omega t]V_{\omega t}^2\right].$$

The efficiency can be computed as

$$\eta = \frac{\mathcal{P}_{\rm mirr}}{\mathcal{J}_{\rm cav}+\mathcal{J}_{\rm at}+\mathcal{P}_{\rm mirr}} = \left(1+\frac{\mathcal{J}_{\rm cav}+\mathcal{J}_{\rm at}}{\mathcal{P}_{\rm mirr}}\right)^{-1},$$

and substituting for the relevant quantities, we find

$$\eta = \left(1+\frac{\hbar\omega_{\rm at}\nu}{\tilde{\gamma}(\Lambda\omega)^2}\frac{\int_0^{\omega\tau} d[\omega t][(1+e^{-\beta\hbar\omega_{\rm at}})n_{\omega t}-e^{-\beta\omega_{\rm at}}]}{\int_0^{\omega\tau} d[\omega t]V_{\omega t}^2} + \frac{\hbar\omega_{\rm cav}^0\kappa}{\tilde{\gamma}(\Lambda\omega)^2}\frac{\int_0^{\omega\tau} d[\omega t](1-\frac{\Lambda}{\ell_0}X_{\omega t})|\alpha_{\omega t}|^2(1-e^{-\beta\hbar\omega_{\rm cav}})}{\int_0^{\omega\tau} d[\omega t]V_{\omega t}^2}\right)^{-1}, \tag{A4}$$

where $n_{\omega t}$ is here the expectation value of the operator n at the dimensionless time ωt.

Specializing to the case with $\nu = 0$ and $\beta\to\infty$, we find, after manipulating the parameters, that

$$\eta \approx \frac{\gamma}{\kappa m}\frac{\Lambda}{\ell_0}\frac{\int_0^{\omega\tau} d[\omega t]V_{\omega t}^2}{\int_0^{\omega\tau} d[\omega t]|\alpha_{\omega t}|^2}, \tag{A5}$$

where we consider only the lowest order in Λ/ℓ_0.

APPENDIX B: METASTABLE TIME-CRYSTAL REGIME

We provide here details of the emergence of a metastable timescale where the optomechanical system works as a time-crystal engine with finite efficiency in the infinite-density limit. This timescale emerges when we consider the parameter $G\Lambda/\omega$ to be small, as we now show.

The evolution equation for $\alpha_{\omega t}$ is given by

$$\dot{\alpha}_{\omega t} = -\frac{\kappa}{2\omega}\alpha_{\omega t} + i\frac{G\Lambda}{\omega}\alpha_{\omega t} - i\frac{g}{\omega}s_{-\,\omega t}.$$

Considering $G\Lambda/\omega$ to be small, we can apply perturbation theory to the mean-field equations. By doing this, we can show that (see Appendix C for details)

$$\alpha_{\omega t} = \alpha_{\omega t}^0 + \frac{G\Lambda}{\omega}\delta\alpha_{\omega t}^1, \tag{B1}$$

where $\alpha_{\omega t}^0$ is obtained through the unperturbed system of mean-field equations, while the term $\delta\alpha_{\omega t}$ is the perturbation around this solution because we consider a small $G\Lambda/\omega$. In Fig. 3 in the main text, we provide the value $\delta\alpha = G\Lambda/\omega\delta\alpha^1$.

Now we proceed by rewriting the second-order differential equation for the mirror oscillations in terms of the dimensionless quantity $\epsilon = Gx/\omega$. We readily obtain

$$\ddot{\epsilon}_{\omega t} + \frac{\gamma}{m\omega}\dot{\epsilon}_{\omega t} + \epsilon_{\omega t} = \frac{G\Lambda}{\omega}|\alpha_{\omega t}|^2.$$

By recalling Eq. (B1), we see that up to first order in $G\Lambda/\omega$ the above equation is fully determined solely by the term $\alpha_{\omega t}^0$, which is given by the same system of equations solved for the finite-density limit and which can show persistent oscillations. However, the correction $\delta\alpha_{\omega t}$ increases linearly with time and thus eventually plays an important role in the dynamics of the mirror. Our exact numerical results show that the perturbation is such that the system will asymptotically approach a stationary state.

APPENDIX C: PERTURBATION THEORY ON THE MEAN-FIELD EQUATIONS

We give here a brief discussion of how we performed the perturbation theory to first order in $G\Lambda/\omega$.

In the dimensionless time, the mean-field equations become (we omit the explicit time dependence)

$$\begin{aligned}\dot{s}_z &= -2\left[i\frac{\Omega}{\omega}s_+ + i\frac{g}{\omega}\alpha s_+ + \text{c.c.}\right],\\ \dot{s}_+ &= -i\left(\frac{\Omega}{\omega}+\frac{g}{\omega}\alpha^\dagger\right)s_z,\\ \dot{\alpha} &= -\frac{\kappa}{2\omega}\alpha + i\left[\frac{G\Lambda}{\omega}X\alpha - \frac{g}{\omega}s_-\right],\end{aligned} \tag{C1}$$

where we used $x = \Lambda X$. This equation is coupled to the second-order differential [see discussion below Eq. (A3)]

$$\ddot{X} + 2\frac{\gamma_0}{\omega}\dot{X} + X = |\alpha|^2.$$

To zeroth order, we simply solve the above system by setting $G\Lambda/\omega \equiv 0$, which gives us the solutions s_z^0, s_+^0, and α^0.

To first order, we expect the solutions to be given by

$$s_z = s_z^0 + \frac{G\Lambda}{\omega}\delta s_z^1, \quad s_+ = s_+^0 + \frac{G\Lambda}{\omega}\delta s_+^1, \quad \alpha = \alpha^0 + \frac{G\Lambda}{\omega}\delta\alpha^1.$$

Substituting into the above system of equations, we find

$$\begin{aligned}
\delta\dot{s}_z^1 &= -2\left[i\frac{\Omega}{\omega}\delta s_+^1 + i\frac{g}{\omega}(\alpha^0\delta s_+^1 + s_+^0\delta\alpha^1) + \text{c.c.}\right],\\
\delta\dot{s}_+^1 &= -i\frac{\Omega}{\omega}\delta s_z^1 - i\frac{g}{\omega}\left(\alpha^{0\,\dagger}\delta s_z^1 + s_z^0\delta\alpha^{1\,\dagger}\right),\\
\delta\dot{\alpha}^1 &= -\frac{\kappa}{2\omega}\delta\alpha^1 + iX^0\alpha^0 - i\frac{g}{\omega}\delta s_-^1.
\end{aligned} \tag{C2}$$

Solving these equations and combining them with the mean-field ones for the unperturbed variables s_z^0, s_+^0, and α^0 give the behavior of $\delta\alpha = (G\Lambda/\omega)\delta\alpha^1$ reported in the main text.

[1] R. Alicki, The quantum open system as a model of the heat engine, J. Phys. A **12**, L103 (1979).

[2] R. Kosloff, A quantum mechanical open system as a model of a heat engine, J. Chem. Phys. **80**, 1625 (1984).

[3] H. T. Quan, Y.-X. Liu, C. P. Sun, and F. Nori, Quantum thermodynamic cycles and quantum heat engines, Phys. Rev. E **76**, 031105 (2007).

[4] R. Kosloff, Quantum thermodynamics: A dynamical viewpoint, Entropy **15**, 2100 (2013).

[5] F. Binder, L. A. Correa, C. Gogolin, J. Anders, and G. Adesso, in *Thermodynamics in the Quantum Regime, Fundamental Aspects and New Directions*, 1st ed., edited by F. Binder, L. A. Correa, C. Gogolin, J. Anders, and G. Adesso, Fundamental Theories of Physics Vol. 195 (Springer, Cham, 2018), p. 998.

[6] S. Deffner and S. Campbell, *Quantum Thermodynamics: An Introduction to the Thermodynamics of Quantum Information* (Morgan and Claypool, San Rafael (USA), 2019).

[7] O. Abah, J. Roßnagel, G. Jacob, S. Deffner, F. Schmidt-Kaler, K. Singer, and E. Lutz, Single-Ion Heat Engine at Maximum Power, Phys. Rev. Lett. **109**, 203006 (2012).

[8] J. Roßnagel, S. T. Dawkins, K. N. Tolazzi, O. Abah, E. Lutz, F. Schmidt-Kaler, and K. Singer, A single-atom heat engine, Science **352**, 325 (2016).

[9] Q. Bouton, J. Nettersheim, S. Burgardt, D. Adam, E. Lutz, and A. Widera, A quantum heat engine driven by atomic collisions, Nat. Commun. **12**, 2063 (2021).

[10] F. Brennecke, T. Donner, S. Ritter, T. Bourdel, M. Köhl, and T. Esslinger, Cavity QED with a Bose–Einstein condensate, Nature (London) **450**, 268 (2007).

[11] F. Brennecke, S. Ritter, T. Donner, and T. Esslinger, Cavity optomechanics with a Bose-Einstein condensate, Science **322**, 235 (2008).

[12] K. W. Murch, K. L. Moore, S. Gupta, and D. M. Stamper-Kurn, Observation of quantum-measurement backaction with an ultracold atomic gas, Nat. Phys. **4**, 561 (2008).

[13] T. P. Purdy, D. W. C. Brooks, T. Botter, N. Brahms, Z.-Y. Ma, and D. M. Stamper-Kurn, Tunable Cavity Optomechanics with Ultracold Atoms, Phys. Rev. Lett. **105**, 133602 (2010).

[14] B. Chen, C. Jiang, J.-J. Li, and K.-D. Zhu, All-optical transistor based on a cavity optomechanical system with a Bose-Einstein condensate, Phys. Rev. A **84**, 055802 (2011).

[15] G. De Chiara, M. Paternostro, and G. M. Palma, Entanglement detection in hybrid optomechanical systems, Phys. Rev. A **83**, 052324 (2011).

[16] H. Ritsch, P. Domokos, F. Brennecke, and T. Esslinger, Cold atoms in cavity-generated dynamical optical potentials, Rev. Mod. Phys. **85**, 553 (2013).

[17] D. M. Stamper-Kurn, in *Cavity Optomechanics*, edited by M. Aspelmeyer, T. J. Kippenberg, and F. Marquardt (Springer, Heidelberg, 2014), Chap. 13, pp. 283–325.

[18] G. Labeyrie, E. Tesio, P. M. Gomes, G. L. Oppo, W. J. Firth, G. R. M. Robb, A. S. Arnold, R. Kaiser, and T. Ackemann, Optomechanical self-structuring in a cold atomic gas, Nat. Photonics **8**, 321 (2014).

[19] F. Mivehvar, F. Piazza, T. Donner, and H. Ritsch, Cavity QED with quantum gases: New paradigms in many-body physics, Adv. Phys. **70**, 1 (2021).

[20] H. Mikaeili, A. Dalafi, M. Ghanaatshoar, and B. Askari, Optomechanically induced gain using a trapped interacting Bose-Einstein condensate, Sci. Rep. **13**, 3659 (2023).

[21] C. Elouard and A. N. Jordan, Efficient Quantum Measurement Engines, Phys. Rev. Lett. **120**, 260601 (2018).

[22] W. Niedenzu, D. Gelbwaser-Klimovsky, A. G. Kofman, and G. Kurizki, On the operation of machines powered by quantum non-thermal baths, New J. Phys. **18**, 083012 (2016).

[23] T. Feldmann and R. Kosloff, Quantum four-stroke heat engine: Thermodynamic observables in a model with intrinsic friction, Phys. Rev. E **68**, 016101 (2003).

[24] Y. Rezek and R. Kosloff, Irreversible performance of a quantum harmonic heat engine, New J. Phys. **8**, 83 (2006).

[25] G. T. Landi and M. Paternostro, Irreversible entropy production: From classical to quantum, Rev. Mod. Phys. **93**, 035008 (2021).

[26] A. Levy and R. Kosloff, The local approach to quantum transport may violate the second law of thermodynamics, Europhys. Lett. **107**, 20004 (2014).

[27] F. Barra, The thermodynamic cost of driving quantum systems by their boundaries, Sci. Rep. **5**, 14873 (2015).

[28] P. Strasberg, G. Schaller, T. Brandes, and M. Esposito, Quantum and Information Thermodynamics: A Unifying Framework Based on Repeated Interactions, Phys. Rev. X **7**, 021003 (2017).

[29] G. D. Chiara, G. Landi, A. Hewgill, B. Reid, A. Ferraro, A. J. Roncaglia, and M. Antezza, Reconciliation of quantum local master equations with thermodynamics, New J. Phys. **20**, 113024 (2018).

[30] K. Micadei, J. P. Peterson, A. M. Souza, R. S. Sarthour, I. S. Oliveira, G. T. Landi, T. B. Batalhão, R. M. Serra, and E. Lutz, Reversing the direction of heat flow using quantum correlations, Nat. Commun. **10**, 2456 (2019).

[31] A. Hewgill, G. De Chiara, and A. Imparato, Quantum thermodynamically consistent local master equations, Phys. Rev. Res. **3**, 013165 (2021).

[32] W. Muschik, Phenomenological non-equilibrium quantum thermodynamics based on modified von Neumann equations, arXiv:2211.12558.

[33] J. T. Stockburger and T. Motz, Thermodynamic deficiencies of some simple Lindblad operators, Fortschr. Phys. **65**, 1600067 (2017).

[34] R. Dann and R. Kosloff, Quantum thermo-dynamical construction for driven open quantum systems, Quantum **5**, 590 (2021).

[35] N. Defenu, T. Donner, T. Macrì, G. Pagano, S. Ruffo, and A. Trombettoni, Long-range interacting quantum systems, arXiv:2109.01063.

[36] A. P. Solon, Y. Fily, A. Baskaran, M. E. Cates, Y. Kafri, M. Kardar, and J. Tailleur, Pressure is not a state function for generic active fluids, Nat. Phys. **11**, 673 (2015).

[37] A. P. Solon, J. Stenhammar, M. E. Cates, Y. Kafri, and J. Tailleur, Generalized thermodynamics of phase equilibria in scalar active matter, Phys. Rev. E **97**, 020602(R) (2018).

[38] A. P. Solon, J. Stenhammar, M. E. Cates, Y. Kafri, and J. Tailleur, Generalized thermodynamics of motility-induced phase separation: Phase equilibria, Laplace pressure, and change of ensembles, New J. Phys. **20**, 075001 (2018).

[39] É. Fodor, R. L. Jack, and M. E. Cates, Irreversibility and biased ensembles in active matter: Insights from stochastic thermodynamics, Annu. Rev. Condens. Matter Phys. **13**, 215 (2022).

[40] É. Fodor and M. E. Cates, Active engines: Thermodynamics moves forward, Europhys. Lett. **134**, 10003 (2021).

[41] C. Nardini, E. Fodor, E. Tjhung, F. van Wijland, J. Tailleur, and M. E. Cates, Entropy Production in Field Theories without Time-Reversal Symmetry: Quantifying the Non-Equilibrium Character of Active Matter, Phys. Rev. X **7**, 021007 (2017).

[42] E. Fodor, C. Nardini, M. E. Cates, J. Tailleur, P. Visco, and F. van Wijland, How Far from Equilibrium Is Active Matter? Phys. Rev. Lett. **117**, 038103 (2016).

[43] A. Riera, C. Gogolin, and J. Eisert, Thermalization in Nature and on a Quantum Computer, Phys. Rev. Lett. **108**, 080402 (2012).

[44] T. J. Kippenberg, H. Rokhsari, T. Carmon, A. Scherer, and K. J. Vahala, Analysis of Radiation-Pressure Induced Mechanical Oscillation of an Optical Microcavity, Phys. Rev. Lett. **95**, 033901 (2005).

[45] A. Jayich, J. Sankey, B. Zwickl, C. Yang, J. Thompson, S. Girvin, A. Clerk, F. Marquardt, and J. Harris, Dispersive optomechanics: A membrane inside a cavity, New J. Phys. **10**, 095008 (2008).

[46] M. Aspelmeyer, T. J. Kippenberg, and F. Marquardt, Cavity optomechanics, Rev. Mod. Phys. **86**, 1391 (2014).

[47] V. Dumont, H.-K. Lau, A. A. Clerk, and J. C. Sankey, Asymmetry-Based Quantum Backaction Suppression in Quadratic Optomechanics, Phys. Rev. Lett. **129**, 063604 (2022).

[48] M. Lei, R. Fukumori, J. Rochman, B. Zhu, M. Endres, J. Choi, and A. Faraon, Many-body cavity quantum electrodynamics with driven inhomogeneous emitters, Nature **617**, 271 (2023).

[49] K. Zhang, F. Bariani, and P. Meystre, Quantum Optomechanical Heat Engine, Phys. Rev. Lett. **112**, 150602 (2014).

[50] K. Zhang, F. Bariani, and P. Meystre, Theory of an optomechanical quantum heat engine, Phys. Rev. A **90**, 023819 (2014).

[51] C. Elouard, M. Richard, and A. Auffèves, Reversible work extraction in a hybrid opto-mechanical system, New J. Phys. **17**, 055018 (2015).

[52] D. Gelbwaser-Klimovsky and G. Kurizki, Work extraction from heat-powered quantized optomechanical setups, Sci. Rep. **5**, 7809 (2015).

[53] A. Mari, A. Farace, and V. Giovannetti, Quantum optomechanical piston engines powered by heat, J. Phys. B **48**, 175501 (2015).

[54] M. Brunelli, A. Xuereb, A. Ferraro, G. D. Chiara, N. Kiesel, and M. Paternostro, Out-of-equilibrium thermodynamics of quantum optomechanical systems, New J. Phys. **17**, 035016 (2015).

[55] F. Reif, *Fundamentals of Statistical and Thermal Physics* (Waveland, Long Grove (USA), 2009).

[56] F. Minganti, A. Biella, N. Bartolo, and C. Ciuti, Spectral theory of Liouvillians for dissipative phase transitions, Phys. Rev. A **98**, 042118 (2018).

[57] W. Casteels, R. Fazio, and C. Ciuti, Critical dynamical properties of a first-order dissipative phase transition, Phys. Rev. A **95**, 012128 (2017).

[58] H. J. Carmichael, Breakdown of Photon Blockade: A Dissipative Quantum Phase Transition in Zero Dimensions, Phys. Rev. X **5**, 031028 (2015).

[59] F. Carollo, K. Brandner, and I. Lesanovsky, Nonequilibrium Many-Body Quantum Engine Driven by Time-Translation Symmetry Breaking, Phys. Rev. Lett. **125**, 240602 (2020).

[60] F. Bibak, U. Delić, M. Aspelmeyer, and B. Dakić, Dissipative phase transitions in optomechanical systems, J. Phys. A **107**, 053505 (2023).

[61] F. Wilczek, Quantum Time Crystals, Phys. Rev. Lett. **109**, 160401 (2012).

[62] B. Buča, J. Tindall, and D. Jaksch, Non-stationary coherent quantum many-body dynamics through dissipation, Nat. Commun. **10**, 1730 (2019).

[63] F. Iemini, A. Russomanno, J. Keeling, M. Schirò, M. Dalmonte, and R. Fazio, Boundary Time Crystals, Phys. Rev. Lett. **121**, 035301 (2018).

[64] K. Sacha and J. Zakrzewski, Time crystals: A review, Rep. Prog. Phys. **81**, 016401 (2018).

[65] F. Carollo and I. Lesanovsky, Exactness of Mean-Field Equations for Open Dicke Models with an Application to Pattern Retrieval Dynamics, Phys. Rev. Lett. **126**, 230601 (2021).

[66] P. Bruno, Impossibility of Spontaneously Rotating Time Crystals: A No-Go Theorem, Phys. Rev. Lett. **111**, 070402 (2013).

[67] H. Watanabe and M. Oshikawa, Absence of Quantum Time Crystals, Phys. Rev. Lett. **114**, 251603 (2015).

[68] F. M. Gambetta, W. Li, F. Schmidt-Kaler, and I. Lesanovsky, Engineering Nonbinary Rydberg Interactions via Phonons in an Optical Lattice, Phys. Rev. Lett. **124**, 043402 (2020).

[69] F. Carollo, F. M. Gambetta, K. Brandner, J. P. Garrahan, and I. Lesanovsky, Nonequilibrium Quantum Many-Body Rydberg Atom Engine, Phys. Rev. Lett. **124**, 170602 (2020).

[70] A. Blais, A. L. Grimsmo, S. M. Girvin, and A. Wallraff, Circuit quantum electrodynamics, Rev. Mod. Phys. **93**, 025005 (2021).

[71] E. T. Jaynes and F. W. Cummings, Comparison of quantum and semiclassical radiation theories with application to the beam maser, Proc. IEEE **51**, 89 (1963).

[72] K. Hepp and E. H. Lieb, On the superradiant phase transition for molecules in a quantized radiation field: The Dicke maser model, Ann. Phys. (NY) **76**, 360 (1973).

[73] K. Hepp and E. H. Lieb, Equilibrium statistical mechanics of matter interacting with the quantized radiation field, Phys. Rev. A **8**, 2517 (1973).
[74] H.-P. Breuer and F. Petruccione, *The Theory of Open Quantum Systems* (Oxford University Press, Oxford, 2002).
[75] T. Tomé and M. J. De Oliveira, *Stochastic Dynamics and Irreversibility* (Springer, New York (USA), 2015).
[76] U. Seifert, Stochastic thermodynamics, fluctuation theorems and molecular machines, Rep. Prog. Phys. **75**, 126001 (2012).
[77] F. Marquardt, J. G. E. Harris, and S. M. Girvin, Dynamical Multistability Induced by Radiation Pressure in High-Finesse Micromechanical Optical Cavities, Phys. Rev. Lett. **96**, 103901 (2006).
[78] S. Seah, S. Nimmrichter, and V. Scarani, Work production of quantum rotor engines, New J. Phys. **20**, 043045 (2018).
[79] K. Brandner and U. Seifert, Periodic thermodynamics of open quantum systems, Phys. Rev. E **93**, 062134 (2016).
[80] P. Kirton, M. M. Roses, J. Keeling, and E. G. Dalla Torre, Introduction to the Dicke Model: From Equilibrium to Nonequilibrium, and Vice Versa, Adv. Quantum Technol. **2**, 1800043 (2019).
[81] H. Spohn, Entropy production for quantum dynamical semigroups, J. Math. Phys. **19**, 1227 (1978).
[82] V. Vedral, The role of relative entropy in quantum information theory, Rev. Mod. Phys. **74**, 197 (2002).
[83] A. Tomadin and R. Fazio, Many-body phenomena in QED-cavity arrays, J. Opt. Soc. Am. B **27**, A130 (2010).
[84] F. Piazza and H. Ritsch, Self-Ordered Limit Cycles, Chaos, and Phase Slippage with a Superfluid inside an Optical Resonator, Phys. Rev. Lett. **115**, 163601 (2015).
[85] F. Benatti, F. Carollo, R. Floreanini, and H. Narnhofer, Non-Markovian mesoscopic dissipative dynamics of open quantum spin chains, Phys. Lett. A **380**, 381 (2016).
[86] F. Benatti, F. Carollo, R. Floreanini, and H. Narnhofer, Quantum spin chain dissipative mean-field dynamics, J. Phys. A **51**, 325001 (2018).
[87] F. Carollo and I. Lesanovsky, Exact solution of a boundary time-crystal phase transition: Time-translation symmetry breaking and non-Markovian dynamics of correlations, Phys. Rev. A **105**, L040202 (2022).
[88] E. Verhagen, S. Deléglise, S. Weis, A. Schliesser, and T. J. Kippenberg, Quantum-coherent coupling of a mechanical oscillator to an optical cavity mode, Nature (London) **482**, 63 (2012).
[89] M. Maldovan and E. L. Thomas, Simultaneous localization of photons and phonons in two-dimensional periodic structures, Appl. Phys. Lett. **88**, 251907 (2006).
[90] M. Eichenfield, R. Camacho, J. Chan, K. J. Vahala, and O. Painter, A picogram- and nanometre-scale photonic-crystal optomechanical cavity, Nature (London) **459**, 550 (2009).
[91] P. Bertet, S. Osnaghi, P. Milman, A. Auffeves, P. Maioli, M. Brune, J. M. Raimond, and S. Haroche, Generating and Probing a Two-Photon Fock State with a Single Atom in a Cavity, Phys. Rev. Lett. **88**, 143601 (2002).
[92] A. Frisk Kockum, A. Miranowicz, S. De Liberato, S. Savasta, and F. Nori, Ultrastrong coupling between light and matter, Nat. Rev. Phys. **1**, 19 (2019).
[93] A. Camacho-Guardian and N. R. Cooper, Moiré-Induced Optical Nonlinearities: Single- and Multiphoton Resonances, Phys. Rev. Lett. **128**, 207401 (2022).

Second publication

Large Deviation Full Counting Statistics in Adiabatic Open Quantum Dynamics

Paulo J. Paulino,[1,*] Igor Lesanovsky,[1,2] and Federico Carollo[1]
[1]Institut für Theoretische Physik, Eberhard Karls Universität Tübingen, Auf der Morgenstelle 14, 72076 Tübingen, Germany
[2]School of Physics and Astronomy and Centre for the Mathematics and Theoretical Physics of Quantum Non-Equilibrium Systems, The University of Nottingham, Nottingham NG7 2RD, United Kingdom

(Received 2 February 2024; accepted 21 May 2024; published 28 June 2024)

The state of an open quantum system undergoing an adiabatic process evolves by following the instantaneous stationary state of its time-dependent generator. This observation allows one to characterize, for a generic adiabatic evolution, the average dynamics of the open system. However, information about fluctuations of dynamical observables, such as the number of photons emitted or the time-integrated stochastic entropy production in single experimental runs, requires controlling the whole spectrum of the generator and not only the stationary state. Here, we show how such information can be obtained in adiabatic open quantum dynamics by exploiting tools from large deviation theory. We prove an adiabatic theorem for deformed generators, which allows us to encode, in a biased quantum state, the full counting statistics of generic time-integrated dynamical observables. We further compute the probability associated with an arbitrary "rare" time history of the observable and derive a dynamics which realizes it in its typical behavior. Our results provide a way to characterize and engineer adiabatic open quantum dynamics and to control their fluctuations.

DOI: 10.1103/PhysRevLett.132.260402

Introduction.—Systems evolving adiabatically, i.e., via slow driving protocols, find many applications in physics. In closed quantum systems, adiabatic dynamics are characterized by the decoupled evolution of the Hamiltonian eigenvectors [1–10], which is crucial for adiabatic quantum computation [11–15] and important experimental protocols such as stimulated Raman adiabatic passage [16]. The presence of decoherence and dissipation typically imposes a fundamental timescale in which this decoupled evolution can be observed [17–21], as explored in the context of optimal control [22–25] and of noisy quantum computation [26,27]. Nevertheless, genuine adiabatic dynamics in open quantum systems occur when the state of the system follows the instantaneous stationary state of its dynamical generator [28–33], as is the case for quasistatic thermodynamic processes [34–37].

Single realizations of open quantum dynamics, or quantum trajectories, are stochastic [38,39], which can manifest in the occurrence of quantum jumps, for instance related to photon emissions [40–45]. For Markovian dynamics, the full counting statistics of jump-related observables, such as entropy production currents [44,46,47], can be obtained using deformed dynamical generators, introduced within the framework of large deviation theory [48–61]. However, much less is known about the characterization of dynamical fluctuations in open quantum dynamics with time-dependent generators [62–64], including the case of adiabatic processes.

In this Letter, we show how to fully characterize the counting statistics of jump-related observables in adiabatic open quantum dynamics in which the system follows the instantaneous stationary state of the dynamical generator [cf. Fig. 1(a)]. We prove an adiabatic theorem for deformed dynamical generators [57,59], which allows us to demonstrate that, in these processes, the statistics of time-integrated observables assumes a large deviation form [48]. Furthermore, we show that adiabatic open quantum dynamics obey a so-called temporal additivity principle [65–68]. That is, the observables follow an instantaneous large deviation principle at all times [cf. Figs. 1(b) and 1(c)]. This fact opens up the possibility of deriving the probability of any time history of the observable, see sketch in Figs. 1(b) and 1(c). Such a probability provides a higher level of description of dynamical fluctuations in the adiabatic process than what can be obtained from the full counting statistics of time-integrated observables. The latter can indeed be obtained from the former through a contraction principle [48], [cf. Fig. 1(c)]. Finally, we construct an auxiliary dynamics [57,59,69] which can realize, as typical realization, any rare realization of the observable time history in the original adiabatic process. Our findings (see Refs. [65–67,70–79] for related results in classical dynamics) shed new insights on open quantum adiabatic processes and provide a powerful approach to control, even as a function of time, their fluctuating properties. Our methods can be used for studying fluctuations in adiabatic quantum machines [43,80,81], both in or out of equilibrium, or for dissipative quantum computation [82–85].

Open quantum dynamics.—We consider quantum systems whose dynamics is described by the master equation $\dot{\rho}(t) = \mathcal{L}(t)[\rho(t)]$, with time-dependent generator

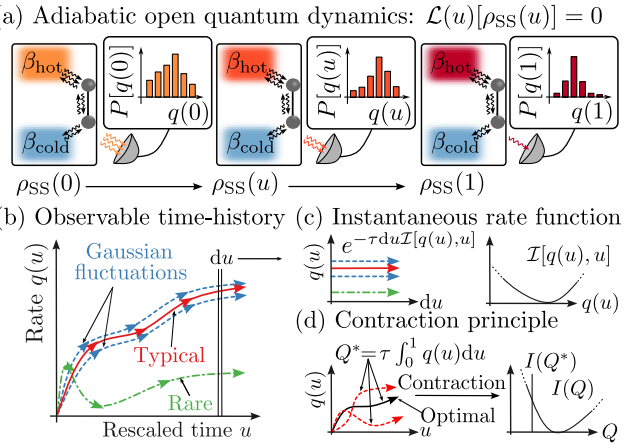

FIG. 1. Adiabatic open quantum dynamics and large deviations. (a) During an adiabatic dynamics (total evolution time τ), the system is described by the instantaneous steady state $\rho_{SS}(u)$ of the dynamical generator $\mathcal{L}(u)$, in the slow rescaled timescale $u = t/\tau$. (b) Sketch of different time histories of the instantaneous "rate" $q(u)$ of an observable of interest, e.g., the instantaneous photonemission rate. We highlight the *typical* time history, two with small Gaussian fluctuations and a rare one displaying a *large deviation* from the typical value. (c) Because of the slow dynamics, the system spends a large amount of time in each rescaled time interval du. This implies that the probability function for each instantaneous rate $q(u)$ [see illustration in panel (a)] obeys a large deviation principle. Combining them provides the probability functional for time histories of the observable. (d) The full counting statistics of the time-integrated observable, $Q(\tau) = \tau \int_0^1 du\, q(u)$, can be obtained from the optimal, i.e., most likely, trajectories providing the values of $Q(\tau) = Q^*$.

$$\mathcal{L}(t)[\rho] = -i[\tilde{H}(t)\rho - \rho\tilde{H}^\dagger(t)] + \sum_j \mathcal{J}_j(t)[\rho]. \quad (1)$$

Here, $\tilde{H}(t) = H(t) - (i/2)\sum_j J_j^\dagger(t)J_j(t)$ is the effective Hamiltonian [39], $\mathcal{J}_j(t)[\rho] = J_j(t)\rho J_j^\dagger(t)$, with $J_j(t)$ being the jump operators. The above equation generates the evolution of the system state $\rho(t)$ averaged over all possible realizations of the system-environment interaction [17,38]. Single dynamical realizations are instead described by quantum jump trajectories [57,59,86], generated by the stochastic process

$$d\psi(t) = \mathcal{B}(t)[\psi(t)]dt + \sum_j \left(\frac{\mathcal{J}_j(t)[\psi(t)]}{\mathrm{Tr}(\mathcal{J}_j(t)[\psi(t)])} - \psi(t)\right) dn_j(t), \quad (2)$$

which evolves pure quantum states $\psi = |\psi\rangle\langle\psi|$. Here, $d\psi(t)$ is the state increment while $dn_j(t)$ are Poisson increments, which can only take the value 0 or 1 with average value $\mathbb{E}_{\psi(t)=\psi}[dn_j(t)] = dt\mathrm{Tr}(\mathcal{J}_j(t)[\psi])$ [17,38], where $\mathbb{E}_{\psi(t)=\psi}$ denotes the expectation over the process conditional to the system being in ψ at time t. When a Poisson increment is equal to 1, the state undergoes a jump associated with the corresponding $\mathcal{J}_j(t)$. When all increments are zero, the system evolves continuously through the map

$$\mathcal{B}(t)[\psi] = -i\tilde{H}(t)\psi + i\psi\tilde{H}^\dagger(t) - \psi\mathrm{Tr}[-i\tilde{H}(t)\psi + i\psi\tilde{H}^\dagger(t)].$$

A generic time-integrated observable associated with quantum-jump events can thus be defined as

$$Q(t) = \sum_j \int_0^t f_j(v)dn_j(v). \quad (3)$$

When $f_j(v) = 1\ \forall\ j$, $Q(t)$ equals the total number of jumps occurred during a trajectory. For other choices, it is instead related to, for instance, stochastic heat or entropy production in thermal machines [43,44,47,87,88]. To characterize the properties of this observable, it is convenient to work with its moment generating function, defined as $Z_s(t) = \mathbb{E}[e^{-sQ(t)}]$ through the field s, which is conjugate to the observable. As shown in Supplemental Material (SM) [89], the moment generating function can be computed as $Z_s(t) = \mathrm{Tr}[\rho_s(t)]$, where $\dot{\rho}_s(t) = \mathcal{L}_s(t)[\rho_s(t)]$ and with $\mathcal{L}_s(t)$ being the deformed dynamical generator [57,90]

$$\mathcal{L}_s(t)[\rho] = \mathcal{L}(t)[\rho] + \sum_j (e^{-sf_j(t)} - 1)\mathcal{J}_j(t)[\rho]. \quad (4)$$

For time-independent deformed generators and large evolution times τ, $Z_s(\tau)$ obeys a large deviation principle, $Z_s(\tau) \approx e^{\tau\theta_s}$ with θ_s being the scaled cumulant generating function of $Q(\tau)$. In such a time-independent framework, θ_s coincides with the dominant eigenvalue of $\mathcal{L}_s$ [48,57] and fully characterizes the probability $P[Q(\tau) = Q^*]$. This also takes a large deviation form $P[Q(\tau) = Q^*] \approx e^{-\tau I(Q^*/\tau)}$, with rate function given by the Legendre-Fenchel transform $I(x) = \sup_{s\in\mathbb{R}}\{-sx - \theta_s\}$ [48]. In what follows, we derive the behavior of $Z_s(\tau)$ for the case of adiabatic open quantum dynamics. To this end, we consider that $\dot{Z}_s(t) = \mathrm{Tr}\{\mathcal{L}_s(t)[\varrho_s(t)]\}Z_s(t)$, where $\varrho_s(t) = \rho_s(t)/\mathrm{Tr}[\rho_s(t)]$, which we can use to express the moment generating function as

$$Z_s(\tau) = e^{\int_0^\tau \mathrm{Tr}(\mathcal{L}_s(t)[\varrho_s(t)])dt}. \quad (5)$$

As we show below, this expression allows us to write θ_s in terms of the instantaneous dominant eigenvalues of $\mathcal{L}_s(t)$.

Adiabatic theorem for deformed generators.—We consider $\mathcal{L}_s(t)$ to vary on the slow timescale $u = t/\tau$, with τ being the total evolution time and we assume it to be diagonalizable with right and left eigenmatrices, $r_s^m(t)$ and $\ell_s^m(t)$. These are such that $\mathcal{L}_s(t)[r_s^m(t)] = \lambda_s^m(t)r_s^m(t)$ and $\mathcal{L}_s^*(t)[\ell_s^m(t)] = \lambda_s^m(t)\ell_s^m(t)$, where $\lambda_s^m(t)$ are the

instantaneous eigenvalues of $\mathcal{L}_s(t)$ and $\mathcal{L}_s^*(t)$ is the dual generator acting on operators. We consider the dominant eigenvalue $\lambda_s^0(t)$ to be unique (and thus real), so that $\lambda_s^0(t) > \mathrm{Re}\{\lambda_s^m(t)\}$, for $m \geq 1$. With these definitions, our adiabatic condition reads (C1) $\|\dot{r}_s^m(t)\|, \|\dot{\ell}_s^m(t)\|, |\dot{\lambda}_s^m(t)| \sim 1/\tau$, encoding that the generator varies slowly for large τ. Our second assumption is related to the uniqueness of the dominant eigenvalue $\lambda_s^0(t)$ and is conveniently expressed as the existence of a finite gap Δ for all times: (C2) $\Delta := \inf_{m>0,\ \forall\ t}\{|\lambda_s^0(t) - \mathrm{Re}\{\lambda_s^m(t)\}|\} > 0$.

Given the two assumptions above, we prove in the SM [89] that, within the rescaled slow timescale $u = t/\tau$,

$$\lim_{\tau\to\infty} \varrho_s(u) = r_s^0(u), \qquad 0 < u \leq 1. \tag{6}$$

Note that, with a slight abuse of notation we denote the dependence on the slow timescale u in the same way as that on the original timescale t. Equation (6) shows that under the evolution with the deformed dynamical generator the normalized state $\varrho_s(u)$ follows the path of the instantaneous dominant right eigenmatrix of $\mathcal{L}_s(t)$. This result thus extends the adiabatic theorem for open quantum systems [28–33] to deformed dynamical generators and includes, for $s = 0$, the case of completely generic open quantum dynamics satisfying conditions (C1)–(C2). Importantly, controlling the evolution of the state under the deformed dynamical generator, as in our result, does only provide information about the stationary state ($s = 0$ case) as in usual adiabatic theorems, but also encodes, in a nontrivial way, some information (for $s \neq 0$) about the spectrum of excitations of the generator of the adiabatic open quantum dynamics. Furthermore, our approach allows us to establish that Eq. (6) holds, for both $s = 0$ and $s \neq 0$, irrespectively of the initial state of the system.

As a consequence of Eq. (6), the moment generating function $Z_s(\tau)$ in Eq. (5) obeys a large deviation principle, in the limit $\tau \to \infty$, with scaled cumulant generating function given by

$$\theta_s^{\mathrm{ad}} = \int_0^1 \lambda_s^0(u)\mathrm{d}u. \tag{7}$$

As such, the statistics of $Q(\tau)$ also obeys a large deviation principle [48], characterized by the function $I(Q/\tau)$, obtained as the Legendre-Fenchel transform of θ_s^{ad}. Interestingly, Eq. (7) remains valid also in the case of degenerate dominant eigenvalues $\lambda_s^0(u)$ [89].

To benchmark these results, we consider a resonantly driven two-level atom, with excited state $|e\rangle$, ground state $|g\rangle$ and Hamiltonian $H(t) = \Omega(t/\tau)(\sigma_+ + \sigma_-)$, where we defined $\sigma_- = \sigma_+^\dagger = |g\rangle\langle e|$. We assume $\Omega(u) = \Omega_0 \cos(u\pi)$ for $u < 1/2$ and $\Omega_0 \sin(u\pi)$ for $u \geq 1/2$. The atom emits photons, which is described by the jump operator $J = \sqrt{\gamma}\sigma_-$, where γ is the emission rate. We focus on the activity, i.e., the total number of quantum jumps, $A(\tau) = \int_0^\tau \mathrm{d}n(t)$ [57]. Figure 2(a) shows the time-averaged fidelity between $r_s^0(u)$ and $\varrho_s(u)$ as a function of the total time τ. The inset displays the fidelity as a function of the rescaled time u, for increasing τ. The results confirm our theorem as well as the convergence of the scaled cumulant generating function to the one in Eq. (7), as $\tau \to \infty$ [see Fig. 2(b)]. They further show that our findings remain valid in the case of piecewise-differentiable dynamical parameters.

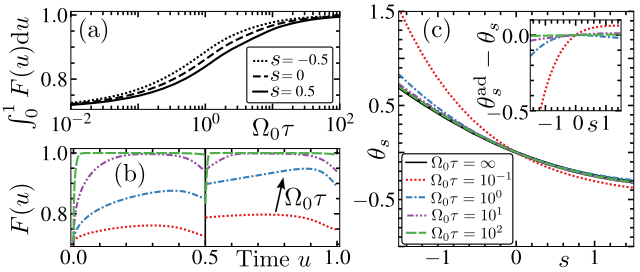

FIG. 2. Driven two-level atom. (a) Time-integrated fidelity $\int_0^1 F(u)\mathrm{d}u$, with $F(u) = \mathrm{Tr}(\sqrt{\varrho_s^{1/2}(u) r_s^0(u) \varrho_s^{1/2}(u)})$, for $s = -0.5$ (dotted line), $s = 0$ (dashed line), and $s = 0.5$ (solid line). (b) The instantaneous fidelity $F(u)$ for different values of $\Omega_0\tau$, see legend in panel (c). The parameters are $\Omega_0 = \gamma$ and $s = -0.5$. (c) Scaled cumulant generating function for the activity. The black solid line corresponds to θ_s^{ad}, while the other lines give the function θ_s for different values of $\Omega_0\tau$. The inset shows how θ_s approaches θ_s^{ad} as $\Omega_0\tau$ is increased.

Time history of the observable.—The scaled cumulant generating function in Eq. (7), together with its Legendre-Fenchel transform, characterizes the time-integrated observable $Q(\tau)$ during an adiabatic process. However, it is also relevant to characterize the probability of the different time histories of the observable [cf. Fig. 1(b)] realizing different values of $Q(\tau)$. To arrive at such a higher level of description of the process, we observe that, due to the adiabatic nature of the open quantum dynamics, the system spends an infinite amount of time in each of the infinitesimal (rescaled) time intervals $\mathrm{d}u$. For each $\mathrm{d}u$, it is possible to define a coarse-grained instantaneous rate $q(u)$, representing the time-averaged value of the observable at the rescaled time u (see Ref. [89] for details). We can thus write $Q(\tau) = \tau \int_0^1 q(u)\mathrm{d}u$, where $\{q(u)\}$ is a (stochastic) time history of the observable rate, as illustrated in Fig. 1(b). Discretizing time and considering that each $q(u)$ obeys an independent large deviation principle, we have that the probability over time histories is given by $P[\{q(u)\}] \approx \prod_u P[q(u)]$ and, in the continuous-time limit, with $\tau \to \infty$,

$$P[\{q(u)\}] \approx e^{-\tau\varphi[\{q(u)\}]}, \qquad \varphi[\{q(u)\}] = \int_0^1 \mathcal{I}[q(u), u]\mathrm{d}u, \tag{8}$$

where $\mathcal{I}[q(u), u]$ is the instantaneous large deviation function of $q(u)$, i.e., the Legendre-Fenchel transform of $\lambda_s^0(u)$

[91]. From a physical perspective, we expect time histories $\{q(u)\}$ to be sufficiently regular, e.g., piecewise analytic functions of time. Essentially, this shows that adiabatic open quantum dynamics obey the so-called temporal additivity principle introduced in Ref. [65]. (See SM for the formal proof [89]).

The functional in Eq. (8) contains the full information about time histories of the observable rate $\{q(u)\}$ and, thus, a complete description of fluctuations at the rescaled timescale u. The typical time history is the one minimizing the functional φ, that is, the one passing through the minima of the instantaneous rate functions $\mathcal{I}[q(u),u]$. The functional φ can further be used to derive the statistics of any observable constructed from the time history $\{q(u)\}$. An example is again the time-integrated observable $Q(\tau)$, whose functional I can be retrieved, via a contraction principle [48], as

$$I(x) = \inf_{\forall\ \{q(u)\}:\ x=\int_0^1 q(u)\mathrm{d}u} \varphi[\{q(u)\}]. \tag{9}$$

Physically, this means that the probability of observing $Q = Q^*$ is equal to the probability of the most likely time history $\{q^*(u)\}$ providing value of the time-integrated observable [cf. Fig. 1(d)].

While the general derivation of the contraction in Eq. (9) is provided in SM [89], we discuss it here using the example of the two-level atom, setting for convenience $\gamma(u) = 4\Omega(u)$ [57]. In this case, we find $\lambda_s^0(u) = 2\Omega(u)(e^{-s/3}-1)$ and $\mathcal{I}[a(u),u] = 3\{a(u)\log[a(u)/a_0(u)] - [a(u)-a_0(u)]\}$, where $a_0(u) = (2/3)\Omega(u)$ is the typical time history of the activity rate. To compute the minimization in Eq. (9), we perform a functional derivative and set it to zero. This results in $a^*(u) = a_0(u)e^{-\mu/3}$ where μ is a Lagrange multiplier introduced to enforce the constraint in Eq. (9). Integrating $a^*(u)$ over time, we find $A^* = A_0 e^{-\mu/3}$ which fixes the Lagrange multiplier to $\mu^* = 3\log(A_0/A^*)$ with A_0 being the typical value of the time-integrated observable $A(\tau)$. Substituting this information into the functional φ [cf. Eq. (8)], we find $I(A^*/\tau) = 3[(A^*/\tau)\log A^*/A_0 - (A^*-A_0)/\tau]$, which is the same result one gets by calculating the Legendre transform of θ_s^{ad} given in Eq. (7) [57].

The functional φ is formally derived as the Legendre-Fenchel transform of the scaled cumulant generating "functional" $\Theta[\{s(u)\}]$, associated with a time dependent field $s(u)$ [89]. The function $\Theta[\{s(u)\}]$ is obtained as in Eq. (7) from the eigenvalues of the deformed operator in Eq. (4) defined with a time-dependent $s(u)$. The knowledge of such a deformed operator gives us a handle to manipulate on-demand time histories of the observable: by choosing $s^*(u)$ such that $-\delta\Theta[\{s^*(u)\}]/\delta s^*(u) = q^*(u)$, we can indeed define a suitable open quantum dynamics which produces, as typical, the rare time history $\{q^*(u)\}$ of the original process [57,59,69]. Such an auxiliary dynamics is given by [89]

$$H^{\mathrm{A}}(u) = \frac{1}{2}\left\{\left[\ell^0_{s^*(u)}(u)\right]^{1/2}\tilde{H}(u)\left[\ell^0_{s^*(u)}(u)\right]^{-1/2} + \mathrm{H.c.}\right\},$$
$$J_j^{\mathrm{A}}(u) = e^{-\frac{s^*(u)}{2}f(u)}\left[\ell^0_{s^*(u)}(u)\right]^{1/2} J_j(u)\left[\ell^0_{s^*(u)}(u)\right]^{-1/2}, \tag{10}$$

where $\ell^0_{s^*(u)}(u)$ is the dominant left eigenmatrix of the deformed operator with time-dependent field $s^*(u)$.

Applications.—As a first application, we consider a system composed by two two-level atoms attached to different thermal baths. The system Hamiltonian is $H = \omega(\sigma_e^{\mathrm{hot}} + \sigma_e^{\mathrm{cold}}) + \Omega(\sigma_-^{\mathrm{hot}}\sigma_+^{\mathrm{cold}} + \mathrm{H.c.})$, with $\sigma_e = |e\rangle\langle e|$ and where the superscripts hot and cold indicate the atom in contact with the corresponding thermal reservoir. The dynamics is governed by a time-dependent Lindblad generator derived via a weak coupling of the system with the thermal baths [17,89]. The jump operators thus read $J_{ij}^b = \sqrt{\gamma}\sqrt{(\omega_{ji}/\omega)^3 N_b(\omega_{ji})}|\epsilon_i\rangle\langle\epsilon_j|$, where b indexes the baths, γ is a rate, $N_b(\omega) = 1/(e^{\beta_b\omega}-1)$, and $\omega_{ij} = \epsilon_j - \epsilon_i$ is the difference between the energies of the eigenstates $|\epsilon_j\rangle$ and $|\epsilon_i\rangle$ of H [17]. They implement transitions between the eigenstates $|\epsilon_i\rangle$ and $|\epsilon_j\rangle$ of H. In addition, we include a phenomenological laser driving term, $H_{\mathrm{laser}} = g(\sigma_x^{\mathrm{hot}} + \sigma_x^{\mathrm{cold}})$ [92–94]. The entropy production associated with any quantum jump in the dynamics is defined as the energy exchanged with the corresponding thermal bath responsible for the transition, $\pm\Delta\sigma_{ij}^b = \pm\omega_{ij}\beta_b$ [43,44,47]. The time-integrated entropy flow from the hot bath to the cold one can thus be defined as $\Sigma(\tau) = \sum_{i,j,b}\int_0^\tau \beta_b(t)\omega_{ij}\mathrm{d}n_{ij}^b(t)$, where $\mathrm{d}n_{ij}^b$ are the increments associated with the different jump operators [47]. The inverse temperature of the hot bath follows the protocol $\beta_{\mathrm{hot}}(t) = \beta_{\mathrm{hot}}^0/[1+(1/2)\sin^2(t\pi/\tau)]$.

Figure 3(a) shows the instantaneous rate function for the stochastic entropy current, which displays a symmetry [95,96] related to the existence of entropy fluctuation relations at all times t [see inset of Fig. 3(a)]. Figure 3(a), also provides numerical results from quantum trajectories for both the original dynamics and an auxiliary one displaying a rare realization of the observables. We note that this analysis can be extended to other quantities, such as stochastic heat and work [88,97,98].

We then consider a three-level system, with basis states $|0\rangle, |1\rangle, |2\rangle$, and time-dependent Hamiltonian $H(t) = \Omega_1(t)|0\rangle\langle 1| + \Omega_2|0\rangle\langle 2| + \mathrm{H.c.}$ The system is subject to decay from state $|1\rangle$ to $|0\rangle$, described by the jump operator $J = \sqrt{\gamma}|0\rangle\langle 1|$. Such a system can be interpreted as a nonequilibrium quantum machine [94]. It can be readily realized in experiments [99] and may find application as a microscopic engine [100,101].

For this three-level system, we consider the activity $A(\tau) = \int_0^\tau \mathrm{d}n(t)$, which is equivalent (up to the rate γ) to the heat dissipated into the environment. We further consider

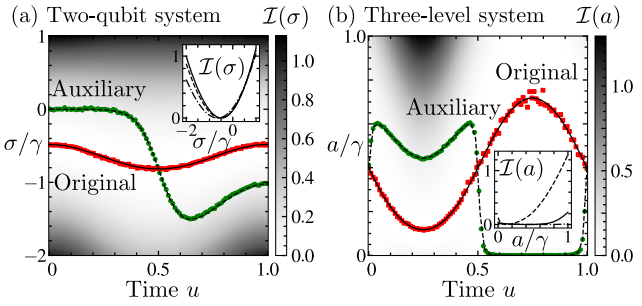

FIG. 3. Stochastic entropy production and heat fluctuations. (a), (b) Instantaneous rate function $\mathcal{I}$ as a function of time for the stochastic entropy production $[\sigma(u)]$ and the heat (proportional to the activity) rates $[a(u)]$ for the two-atom and the three-level systems, respectively. The black solid line shows the typical time history while the dashed line a rare one. Red squares are estimates obtained by running a quantum trajectory evaluated at $s = 0$, while the green bullets a quantum trajectory with the auxiliary system in Eq. (10), for $s(u) = (1/2)\tanh(10u - 5)$ in panel (a) and $s(u) = -\sin(2\pi u)$ in panel (b). The total evolution for (a) and (b) are, respectively, $\gamma\tau = 2 \times 10^6$ and $\gamma\tau = 5 \times 10^6$. Both insets show the instantaneous rate function for $u = 0$ (solid line), $u = 1/4$ (dashed line), and the dot-dashed line for (a) represents $u = 1/2$ while for (b) $u = 3/4$. The parameters for (a) are $g = 2\Omega = \omega = \gamma$ and the temperatures are $\beta^0_{\rm hot} = \beta_{\rm cold}/2 = 1$, in units of $1/\omega$. For panel (b), $10\Omega_2 = \gamma/4 = \Omega^0_1$.

$\Omega_1(t) = \Omega^0_1[1 - \sin(2\pi t/\tau)/2]$. Typical trajectories of the system feature coexistence between an active phase (frequent emissions) and an inactive one (no emissions) [57,99,102]. As such, the instantaneous rate function of the activity shows a broad minimum associated with very large fluctuations, which can also be observed in a single realization of the quantum dynamics [see red squares in Fig. 3(b)]. We then bias the system dynamics in a way that it is found in the active phase for $u < 1/2$ and in the inactive one for $u \geq 1/2$. In this case, the total dissipated heat is essentially determined by the emissions during the active phase. This simple example highlights the importance of investigating fluctuations of thermodynamic quantities in quantum machines as well as of controlling their full time history beyond the global time-integrated value.

Discussion.—We have derived a complete statistical characterization for open quantum systems in the adiabatic regime. Our analysis can be extended to different quantum stochastic processes, such as diffusive quantum trajectories associated with homodyne-detection experiments [103]. It would be interesting to explore whether the auxiliary quantum dynamics derived here can be exploited to control the performance of (adiabatic) quantum machines [104–106]. With regard to applications in adiabatic quantum computing [21,107], it would be important to generalize our analysis to characterize the full counting statistics of state-dependent observables [50], such as the fidelity. This would require the application of numerical schemes as in Ref. [108] or the derivation of a level 2.5 formalism for adiabatic open quantum dynamics [50,109]. Full counting statistics find applications in quantum sensing and interferometry [110–113]. Our results may thus allow for novel protocols for sensing critical values of dynamical parameters by detecting sudden changes, during an adiabatic evolution, of the statistics of emission related observables.

The codes used to produce the numerical results of this Letter are available on Zenodo [114].

We are grateful to Stefan Teufel and Tom Wessel for useful discussions on adiabatic theorems and to Robert L. Jack for drawing our attention to related literature. We acknowledge funding from the Deutsche Forschungsgemeinschaft (DFG, German Research Foundation) under Project No. 435696605 and through the Research Units FOR 5413/1, Grant No. 465199066 and FOR 5522/1, Grant No. 499180199. This project has also received funding from the European Union's Horizon Europe research and innovation program under Grant Agreement No. 101046968 (BRISQ). F. C. is indebted to the Baden-Württemberg Stiftung for the financial support of this research project by the Eliteprogramme for Postdocs.

*paulo.paulino.souza96@gmail.com

[1] M. Born and V. Fock, Beweis des adiabatensatzes, Z. Phys. **51**, 165 (1928).
[2] T. Kato, On the adiabatic theorem of quantum mechanics, J. Phys. Soc. Jpn. **5**, 435 (1950).
[3] L. E. Ballentine, *Quantum Mechanics: A Modern Development* (World Scientific, Singapore, 2014).
[4] M. S. Sarandy, L.-A. Wu, and D. A. Lidar, Consistency of the adiabatic theorem, Quantum Inf. Process. **3**, 331 (2004).
[5] D. M. Tong, Quantitative condition is necessary in guaranteeing the validity of the adiabatic approximation, Phys. Rev. Lett. **104**, 120401 (2010).
[6] M. V. Berry, Quantal phase factors accompanying adiabatic changes, Proc. R. Soc. A **392**, 45 (1984).
[7] D. Xiao, M.-C. Chang, and Q. Niu, Berry phase effects on electronic properties, Rev. Mod. Phys. **82**, 1959 (2010).
[8] A. Shapere and F. Wilczek, *Geometric Phases in Physics* (World Scientific, Singapore, 1989), Vol. 5.
[9] S. Teufel, *Adiabatic Perturbation Theory in Quantum Dynamics*, Lecture Notes in Mathematics (Springer, New York, 2003).
[10] S. Teufel, Non-equilibrium almost-stationary states and linear response for gapped quantum systems, Commun. Math. Phys. **373**, 621 (2020).
[11] T. Albash and D. A. Lidar, Adiabatic quantum computation, Rev. Mod. Phys. **90**, 015002 (2018).
[12] J. Roland and N. J. Cerf, Quantum search by local adiabatic evolution, Phys. Rev. A **65**, 042308 (2002).
[13] E. Farhi and S. Gutmann, Analog analogue of a digital quantum computation, Phys. Rev. A **57**, 2403 (1998).
[14] A. Mizel, D. A. Lidar, and M. Mitchell, Simple proof of equivalence between adiabatic quantum computation and the circuit model, Phys. Rev. Lett. **99**, 070502 (2007).

[15] D. M. Tong, K. Singh, L. C. Kwek, and C. H. Oh, Sufficiency criterion for the validity of the adiabatic approximation, Phys. Rev. Lett. **98**, 150402 (2007).
[16] N. V. Vitanov, A. A. Rangelov, B. W. Shore, and K. Bergmann, Stimulated raman adiabatic passage in physics, chemistry, and beyond, Rev. Mod. Phys. **89**, 015006 (2017).
[17] H.-P. Breuer and F. Petruccione, *The Theory of Open Quantum Systems* (Oxford University Press on Demand, New York, 2002).
[18] T. Albash, S. Boixo, D. A. Lidar, and P. Zanardi, Quantum adiabatic Markovian master equations, New J. Phys. **14**, 123016 (2012).
[19] M. S. Sarandy and D. A. Lidar, Adiabatic approximation in open quantum systems, Phys. Rev. A **71**, 012331 (2005).
[20] X. Yi, D. Tong, L. Kwek, and C. Oh, Adiabatic approximation in open systems: An alternative approach, J. Phys. B **40**, 281 (2007).
[21] M. S. Sarandy and D. A. Lidar, Adiabatic quantum computation in open systems, Phys. Rev. Lett. **95**, 250503 (2005).
[22] S. Alipour, A. Chenu, A. T. Rezakhani, and A. del Campo, Shortcuts to adiabaticity in driven open quantum systems: Balanced gain and loss and non-Markovian evolution, Quantum **4**, 336 (2020).
[23] Z. Yin, C. Li, J. Allcock, Y. Zheng, X. Gu, M. Dai, S. Zhang, and S. An, Shortcuts to adiabaticity for open systems in circuit quantum electrodynamics, Nat. Commun. **13**, 188 (2022).
[24] A. C. Santos and M. S. Sarandy, Generalized transitionless quantum driving for open quantum systems, Phys. Rev. A **104**, 062421 (2021).
[25] A. C. Santos, C. J. Villas-Boas, and R. Bachelard, Quantum adiabatic brachistochrone for open systems, Phys. Rev. A **103**, 012206 (2021).
[26] M. H. S. Amin, P. J. Love, and C. J. S. Truncik, Thermally assisted adiabatic quantum computation, Phys. Rev. Lett. **100**, 060503 (2008).
[27] C.-K. Hu, A. C. Santos, J.-M. Cui, Y.-F. Huang, M. S. Sarandy, C.-F. Li, and G.-C. Guo, Adiabatic quantum dynamics under decoherence in a controllable trapped-ion setup, Phys. Rev. A **99**, 062320 (2019).
[28] E. B. Davies and H. Spohn, Open quantum systems with time-dependent Hamiltonians and their linear response, J. Stat. Phys. **19**, 511 (1978).
[29] J. E. Avron, M. Fraas, G. M. Graf, and P. Grech, Adiabatic theorems for generators of contracting evolutions, Commun. Math. Phys. **314**, 163 (2012).
[30] J. E. Avron, M. Fraas, and G. M. Graf, Adiabatic response for Lindblad dynamics, J. Stat. Phys. **148**, 800 (2012).
[31] L. C. Venuti, T. Albash, D. A. Lidar, and P. Zanardi, Adiabaticity in open quantum systems, Phys. Rev. A **93**, 032118 (2016).
[32] V. Cavina, A. Mari, and V. Giovannetti, Slow dynamics and thermodynamics of open quantum systems, Phys. Rev. Lett. **119**, 050601 (2017).
[33] L. C. Venuti, T. Albash, M. Marvian, D. Lidar, and P. Zanardi, Relaxation versus adiabatic quantum steady-state preparation, Phys. Rev. A **95**, 042302 (2017).
[34] H. B. Callen, *Thermodynamics and an Introduction to Thermostatistics* (John Wiley, New York, 1985).
[35] S. Deffner and S. Campbell, *Quantum Thermodynamics* (Morgan & Claypool Publishers, San Rafael, 2019).
[36] A. Bérut, A. Arakelyan, A. Petrosyan, S. Ciliberto, R. Dillenschneider, and E. Lutz, Experimental verification of Landauer's principle linking information and thermodynamics, Nature (London) **483**, 187 (2012).
[37] C. K. Hu, A. C. Santos, J. M. Cui, J. Jing, L. C. Kwek, and X. B. Wang, Quantum thermodynamics in adiabatic open systems and its trapped-ion experimental realization, npj Quantum Inf. **6**, 73 (2020).
[38] H. M. Wiseman and G. J. Milburn, *Quantum Measurement and Control* (Cambridge University Press, Cambridge, England, 2009).
[39] M. B. Plenio and P. L. Knight, The quantum-jump approach to dissipative dynamics in quantum optics, Rev. Mod. Phys. **70**, 101 (1998).
[40] F. Minganti, A. Biella, N. Bartolo, and C. Ciuti, Spectral theory of Liouvillians for dissipative phase transitions, Phys. Rev. A **98**, 042118 (2018).
[41] C. Guerlin, J. Bernu, S. Deléglise, C. Sayrin, S. Gleyzes, S. Kuhr, M. Brune, J.-M. Raimond, and S. Haroche, Progressive field-state collapse and quantum non-demolition photon counting, Nature (London) **448**, 889 (2007).
[42] K. W. Yip, T. Albash, and D. A. Lidar, Quantum trajectories for time-dependent adiabatic master equations, Phys. Rev. A **97**, 022116 (2018).
[43] P. Menczel, C. Flindt, and K. Brandner, Quantum jump approach to microscopic heat engines, Phys. Rev. Res. **2**, 033449 (2020).
[44] G. Manzano and R. Zambrini, Quantum thermodynamics under continuous monitoring: A general framework, AVS Quantum Sci. **4**, 025302 (2022).
[45] S. Gleyzes, S. Kuhr, C. Guerlin, J. Bernu, S. Deléglise, U. Busk Hoff, M. Brune, J.-M. Raimond, and S. Haroche, Quantum jumps of light recording the birth and death of a photon in a cavity, Nature (London) **446**, 297 (2007).
[46] K. Brandner and K. Saito, Thermodynamic geometry of microscopic heat engines, Phys. Rev. Lett. **124**, 040602 (2020).
[47] G. Manzano, J. M. Horowitz, and J. M. R. Parrondo, Quantum fluctuation theorems for arbitrary environments: Adiabatic and nonadiabatic entropy production, Phys. Rev. X **8**, 031037 (2018).
[48] H. Touchette, The large deviation approach to statistical mechanics, Phys. Rep. **478**, 1 (2009).
[49] R. Chetrite and H. Touchette, Nonequilibrium Markov processes conditioned on large deviations, Ann. Henri Poincaré **16**, 2005 (2015).
[50] F. Carollo, R. L. Jack, and J. P. Garrahan, Unraveling the large deviation statistics of Markovian open quantum systems, Phys. Rev. Lett. **122**, 130605 (2019).
[51] A. Gambassi and A. Silva, Large deviations and universality in quantum quenches, Phys. Rev. Lett. **109**, 250602 (2012).
[52] V. Lecomte, C. Appert-Rolland, and F. van Wijland, Chaotic properties of systems with Markov dynamics, Phys. Rev. Lett. **95**, 010601 (2005).

[53] V. Lecomte, C. Appert-Rolland, and F. van Wijland, Thermodynamic formalism for systems with Markov dynamics, J. Stat. Phys. **127**, 51 (2007).
[54] R. Hurtado-Gutiérrez, F. Carollo, C. Pérez-Espigares, and P. I. Hurtado, Building continuous time crystals from rare events, Phys. Rev. Lett. **125**, 160601 (2020).
[55] T. Bodineau and B. Derrida, Cumulants and large deviations of the current through non-equilibrium steady states, C.R. Phys. **8**, 540 (2007).
[56] T. Bodineau and B. Derrida, Distribution of current in nonequilibrium diffusive systems and phase transitions, Phys. Rev. E **72**, 066110 (2005).
[57] J. P. Garrahan and I. Lesanovsky, Thermodynamics of quantum jump trajectories, Phys. Rev. Lett. **104**, 160601 (2010).
[58] J. P. Garrahan, Classical stochastic dynamics and continuous matrix product states: Gauge transformations, conditioned and driven processes, and equivalence of trajectory ensembles, J. Stat. Mech. (2016) 073208.
[59] F. Carollo, J. P. Garrahan, I. Lesanovsky, and C. Pérez-Espigares, Making rare events typical in Markovian open quantum systems, Phys. Rev. A **98**, 010103(R) (2018).
[60] D. Cilluffo, G. Buonaiuto, I. Lesanovsky, A. Carollo, S. Lorenzo, G. M. Palma, F. Ciccarello, and F. Carollo, Microscopic biasing of discrete-time quantum trajectories, Quantum Sci. Technol. **6**, 045011 (2021).
[61] M. Cech, I. Lesanovsky, and F. Carollo, Thermodynamics of quantum trajectories on a quantum computer, Phys. Rev. Lett. **131**, 120401 (2023).
[62] T. D. Honeychurch and D. S. Kosov, Full counting statistics for electron transport in periodically driven quantum dots, Phys. Rev. B **102**, 195409 (2020).
[63] F. Liu, Auxiliary open quantum system for the Floquet quantum master equation, Phys. Rev. E **103**, 022116 (2021).
[64] F. Liu and S. Su, Stochastic Floquet quantum heat engines and stochastic efficiencies, Phys. Rev. E **101**, 062144 (2020).
[65] R. J. Harris and H. Touchette, Current fluctuations in stochastic systems with long-range memory, J. Phys. A **42**, 342001 (2009).
[66] R. J. Harris, Fluctuations in interacting particle systems with memory, J. Stat. Mech. (2015) P07021.
[67] N. R. Smith and O. Farago, Nonequilibrium steady state for harmonically confined active particles, Phys. Rev. E **106**, 054118 (2022).
[68] R. L. Jack and R. J. Harris, Giant leaps and long excursions: Fluctuation mechanisms in systems with long-range memory, Phys. Rev. E **102**, 012154 (2020).
[69] R. L. Jack and P. Sollich, Large deviations and ensembles of trajectories in stochastic models, Prog. Theor. Phys. Suppl. **184**, 304 (2010).
[70] M. Cavallaro, R. J. Mondragón, and R. J. Harris, Temporally correlated zero-range process with open boundaries: Steady state and fluctuations, Phys. Rev. E **92**, 022137 (2015).
[71] M. Cavallaro and R. J. Harris, A framework for the direct evaluation of large deviations in non-Markovian processes, J. Phys. A **49**, 47LT02 (2016).
[72] L. Bertini, R. Chetrite, A. Faggionato, and D. Gabrielli, Level 2.5 large deviations for continuous-time Markov chains with time periodic rates, Ann. Henri Poincaré **19**, 3197 (2018).
[73] A. C. Barato, R. Chetrite, A. Faggionato, and D. Gabrielli, Bounds on current fluctuations in periodically driven systems, New J. Phys. **20**, 103023 (2018).
[74] E. Potanina, K. Brandner, and C. Flindt, Optimization of quantized charge pumping using full counting statistics, Phys. Rev. B **99**, 035437 (2019).
[75] N. Sinitsyn and I. Nemenman, The berry phase and the pump flux in stochastic chemical kinetics, Europhys. Lett. **77**, 58001 (2007).
[76] J. Ren, P. Hänggi, and B. Li, Berry-phase-induced heat pumping and its impact on the fluctuation theorem, Phys. Rev. Lett. **104**, 170601 (2010).
[77] J. Hoppenau and A. Engel, On the work distribution in quasi-static processes, J. Stat. Mech. (2013) P06004.
[78] J. Gu, Work statistics in slow thermodynamic processes, J. Chem. Phys. **158** (2023).
[79] N. A. Sinitsyn and I. Nemenman, Universal geometric theory of mesoscopic stochastic pumps and reversible ratchets, Phys. Rev. Lett. **99**, 220408 (2007).
[80] M. Josefsson, A. Svilans, A. M. Burke, E. A. Hoffmann, S. Fahlvik, C. Thelander, M. Leijnse, and H. Linke, A quantum-dot heat engine operating close to the thermodynamic efficiency limits, Nat. Nanotechnol. **13**, 920 (2018).
[81] G. Manzano, R. Silva, and J. M. R. Parrondo, Autonomous thermal machine for amplification and control of energetic coherence, Phys. Rev. E **99**, 042135 (2019).
[82] F. Verstraete, M. M. Wolf, and J. Ignacio Cirac, Quantum computation and quantum-state engineering driven by dissipation, Nat. Phys. **5**, 633 (2009).
[83] Y. Lin, J. Gaebler, F. Reiter, T. R. Tan, R. Bowler, A. Sørensen, D. Leibfried, and D. J. Wineland, Dissipative production of a maximally entangled steady state of two quantum bits, Nature (London) **504**, 415 (2013).
[84] L. Del Re, B. Rost, A. F. Kemper, and J. K. Freericks, Driven-dissipative quantum mechanics on a lattice: Simulating a fermionic reservoir on a quantum computer, Phys. Rev. B **102**, 125112 (2020).
[85] M. Cattaneo, M. A. C. Rossi, G. García-Pérez, R. Zambrini, and S. Maniscalco, Quantum simulation of dissipative collective effects on noisy quantum computers, PRX Quantum **4**, 010324 (2023).
[86] P. Zoller, M. Marte, and D. F. Walls, Quantum jumps in atomic systems, Phys. Rev. A **35**, 198 (1987).
[87] J. M. Horowitz, Quantum-trajectory approach to the stochastic thermodynamics of a forced harmonic oscillator, Phys. Rev. E **85**, 031110 (2012).
[88] G. T. Landi, M. J. Kewming, M. T. Mitchison, and P. P. Potts, Current fluctuations in open quantum systems: Bridging the gap between quantum continuous measurements and full counting statistics, PRX Quantum **5**, 020201 (2024).
[89] See Supplemental Material at http://link.aps.org/supplemental/10.1103/PhysRevLett.132.260402 for a detailed proof of the adiabatic theorem for deformed generators, additional details on large deviations results, and the

derivation of the master equation of the two-qubit model used in the main text.

[90] R. Chetrite and H. Touchette, Nonequilibrium microcanonical and canonical ensembles and their equivalence, Phys. Rev. Lett. **111**, 120601 (2013).

[91] R. K. P. Zia, E. F. Redish, and S. R. McKay, Making sense of the Legendre transform, Am. J. Phys. **77**, 614 (2009).

[92] F. Carollo, F. M. Gambetta, K. Brandner, J. P. Garrahan, and I. Lesanovsky, Nonequilibrium quantum many-body Rydberg atom engine, Phys. Rev. Lett. **124**, 170602 (2020).

[93] C. Nill, K. Brandner, B. Olmos, F. Carollo, and I. Lesanovsky, Many-body radiative decay in strongly interacting Rydberg ensembles, Phys. Rev. Lett. **129**, 243202 (2022).

[94] P. J. Paulino, I. Lesanovsky, and F. Carollo, Nonequilibrium thermodynamics and power generation in open quantum optomechanical systems, Phys. Rev. A **108**, 023516 (2023).

[95] S. Marcantoni, C. Pérez-Espigares, and J. P. Garrahan, Symmetry-induced fluctuation relations for dynamical observables irrespective of their behavior under time reversal, Phys. Rev. E **101**, 062142 (2020).

[96] S. Marcantoni, C. Pérez-Espigares, and J. P. Garrahan, Symmetry-induced fluctuation relations in open quantum systems, Phys. Rev. E **104**, 014108 (2021).

[97] H. J. D. Miller, M. H. Mohammady, M. Perarnau-Llobet, and G. Guarnieri, Joint statistics of work and entropy production along quantum trajectories, Phys. Rev. E **103**, 052138 (2021).

[98] G. Manzano, R. Sánchez, R. Silva, G. Haack, J. B. Brask, N. Brunner, and P. P. Potts, Hybrid thermal machines: Generalized thermodynamic resources for multitasking, Phys. Rev. Res. **2**, 043302 (2020).

[99] Z. K. Minev, S. O. Mundhada, S. Shankar, P. Reinhold, R. Gutiérrez-Jáuregui, R. J. Schoelkopf, M. Mirrahimi, H. J. Carmichael, and M. H. Devoret, To catch and reverse a quantum jump mid-flight, Nature (London) **570**, 200 (2019).

[100] D. von Lindenfels, O. Gräb, C. T. Schmiegelow, V. Kaushal, J. Schulz, M. T. Mitchison, J. Goold, F. Schmidt-Kaler, and U. G. Poschinger, Spin heat engine coupled to a harmonic-oscillator flywheel, Phys. Rev. Lett. **123**, 080602 (2019).

[101] J. Roßnagel, S. T. Dawkins, K. N. Tolazzi, O. Abah, E. Lutz, F. Schmidt-Kaler, and K. Singer, A single-atom heat engine, Science **352**, 325 (2016).

[102] J. P. Garrahan and M. Guţă, Catching and reversing quantum jumps and thermodynamics of quantum trajectories, Phys. Rev. A **98**, 052137 (2018).

[103] C. Gardiner and P. Zoller, *Quantum Noise: A Handbook of Markovian and Non-Markovian Quantum Stochastic Methods with Applications to Quantum Optics* (Springer Science & Business Media, New York, 2004).

[104] Y. Zheng, S. Campbell, G. De Chiara, and D. Poletti, Cost of counterdiabatic driving and work output, Phys. Rev. A **94**, 042132 (2016).

[105] M. Kieferová and N. Wiebe, On the power of coherently controlled quantum adiabatic evolutions, New J. Phys. **16**, 123034 (2014).

[106] I. B. Coulamy, A. C. Santos, I. Hen, and M. S. Sarandy, Energetic cost of superadiabatic quantum computation, Front. ICT **3**, 19 (2016).

[107] A. C. Santos and M. S. Sarandy, Sufficient conditions for adiabaticity in open quantum systems, Phys. Rev. A **102**, 052215 (2020).

[108] F. Carollo and C. Pérez-Espigares, Entanglement statistics in Markovian open quantum systems: A matter of mutation and selection, Phys. Rev. E **102**, 030104(R) (2020).

[109] F. Carollo, J. P. Garrahan, and R. L. Jack, Large deviations at level 2.5 for Markovian open quantum systems: Quantum jumps and quantum state diffusion, J. Stat. Phys. **184**, 13 (2021).

[110] F. Albarelli, M. A. Rossi, D. Tamascelli, and M. G. Genoni, Restoring Heisenberg scaling in noisy quantum metrology by monitoring the environment, Quantum **2**, 110 (2018).

[111] A. Cabot, F. Carollo, and I. Lesanovsky, Continuous sensing and parameter estimation with the boundary time crystal, Phys. Rev. Lett. **132**, 050801 (2024).

[112] J. Sperling, W. Vogel, and G. S. Agarwal, Sub-binomial light, Phys. Rev. Lett. **109**, 093601 (2012).

[113] J. D. Cohen, S. M. Meenehan, G. S. MacCabe, S. Gröblacher, A. H. Safavi-Naeini, F. Marsili, M. D. Shaw, and O. Painter, Phonon counting and intensity interferometry of a nanomechanical resonator, Nature (London) **520**, 522 (2015).

[114] P. J. Paulino, I. Lesanovsky, and F. Carollo, Data of "Large Deviation Full Counting Statistics in Adiabatic Open Quantum Dynamics" (2024), 10.5281/zenodo.11550106.

SUPPLEMENTAL MATERIAL

Large deviation full counting statistics in adiabatic open quantum dynamics

Paulo J. Paulino[1], Igor Lesanovsky[1,2] and Federico Carollo[1]

[1]*Institut für Theoretische Physik, Universität Tübingen, Auf der Morgenstelle 14, 72076 Tübingen, Germany, Auf der Morgenstelle 14, 72076 Tübingen, Germany*
[2]*School of Physics and Astronomy and Centre for the Mathematics and Theoretical Physics of Quantum Non-Equilibrium Systems, The University of Nottingham, Nottingham, NG7 2RD, United Kingdom*

I. DERIVATION OF THE DEFORMED DYNAMICAL GENERATOR

In this Section, we derive the deformed dynamical generator $\mathcal{L}_s(t)$, which is given in Eq. (4) of the main text. We start by defining the time-integrated observable

$$Q(t) = \sum_j \int_0^t f_j(v) \mathrm{d}n_j(v) \,, \tag{S1}$$

where $\mathrm{d}n_j(v)$ is a Poisson increment associated with a jump through the j-th channel, at time t. The noises are such that $\mathrm{d}n_j^2(t) = \mathrm{d}n_j(t)$.

To calculate the moment generating function, we have to evaluate $Z_s(t) = \mathbb{E}[K(t)]$, where $K(t) = e^{-sQ(t)}$. To this end, it is convenient to turn the problem into finding the evolution of the biased density matrix

$$\rho_s(t) = \mathbb{E}[K(t)\psi(t)] = \int_0^t P[\psi(t)=\psi]\mathbb{E}\big|_{\psi(t)=\psi}[K(t)\psi(t)]\mathrm{d}\psi = \int_0^t P_s[\psi(t)=\psi]\psi \mathrm{d}\psi \,, \tag{S2}$$

where $P_s[\psi(t)=\psi] = P[\psi(t)=\psi]\mathbb{E}\big|_{\psi(t)=\psi}[K(t)]$. The moment generating function can be retrieved using the fact that $Z_s(t) = \mathrm{Tr}(\rho_s(t))$.

In order to find the map that generates the dynamics of the deformed density matrix, $\rho_s(t)$, we consider the differential equation

$$\mathrm{d}\rho_s(t) = \int_0^t P[\psi(t)=\psi]\mathbb{E}\big|_{\psi(t)=\psi}[\mathrm{d}(K(t)\psi(t))]\mathrm{d}\psi \,. \tag{S3}$$

The differential inside the integral can be written as the sum of three different components, since

$$\mathrm{d}(K(t)\psi(t)) = \mathrm{d}(K(t))\psi(t) + K(t)\mathrm{d}(\psi(t)) + \mathrm{d}(K(t))\mathrm{d}(\psi(t)) \,, \tag{S4}$$

and we evaluate each of the above increments independently. For the term $K(t)$, we have

$$K(t+\mathrm{d}t) = e^{-\sum_j \int_0^{t+\mathrm{d}t} s(v) f_j(v) \mathrm{d}n_j(v)} = K(t) e^{-s(t)\sum_j f_j(t)\mathrm{d}n_j(t)} \,. \tag{S5}$$

We now can explicitly calculate the exponential exploiting the relation $\mathrm{d}n_i(t)\mathrm{d}n_j(t) = \mathrm{d}n_i(t)\delta_{ij}$, where δ_{ij} is a Kronecker delta. With this we can write

$$\mathrm{d}K(t) = K(t+\mathrm{d}t) - K(t) = K(t)\sum_j \mathrm{d}n_j(t)(e^{-s(t)f_j(t)} - 1) \,, \tag{S6}$$

which allows us to calculate the expectation of the first term appearing on the right hand side of Eq. (S4) as

$$\mathbb{E}\big|_{\psi(t)=\psi}[\mathrm{d}K(t)\psi(t)] = \mathbb{E}\big|_{\psi(t)=\psi}[K(t)]\psi \sum_j \Big(e^{-sf_j(t)} - 1\Big)\,\mathrm{Tr}\Big\{\mathcal{J}_j[\psi]\Big\}\mathrm{d}t \,. \tag{S7}$$

The stochastic equation for the pure state $\psi(t)$ is given by

$$\mathrm{d}\psi(t) = \mathcal{B}(t)[\psi(t)]\mathrm{d}t + \sum_j \left(\frac{\mathcal{J}_j(t)[\psi(t)]}{\mathrm{Tr}\left(\mathcal{J}_j(t)[\psi(t)]\right)} - \psi(t) \right) \mathrm{d}n_j(t)\,, \tag{S8}$$

where $\tilde{H}(t) = H(t) - (i/2)\sum_j J_j^\dagger(t)J_j(t)$ is the effective Hamiltonian. As defined in the main text, we have $\mathcal{B}(t)[\psi] = -i\tilde{H}(t)\psi + i\psi\tilde{H}^\dagger(t) - \psi\mathrm{Tr}[-i\tilde{H}(t)\psi + i\psi\tilde{H}^\dagger(t)]$, and $\mathcal{J}_j(t)[\rho] = J_j(t)\rho J_j^\dagger(t)$, with $J_j(t)$ being the jump operators. Therefore, we have

$$\mathbb{E}\big|_{\psi(t)=\psi}[K(t)\mathrm{d}\psi(t)] = \mathbb{E}\big|_{\psi(t)=\psi}[K(t)]\mathcal{L}[\psi]\mathrm{d}t\ . \tag{S9}$$

For the last term, $\mathrm{d}K(t)\mathrm{d}\psi(t)$, we further consider that $\mathrm{d}t\mathrm{d}n_j(t)$ is of higher-order in $\mathrm{d}t$ and we obtain

$$\mathrm{d}K(t)\mathrm{d}\psi(t) = K(t)\sum_j \left(\frac{\mathcal{J}_j(t)[\psi(t)]}{\mathrm{Tr}\left(\mathcal{J}_j(t)[\psi(t)]\right)} - \psi(t) \right) \left(e^{-sf_j(t)} - 1 \right) \mathrm{d}n_j(t)\ . \tag{S10}$$

By taking the expectation value, we find

$$\mathbb{E}\big|_{\psi(t)=\psi}[\mathrm{d}K(t)\mathrm{d}\psi(t)] = \mathbb{E}\big|_{\psi(t)=\psi}[K(t)]\sum_j \left(\mathcal{J}_j[\psi] - \psi\mathrm{Tr}\Big\{ \mathcal{J}_j[\psi] \Big\} \right) \left(e^{-sf_j(t)} - 1 \right) \mathrm{d}t\ . \tag{S11}$$

Summing all three contributions we find

$$\mathbb{E}\big|_{\psi(t)=\psi}[\mathrm{d}(K(t)\psi(t))] = \mathbb{E}\big|_{\psi(t)=\psi}[K(t)] \left(\mathcal{B}[\psi] + \sum_j e^{-sf_j(t)}\mathcal{J}_j[\psi] \right) \mathrm{d}t\ . \tag{S12}$$

To conclude the derivation, we note that

$$\mathrm{d}\rho_s(t) = \int_0^t P[\psi(t)=\psi]\mathbb{E}\big|_{\psi(t)=\psi}[\mathrm{d}(K(t)\psi(t))]\mathrm{d}\psi = \int_0^t P[\psi(t)=\psi]\mathbb{E}\big|_{\psi(t)=\psi}[K(t)]\mathcal{L}_s(t)[\psi]\mathrm{d}\psi = \mathcal{L}_s(t)[\rho_s(t)]\ , \tag{S13}$$

where

$$\mathcal{L}_s(t)[\rho] = -i\left[\tilde{H}(t)\rho - \rho\tilde{H}^\dagger(t)\right] + \sum_j e^{-sf_j(t)}J_j(t)\rho J_j^\dagger(t)\ . \tag{S14}$$

II. ADIABATIC THEOREM FOR DEFORMED DYNAMICAL GENERATORS

In this Section, we provide a proof for the result presented in Eq. (6) in the main text. Assuming that the deformed generator $\mathcal{L}_s(t)$ can be diagonalized, we can write the deformed state of the system at time t, $\rho_s(t)$, as

$$\rho_s(t) = \sum_m c_s^m(t) r_s^m(t)\,. \tag{S15}$$

Here, $c_s^m(t) = \mathrm{Tr}(\ell_s^m(t)\rho_s(t))$ and $\ell_s^m(t), r_s^m(t)$ are the left and right eigenmatrices of the instantaneous generator $\mathcal{L}_s(t)$. The first step of the proof is to determine the time evolution of the coefficients $c_s^m(t)$. To this end, we take the time derivative of $\rho_s(t)$ which gives

$$\dot{\rho}_s(t) = \sum_m \left[\dot{c}_s^m(t)r_s^m(t) + c_s^m(t)\dot{r}_s^m(t)\right] = \sum_m \lambda_s^m(t)c_s^m(t)r_s^m(t)\,, \tag{S16}$$

where the second equality comes from acting on $\rho_s(t)$ with the deformed generator $\mathcal{L}_s(t)$. To find an equation for the coefficients $c_s^m(t)$, we "project" the above equation onto $\ell_s^k(t)$, exploiting the orthogonality relation $\mathrm{Tr}(\ell_s^k(t)r_s^m(t)) = \delta_{km}$, to get

$$\dot{c}_s^k(t) = \lambda_s^k(t)c_s^k(t) - \sum_m c_s^m(t)\mathrm{Tr}\left(\ell_s^k(t)\dot{r}_s^m(t)\right)\ . \tag{S17}$$

Introducing the vector $\mathbf{c}_s(t) = [c_s^0(t), c_s^1(t), \dots]^T$, we can recast the above system of differential equations as

$$\dot{\mathbf{c}}_s(t) = \left[\Lambda(t) + \frac{1}{\tau}M(t)\right]\mathbf{c}_s(t)\,, \tag{S18}$$

where $\Lambda(t)$ is a diagonal matrix containing the eigenvalues $\lambda_s^m(t)$ and where

$$M_{km}(t) = -\tau \mathrm{Tr}\left(\ell_s^k(t)\dot{r}_s^m(t)\right)\,.$$

The latter matrix has finite values which further remain finite in the large τ limit, since we are considering finite-dimensional systems and $\dot{r}_s^m(t)$ of order $1/\tau$. This implies that there exists a constant $M_{\max}$ such that $\|M(t)\| \leq M_{\max}$ for all $t \geq 0$. (We note that the diagonal elements of the matrix M are analogous to the geometric phase in the Hamiltonian case [6–8].) The full propagator for the time evolution of the coefficients as expressed by Eq. (S18) is given by the time-order exponential $U(t) = \mathcal{T}\exp\{\int_0^t[\Lambda(v) + \tau^{-1}M(v)]\mathrm{d}v\}$. This shows that the coefficients $\mathbf{c}_s(t)$ evolves through a diagonal matrix $\Lambda(t)$ plus an off-diagonal one of order $1/\tau$. Our aim is to show that, in the large τ limit, all coefficients $c_s^m(t)$ are vanishingly small when compared with the coefficient $c_s^0(t)$, which is enough to prove Eq. (6).

We start by expanding the propagator $U(t)$ into a Dyson series using the matrix $M(t)$ as a perturbation and the parameter $1/\tau$ as the perturbation strength. The Dyson series reads $U(t) = \sum_{n=0}^{\infty} V_n$, with

$$V_n = \frac{1}{\tau^n}\int_0^t \mathrm{d}v_n \int_0^{v_n} \mathrm{d}v_{n-1}\cdots\int_0^{v_2}\mathrm{d}v_1 B(t,v_n)M(v_n)B(v_n,v_{n-1})M(v_{n-1})\dots B(v_2,v_1)M(v_1)B(v_1,0)\,,$$

where we have defined

$$B(t,t_0) = e^{\int_{t_0}^t \Lambda(v)\mathrm{d}v}\,.$$

The evolution of the coefficients $\mathbf{c}_s(t)$ is then given by

$$\mathbf{c}_s(t) = B(t,0)\mathbf{c}_s(0) + \sum_{n=1}^{\infty} V_n\mathbf{c}_s(0)\,,$$

where we have singled out the zeroth term of the series. From this term, it is clear that the dominant contribution is given by the term $e^{\int_0^t \mathrm{d}v\lambda_s^0(v)}$ included in $B(t,0)$. We thus want to understand how all the coefficients behave in comparison with this quantity. We take a generic element $c_s^m(t)$ in the vector $\mathbf{c}_s(t)$ and consider the ratio

$$\frac{c_s^m(t)}{e^{\int_0^t \mathrm{d}v\lambda_s^0(v)}} = \frac{e^{\int_0^t \mathrm{d}v\lambda_s^m(v)}}{e^{\int_0^t \mathrm{d}v\lambda_s^0(v)}}c_s^m(0) + \sum_{n=1}^{\infty}\frac{\mathbf{e}_m\cdot V_n\mathbf{c}_s(0)}{e^{\int_0^t \mathrm{d}v\lambda_s^0(v)}}\,, \tag{S19}$$

where $\mathbf{e}_m$ is the basis vector with 1 in the mth position and 0 otherwise. We now want to bound each term on the right hand side of the above equation for $m \neq 0$. For the first term we find

$$\left|\frac{e^{\int_0^t \mathrm{d}v\lambda_s^m(v)}}{e^{\int_0^t \mathrm{d}v\lambda_s^0(v)}}c_s^m(0)\right| \leq \left|\frac{e^{\int_0^t \mathrm{d}v\lambda_s^m(v)}}{e^{\int_0^t \mathrm{d}v\lambda_s^0(v)}}\right| c_{\max}\,,$$

where $c_{\max}$ is such that $|c_s^m(0)| \leq c_{\max}$, $\forall m$. Considering that we can write the ratio of the exponential as

$$\left|\frac{e^{\int_0^t \mathrm{d}v\lambda_s^m(v)}}{e^{\int_0^t \mathrm{d}v\lambda_s^0(v)}}\right| = \left|e^{\int_0^t \mathrm{d}v[\lambda_s^m(v)-\lambda_s^0(v)]}\right|\,,$$

and using our finite-gap condition (C2), we find (recalling that $m \neq 0$)

$$\left|\frac{e^{\int_0^t \mathrm{d}v\lambda_s^m(v)}}{e^{\int_0^t \mathrm{d}v\lambda_s^0(v)}}c_s^m(0)\right| \leq e^{-\Delta t}c_{\max}\,. \tag{S20}$$

Now, we consider the generic term in the series of Eq. (S19). Explicitly, we have

$$\begin{aligned}\frac{\mathbf{e}_m\cdot V_n\mathbf{c}_s(0)}{e^{\int_0^t \mathrm{d}v\lambda_s^0(v)}} = \frac{1}{\tau^n}\int_0^t \mathrm{d}v_n\int_0^{v_n}\mathrm{d}v_{n-1}\cdots\int_0^{v_2}\mathrm{d}v_1\times \\ \times\frac{e^{\int_{v_n}^t \mathrm{d}r_n\lambda_s^m(r_n)}\mathbf{e}_m\cdot M(v_n)B(v_n,v_{n-1})M(v_{n-1})\dots B(v_2,v_1)M(v_1)B(v_1,0)\mathbf{c}_s(0)}{e^{\int_0^t \mathrm{d}v\lambda_s^0(v)}}\,.\end{aligned} \tag{S21}$$

We now split the exponential $e^{\int_0^t \mathrm{d}v\lambda_s^0(v)}$, which does not depend on the integration variables, into the product

$$e^{\int_0^t \mathrm{d}v\lambda_s^0(v)} = e^{\int_{v_n}^t \mathrm{d}r_n\lambda_s^0(r_n)} e^{\int_{v_{n-1}}^{v_n} \mathrm{d}r_{n-1}\lambda_s^0(r_{n-1})} \cdots e^{\int_{v_1}^{v_2} \mathrm{d}r_1\lambda_s^0(r_1)} e^{\int_0^{v_1} \mathrm{d}r\lambda_s^0(r)}$$

and assign each term to the corresponding $B(v_k, v_{k-1})$ and to the first exponential. We can thus write

$$\begin{aligned}\frac{\mathbf{e}_m \cdot V_n \mathbf{c}_s(0)}{e^{\int_0^t \mathrm{d}v\lambda_s^0(v)}} = \frac{1}{\tau^n}\int_0^t \mathrm{d}v_n \int_0^{v_n} \mathrm{d}v_{n-1}\cdots \int_0^{v_2} \mathrm{d}v_1 e^{\int_{v_n}^t \mathrm{d}r_n[\lambda_s^m(r_n)-\lambda_s^0(r_n)]}\times \\ \times\, \mathbf{e}_m \cdot M(v_n)\frac{B(v_n, v_{n-1})}{e^{\int_{v_{n-1}}^{v_n} \mathrm{d}r_{n-1}\lambda_s^0(r_{n-1})}} M(v_{n-1}) \cdots \frac{B(v_2, v_1)}{e^{\int_{v_1}^{v_2} \mathrm{d}r_1\lambda_s^0(r_1)}} M(v_1) \frac{B(v_1, 0)}{e^{\int_0^{v_1} \mathrm{d}r\lambda_s^0(r)}} \mathbf{c}_s(0)\,.\end{aligned} \tag{S22}$$

Taking the absolute value of the above quantity, using the Cauchy-Schwarz inequality for the matrix element in the second line, and noticing that $\left\| \frac{B(v_k, v_{k-1})}{e^{\int_{v_{k-1}}^{v_k} \mathrm{d}r_{k-1}\lambda_s^0(r_{k-1})}} \right\| \leq 1$, we find

$$\left| \frac{\mathbf{e}_m \cdot V_n \mathbf{c}_s(0)}{e^{\int_0^t \mathrm{d}v\lambda_s^0(v)}} \right| \leq \frac{\|\mathbf{c}_s(0)\| M_{\max}^n}{\tau^n} \int_0^t \mathrm{d}v_n e^{-\Delta(t-v_n)} \int_0^{v_n} \mathrm{d}v_{n-1}\cdots \int_0^{v_2} \mathrm{d}v_1\,,$$

where we have exploited our gap condition for the first exponential. Calculating the integrals up to the integration variable v_{n-1} we find

$$\int_0^{v_n} \mathrm{d}v_{n-1}\cdots \int_0^{v_2} \mathrm{d}v_1 = \frac{v_n^{n-1}}{(n-1)!} \leq \frac{\tau^{n-1}}{(n-1)!}\,,$$

which, when substituted in the bound above, gives

$$\left| \frac{\mathbf{e}_m \cdot V_n \mathbf{c}_s(0)}{e^{\int_0^t \mathrm{d}v\lambda_s^0(v)}} \right| \leq \frac{c_{\max} D^2}{\tau\Delta}\left(1 - e^{-\Delta t}\right)\frac{M_{\max}^n}{(n-1)!}\,,$$

where we further used that $\|\mathbf{c}_s(0)\| \leq c_{\max} D^2$ with D being the dimension of the Hilbert space of the system. Putting all together, this shows that, for $m \neq 0$,

$$\left| \frac{c_s^m(t)}{e^{\int_0^t \mathrm{d}v\lambda_s^0(v)}} \right| \leq c_{\max}\left[e^{-t\Delta} + \frac{D^2}{\tau\Delta}(1 - e^{-t\Delta}) \sum_{n=1}^{\infty} \frac{M_{\max}^n}{(n-1)!} \right],$$

which vanishes when introducing the rescaled time $u = t/\tau$ and sending $\tau \to \infty$. Doing a similar manipulation to the one performed above one can instead show that $c_s^0(t)/e^{\int_0^t \mathrm{d}r\lambda_s^0(r)}$ remains finite in the large-τ limit. The above result implies that $\rho_s(u) \approx c_s^0(u) r_s^0(u)$ for large τ and thus that

$$\lim_{\tau\to\infty} \varrho_s(u) := \lim_{\tau\to\infty} \frac{\rho_s(u)}{\mathrm{Tr}(\rho_s(u))} = r_s^0(u)\,,$$

where we defined $r_s^0(u)$ to be unit trace.

We conclude this section by briefly discussing the case of a degenerate dominant eigenvalue $\lambda_s^0(s)$. Even with such a degeneracy, it is still possible to do the same steps done above to show that all the coefficients c_s^m, which are not associated with the dominant eigenvalue, would be vanishing in the large-τ limit. That is, the quantum state $\varrho_s(u)$ would only contain eigenmatrices $r_s^m(u)$ related to the dominant eigenvalue. As such, even though the form of $\varrho_s(u)$ would not be completely determined by the above calculation, one can still conclude that $\mathcal{L}_s(u)[\varrho_s(u)] = \lambda_s^0(u)\varrho_s(u)$, which is all that is needed to arrive at Eq. (7).

III. OBSERVABLE RATES AND PROBABILITY FUNCTIONAL FOR TIME-HISTORIES

Due to adiabatic character of the dynamics, the system essentially spends an infinite amount of time in each of the rescaled times $u = t/\tau$. For each of these times, we can thus define a time-averaged value of the observable $q(u)$, which represents an instantaneous rate for the observable $Q(\tau)$. As a special case of the derivation we present below,

the latter can indeed be written as $Q(\tau) = \tau \int_0^1 q(u)\mathrm{d}u$. In this Section, we show how the functional providing the probability of any time-history, or path, $\{q(u)\}$ can be derived.

The first step consists in showing that the moment generating function for the time-histories $\{q(u)\}$ can be defined by considering a time-dependent *path* for the conjugate field $s(u)$, which only varies on the slow timescale u. To this end, we start defining the quantity

$$\hat{Q}(\tau) = \sum_j \int_0^\tau s(v/\tau) f_j(v/\tau) \mathrm{d}n_j(v)\,, \tag{S23}$$

where the factor $1/\tau$ in the arguments of the functions s and f_j explicitly accounts for the fact that these functions vary on the slow timescale. To proceed, we now divide the total evolution time τ into M time-intervals so that we can write

$$\hat{Q}(\tau) = \sum_{k=1}^{M} \sum_j \int_{\frac{\tau}{M}(k-1)}^{\frac{\tau}{M}k} s(v/\tau) f_j(v/\tau) \mathrm{d}n_j(v)\,.$$

For M large enough, the functions s and f_j are essentially constant inside each time interval so that we have

$$\hat{Q}(\tau) \approx \sum_{k=1}^{M} \sum_j s(k/M) f_j(k/M) \int_{\frac{\tau}{M}(k-1)}^{\frac{\tau}{M}k} \mathrm{d}n_j(v) = \frac{\tau}{M} \sum_{k=1}^{M} s(k/M) \left[\sum_j f_j(k/M) \frac{1}{\tau/M} \int_{\frac{\tau}{M}(k-1)}^{\frac{\tau}{M}k} \mathrm{d}n_j(v) \right],$$

where for the second equality we only multiplied and divided by the factor τ/M. The term inside the square bracket is essentially the average rate of the considered observable at the rescaled time k/M, which we call $q(k/M)$. With such a definition, we can write

$$\hat{Q}(\tau) \approx \frac{\tau}{M} \sum_{k=1}^{M} s(k/M) q(k/M)\,.$$

Taking the limit $M \to \infty$ we find

$$\hat{Q}(\tau) = \tau \int_0^1 s(u) q(u) \mathrm{d}u\,.$$

The above expression thus shows that a time-dependent field $s(u)$ is conjugated to the time-history of the rate $\{q(u)\}$, whose moment generating function can thus be written as $Z_{\{s(u)\}} = \mathbb{E}[e^{-\hat{Q}(\tau)}]$.

The second step to arrive at a probability function for time-histories is to recognize that the tilted operator for $Z_{\{s(u)\}}$ is exactly the one presented in Eq. (4) but with a time-dependent s, $\mathcal{L}_{s(u)}(u)$ varying on the slow timescale u. This thus also implies that our adiabatic theorem is also valid for this tilted generator and that we can write the scaled cumulant generating functional for time-histories as

$$\Theta[\{s(u)\}] = \int_0^1 \lambda^0_{s(u)}(u) \mathrm{d}u\,,$$

where $\lambda^0_{s(u)}(u)$ is the dominant eigenvalue of $\mathcal{L}_{s(u)}(u)$.

With the scaled cumulant generating function at hand, we can calculate the probability functional for time-histories as its Legendre-Fenchel transform. That is, the large deviation rate function for $\{q(u)\}$ is defined as

$$\varphi[\{q(u)\}] = \sup_{\{s(u)\}} \left[-\int_0^1 s(u) q(u) \mathrm{d}u - \Theta[\{s(u)\}] \right].$$

Taking the functional derivative with respect to $\delta s(r)$, we find

$$\frac{\delta}{\delta s(r)} \left[-\int_0^1 s(u) q(u) \mathrm{d}u - \Theta[\{s(u)\}] \right] = -q(r) - \frac{\delta \lambda_{s(r)}(r)}{\delta s(r)}.$$

Then, assuming that it is possible to find the suitable path $s^*(r)$ such that the above equality can be set to zero, we find

$$q(r) = -\frac{\delta \lambda_{s^*(r)}(r)}{\delta s^*(r)}\,.$$

Substituting into the equation for φ, we obtain

$$\varphi[\{q(u)\}] = \int_0^1 \left[s^*(u) \frac{\delta \lambda_{s^*(u)}(u)}{\delta s^*(u)} - \lambda_{s^*(u)}(u) \right] \mathrm{d}u \,.$$

For each u, the term inside the integral corresponds to the Legendre-Fenchel transform of the instantaneous dominant eigenvalue, calculated in $q(u)$, so that we finally have

$$\varphi[\{q(u)\}] = \int_0^1 \mathcal{I}(q(u), u) \mathrm{d}u \,.$$

Contraction to the full counting statistics of the time-integrated observable

In this Section, we explicitly show how to go from the functional over time-histories φ to the large deviation rate function I for the time-integrated observable $Q(\tau) = \tau \int_0^\tau q(u)\mathrm{d}u$. This can be done via the contraction principle given that the observable Q is a function of the different time-histories. Due to the contraction principle, we can define, as done in the main text,

$$I(Q^*/\tau) = \min_{\forall \{q(u)\} : \int_0^1 q(u)\mathrm{d}u = Q^*/\tau} \left[\int_0^1 \mathcal{I}(q(u), u) \mathrm{d}u \right] .$$

To perform the constrained minimization we introduce the Lagrange multiplier μ and construct the functional

$$Y[\{q(u)\}, \mu] = \int_0^1 \mathcal{I}(q(u), u)\mathrm{d}u - \mu \left[\int_0^1 q(u)\mathrm{d}u - Q^*/\tau \right] .$$

We then take the functional derivative of Y with respect to $\delta q(r)$ to find

$$\frac{\delta Y}{\delta q(r)} = \frac{\delta \mathcal{I}(q(r), r)}{\delta q(r)} - \mu \,. \tag{S24}$$

We assume that it is possible to find the path $q^*(r)$, which depends on μ, such that the above quantity can be made equal to zero. Then, to fix the value of $\mu = \mu^*$, we integrate $q^*(r)$ and insist that

$$\int_0^1 q^*(r)\mathrm{d}r = Q^*/\tau \,.$$

We can then substitute this into the functional to obtain

$$Y(\{q^*(u)\}, \mu^*) = \int_0^1 \mathcal{I}(q^*(r), r)\mathrm{d}r \,.$$

The task now is to find a convenient expression for the large deviation rate function $\mathcal{I}(q^*(r), r)$. To this end, we note that this is the Legendre-Fenchel transform of the instantaneous dominant eigenvalue $\lambda_\mu(r)$. This means that we also have the inverse relation

$$\lambda_{\mu^*}(r) = -\inf_{\forall q(r)} \left[\mathcal{I}(q(r), r) + \mu^* q(r) \right] .$$

Performing the minimization we find the same relation as in Eq. (S24), i.e., $\delta \mathcal{I}(q(r), r)/\delta q^*(r) = \mu^*$. Substituting this in the equation for $\lambda^*_\mu(r)$ we obtain the relation

$$\lambda_{\mu^*}(r) = -\mathcal{I}(q^*(r), r) - \mu^* q^*(r) \,.$$

Solving this for $\mathcal{I}(q^*(r), r)$ and substituting the in the Y functional we find

$$I(Q^*/\tau) = Y(\{q^*(u), \mu^*\} = -\mu^* \int_0^1 q^*(u)\mathrm{d}u - \int_0^1 \lambda_{\mu^*}(u)\mathrm{d}u = -\mu^* Q^*/\tau - \theta^{\mathrm{ad}}_{\mu^*} \,,$$

which is exactly the Legendre-Fenchel transform of θ^{ad}_μ as it should be.

IV. QUANTUM DOOB TRANSFORM FOR TIME-DEPENDENT GENERATORS

In this Section, we discuss how it is possible to define an auxiliary process that gives a desired time-history for the observable as its typical one. This is achieved by exploiting ideas put forward in Refs. [57, 59] in the context of quantum generalizations of the *Doob transform* introduced in Ref. [69].

We start by considering the evolution under the deformed dynamical generator and Trotterize this in the slow time-scale. We can thus write

$$\rho_s(\tau) = \mathcal{T} e^{\tau \int_0^1 \mathcal{L}_{s(u)}(u) \mathrm{d}u}[\rho(0)] \approx \prod_{k=1}^{M} e^{\tau \mathcal{L}_{s(k/M)}(k/M) \mathrm{d}u}[\rho(0)] \ ,$$

where we considered the same partitioning of the τ exploited in Section III. For a given path $\{s(u)\}$ this deformed generator enhances the probability of observing as typical time-history the one given by $q(u) = -\delta\Theta/\delta s(u)$. However, the above evolution is not a physical dynamics. To obtain a suitable, we can proceed by applying at each rescaled time the time-independent Doob transform introduced in Refs. [57, 59]. Essentially, we want to find a generalized rotation of the deformed generator at each rescaled time u, $\mathcal{L}_{s(u)}(u)$, such that the latter becomes a well-defined quantum map. Following [57], this is achieved by exploiting the left dominant eigenmatrix of the deformed generator and defined the auxiliary dynamics via the dynamical generator

$$\mathcal{L}^{\mathrm{A}}(u)[\rho] = -i[H^{\mathrm{A}}(u), \rho] + \sum_j \left[J_j^{\mathrm{A}}(u) \rho (J_j^{\mathrm{A}}(u))^\dagger - \frac{1}{2} \left\{ (J_j^{\mathrm{A}}(u))^\dagger J_j^{\mathrm{A}}(u), \rho \right\} \right] \ ,$$

with Hamiltonian and jump operators given in Eq. (10) of the main text. The dynamics resulting from the generator $\mathcal{L}^{\mathrm{A}}(u)$ is still an adiabatic dynamics by construction and such that the typical path is the one given by $q(u) = -\delta\Theta/\delta s(u)$ as desired.

V. MASTER EQUATION OF THE TWO-QUBIT SYSTEM

In this Section, we provide details on the quantum master equation for the two-qubit system coupled to two different thermal baths, a hot one and a cold one.

We consider the Hamiltonian

$$H = \omega(\sigma_e^{\mathrm{hot}} + \sigma_e^{\mathrm{cold}}) + \Omega(\sigma_+^{\mathrm{hot}} \sigma_-^{\mathrm{cold}} + \sigma_-^{\mathrm{hot}} \sigma_+^{\mathrm{cold}}) \ , \tag{S25}$$

where Ω is the interaction strength, $x^{\mathrm{hot}} = x \otimes \mathbb{1}$ and $x^{\mathrm{cold}} = \mathbb{1} \otimes x$ concern the qubit in contact with the hot bath and the cold one, respectively. The operator σ_e is the project onto the excited state $n = |e\rangle\langle e|$ while $\sigma_- = |g\rangle\langle e|$ and $\sigma_+ = \sigma_-^\dagger$. Under the assumption that the qubits are interacting with a hot and a cold thermal bath, we find that, under a weak-coupling assumption, the dynamics of the state of the system is described by the Lindblad generator

$$\dot{\rho}(t) = -i[H, \rho(t)] + \sum_j \left(J_j \rho(t) J_j^\dagger - \frac{1}{2} \{ J_i^\dagger J_i, \rho(t) \} \right) \ , \tag{S26}$$

where we have the jump operators

$$J_{01}^b = \sqrt{\gamma} \sqrt{\left(\frac{\omega - \Omega}{\omega}\right)^3 \left(1 + \frac{1}{e^{\beta_b(\omega-\Omega)} - 1}\right)} |\epsilon_0\rangle\langle\epsilon_1| \ , \quad J_{10}^b = \sqrt{\gamma} \sqrt{\left(\frac{\omega - \Omega}{\omega}\right)^3 \frac{1}{e^{\beta_b(\omega-\Omega)} - 1}} |\epsilon_1\rangle\langle\epsilon_0| \ , \tag{S27}$$

$$J_{02}^b = \sqrt{\gamma} \sqrt{\left(\frac{\omega + \Omega}{\omega}\right)^3 \left(1 + \frac{1}{e^{\beta_b(\omega+\Omega)} - 1}\right)} |\epsilon_0\rangle\langle\epsilon_2| \ , \quad J_{20}^b = \sqrt{\gamma} \sqrt{\left(\frac{\omega + \Omega}{\omega}\right)^3 \frac{1}{e^{\beta_b(\omega+\Omega)} - 1}} |\epsilon_2\rangle\langle\epsilon_0| \ , \tag{S28}$$

$$J_{13}^b = \sqrt{\gamma} \sqrt{\left(\frac{\omega + \Omega}{\omega}\right)^3 \left(1 + \frac{1}{e^{\beta_b(\omega+\Omega)} - 1}\right)} |\epsilon_1\rangle\langle\epsilon_3| \ , \quad J_{31}^b = \sqrt{\gamma} \sqrt{\left(\frac{\omega + \Omega}{\omega}\right)^3 \frac{1}{e^{\beta_b(\omega+\Omega)} - 1}} |\epsilon_3\rangle\langle\epsilon_1| \ , \tag{S29}$$

$$J_{23}^b = \sqrt{\gamma} \sqrt{\left(\frac{\omega - \Omega}{\omega}\right)^3 \left(1 + \frac{1}{e^{\beta_b(\omega-\Omega)} - 1}\right)} |\epsilon_2\rangle\langle\epsilon_3| \ , \quad J_{32}^b = \sqrt{\gamma} \sqrt{\left(\frac{\omega - \Omega}{\omega}\right)^3 \frac{1}{e^{\beta_b(\omega-\Omega)} - 1}} |\epsilon_3\rangle\langle\epsilon_2| \ . \tag{S30}$$

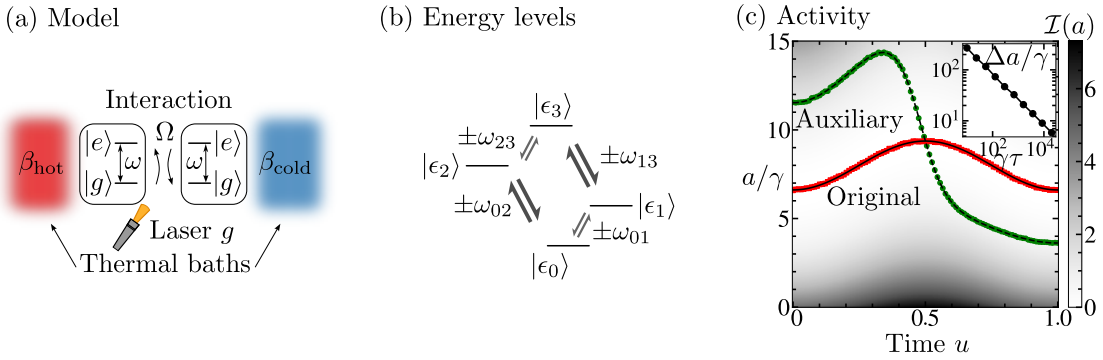

FIG. S1. **Two-atom system.** (a) Two atoms (bare energy ω) interact by exchanging excitations at rate Ω. The atom on the left (right) is in contact with a hot (cold) bath, with inverse temperature $\beta_{\rm hot}$ ($\beta_{\rm cold}$). The whole system is also subject to a laser driving with Rabi frequency g. (b) Transitions implemented by the jump operators, with ω_{ij} representing the energy exchanges with the thermal baths given by $\omega_{02} = \omega_{13} = (\omega + \Omega)$ and $\omega_{01} = \omega_{23} = (\omega - \Omega)$. (c) Instantaneous rate function $\mathcal{I}(a(u), u)$ for the the activity rate as a function of time. The black solid line shows the typical time-history of the rates while the dashed line a rare one. Red squares are estimates obtained by running a (typical) quantum trajectory evaluated at $s = 0$, while the green bullets a quantum trajectory with the auxiliary system in Eq. (10), for $s(u) = (1/2)\tanh(10u - 5)$. The total evolution is $\gamma\tau = 2 \times 10^6$. The inset in (c) shows the error between the activity rate estimated through a quantum trajectory, $a(u)$, and the expected behavior, $a_0(u)$, in the adiabatic limit, $\Delta a = \int_0^\tau |a(u) - a_0(u)|{\rm d}u$, as a function of $\gamma\tau$. The parameters are $g = 2\Omega = \omega = \gamma$ and the temperatures are $\beta^0_{\rm hot} = \beta_{\rm cold}/2 = 1$, in units of $1/\omega$.

Here, γ is a rate and β_b, with $b = \text{hot}, \text{cold}$, is the inverse temperature of the bath. The vectors $|\epsilon_i\rangle$ are the eigenstates of the Hamiltonian H, given by

$$|\epsilon_0\rangle = |gg\rangle\,, \quad |\epsilon_{1,2}\rangle = \frac{1}{\sqrt{2}}\left(|ge\rangle \mp |eg\rangle\right)\,, \quad |\epsilon_3\rangle = |ee\rangle\,, \tag{S31}$$

where $|ij\rangle = |i\rangle \otimes |j\rangle$, associated with the energies $\epsilon_0 = 0$, $\epsilon_{1,2} = \omega \mp \Omega$, and $\epsilon_3 = 2\omega$. In addition to these terms, we further consider phenomenologically a laser driving given by $H_S = H + H_{\rm laser}$ with $H_{\rm laser} = g(\sigma_x^{\rm hot} + \sigma_x^{\rm cold})$. Figs. S1(a-b) show the model and the transitions implemented by the jump operators, respectively. In Fig. S1(c) we instead analyze the activity, $A(\tau) = \sum_{i,j,b}\int_0^\tau {\rm d}n_{ij}^b(t)$. The inset shows that the error of the adiabatic approximation approaches to zero as the dynamics total time τ increases, being therefore consistent with the Eq. (6) in the main text and the results in the Sec. II of the supplemental material.

Third publication

Thermodynamics of coupled time crystals with an application to energy storage

Paulo J. Paulino[1], Albert Cabot[1], Gabriele De Chiara[2], Mauro Antezza[3,4], Igor Lesanovsky[1,5] and Federico Carollo[1]

[1]Institut für Theoretische Physik and Center for Integrated Quantum Science and Technology, Universität Tübingen, Auf der Morgenstelle 14, 72076 Tübingen, Germany

[2] Centre for Quantum Materials and Technology, School of Mathematics and Physics, Queen's University Belfast, Belfast BT7 1NN, United Kingdom

[3] Laboratoire Charles Coulomb (L2C) UMR 5221 CNRS-Université de Montpellier, F- 34095 Montpellier, France

[4] Institut Universitaire de France, 1 rue Descartes, F-75231 Paris Cedex 05, France

[5] School of Physics and Astronomy and Centre for the Mathematics and Theoretical Physics of Quantum Non-Equilibrium Systems, The University of Nottingham, Nottingham, NG7 2RD, United Kingdom

Abstract. Open many-body quantum systems can exhibit intriguing nonequilibrium phases of matter, such as time crystals. In these phases, the state of the system spontaneously breaks the time-translation symmetry of the dynamical generator, which typically manifests through persistent oscillations of an order parameter. A paradigmatic model displaying such a symmetry breaking is the *boundary time crystal*, which has been extensively analyzed experimentally and theoretically. Despite the broad interest in these nonequilibrium phases, their thermodynamics and their fluctuating behavior remain largely unexplored, in particular for the case of coupled time crystals. In this work, we consider two interacting boundary time crystals and derive a consistent interpretation of their thermodynamic behavior. We fully characterize their average dynamics and the behavior of their quantum fluctuations, which allows us to demonstrate the presence of quantum and classical correlations in both the stationary and the time-crystal phases displayed by the system. We furthermore exploit our theoretical derivation to explore possible applications of time crystals as quantum batteries, demonstrating their ability to efficiently store energy.

1. Introduction

Interacting open many-body quantum systems can display phases that break the time-translation symmetry of the dynamical generator, referred to as time crystals [1, 2, 3, 4]. Such a symmetry breaking constitutes a genuine nonequilibrium phenomenon [5, 6], that can emerge due to the interplay between driving, dissipation and interactions [3, 4]. In these settings, observables of the system, e.g., the average magnetization, exhibit persistent oscillations rather than approaching stationary values [7, 3, 8, 9]. These dissipative time crystals have been extensively explored theoretically and have been found to emerge in a variety of different settings [4, 10, 11, 12, 13, 14, 15, 16, 17, 3, 18, 19, 20, 21]. Several experimental observations on the realization of time crystals have also been reported [22, 23, 24, 25, 26].

Technological applications of time crystals have been proposed in the context of quantum metrology [27, 28, 29, 30] and of quantum thermodynamics, for instance in nonequilibrium quantum engines [21, 31]. In order to be able to assess this potential, there is the need of a consistent thermodynamic description that accounts for their intrinsic nonequilibrium nature [32, 33]. One way to achieve this is by exploiting a collision-model approach for modelling their interaction with the surroundings [34, 35, 36, 37, 38, 39]. Within this framework, the environment consists of a set of ancillae that individually, and unitarily, interact with the system [see Fig. 1(a)]. By evaluating the energy and the information exchange with the ancillae, it is possible to provide a fully consistent characterization of the thermodynamic quantities related to the system [36, 40, 35, 41, 42].

Quantum thermodynamics is also concerned with the use of quantum systems for energy storage. Quantum devices performing this task are also known as quantum batteries [43, 44, 45, 46, 47, 48, 49] and are being studied in the context of closed [50, 51, 52] and open quantum systems [53, 54, 55, 56, 57, 58, 59, 60, 61], for which experimental realisations have been reported [62, 63, 64, 65]. An important platform in this field are driven-dissipative quantum batteries, where a persistent external energy input is used to compete with dissipation effects in order for the system to store a finite amount of energy [56, 57, 66, 45, 67]. However, the possibility of exploiting time crystals as quantum batteries in these driven-dissipative settings has remained unexplored so far.

In this work, we consider a system consisting of two interacting boundary time crystals and explore its potential for energy storage [see Fig. 1]. We investigate the coupled systems focusing on two different setups. In one setup, both boundary time crystals are used for energy storage and the charging occurs due to input from external lasers [see Fig. 1(b)]. This setup is also known as parallel charging process [68, 69]. In the other setup, one boundary time crystal is driven by a laser and is considered to be the charger, while the other one is the battery and is not subject to any external driving. In this way, energy can be transferred from the charger to the battery, which in the time-crystal phase happens via seeding crystallization in time [70] [see Fig. 1(c)]. Through a collision-model approach, we characterize the thermodynamics of these systems which

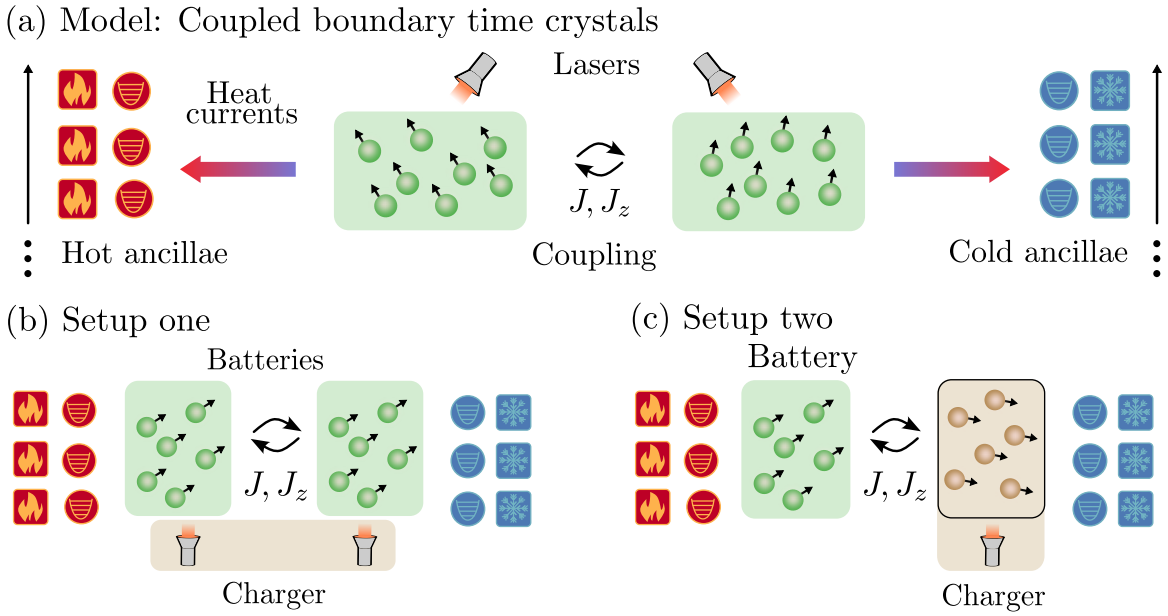

Figure 1. Collision-model setup for a system of two interacting boundary time crystals. (a) A hot ancillary system, in a thermal state with inverse temperature β_1, interacts with one boundary time crystal (BTC), while a cold ancillary system, in a thermal state with inverse temperature β_2, interacts with the other BTC. The two BTCs are also driven by two independent lasers and coupled through an interaction Hamiltonian parametrized by the coupling strengths J, in the x and y directions, and J_z, in the z direction (see main text). (b) Two interacting BTCs working as batteries driven by the lasers. (c) One BTC charging the other one via seeding crystallization in time.

allows us to define a measure of efficiency for the charging process, given by the ratio between stored energy and charging cost. We then compare the energy stored in the batteries and their efficiency when operating in a variety of time-crystal and stationary phases emerging in both setups. Our analysis shows that when the system is found in the time-crystal phase it can store more energy, with a higher efficiency compared to the stationary phase. We also analyze quantum fluctuations in the system and compute quantum and classical correlations between the coupled boundary time crystals. We find that the first setup considered [Fig. 1(b)] exhibits entanglement in the stationary phase, while the second one [Fig. 1(c)] displays entanglement within the time-crystal phase.

2. Model

We consider two ensembles of atoms with N two-level atoms each. Their bare Hamiltonian is ($\hbar = 1$) $H_{\rm at}^{(j)} = \omega_{\rm at} S_z^{(j)}/\sqrt{2}$, where $j = 1, 2$ refers to the atomic systems, and $\omega_{\rm at} > 0$ is the energy splitting between the atomic levels. Here, $S_\alpha^{(j)} = 1/\sqrt{2}\sum_{m=1}^{N} \sigma_{\alpha,m}^{(j)}$ is a collective operator, representing the atoms in the different

ensembles, such that $\sigma^{(j)}_{\alpha,m}$ is the Pauli matrix in the α direction, $\alpha = x, y, z$, for the m-th atom in the j-th ensemble. The two ensembles interact collectively through the Hamiltonian

$$H_{\rm int} = \frac{J}{N}\left(S^{(1)}_x S^{(2)}_x + S^{(1)}_y S^{(2)}_y\right) + \frac{J_z}{N} S^{(1)}_z S^{(2)}_z, \tag{1}$$

where J is the coupling strength in both x and y direction, while J_z is the one in the z directions. The factor $1/N$ is included to ensure a well defined thermodynamic limit [71]. The two ensembles are driven by external lasers that are modelled by the Hamiltonian

$$H^{(j)}_{\rm las} = \frac{\Omega_j}{\sqrt{2}}(S^{(j)}_- e^{i\omega_{\rm las}t} + S^{(j)}_+ e^{-i\omega_{\rm las}t}), \tag{2}$$

where $S^{(j)}_\pm = S^{(j)}_x \pm i S^{(j)}_y$, $\omega_{\rm las}$ is the laser frequency, which we assume to be the same for both ensembles, and Ω_j is the Rabi frequency. The Hamiltonian of the full system is $H_{\rm s} = H^{(1)}_{\rm at} + H^{(2)}_{\rm at} + H^{(1)}_{\rm las} + H^{(2)}_{\rm las} + H_{\rm int}$, which in the frame rotating with the laser frequency, becomes

$$H^{\rm rot}_{\rm s} = \frac{\Omega_1}{\sqrt{2}} S^{(1)}_x + \frac{\Omega_2}{\sqrt{2}} S^{(2)}_x + \frac{\delta}{\sqrt{2}} S^{(1)}_z + \frac{\delta}{\sqrt{2}} S^{(2)}_z + H_{\rm int}. \tag{3}$$

Here $\delta = \omega_{\rm at} - \omega_{\rm las}$ is the detuning between the laser frequency and the energy splitting $\omega_{\rm at}$. Each of the atomic ensembles is coupled to a thermal bath with inverse temperature β_j. The driven-dissipative dynamics is then governed by the master equation $\dot\rho = \mathcal{L}[\rho]$, where

$$\mathcal{L}[\rho] = -i[H^{\rm rot}_{\rm s}, \rho] + \sum_{j,\alpha}\left[L^{(j)}_\alpha \rho (L^{(j)}_\alpha)^\dagger - \frac{1}{2}\left\{(L^{(j)}_\alpha)^\dagger L^{(j)}_\alpha, \rho\right\}\right]. \tag{4}$$

The jump operators that describe the dissipative processes are

$$L^{(j)}_+ = \sqrt{\frac{\kappa n_j}{N}} S^{(j)}_+, L^{(j)}_- = \sqrt{\frac{\kappa(1+n_j)}{N}} S^{(j)}_-, \tag{5}$$

where $n_j = (e^{\beta_j \nu} - 1)^{-1}$ is the occupation number of the environment degrees of freedom, β_j is the inverse temperature and ν the energy scale for the environment. Here, the parameter κ encodes the decay rate. Essentially, the considered system consists of two interacting boundary time crystals and immersed in two separate environments at finite temperature [see sketch in Fig. 1(a)].

3. Quantum thermodynamics

The master equation describing the dynamics of the system, Eq. (4), is a so-called local master equation, characterized by jump operators which do not implement transitions between the eigenstates of the system Hamiltonian [36, 72, 41, 42]. This equation could be obtained by considering that the interaction between the subsystems and the laser driving do not affect the coupling between the bare systems and their environment [73, 32, 74]. Although this phenomenological approach is successfully employed to model and interpret several experiments [75, 76, 77, 78, 79], it can lead

to thermodynamic inconsistencies if the relevant quantities are not properly defined. For example, it can lead to nonequilibrium stationary states featuring persistent heat currents that do not obey Spohn's inequality [80, 32, 81, 21]. In other words, these master equations may apparently violate the laws of thermodynamics as formulated for a system weakly coupled to an external thermal bath [33]. Nevertheless, a consistent description of systems governed by local master equations can be obtained, for instance, by considering a collision-model interpretation of their interaction with the surroundings [38, 39, 37, 35, 36].

In our setup, the two atomic ensembles are coupled to different thermal baths. Within the collision-model approach [38, 39, 37, 35, 36], we model each environment as a stream of ancillary units consisting of bosonic modes. The dynamics follows from the joint unitary time evolution of the system and the ancillae. Each ancilla interacts with the system only once and for a time δt, after which it can be discarded from the description. The process is then repeated with the next ancilla. In the continuum limit $\delta t \to 0$, the sequence of collisions can reproduce the dynamics of the master equation in Eq. (4) [see Fig. 1(a)]. The ancillary systems are described by the bare Hamiltonian $H_{\rm e} = \sum_k [H_{{\rm e}_k}^{(1)} + H_{{\rm e}_k}^{(2)}]$, where $H_{{\rm e}_k}^{(j)} = \nu a_k^{(j)\dagger} a_k^{(j)}$ is the free Hamiltonian of the ancilla corresponding to the k-th collision in system j, ν is its bare frequency, and $a_k^{(j)}$ ($a_k^{(j)\dagger}$) are the bosonic annihilation (creation) operators. The Hamiltonian describing the k-th ancilla interacting with the j-th atomic ensemble is

$$H_{{\rm se}_k}^{(j)}(t) = \sqrt{\frac{\kappa}{N\delta t}}\theta(t,k)\left(a_k^{(j)\dagger} S_-^{(j)} + a_k^{(j)} S_+^{(j)}\right), \tag{6}$$

where $\theta(t,k)$ is defined as $\theta(t,k) = 1$ for $k\delta t < t < (k+1)\delta t$ and 0 otherwise. In order to ensure a completely positive Markovian dynamics for the system, we consider the *ancillae* to be initially in a product state, with each ancilla being in the thermal state with occupation number given by $\langle (a_k^{(j)})^\dagger a_k^{(j)} \rangle = n_j$ [see definition after Eq. (5)]. This collision-model description of the system-environment interaction allows us to derive a consistent thermodynamic description of the system [36, 34].

To this end, we consider the thermodynamic behaviour of the two atomic ensembles in the laboratory frame, in which the contribution from the bare atomic frequency, $H_{\rm at}$, is taken into account. Thus, we start with $H_{\rm s}$ and we consider the variation of the density matrix after a collision,

$$\Delta\rho_{{\rm se}_k} = V_k\left(\rho_{\rm s}\otimes\rho_{{\rm e}_k}\right)V_k^\dagger - \rho_{\rm s}\otimes\rho_{{\rm e}_k}, \tag{7}$$

where $\rho_{{\rm e}_k} = \rho_{{\rm e}_k}^{(1)} \otimes \rho_{{\rm e}_k}^{(2)}$. Here, the unitary evolution of the system and the ancillae reads $V_k = \mathcal{T} e^{-i\int_t^{t+\delta t}\left(H_{\rm s}+H_{{\rm e}_k}^{(1)}+H_{{\rm e}_k}^{(2)}+H_{{\rm se}_k}^{(1)}+H_{{\rm se}_k}^{(2)}\right){\rm d}t'}$. Also, $\mathcal{T}$ is a time-ordering operator, which is needed given that in the laboratory frame $H_{\rm s}$ is time-dependent due to the laser driving and given that the interaction with the ancillae is also time-dependent. The heat dissipated by the j-th system after a collision is defined as minus the energy variation of the ancilla,

$$\Delta Q^{(j)}(t) = -\,{\rm Tr}_k\{H_{{\rm e}_k}^{(j)}\Delta\rho_{{\rm se}_k}\}, \tag{8}$$

where $t = k\delta t$. Similarly, we define the variation of the internal energy of the system after a collision as

$$\Delta U = \Delta U_{\rm s} + \Delta W_{\rm las}, \tag{9}$$

where $\Delta W_{\rm las} = {\rm Tr}_k \{\Delta H_{\rm las}\rho_{{\rm se}_k}\}$ is the work done on the system due to the time-dependence of the laser Hamiltonian and $\Delta U_{\rm s} = {\rm Tr}_k\{H_{\rm s}\Delta\rho_{{\rm se}_k}\}$. We find the first law of thermodynamics by considering that the total work input in the system can be computed as the difference between the variation of the internal energy of the system and the total dissipated heat

$$\dot{W} = \lim_{\delta t\to 0}\frac{1}{\delta t}\left(\Delta W_{\rm env} - \Delta W_{\rm las}\right) = \dot{U}_{\rm s} - \dot{Q}, \tag{10}$$

where $\dot{A} = \lim_{\delta t\to 0}\Delta A/\delta t$, $\dot{Q} = \dot{Q}^{(1)} + \dot{Q}^{(2)}$ and $\Delta W_{\rm env}$ is the work done by turning on the interaction between the system and the different ancillae (see Appendix A for details on the second law of thermodynamics for the coupled boundary time crystals). In the following, we exploit the above thermodynamic quantities to characterize energy storage and its efficiency in two different setups of the coupled boundary time crystals [see an illustration in Fig. 1(b)-(c)].

4. Energy storage with interacting time-crystal batteries

In this section we consider the setup in which the boundary time crystals act as a battery charged by the external lasers and the interaction with the environment [see Fig. 1(b)], such that the system follows a parallel charging process [68, 69]. To lay the foundation for this investigation we first characterize the phase diagram of the system in the thermodynamic limit. We consider both atomic systems to have the same parameters, $\Omega_1 = \Omega_2 = \Omega$ and $\delta = 0$, with all atoms initially in the ground state of the bare atomic Hamiltonian.

We define the average expected values $m_\alpha^{(j)} = \langle S_\alpha^{(i)}/N\rangle$, whose equations of motion can be obtained from the master equation in Eq. (4). In the thermodynamic limit, $N\to\infty$, the average dynamics of the system is exactly described by the mean-field equations [82, 83], which in the rotating frame read

$$\dot{m}_x = (J - J_z)\sqrt{2}m_y m_z + \kappa\sqrt{2}m_x m_z, \tag{11}$$

$$\dot{m}_y = (J_z - J)\sqrt{2}m_x m_z + \kappa\sqrt{2}m_y m_z - \Omega m_z, \tag{12}$$

$$\dot{m}_z = -\kappa\sqrt{2}(m_x^2 + m_y^2) + \Omega m_y. \tag{13}$$

Here $m_\alpha = m_\alpha^{(1)} = m_\alpha^{(2)}$, as for the considered initial conditions both systems feature the same mean-field dynamics. We note that the mean-field equations are not dependent on the temperature of the environments [34]. Besides the conservation of the norm of the vector $\vec{m} = [m_x(t), m_y(t), m_z(t)]$, the system of equations features another conserved quantity. This is given by the expression [3]

$$\Gamma = i\left[\lambda_- \log\left(\lambda_+\eta_+ - \frac{\Omega}{\sqrt{2}}\right) - \lambda_+\log\left(\lambda_-\eta_- - \frac{\Omega}{\sqrt{2}}\right)\right], \tag{14}$$

where $\lambda_\pm = \sqrt{2}(\kappa \pm i(J - J_z))$, and $\eta_\pm = (\pm i m_x + m_y)/\sqrt{2}$, so that its value depends both on system parameters and initial conditions. The system features a stationary phase, a time-crystal phase, and a region in which both phases coexist. In the stationary phase, we find the following stationary solutions for the magnetizations

$$m_x^{\mathrm{s}} = \frac{1}{\sqrt{2}} \frac{\Omega(J_z - J)}{(J_z - J)^2 + \kappa^2}, \tag{15}$$

$$m_y^{\mathrm{s}} = \frac{1}{\sqrt{2}} \frac{\kappa\Omega}{(J_z - J)^2 + \kappa^2}, \tag{16}$$

$$m_z^{\mathrm{s}} = \frac{\pm 1}{\sqrt{2}} \sqrt{1 - \frac{\Omega^2}{(J_z - J)^2 + \kappa^2}}, \tag{17}$$

which exist as long as the condition $(J_z - J)^2 + \kappa^2 \geq \Omega^2$ is satisfied. We note that the magnetization in the z-direction has two possible values, a negative one which is stable and a positive one which is unstable. When the above condition is not fulfilled, the system displays oscillations. The time-crystal phase is characterized by a continuous family of oscillatory solutions, or limit cycles, each one associated with a possible value of the conserved quantity in Eq. (14). This is similar to what is observed in the single boundary time-crystal case [7, 84, 3]. These different oscillatory solutions can be accessed by varying the initial conditions.

Concerning thermodynamic quantities, the heat exchanged with the j-th environment is given by

$$\dot{Q}^{(j)} = -\frac{\kappa\nu}{N} \left\langle (S_x^{(j)})^2 + (S_y^{(j)})^2 + \sqrt{2}(2n_j + 1) S_z^{(j)} \right\rangle, \tag{18}$$

(see Appendix A for details). The heat currents are characterized by a dominant part, proportional to N, and another contribution dependent on the temperature (through n_j) that is intensive with N. This results from the factorization $\langle S_\alpha^{(i)} S_\beta^{(j)}/N^2 \rangle = m_\alpha^{(i)} m_\beta^{(j)} + \mathcal{O}(N^{-1})$, where $\mathcal{O}(N^{-1})$ denotes a contribution of order N^{-1}, which is exact in the thermodynamic limit [34]. Therefore, in this limit, the heat exchanged (per atom) with the j-th environment becomes

$$\dot{q}^{(j)} = -\kappa\nu \left[(m_x^{(j)})^2 + (m_y^{(j)})^2 \right], \tag{19}$$

where we denote $\lim_{N\to\infty} \dot{Q}^{(j)}/N = \dot{q}^{(j)}$. Noteworthily, the heat $\dot{q}^{(j)}$ does not depend on the temperature of environment since the latter does not appear in the mean-field dynamics [34]. Also, the heat is always negative, meaning that energy is dissipated and always flows from the system to the environment. This suggests that no efficient heat engine could be devised from our model [85]. The time-average of $\dot{q}(t)$ during a long time-window, reduces the first law, Eq. (10), to

$$\bar{\dot{w}} = -\bar{\dot{q}}, \tag{20}$$

where $\bar{\dot{a}} = \lim_{t\to\infty} t^{-1} \int_0^t \dot{a}(t')\mathrm{d}t'$. In deriving this expression, we use the fact that the internal energy rescaled by $1/N$ does not grow indefinitely with time, such that $t^{-1} \int_0^t \dot{u}\mathrm{d}t' = t^{-1}(u_t - u_0)$ goes to zero for large times t.

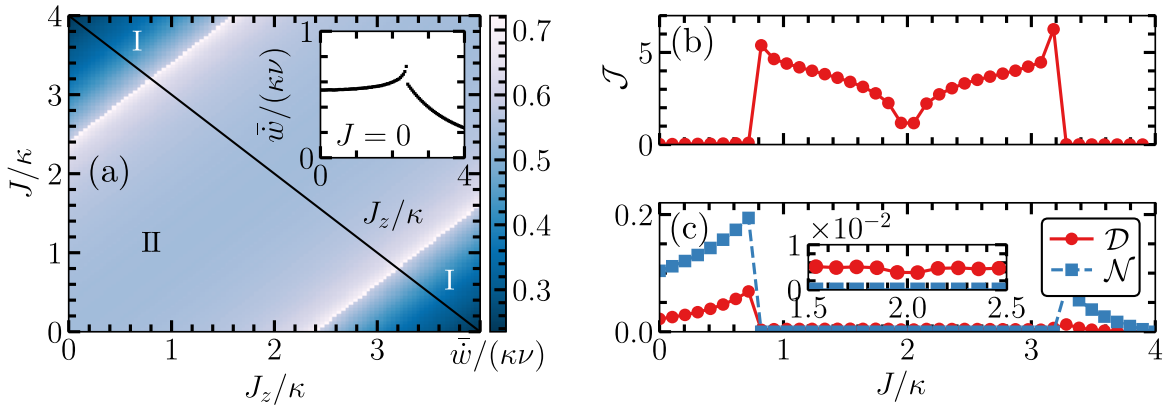

Figure 2. Time-averaged work input and correlations. (a) Total time-averaged work input for varying J_z and J. Region I denotes the stationary phase, while region II the time-crystal phase. The inset shows the phase transition for $J = 0$. The other parameters are $\delta = 0$, $n_1 = n_2 = 0$ and $\Omega_1/2 = \Omega_2/2 = \kappa$. The initial state is $\vec{m}^{(j)} = [0, 0, -1/\sqrt{2}]$ for both systems in every point of the phase-diagram. (b) Time-averaged classical correlations $\mathcal{J}$ and (c) time-averaged quantum discord $\mathcal{D}$ and negativity $\mathcal{N}$ as function of J, such that $J + J_z = 4\kappa$ [see the diagonal in panel (a)]. The mean-field quantities were evolved from $t = 0$ to $t\kappa = 10^3$ and the average was computed by integrating over the second half of the evolution time. The correlations (see Sec. 4.1) were computed considering trajectories between $t = 0$ and $t\kappa = 200$, and the integration was done over the second half of such interval. The remaining parameters are $\Omega_1 = \Omega_2 = 2\kappa$, and $n_1 = n_2 = 0$.

In Fig. 2(a) we show the behavior of the time-averaged work input in the system, $\bar{w}$, which exhibits two distinct dynamical regions. In region I, the mean-field dynamics has a stationary solution, while in region II it only exhibits persistent oscillations. However, in region I, we also observe oscillatory solutions, indicating a bistable regime with coexistence of oscillatory and stationary solutions approached by different initial conditions, see Fig. 3(a) [see also Appendix B for more details]. For the stationary solutions, the total time-averaged work input per particle is given by $\bar{w} = \kappa\nu\Omega^2/[(J - J_z)^2 + \kappa^2]$. This shows that the work input grows higher close to the phase transition, approaching $\bar{w} = \kappa\nu$ near the transition point. In contrast, the work input goes to zero when $(J - J_z)^2 \gg \kappa^2$. In Fig. 2(a), we observe that the work input is higher in the time-crystal phase than in the stationary one, see inset in Fig. 2(a).

4.1. Quantum and classical correlations

Beyond the mean-field description, it is possible to investigate the behavior of quantum fluctuations within the system [86, 87, 34, 16, 88]. Quantum fluctuations can be described through the operators

$$F_\alpha^{(j)} = \frac{S_\alpha^{(j)} - \langle S_\alpha^{(j)} \rangle}{\sqrt{N}}, \tag{21}$$

which describe the deviation of $S_\alpha^{(j)}$ from its average value. These operators account for the leading correction to $\langle S_\alpha^{(j)} S_\beta^{(k)}\rangle/N^2 - m_\alpha^{(j)} m_\beta^{(k)} \approx \langle F_\alpha^{(j)} F_\beta^{(k)}\rangle/N$ and capture both thermal and quantum effects. In the thermodynamic limit, $N \to \infty$, the fluctuations behave as bosonic operators and they follow Gaussian statistics with zero average. Therefore, the states of the fluctuations are fully characterized by the 6×6 covariance matrix $G_{\alpha\beta}^{(j,k)} = \langle\{F_\alpha^{(j)}, F_\beta^{(k)}\}\rangle/2$ [89, 90]. Additionally, these operators obey the commutation relations

$$\lim_{N\to\infty} -i\langle[F_\alpha^{(j)}, F_\beta^{(k)}]\rangle = \sqrt{2}\sum_\gamma \epsilon_{\alpha\beta\gamma}\delta_{jk} m_\gamma^{(j)} = \delta_{jk} s_{\alpha\beta}, \tag{22}$$

where $\epsilon_{\alpha\beta\gamma}$ is a Levi-Civita tensor, δ_{jk} is the Kronecker delta and $s_{\alpha\beta}$ is a symplectic matrix. These commutation relations entail the fact that the fluctuations remain quantum in the thermodynamic limit and can thus be used to describe collective non-classical correlations [86, 90]. The dynamics of the covariance matrix can be computed through Eq. (4) in the Heisenberg picture, and it is given in Appendix C.

To evaluate the correlations among the boundary time crystals, we can analyse the fluctuations in the reference frame which rotates solidly with the mean-field observables, such that the commutation relations in Eq. (22) become time independent [8, 16]. To obtain this rotated frame, we first consider a time-dependent rotation matrix $R(t)$ that evolves the mean-field equations, $\vec{m}(t) = R(t)\vec{m}(0)$. To find $R(t)$, we rewrite the mean-field equations as $\dot{\vec{m}}(t) = D(t)\vec{m}(t)$, where $D(t)$ is a time-dependent matrix and $\vec{m} = [m_x^{(1)}, m_y^{(1)}, m_z^{(1)}, m_x^{(2)}, m_y^{(2)}, m_z^{(2)}]$ is the vector of the mean-field variables. The rotation $R(t)$ follows from the integration of $\dot{\vec{m}}(t)$ (see Appendix C for more details). Thereafter, we define the rotated fluctuation operators $\vec{X} = R^T(t)\vec{F} = [x_1, p_1, w_1, x_2, p_2, w_2]$, where $\vec{F} = [F_x^{(1)}, F_y^{(1)}, F_z^{(1)}, F_x^{(2)}, F_y^{(2)}, F_z^{(2)}]$ is the vector of the quantum fluctuation operators of the atomic ensemble. In the rotated reference frame, the quantum fluctuations obey a two-mode bosonic algebra $[x_j, p_k] = i\delta_{jk}$ and w_j commutes with all the other operators. Hence, w_j does not contribute to the dynamics of the bosonic fluctuations. Finally, we define the rotated covariance matrix $\bar{G} = R^T(t)G(t)R(t)$, which represents a two-mode Gaussian system [86] (see Appendix C for more details).

Using the symplectic eigenvalues of $\bar{G}$ [91], we can evaluate the von Neumann entropy, defined as $S(\rho) = -\operatorname{Tr}[\rho \ln \rho]$, for the coupled boundary time crystals [34]. Additionally, we can use the results on Gaussian bosonic systems to calculate classical and quantum correlations within the system, denoted by $\mathcal{J}$, and the quantum discord, $\mathcal{D}$, respectively. Here, we note that the mutual information between the two modes is $I = \mathcal{D} + \mathcal{J}$. In addition to that, we can also evaluate the negativity, $\mathcal{N}$, which measures collective entanglement between fluctuations of the coupled systems [92, 93] (see Appendix C.2 for more details).

The behavior of correlations is shown in Fig. 2(b)-(c). We evaluate the quantities calculated from fluctuations along the diagonal line in Fig. 2(a) given by $J + J_z = 4\kappa$, such that we can visualize correlations in both phases. When starting from the time-crystal phase, the classical correlations exhibit a sudden jump from the stationary phase to the time-crystalline phase. On the other hand, the discord and the entanglement

negativity have higher values in the stationary phase as compared to the time-crystal one. We note that in the time-crystal phase both discord and classical correlations are minimized at the point $J = J_z$. Remarkably, there is no entanglement in the time-crystal phase.

When $J = J_z$ the mean-field equations recover those of a single boundary time crystal. This can be understood in the context of synchronization blockade [94, 95, 96], where the systems dynamics are effectively decoupled in spite of the interaction terms. Also, along this line of the phase-diagram, an analytical solution for the mean-field equations is known [8], allowing us to write down the Hamiltonian and jump operators describing the dynamics of the Gaussian fluctuations [8, 16]. In particular, we find the Hamiltonian in the rotated frame to be

$$H_{\rm f} = J\left[x_1 x_2 + p_1 p_2\right], \tag{23}$$

which is time-independent and represents just an exchange of excitations term. Also, each mode is affected by the jump operators

$$V^{(j)}(t) = x_j - i\sqrt{2} m_z^{(j)}(t) p_j \tag{24}$$

and $[V^{(j)}(t)]^\dagger$. This analysis shows that although the atomic systems become decoupled at the mean-field level when $J = J_z$, they still develop collective correlations which are captured by quantum fluctuations.

4.2. Energy storage

In order to quantify the amount of energy stored within the system, we consider the difference between the instantaneous intensive energy in the system and the energy contained at the initial time, $\mathcal{E}(t) = \mathrm{Tr}\{[\rho(t) - \rho(0)]H_{\rm ref}\}/N$, where $H_{\rm ref}$ is a Hamiltonian operator encoding the accessible energy which can be stored in the system [97, 82, 98]. In particular, we shall consider $H_{\rm ref}$ to be related to the bare energy of the atoms, which is also justified by the fact that typically $\omega_{\rm at} \gg J, J_z, \Omega$. The mean-field description of the system provides a way to estimate the intensive quantity $\mathcal{E}(t)$ in the thermodynamic limit.

When the lasers are turned off, the dissipation brings the system toward the ground state of the bare atom Hamiltonian from which no energy can be extracted [99, 100]. To store energy within the system, one thus needs an external energy input from the laser which constitute a charging "cost" necessary to sustain a nonequilibrium state featuring a finite energy. As a consequence, an important quantity to characterize driven-dissipative batteries is the charging efficiency, which measures the ratio between the stored energy and the total energy input to keep the battery charged [46, 56, 57]

$$\eta(t) = \frac{\mathcal{E}(t)}{\int_0^t \dot{w}(u)\mathrm{d}u} = \frac{\mathcal{E}(t)}{\Delta u_{\rm s}(t) - \int_0^t \dot{q}(u)\mathrm{d}u}, \tag{25}$$

where $\Delta u_{\rm s}(t) = \mathrm{Tr}\{[\rho(t) - \rho(0)]H_{\rm s}\}/N$, and the second equality follows from the first law of thermodynamics given in Eq. (10). Here, $H_{\rm s}$ is the Hamiltonian of the system

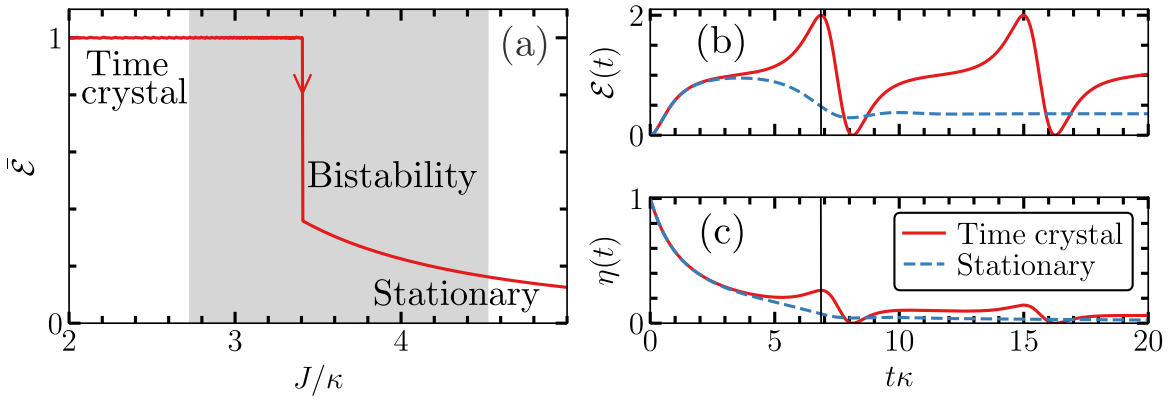

Figure 3. Stored energy and charging efficiency. (a) Time-averaged stored energy in both atomic ensembles, defined as $\bar{\mathcal{E}} = \lim_{t\to\infty} t^{-1} \int_0^t \mathcal{E}(t')\mathrm{d}t'$, in units of $\omega_{\rm at}$. Here, we consider the initial condition to be with all atoms in the ground state. The gray region indicates a bistable regime, that we can access by following adiabatically the time-crystal solution as the interaction parameter J is increased. When starting from the ground state, the systems goes to the stationary phase before the end of the bistable region. The other parameters are $\Omega = 2\kappa$ and $J_z = \kappa$. (b)-(c) Stored energy (in units of $\omega_{\rm at}$) and efficiency as function of time for a time-crystal solution (red solid line) and a stationary one (blue dashed line). In both cases, the initial conditions were $\vec{m} = [0, 0, -1/\sqrt{2}]$ and for the time-crystal solution we set $J = 3.4\kappa$ while for stationary we use $J = 3.41\kappa$. The vertical black lines show that the second peak of efficiency correspond to the maximum stored energy. The remaining parameters are: $\Omega = 2J_z = 2\kappa$ and $\omega_{\rm at} = \nu$.

in the laboratory frame and we note that $\dot{q}$ is always negative. Given the assumption $\omega_{\rm at} \gg J, J_z, \Omega$, we can consider that $H_{\rm s} \approx H_{\rm at}^{(1)} + H_{\rm at}^{(2)}$ so that $\Delta u_{\rm s}(t)$ is well approximated by the variation of the bare atom energy in both atomic ensembles. The quantity $\eta(t)$ provides the efficiency of the charging process when $\mathcal{E}(t) > 0$, otherwise the process is actually removing energy from the system. Given that the stored energy is bounded in time while the cost to keep the energy stored grows linearly with time, $\eta(t)$ approaches zero as the dynamics total time goes to infinity.

For the setup considered in this section [cf. Fig. 1(b)], the reference Hamiltonian is $H_{\rm ref} = H_{\rm at}^{(1)} + H_{\rm at}^{(2)}$ and we further consider all atoms initially in the ground state. In this case, we have $\Delta u_{\rm s}(t) \approx \mathcal{E}(t) \geq 0$. Fig. 3(a) shows that, averaging over the charging time, the time-crystal phase can store large amounts of energy. Note that there is a bistable region, in gray, in which the stationary solution and the time-crystal solution coexist. Upon varying the parameter J, the system jumps from the time-crystal phase to the stationary one and the amount of stored energy drastically decreases. In Fig. 3(b)-(c) we plot the stored energy and the efficiency of the charging process as a function of time. Here, we compare the time-crystal phase with the stationary one. To this end, we consider two values of the interaction strength J which are extremely close one another, but with one giving rise to a time-crystal and the other to a stationary phase. Essentially, one interaction strength is on the left and the other one on the right of the

value at which the stored energy drops in Fig. 3(a). We clearly see that the time-crystal phase allows to store more energy than the stationary phase [cf. Fig. 3(b)]. These peaks could serve as optimal times for energy extraction. In Fig. 3(c), we also see that the charging efficiency, as a function of time, is typically higher in the time-crystal regime.

5. Charging by seeding crystallization in time

We now investigate the energy storage and its efficiency in a battery which is charged via seeding crystallization in time [70]. In this setup, [cf. Fig. 1(c)], we consider one atomic ensemble without external driving as the battery, while the second atomic ensemble, referred to as the charger, is driven by a laser. For simplicity, we consider, apart from the laser driving, both atomic systems with the same parameters, and $\delta = J_z = 0$. In addition to that, we consider initial conditions with $m_x^{(2)} = m_y^{(1)} = 0$, which leads to $m_x^{(2)}(t) = m_y^{(1)}(t) = 0$ for all times. Given that the the norm of the vector $\vec{m}^{(j)}(t) = [m_x^{(j)}(t), m_y^{(j)}(t), m_z^{(j)}(t)]$ is conserved in each system, we can express the magnetizations as

$$\begin{aligned} m_x^{(1)}(t) &= m_0 \sin[f^{(1)}(t)], \quad m_z^{(1)}(t) = m_0 \cos[f^{(1)}(t)], \\ m_y^{(2)}(t) &= m_0 \sin[f^{(2)}(t)], \quad m_z^{(2)}(t) = m_0 \cos[f^{(2)}(t)], \end{aligned} \tag{26}$$

where $m_0 = -1/\sqrt{2}$. By exploiting the aforementioned conditions, one can show that the dynamics of the coupled system is determined by

$$\begin{aligned} \dot{f}^{(1)} &= -J \sin(f^{(2)}) - \kappa \sin(f^{(1)}), \\ \dot{f}^{(2)} &= J \sin(f^{(1)}) - \kappa \sin(f^{(2)}) - \Omega. \end{aligned} \tag{27}$$

This dynamical system features a rich phase diagram containing limit cycles, quasi-periodic oscillations, stationary solutions, as well as bistable regimes, as illustrated in Fig. 4(a). In the stationary regime, the stationary solutions of Eq. (27) are given by

$$m_z^{(1)} = \frac{\pm 1}{\sqrt{2}} \sqrt{1 - \frac{(J\Omega)^2}{(J^2+\kappa^2)^2}}, \qquad m_z^{(2)} = \frac{\pm 1}{\sqrt{2}} \sqrt{1 - \frac{(\kappa\Omega)^2}{(J^2+\kappa^2)^2}}, \tag{28}$$

where only the negative $m_z^{(j)}$ is stable. Here, we observe two conditions that have to be simultaneously satisfied for the existence of stationary solutions, $\mathcal{C}_1 : J^2 + \kappa^2 \geq \kappa\Omega$ and $\mathcal{C}_2 : J^2 + \kappa^2 \geq J\Omega$. Using these conditions, we can find the critical interaction strength determining the transition between the stationary and non-stationary phases,

$$J_c = \max_{J \in \mathbb{R}} \left(J = \sqrt{\Omega\kappa - \kappa^2}, 2J = \Omega + \sqrt{\Omega^2 - 4\kappa^2} \right). \tag{29}$$

We note the same behavior observed in the first setup, with strong interactions driving the system towards a stationary phase.

In Fig. 4(a) we show the phase diagram for the time-averaged total work input in both battery and charger starting from the initial condition in which all atoms are in the ground state. Under these conditions, we can identify four distinct dynamical regions. We have region Ia featuring stationary solutions, region II displaying quasi-periodic

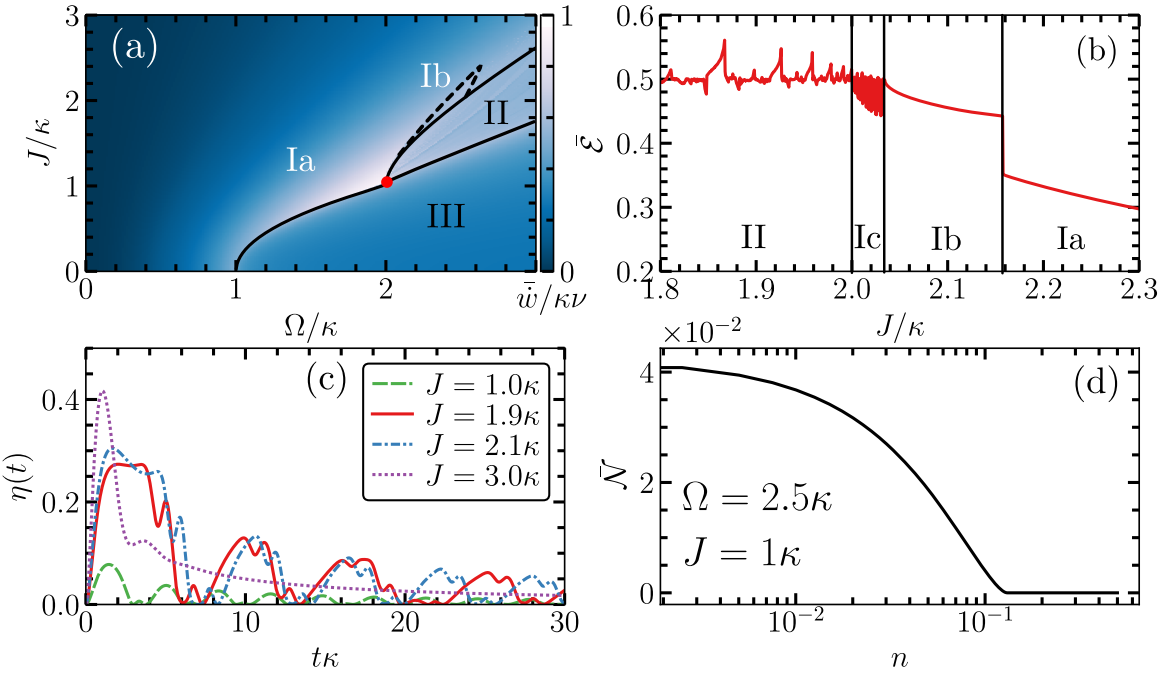

Figure 4. Work input, efficiency, and entanglement. (a) Time-integrated average work input as a function of J and Ω. We compute this phase-diagram by considering all atoms initially in the ground state for all points. We identify four regions: stationary (Ia), limit cycle (Ib), oscillatory regime between limit cycle and stationary (Ic), quasi-periodic oscillations (II) and limit cycle (III). (b) A section of the phase diagram (a) for the time-averaged stored energy in units of $\omega_{\rm at}$ as function of J/κ for $\Omega = 2.5\kappa$. In region II, we have the stored energy in the quasi-periodic regime. In Ic, the system oscillates between limit-cycles and stationary values for small variations of J/κ. After this intermediate region, it goes to region Ib until it reaches region Ia. Here we time-average trajectories with total time $t\kappa = 10^3$. The stored energy is given in units of $\omega_{\rm at}$. (c) The efficiency $\eta(t)$ as function of time, for four values of J, as indicated in the legend. Here $\Omega = 2.5\kappa$. The blue dashed line correspond to a limit-cycle solution found in region I with initial state being the ground state of $H_{\rm at}$ (d) Time-averaged entanglement negativity between the charger and the battery as function of the occupation number $n_1 = n_2 = n$. We further set $\omega_{\rm at} = \nu$.

solutions, region III characterized by one limit cycle solution, and region Ib characterized by limit-cycle phase when starting from all atoms down (a stationary solution is also possible when starting from a different initial condition). From the condition in Eq. (29), we identify a tricritical point [red dot in Fig. 4(a)], given by $J = \kappa$ and $\Omega = 2\kappa$, between regions I, II, and II, as well as the curve separating the stationary phase from the other ones. We can interpret the emergence of quasi-periodicity as follows: in region I, both stationary conditions are satisfied, while in region III, the condition for non-stationarity $\mathcal{C}_2$ is not valid, regardless of the validity of $\mathcal{C}_1$. For this region, the charger seeds time crystallization in the battery. Conversely, in region II, only $\mathcal{C}_1$ is not satisfied. This suggests that the competition between the battery preferring an oscillatory solution

while the charger a stationary one gives rise to the quasi-periodic regime. Moreover, in the stationary region, the total work input assumes the same form as the setup we considered in Sec. 4, i.e. $\bar{\dot{w}} = \kappa\nu\Omega^2/[J^2+\kappa^2]$.

For this setup [cf. Fig. 1(c)] we consider that energy can only be stored in the atomic ensemble which is not directly driven by the laser, i.e., $H_{\rm ref} = \omega_{\rm at} S_z^{(1)}/\sqrt{2}$. Recalling that $H_{\rm s} \approx H_{\rm at}^{(1)} + H_{\rm at}^{(2)}$ due to our assumption $\omega_{\rm at} \gg J, J_z, \Omega$ and considering all atoms initially in the ground state, the efficiency $\eta(t)$ is always between 0 and 1, since $\Delta u_s(t) \geq \mathcal{E}(t)$. Here, we consider a cut in the phase diagram with a fixed laser driving and we vary the interaction, Fig. 4(b). For these parameters, we evaluate the time-averaged stored energy in the process. We observe that in the quasi-periodic phase the system can store, on average, more energy than in the other phases. Also, in region Ib the system attains higher values of time-averaged stored energy. However, when the system parameters belong to region Ia, the amount of stored energy drops considerably. We note that region Ib coexists with region Ia and in region Ic, the system oscillates between limit-cycles and stationary solutions for small variations of J/κ (see Appendix E for more details on the presence of multistability in this parameter regime).

In Fig. 4(c) we plot the efficiency $\eta(t)$ for fixed driving and varying coupling, showing that it reaches a maximum value during the transient phase of the stationary solution. After this, the efficiency assumes higher values for the quasi-periodic and limit cycle solutions. We interpret this result as follows. A small J limits the flux of energy from the charger to the battery, which makes the limit cycle phase in region III not efficient in storing energy, since the battery oscillates close to its ground state. On the other hand, in the region of quasi-periodicity and for limit cycles solutions in region Ib, the internal energy in the battery system oscillates around half of its maximum value and with high amplitude, thereby achieving large values of both $\mathcal{E}(t)$ and $\eta(t)$.

In addition to the stored energy, we investigate correlation properties in this setup. We observe a finite entanglement negativity in the time-crystal phase, which vanishes as the temperature increases, as shown in Fig. 4(d). To further understand this behaviour in the limit-cycle phase, we look at the Hamiltonian of the fluctuation operators

$$H_{\rm f}(t) = J\sqrt{2}[m_z^{(2)}(t)x_1x_2 + m_z^{(1)}(t)p_1p_2]. \tag{30}$$

This Hamiltonian contains two time-dependent terms, that are related to two-mode squeezing and excitation exchange, and allow for entanglement during limit cycle phases [16]. The jump operators of system j, have the same form of the one reported for the other setup. The persistent entanglement may be further explored, for instance, for metrological applications [27, 101, 102] (see Appendix C for furthers details).

6. Conclusions

We have fully characterized of the non-linear dynamics and thermodynamics of two coupled boundary time crystals. Using this characterization, we have investigated the coupled systems in the context of energy storage. Our thermodynamic analysis allowed

us to assess the efficiency of driven-dissipative quantum batteries operating in both stationary and oscillatory phases. We have explored energy storage within two different setups and observed distinct features. In the first setup, where both atomic ensembles are regarded as the batteries and the charging is provided by external lasers following a parallel charging process, we have found that the time-crystal phase surpasses the stationary phase in both the amount of stored energy and efficiency. In addition to that, we have shown that in this setup the batteries develop quantum correlations in both phases, but with non-zero entanglement only within the stationary phase. In the second setup, where one atomic ensemble transfers energy to the other one, we have found that the dynamics is described by a set of non-linear coupled phase equations. These equations provide the critical lines, separating the stationary solutions from the limit cycle and the quasi-periodic solutions. Regarding this setup, our analysis suggests that the optimal time for energy storage occurs during a transient phase toward the stationary state. However, we also observe that when the system operates in oscillatory phases, it demonstrates high efficiency in storing energy for longer periods of time. Furthermore, we show that the battery and the charger can remain entangled during the limit cycle phase. Our findings suggest that coupled boundary time crystals can be used as quantum batteries that operate in both oscillatory and stationary phases.

The codes used to produce the numerical results of this paper are available on Github [103].

Acknowledgments

We are grateful to Farokh Mivehvar and Parvinder Solanki for useful discussions. We acknowledge funding from the Deutsche Forschungsgemeinschaft (DFG, German Research Foundation) under Project No. 435696605 and through the Research Units FOR 5413/1, Grant No. 465199066 and FOR 5522/1, Grant No. 499180199. This project has also received funding from the European Union's Horizon Europe research and innovation program under Grant Agreement No. 101046968 (BRISQ). F.C. is indebted to the Baden-Württemberg Stiftung for the financial support of this research project by the Eliteprogramme for Postdocs. A.C. is grateful for financing from the Deutsche Forschungsgemeinschaft (DFG, German Research Foundation) through the Walter Benjamin programme, Grant No. 519847240. G.D.C. acknowledges support from the UK EPSRC through Grant No. EP/S02994X/1. This work was funded by the QuantERA II Programme (project CoQuaDis, DFG Grant No. 532763411) that has received funding from the EU H2020 research and innovation programme under GA No. 101017733.

Appendix

Appendix A. Thermodynamics of collision models

In this Appendix, we provide additional details on the derivation of a consistent thermodynamic description for the coupled boundary time crystal system. In order to do so, we consider the dynamics of the system composed by the coupled atomic ensembles together with the ancillae, defining the collision model. Our derivation follows closely the ones presented in Refs. [36, 34].

The dynamics of the atomic systems interacting with the ancillae is governed by the following Hamiltonian in the laboratory frame

$$H_k(t) = \sum_{j=1,2} [H_{\rm at}^{(j)} + H_{\rm e_k}^{(j)} + H_{\rm se_k}^{(j)}(t)] + H_{\rm int} \tag{A.1}$$

$$+ \sum_{j=1,2} \frac{\Omega_j}{\sqrt{2}} (S_-^{(j)} e^{i\omega_{\rm las} t} + S_+^{(j)} e^{-i\omega_{\rm las} t}), \tag{A.2}$$

where we consider both lasers with the same frequency and the Hamiltonians for the atomic ensembles and k-th ancilla are defined in the main text. In this way, we now evaluate the quantities related to the first law of thermodynamics. To this end, we consider the variation of the density matrix after a single collision between the system and an ancilla

$$\Delta\rho_{\rm se_k} = V_k \left(\rho_{\rm s} \otimes \rho_{\rm e_k}\right) V_k^\dagger - \rho_{\rm s} \otimes \rho_{\rm e_k}, \tag{A.3}$$

where $\rho_{\rm e_k} = \rho_{\rm e_k}^{(1)} \otimes \rho_{\rm e_k}^{(2)}$ and

$$V_k = \mathcal{T} e^{-i \int_t^{t+\delta t} H_k(t) {\rm d}t'}, \tag{A.4}$$

where $\mathcal{T}$ is the time-ordering operator.

The dissipated heat to the environment j is given by the energy absorbed by the k-th ancilla during the collision with the system

$$\Delta Q_k^{(j)} = -\lim_{\delta t \to 0} \frac{1}{\delta t} {\rm Tr}_k \{\nu (a_k^{(j)})^\dagger a_k^{(j)} \Delta\rho_{\rm se_k}\}. \tag{A.5}$$

In addition to that, the change in the internal energy of the system reads

$$\Delta U_k = \lim_{\delta t \to 0} \frac{1}{\delta t} {\rm Tr}_k \{H_{\rm s} \Delta\rho_{\rm se_k} + \Delta H_{\rm s} \rho_{\rm s} \otimes \rho_{\rm e_k}\}$$

where the second term accounts for the change in the Hamiltonian due the time-dependency. In order to compute the quantities above, we can go to the Heisenberg picture

$$\Delta\langle\mathcal{O}\rangle = \langle V_k^\dagger \mathcal{O} V_k - \mathcal{O}\rangle.$$

For calculating the above expression, we expand the unitary operator in Eq. (A.4) up to the second order in δt, finding

$$\Delta\langle\mathcal{O}\rangle = i\delta t \langle[H_k, \mathcal{O}]\rangle - \frac{\delta t^2}{2} \langle[H_k, [H_k, \mathcal{O}]]\rangle.$$

We use the limit $\delta t \ll \omega_{\rm las}^{-1}$, such that the time-dependent laser term remains approximately constant during one collision. Using that the ancillary system is in a product and thermal state, the dynamics of the Hamiltonians simplifies to

$$\begin{aligned}\Delta\langle H_{\rm s}\rangle &= -\frac{\delta t^2}{2}\langle[H_{{\rm se}_k},[H_{{\rm se}_k},H_{\rm s}]]\rangle + \delta t\langle\dot{H}_{\rm s}\rangle,\\ \Delta\langle H^{(j)}_{e_k}\rangle &= -\frac{\delta t^2}{2}\langle[H^{(j)}_{{\rm se}_k},[H^{(j)}_{{\rm se}_k},H^{(j)}_{{\rm e}_k}]]\rangle.\end{aligned}$$

The quantity $\langle\dot{H}_{\rm s}\rangle$ is referred as an external work input from the lasers. In order to perform the calculations, it is more convenient to move to the frame rotating with the laser. This can be achieved through the unitary transform for the k-th collision

$$\mathcal{V}_k = e^{-i\omega_{\rm las}t\left[(a_k^{(1)})^\dagger a_k^{(1)}+(a_k^{(2)})^\dagger a_k^{(2)}+\frac{S_z^{(1)}}{\sqrt{2}}+\frac{S_z^{(2)}}{\sqrt{2}}\right]},$$

such that $\tilde{\rho}_{{\rm se}_k} = \mathcal{V}_k\rho_{{\rm se}_k}\mathcal{V}_k^\dagger$. With this, we find the Hamiltonian in the rotating frame

$$H_{\rm s}^{\rm rot} = H_{\rm int} + H^{(1)}_{{\rm se}_k} + H^{(2)}_{{\rm se}_k} \tag{A.6}$$

$$+\frac{\Omega_1}{\sqrt{2}}S_x^{(1)} + \frac{\Omega_2}{\sqrt{2}}S_x^{(2)} + \frac{\delta}{\sqrt{2}}S_z^{(1)} + \frac{\delta}{\sqrt{2}}S_z^{(2)} \tag{A.7}$$

$$+\tilde{\delta}(a_k^{(1)})^\dagger a_k^{(1)} + \tilde{\delta}(a_k^{(2)})^\dagger a_k^{(2)}, \tag{A.8}$$

where $\tilde{\delta} = \nu - \omega_{\rm las}$. In the first line, the Hamiltonians remain unchanged, in the second and third lines we have the Hamiltonians of the atomic systems and of the ancillae in the rotating frame, respectively. We remark that when performing the collision dynamics within this Hamiltonian using $\delta t \to 0$, we find the Lindblad equation reported in the main text, Eq. (4).

Here we provide details about the calculation of the dissipated heat. We start with the dissipated heat in the laboratory frame and we use identities $\mathcal{V}_k^\dagger\mathcal{V}_k = \mathcal{V}_k\mathcal{V}_k^\dagger = I$ and the cyclic property of the trace, such that we can use the state evaluated in the rotating frame to compute the observables of interest in the laboratory frame. In this way, we obtain the heat dissipated to the j-th environment

$$\begin{aligned}\Delta Q^{(j)} &= -\Delta\langle H^{(j)}_{{\rm e}_k}\rangle\\ &= -\frac{\delta t\kappa\nu}{2N}{\rm Tr}\left\{\left[S_+^{(j)}S_-^{(j)} + S_-^{(j)}S_+^{(j)}\right.\right.\\ &\left.\left.+2\sqrt{2}S_z\left(2(a_k^{(j)})^\dagger a_k^{(j)}+1\right)\right]\tilde{\rho}_{{\rm se}_k}\right\}.\end{aligned} \tag{A.9}$$

We note that when considering a mesoscopic scale, $1 \ll N < \infty$, we can approximate the dissipated heat by the j-th system to [34]

$$\dot{Q}^{(j)}(t) \approx N\dot{Q}^{(j)}_{\rm mf}(t) + \dot{Q}^{(j)}_{\rm sub}(t) \tag{A.10}$$

where $\dot{Q}^{(j)}_{\rm mf}(t) = -\kappa\nu[(m_x^{(j)})^2 + (m_y^{(j)})^2]$ and

$$\dot{Q}^{(j)}_{\rm sub} = -\kappa\nu\left[G^N_{x_jx_j} + G^N_{y_jy_j} + \sqrt{2}m_z^{(j)}(2n_j+1)\right], \tag{A.11}$$

where total dissipated heat is given by an extensive contribution from the mean-field, $\dot{Q}^{(j)}_{\rm mf}$, and a intensive contribution that accounts for the fluctuations effects, $\dot{Q}^{(j)}_{\rm sub}$. The matrix G is defined in the Appendix C.

Moreover, given that the collision model reproduces the Lindblad equation reported in the main text, the variation of the internal energy can be calculated through the equation

$$\dot{U} = \sum_{j,\alpha} \langle \mathcal{D}^*_{j,\alpha}[H_{\rm s}] \rangle + \dot{W}^{(1)}_{\rm las} + \dot{W}^{(2)}_{\rm las}, \tag{A.12}$$

where $\mathcal{D}^*_{j,\alpha}$ is the dual generator of the dissipative part of the dynamical generator, given by

$$D^*_{j,\alpha}[X] = \sum_{j,\alpha} \left[(L^{(j)}_\alpha)^\dagger X L^{(j)}_\alpha - \frac{1}{2} \left\{ (L^{(j)}_\alpha)^\dagger L^{(j)}_\alpha, X \right\} \right], \tag{A.13}$$

where X is an arbitrary operator. Here we note that the unitary $\mathcal{V}_k$ leaves the dissipative part unchanged. Finally, the work input from the lasers is calculated by considering the time-derivative of the Hamiltonian of the laser

$$\dot{W}^{(j)}_{\rm las} = \frac{\Omega_j}{\sqrt{2}} \, {\rm Tr} \left[\frac{\rm d}{{\rm d}t} (S^{(j)}_- e^{-i\omega_{\rm las} t} + S^{(j)}_+ e^{+i\omega_{\rm las} t}) \rho_{\rm s} \otimes \rho_{{\rm e}_k} \right]. \tag{A.14}$$

Then, we remove the time-dependency by inserting the identities $\mathcal{V}$, such that we find

$$\dot{W}^{(j)}_{\rm las} = -i \frac{\omega_{\rm las} \Omega_j}{\sqrt{2}} \, {\rm Tr} \left\{ (S^{(j)}_- - S^{(j)}_+)(\rho_{\rm s} \otimes \rho_{{\rm e}_k})_{\rm rot} \right\} = -\omega_{\rm las} \Omega_j \sqrt{2} \langle S^{(j)}_y \rangle. \tag{A.15}$$

Appendix A.1. The second law

In this section, we are going to derive the second law of thermodynamics for the coupled boundary time crystals. This follows closely the derivations presented in Refs. [34, 104].

We start by defining the states, $\rho'_{{\rm se}_k} \equiv V_k \left(\rho_{\rm s} \otimes \rho_{{\rm e}_k} \right) V_k^\dagger$, $\rho'_{\rm s} \equiv {\rm Tr}_k[\rho_{{\rm se}_k}]$, $\rho'_{{\rm e}_k} \equiv {\rm Tr}_{\rm s}[\rho'_{{\rm se}_k}]$, $\rho^{(1)\prime}_{{\rm e}_k} \equiv {\rm Tr}_2[\rho'_{{\rm e}_k}]$, and $\rho^{(2)\prime}_{{\rm e}_k} \equiv {\rm Tr}_1[\rho'_{{\rm e}_k}]$. Here we remark that for the derivation of the first law of thermodynamics, we look to the energy exchanged between the system and the ancillae system. For the second law, however, we consider the information loss when we trace-out the ancillae degrees of freedom. In this way, we can express the entropy production for this system as

$$\Sigma = \mathcal{I}_{{\rm e}_k}({\rm s} : {\rm e}_k) + S(\rho'_{{\rm e}_k} || \rho_{{\rm e}_k}) \geq 0, \tag{A.16}$$

where $\mathcal{I}_{{\rm e}_k}({\rm s} : {\rm e}_k) = S(\rho'_{{\rm e}_k}) + S(\rho'_{\rm s}) - S(\rho'_{{\rm se}_k})$ denotes the mutual information between the ancilla after the j-th collision and the system. $S(A||B) = {\rm Tr}[A \ln A - A \ln B]$ is the is the relative entropy between the states A and B. Here, $S(A) = -{\rm Tr}[A \ln A]$ is the von Neumann entropy. The positivity of the entropy production is valid since both mutual information and relative entropy are positive. Moreover, we can rewrite the entropy production above as

$$\Sigma = \Delta S - \Phi_k, \tag{A.17}$$

where $\Phi_k = \Phi^{(1)}_k + \Phi^{(2)}_k$, is the entropy flux from the system to the environments during the k-th collision, with

$$\Phi^{(j)}_k = {\rm Tr}[(\rho^{(j)\prime}_{{\rm e}_k} - \rho^{(j)}_{{\rm e}_k}) \ln \rho^{(j)}_{{\rm e}_k}]. \tag{A.18}$$

ΔS is the variation of the von Neumann entropy of the system. When dividing the above equation by δt and taking the limit of δt to zero, we go to the continuous limit, with $\dot{\Sigma} = \dot{S} - \dot{\Phi}$. In our model, we consider that the ancillary systems are initially in a thermal state, given by $\rho_{\mathrm{e}_k}^{(j)} = e^{-\beta_j H_{\mathrm{e}_k}^{(j)}}/Z_{\mathrm{e}_k}^{(j)}$, where $Z_{\mathrm{e}_k}^{(j)}$ is the partition function of the thermal ancilla k interacting with the j-th environment. In this scenario, the entropy flux reduces to

$$\dot{\Phi}^{(j)}(t) = -\beta_j \lim_{\delta t \to 0} \frac{1}{\delta t} \mathrm{Tr}\{(\rho_{\mathrm{e}_k}^{(j)\prime} - \rho_{\mathrm{e}_k}^{(j)})\nu (a_k^{(j)})^\dagger a_k^{(j)}\} = \beta \dot{Q}^{(j)}(t). \tag{A.19}$$

This result shows that when the ancillae are in a thermal state, the entropy flux to the environment is proportional to the heat current flowing between the system and the bath [34, 104]. In the thermodynamic limit, the heat currents are always negative for our model.

Appendix B. Mean-field dynamics

In this appendix we write down the full system of equations describing the mean-field dynamics of the coupled boundary time crystals. This is given by

$$\begin{aligned}
\dot{m}_x^{(1)} =& -J_z\sqrt{2}m_y^{(1)}m_z^{(2)} + J\sqrt{2}m_y^{(2)}m_z^{(1)} \\
& -\delta m_y^{(1)} + \kappa\sqrt{2}m_x^{(1)}m_z^{(1)}, \\
\dot{m}_y^{(1)} =& -J\sqrt{2}m_z^{(1)}m_x^{(2)} + J_z\sqrt{2}m_x^{(1)}m_z^{(2)} \\
& -\Omega_1 m_z^{(1)} + \delta m_x^{(1)} + \kappa\sqrt{2}m_y^{(1)}m_z^{(1)}, \\
\dot{m}_z^{(1)} =& J\sqrt{2}\left(m_y^{(1)}m_x^{(2)} - m_y^{(2)}m_x^{(1)}\right) \\
& +\Omega_1 m_y^{(1)} - \kappa\sqrt{2}((m_x^{(1)})^2 + (m_y^{(1)})^2), \\
\dot{m}_x^{(2)} =& -J_z\sqrt{2}m_y^{(2)}m_z^{(1)} + J\sqrt{2}m_y^{(1)}m_z^{(2)} \\
& -\delta m_y^{(2)} + \kappa\sqrt{2}m_x^{(2)}m_z^{(2)}, \\
\dot{m}_y^{(2)} =& -J\sqrt{2}m_z^{(2)}m_x^{(1)} + J_z\sqrt{2}m_x^{(2)}m_z^{(2)} \\
& -\Omega_2 m_z^{(2)} + \delta m_x^{(2)} + \kappa\sqrt{2}m_y^{(2)}m_z^{(2)}, \\
\dot{m}_z^{(2)} =& J\sqrt{2}\left(m_y^{(2)}m_x^{(1)} - m_y^{(1)}m_x^{(2)}\right) \\
& +\Omega_2 m_y^{(2)} - \kappa\sqrt{2}((m_x^{(2)})^2 + (m_y^{(2)})^2).
\end{aligned}$$

We observe that, as in Ref. [34], the mean-field equations do not depend on the temperature of the baths. Moreover, this systems of equations reduces to Eq. (11) and Eq. (27), when considering the parameter choices and initial conditions for setup one, Sec. 4 or two, Sec. 5, respectively.

Appendix C. Dynamics of the fluctuations

In this Appendix, we provide the detailed calculations for the dynamics of the covariance matrix. For convenience, we make use of a different notation as in the rest of the text.

In this way, we define the quantum fluctuation operators as

$$F_j^N = \frac{S_j - \langle S_j \rangle}{\sqrt{N}}. \tag{C.1}$$

Here, instead of two indexes, one referring to the atomic system and the other to the operator, we have just one. Our new index ranges from 1 to 6 such that it represents the ordered set $\{(x,1),(y,1),(z,1),(x,2),(y,2),(z,2)\}$, where we have the coordinate and the system, respectively. We note that we include the upper index N indicating that the fluctuation operator corresponds to a finite system. The dynamics of the quantum fluctuations is fully characterized by the covariance matrix [89, 102]

$$G_{jk} = \lim_{N\to\infty} G_{jk}^N, \quad G_{jk}^N = \frac{1}{2}\langle\{F_j^N, F_k^N\}\rangle. \tag{C.2}$$

Moreover, we denote the symplectic matrix as $s = s^{(1)} \oplus s^{(2)}$, and the Levi-Civita tensor as $\epsilon = \epsilon^{(1)} \oplus \epsilon^{(2)}$. We note that the dynamics of the symplectic matrix s can be computed directly from the dynamics of the mean-field operators. For evaluating the dynamics of the covariance matrix, we introduce the matrix K, defined as

$$K_{jk} = \lim_{N\to\infty} K_{jk}^N, \qquad K_{jk}^N = \langle F_j^N F_k^N \rangle. \tag{C.3}$$

With this, we note that $G = (K + K^{\mathrm{T}})/2$, so we can look at the dynamics of K to characterize G. For this purpose, we calculate $\dot{K}_{jk} = \lim_{N\to\infty} \langle \mathcal{L}^*[F_j^N F_k^N]\rangle$, where $\mathcal{L}^*$ is the dual of the Lindblad generator. The dual can be rewritten in a more convenient way by rewriting the raising and lowering operators in terms of the x and y components, becoming

$$\mathcal{L}^*[O] = i[H_{\mathrm{s}}, O] + \sum_{jk}\left(\frac{A_{jk}}{2N}[[S_j, O], S_k] + i\frac{B_{jk}}{2N}\{[S_j, O], S_k\}\right). \tag{C.4}$$

Here we have defined the matrices $A = A^{(1)} \oplus A^{(2)}$ and $B = B^{(1)} \oplus B^{(2)}$ with

$$A^{(j)} = \kappa(2n_j + 1)\begin{pmatrix} 1 & 0 & 0 \\ 0 & 1 & 0 \\ 0 & 0 & 0 \end{pmatrix}, \; B^{(j)} = \kappa\begin{pmatrix} 0 & -1 & 0 \\ 1 & 0 & 0 \\ 0 & 0 & 0 \end{pmatrix}.$$

Additionally, we can express the Hamiltonian of the coupled system as

$$H = H_{\mathrm{M}} + H_{\mathrm{L}}, \quad H_{\mathrm{M}} = \sum_{jk}\frac{M_{jk}}{N} S_j S_k, \quad H_{\mathrm{L}} = \sum_j \frac{h_{jj}}{\sqrt{2}} S_j,$$

with $h = \mathrm{diag}(\Omega_1, 0, \delta, \Omega_2, 0, \delta)$ and

$$M = \frac{1}{2}\begin{pmatrix} 0 & 0 & 0 & J & 0 & 0 \\ 0 & 0 & 0 & 0 & J & 0 \\ 0 & 0 & 0 & 0 & 0 & J_z \\ J & 0 & 0 & 0 & 0 & 0 \\ 0 & J & 0 & 0 & 0 & 0 \\ 0 & 0 & J_z & 0 & 0 & 0 \end{pmatrix}, \tag{C.5}$$

where the factor $1/2$ deals with an over count.

For calculating the fluctuation dynamics, we start with the Hamiltonian part. This can be splitted in two terms by using the commutation relation

$$[H, F_l^N F_m^N] = [H, F_l^N]F_m^N + F_l^N[H, F_m^N].$$

For the first term after in the right-hand side of the equation, we have

$$i[H_{\rm M}, F_l^N] = i\sum_{jk} M_{jk}\Bigg(F_j^N[F_k^N, F_l^N] + \frac{\langle S_j\rangle}{N}[S_k, F_l^N] + \\ + [F_j^N, F_l^N]F_k^N + [S_j, F_l^N]\frac{\langle S_k\rangle}{N}\Bigg).$$

In order to find this expression, we have just added and subtracted the expected values inside the commutators. Moreover, the terms regarding the commutation between the fluctuation operators can be factorized together and written as

$$\sum_{jk} M_{jk}\left(F_j^N[F_k^N, F_l^N] + [F_j^N, F_l^N]F_k^N\right) \approx -i\sum_j C_{lj}F_j.$$

Here, the approximation is exact when $N \to \infty$ and we define

$$C = s\left(M^{\rm T} + M\right).$$

The terms with the diagonal part in the subsystems read

$$i\sum_{jk} M_{jk}\left(\frac{\langle S_j\rangle}{N}[S_k, F_l^N] + [S_j, F_l^N]\frac{\langle S_k\rangle}{N}\right) = -\sum_w D_{lw}^{\rm M}\frac{S_w}{\sqrt{N}},$$

where $D_{lw}^{\rm M} = -\sqrt{2}\sum_{jk} m_k\left(M_{jk} + M_{jk}^{\rm T}\right)\epsilon_{klw}$. In this way, we have that

$$\lim_{N\to\infty} i\langle[H_{\rm M}, F_l^N]F_w^N]\rangle = \left[(D^{\rm M} + C)K\right]_{lw}.$$

In summary, the full contribution of the quadratic Hamiltonians for the dynamics of the covariance reads

$$\lim_{N\to\infty} i\langle[H_{\rm M}, F_l^N F_w^N]]\rangle = \left[\left(D^{\rm M} + C\right)K + K\left(D^{\rm M} + C\right)^{\rm T}\right]_{lw}.$$

The term involving the matrix K on the left side can be easily derived by exploiting the symmetry of the matrices and their indexes.

Moreover, the linear part of the Hamiltonian, $H_{\rm L}$, has a similar structure of the above equation,

$$i[H_{\rm L}, F_l^N] = \sum_k D_{lk}^{\rm L}\frac{S_k}{\sqrt{N}},$$

where $D_{lk}^L = -\sqrt{2}\sum_j h_j\epsilon_{jlk}$. The expected value for this term reads

$$\lim_{N\to\infty} i\langle[H_{\rm L}, F_l^N]F_k^N]\rangle = \left[D^{\rm L}K\right]_{lk},$$

where we have used that the mean value of the fluctuation operators is zero. The full Hamiltonian dynamics for the matrix K reads

$$\lim_{N\to\infty} i\langle[H_{\rm L}, F_l^N F_m^N]]\rangle = \left[D^{\rm L}K + K\left(D^{\rm L}\right)^{\rm T}\right]_{lm},$$

where the second term on the right-hand side of the equation follows by using the antisymmetric property of ϵ_{jkl}. With this we conclude the analysis of the Hamiltonian part.

We now address the dissipative contribution of the Lindbladian on the fluctuation dynamics. We first consider the the term multiplied by the matrix A in Eq. (C.4). The contribution of this term follows by evaluating the commutator

$$\begin{aligned}&\frac{1}{N}\langle[S_j,[F_l^N F_w^N,S_k]]\rangle = \\ &-\langle[F_j^N,[F_k,F_l^N]]F_w^N \;- F_l^N[F_j^N,[F_k,F_w^N]] \\ &-[F_j^N,F_l^N][F_k,F_w^N] \;- [F_k,F_l^N][F_j^N,F_w^N]\rangle.\end{aligned}$$

When we consider the thermodynamic limit, the terms in the second line become zero. This follows due to a further scaling $1/\sqrt{N}$ that appears after evaluating the commutators. The third line can be rewritten by means of the symplectic matrix

$$[F_k^N,F_l^N][F_j,F_w^N]+[F_j,F_l^N][F_k^N,F_w^N] = -s_{kl}s_{jw}-s_{jl}s_{kw}.$$

Then, the expected value of this term becomes

$$\lim_{N\to\infty}\sum_{jk}\frac{A_{jk}}{2N}\langle[S_j,[S_k,F_l^N F_w^N]]\rangle = -(sAs)_{lw}.$$

We note that the sign changes due to the odd permutation in the indexes of the symplectic matrix.

We now move to the last term, the one involving the matrix B. To this end, we start by rewriting the anti-commutator as

$$\frac{1}{N}\langle\{S_j,[F_l^N F_m^N,S_k]\}\rangle = -\langle\{F_j^N,[F_k^N,F_l^N F_m^N]\}\rangle - 2\frac{\langle S_j\rangle}{N}[S_k,F_l^N F_m^N].$$

To find this expression we simply added and subtracted the expected value. We now focus on the first term after the equality sign, since the last term will be similar to the Hamiltonian contributions. In this way, we can expand the commutator as

$$\langle\{F_j^N,[F_k^N,F_l^N F_m^N]\}\rangle \approx i\left(s_{kl}\langle\{F_j^N,F_m^N\}\rangle + s_{km}\langle\{F_j^N,F_l^N\}\rangle\right).$$

The approximation sign is valid in the thermodynamics limit, since in this limit we have $\langle S_jS_k\rangle \to \langle S_j\rangle\langle S_k\rangle$. Then, after applying the sum we find

$$\lim_{N\to\infty} i\sum_{jk}\frac{B_{jk}}{2N}(-\langle\{F_j^N,[F_k^N,F_l^N F_m^N]\}\rangle) = (sBG+GBs)_{lm}.$$

Finally, we evaluate the last term

$$\begin{aligned}&i\sum_{jk}\frac{B_{jk}}{N}\left(-\frac{\langle S_j\rangle}{N}\langle[S_k,F_l^N F_m^N]\rangle\right) = \\ &i\sum_{w}\sum_{jk}\sqrt{2}\frac{B_{jk}}{N}\frac{\langle S_j\rangle}{N}\langle i\epsilon_{klw}F_w^N F_m^N + i\epsilon_{kmw}F_l^N F_w^N\rangle.\end{aligned}$$

Therefore, we can write the above expression as

$$\lim_{N\to\infty} i\sum_{jk}B_{jk}\frac{\langle S_j\rangle}{N}\langle[S_k,F_l^N F_m^N]\rangle = \left[D^B K + K(D^B)^{\mathrm{T}}\right]_{lm},$$

where $D^{\mathrm{B}}_{lw} = \sum_{jk} \sqrt{2} B_{jk} m_j \epsilon_{klw}$.

From these calculations, we have the full dynamics of the covariance matrix. In order to write the dynamics of the fluctuation operators more compactly, we define $D \equiv D^{\mathrm{L}} + D^{\mathrm{M}} + D^{\mathrm{B}}$. Then, the final expression for the matrix K reads

$$\dot{K} = (D+Q)K + K(D+Q)^{\mathrm{T}} + sBG + G\,(sB)^{\mathrm{T}} - sAs.$$

With this, we have the dynamics of the covariance matrix, $G = (K + K^{\mathrm{T}})/2$, given by the Lyapunov equation

$$\dot{G} = PG + GP^{\mathrm{T}} - sAs, \tag{C.6}$$

where $P = D + C + sB$. Here, we note that the matrix D is anti-symmetric and it gives the evolution of the mean-field operators, such that we have $\dot{\vec{m}} = D(\vec{m})\vec{m}$. The other two matrices capture the part that can not be accessed by the mean-field equations.

For convenience, we rewrite the matrices composing the dynamics of the fluctuation operators

$$\begin{aligned}
(D^{\mathrm{L}})_{lk} &= -\sqrt{2}\sum_{j} h_j \epsilon_{jlk}, \\
(D^{\mathrm{M}})_{lw} &= -\sqrt{2}\sum_{jk} m_k (M_{jk} + M_{jk}) \epsilon_{klw}, \\
(D^{\mathrm{B}})_{lw} &= \sqrt{2}\sum_{jk} B_{jk} m_w \epsilon_{klw},
\end{aligned} \tag{C.7}$$

and

$$C = s(M + M^{\mathrm{T}}). \tag{C.8}$$

Appendix C.1. Covariance matrix in the rotating frame

In this section, we analyze the covariance matrix in a frame that rotates in the opposite direction of the mean-field dynamics, such that the commutation relations of the fluctuations are time-independent. Particularly, in this reference frame the fluctuations obey a bosonic algebra, such that we can use the results for Gaussian bosonic mode, to calculate the classical correlations, $\mathcal{J}$, the quantum discord, $\mathcal{D}$, and the entanglement negativity, $\mathcal{N}$ [92, 93].

We start by considering a time-dependent rotation matrix $R(t)$ that has the property to evolve the mean-field equations. In this sense, the time-derivative of the rotation reads $\dot{R}(t) = DR(t)$, where D is defined in Eq. (C.7). Here $m(t) = [m_x^{(1)}, m_y^{(1)}, m_z^{(1)}, m_x^{(2)}, m_y^{(2)}, m_z^{(2)}]$ is the vector of the mean-field variables of both ensembles. We now consider the rotated covariance matrix $\mathrm{d}_t(\bar{G}) = \mathrm{d}_t(R^{\mathrm{T}} G R)$, which also obeys a Lyapunov equation. The symplectic matrix assumes the bosonic form

$$(\sigma)^{(j)} = (R^{\mathrm{T}}(t) s R(t))^{(j)} = \begin{pmatrix} 0 & 1 & 0 \\ -1 & 0 & 0 \\ 0 & 0 & 0 \end{pmatrix}. \tag{C.9}$$

We now can define the new bosonic quantum fluctuations as $\vec{X} = R^{\mathrm{T}}\vec{F} = (x_1, p_1, w_1, x_2, p_2, w_2)$, where $\vec{F} = (F_j)_{j=1}^{6}$ is the vector of the fluctuation operators. From the rotated covariance matrix, one can evaluate the correlations within the bosonic system, as shown in the Refs. [93]. For convenience, we review the procedure for computing these correlations in Appendix C.2.

Furthermore, one does not need the analytical form of $R(t)$ to evaluate the correlations between the atomic systems. However, having this information allows us to derive an effective Lindblad generator for the fluctuation operators, as reported in the main text in Eqs. (23)-(30). In general the rotation matrix $R(t)$ can not be found analytically, since it requires the analytical solution of the mean-field dynamics. However, one can find the expression of this matrix in some scenarios. For the first setup, described in Sec. 4, in the regime of $J = J_z$ and with the atoms initially in the ground state, the mean-field variables have the property that $m_x(t)$ is zero for all times, as reported in Refs. [3, 8]. By using this information and that the magnetization is conserved in each atomic system,

$$(m_x^{(j)})^2(t) + (m_y^{(j)})^2(t) + (m_z^{(j)})^2(t) = (m^{(j)})^2(0), \tag{C.10}$$

we find $R(t) = R^{(1)}(t) \oplus R^{(2)}(t)$, with

$$R^{(j)}(t) = \sqrt{2}\begin{pmatrix} 1/\sqrt{2} & 0 & 0 \\ 0 & m_z^{(j)}(t) & m_y^{(j)}(t) \\ 0 & -m_y^{(j)}(t) & m_z^{(j)}(t) \end{pmatrix}. \tag{C.11}$$

Here, the rotation matrix is the same for each atomic system, $R^{(j)}(t) = R^{(1)}(t) = R^{(2)}(t)$, since in this regime, they exhibit the same mean-field equations. The fluctuation operators in this frame assume the form

$$\begin{aligned} x_j &= F_x^{(j)}, \\ p_j &= \sqrt{2}(m_z^{(j)} F_y^{(j)} - m_y^{(j)} F_z^{(j)}), \\ w_j &= \sqrt{2}(m_y^{(j)} F_y^{(j)} + m_z^{(j)} F_z^{(j)}). \end{aligned} \tag{C.12}$$

Although we have the fluctuation operator w_j, it does not contribute to the dynamics of the correlation matrix in the bosonic frame, since it commutes with both x_j and p_j.

In the second setup, described in Sec. 5, we have an analogous property in the mean-field dynamics, wherein each system can be represented by a phase, as we write in Eq. (26) of the main text. Using this property, we find the form of the rotation matrix of setup two, $R(t) = R^{(1)}(t) \oplus R^{(2)}(t)$, where $R^{(2)}(t)$ is given by Eq. (C.11), and

$$R^{(1)}(t) = \sqrt{2}\begin{pmatrix} m_z^{(1)}(t) & 0 & m_x^{(1)}(t) \\ 0 & 1/\sqrt{2} & 0 \\ -m_x^{(1)}(t) & 0 & m_z^{(1)}(t) \end{pmatrix}. \tag{C.13}$$

Appendix C.2. Quantum information for Gaussian systems

We now review how one can calculate the quantum and classical correlations in Gaussian systems [93]. When we apply this rotation to the covariance matrix we find that it can

be expressed as

$$2\bar{G} = 2RGR^{\mathrm{T}} = \begin{pmatrix} \alpha & \gamma \\ \gamma^{\mathrm{T}} & \beta \end{pmatrix}, \tag{C.14}$$

where the coefficients α, β, and γ are matrices representing the covariance between the new bosonic variables. Moreover, we define the symplectic invariants $c_\alpha = \det \alpha$, $c_\beta = \det \beta$, $c_\gamma = \det \gamma$, and $c_\delta = \det \delta$. The covariance matrix will correspond to a physical state if $c_\alpha, c_\beta \geq 1$ and $\lambda_\pm \geq 1$, where $\lambda_\pm$ are the symplectic eigenvalues defined as $2\lambda_\pm^2 = \Delta \pm \sqrt{\Delta^2 - 4c_\delta}$, where $\Delta = c_\alpha + c_\beta + 2c_\gamma$. We further define the function

$$f(x) = \left(\frac{x+1}{2}\right)\log\left(\frac{x+1}{2}\right) - \left(\frac{x-1}{2}\right)\log\left(\frac{x-1}{2}\right). \tag{C.15}$$

Using this equation, one can evaluate the von Neumann entropy of the system using that $S = \sum_{m=1}^{N} f(\lambda_m)$, where λ_m are the symplectic eigenvalues. This can be interpreted in terms of the Williamson theorem [105], which states that the symplectic eigenvalues of the covariance matrix represents a thermal state given as $\rho_{\mathrm{th}} = \rho_{\mathrm{th}}^{(1)} \otimes \rho_{\mathrm{th}}^{(2)}$, where

$$\rho_{\mathrm{th}}^{(j)} = \sum_{k=0}^{\infty} \frac{\bar{n}_j^k}{(\bar{n}_j + 1)^{(k+1)}} |k\rangle\langle k|, \tag{C.16}$$

where $|k\rangle$ is a Fock state and $\bar{n}_j$ is a occupation number of the j-th mode and it relates to the respective symplectic eigenvalue of the j-th mode as $\bar{n}_j = (\lambda_j - 1)/2$. In other words, the symplectic transformation removes the Gaussian unitary operations in the state, bringing the system to a locally thermal state.

Furthermore, by using these quantities we can compute the one-way quantum discord and the one-way classical correlation, respectively,

$$\mathcal{D} = f(\sqrt{c_\beta}) - f(\lambda_+) - f(\lambda_-) + f(\sqrt{E_{\min}}) \tag{C.17}$$

$$\mathcal{J} = f(\sqrt{c_\alpha}) - f(\sqrt{E_{\min}}), \tag{C.18}$$

where

$$E_{\min} = \frac{2c_\gamma^2 + (c_\beta - 1)(c_\delta - c_\alpha)}{(c_\beta - 1)^2} + \frac{2|c_\gamma|\sqrt{c_\gamma^2 + (c_\beta - 1)(c_\delta - c_\alpha)}}{(c_\beta - 1)^2}$$

if $(c_\delta - c_\alpha c_\beta)^2 \leq (1 + c_\beta)(c_\gamma^2)(c_\alpha + c_\delta)$ and

$$E_{\min} = \frac{c_\alpha c_\beta - c_\gamma^2 + c_\delta}{2c_\beta} - \frac{\sqrt{c_\gamma^4 + (c_\delta - c_\alpha c_\beta)^2 - 2c_\gamma^2(c_\alpha c_\beta + c_\delta)}}{2c_\beta},$$

otherwise.

The last quantity we consider is the logarithmic negativity, which is a witness of the amount of bipartite entanglement between the two bosonic systems. This quantity is given by

$$\mathcal{N} = \max(0, -\ln \tilde{\lambda}_-), \tag{C.19}$$

where $\tilde{\lambda}_-$ is the smallest symplectic eigenvalue of the partially transposed covariance matrix, obtained by replacing c_γ to $-c_\gamma$ [93].

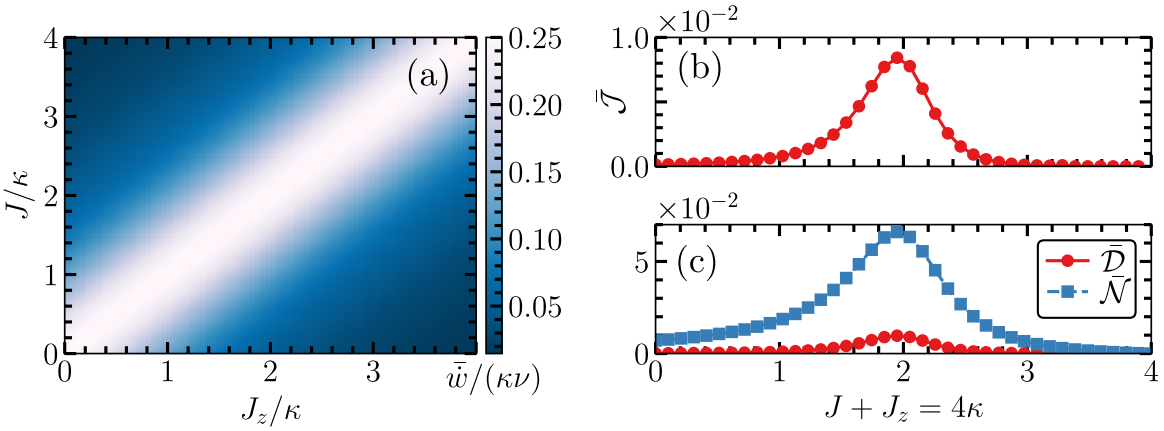

Figure D1. Time-averaged work input and quantum correlations for the stationary phase. (a) Time-averaged work input for varying J_z and J, for the stationary phase $\Omega_1 = \Omega_2 = \kappa/2$, respectively. Here, we start with $J = 0$ and $J_z = 4\kappa$ and we increase J and decrease J_z. (b)-(c) Time-averaged classical and quantum correlations, respectively, as function of J, such that $J_z + J = 4\kappa$. The mean-field quantities were evolved from $t = 0$ to $t\kappa = 10^3$ and only their second half were integrated. The correlations were computed considering time intervals $t \in [0, 200]$, and the integration was done over the second half of the interval. The remaining parameters are $\delta = 0$, $n_1 = n_2 = 0$ and $\kappa = 2\Omega_1 = 2\Omega_2$. The initial state is $\vec{m} = [0, 0, -1/\sqrt{2}]$.

Appendix D. Additional information for setup one

In this section we provide further information about the results concerning the setup one for the mean-field and fluctuation dynamics.

We start by analysing the time-averaged work input and correlations for the system in the stationary phase emerging when $\Omega^2 < \kappa^2 + (J - J_z)^2$. In Fig. D1(a) we show the total time-averaged work input in the system. This can be understood from the analytical solutions of the stationary phase from which we obtain an analytical expression for this quantity $\bar{w} = \kappa\nu\Omega^2/[(J - J_z)^2 + \kappa^2]$. In Fig. D1(b)-(c) we show the behaviour of the correlations. In contrast to the results for the time-crystal phase, we observe that both correlations are maximized when $J = J_z$.

We now address in more detail the continuous family of oscillatory solutions that emerge in the time-crystal phase due to the presence of the conserved quantity Γ [see Eq. (11)]. To this end, we exemplify in Fig. D2(a) some of the time-crystal solutions that can be accessed through different initial conditions. The figure shows that the amplitude in the z direction decreases until it reaches zero, thereby becoming a stationary point in the time-crystal region, for when $m_z(0) = 0$, $m_x(0) = \cos(\pi/6)$, and $m_y(0) = \sin(\pi/6)$. Moreover, in Fig. D2(b) we show a comparison between two time-crystal solutions for different J, showing that the interaction strength does not change much the efficiency. This fact is supported by the results shown in Fig. 3 in the main text, where we observe that the time-averaged stored energy does not depend on J inside the time-crystal

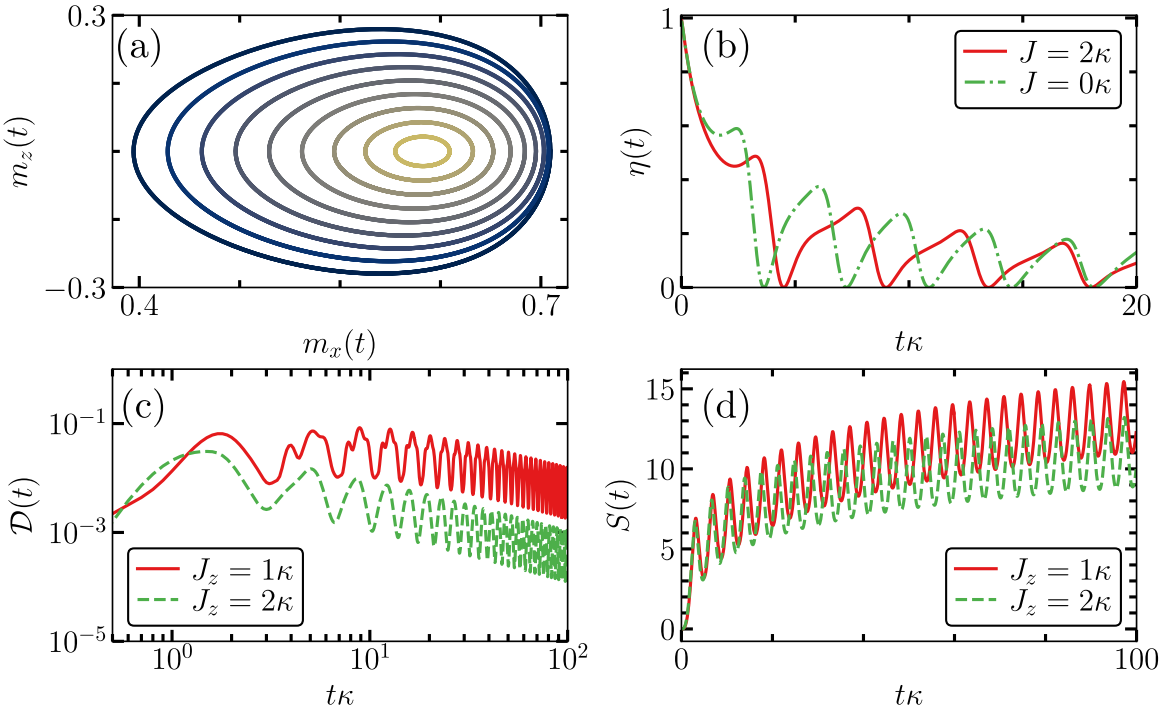

Figure D2. Continuous family of oscillations, efficiency, quantum discord, and entropy. (a) Time-crystal solutions accessed with different initial conditions, $m_z(0) = 0$, $m_x(0) = \sqrt{1/2}\cos(\phi)$ and $m_y(0) = \sqrt{1/2}\sin(\phi)$. Here we vary ϕ from 0 to $\pi/6$ in ten intervals. The amplitude of the solutions decrease as ϕ increases, being zero when $\phi = \pi/6$. Also, we consider $J = \Omega = 2J_z = 2\kappa$. In (b), we plot the efficiency when the system starts in the ground state for different J, as indicated in the legend, for $\Omega = 2\kappa$ and $J_z = 0$. Moreover, in (c)-(d) we plot the quantum discord and the entropy as function of time, respectively. In these plots, we consider $J = \Omega = 2\kappa$ and $\omega_{\rm at} = \nu$.

region. Moreover, in Fig. D2(c)-(d), we show the discord and the entropy for two scenarios, respectively. In the first one, given in red solid lines, we have $J \neq J_z$, and $J = J_z$ is given by the green dashed line. This shows the asymptotic behavior of both quantities, where the quantum correlations increase in the beginning of the dynamics, and then they decrease in time with a power law. On the other hand, the entropy of both systems increases. This behavior of the entropy is analogous to the one observed in the single boundary time-crystal, as reported in the Refs. [106, 8] Here, we note that when the interactions are different, the system entropy grows with a higher rate.

Appendix E. Additional information for setup two

In this section, we provide further information on the mean-field and quantum fluctuations dynamics concerning the setup two.

We start by investigating the Fourier spectrum of the magnetization in the z-direction for a fixed value of Rabi frequency and different values of J, as shown by

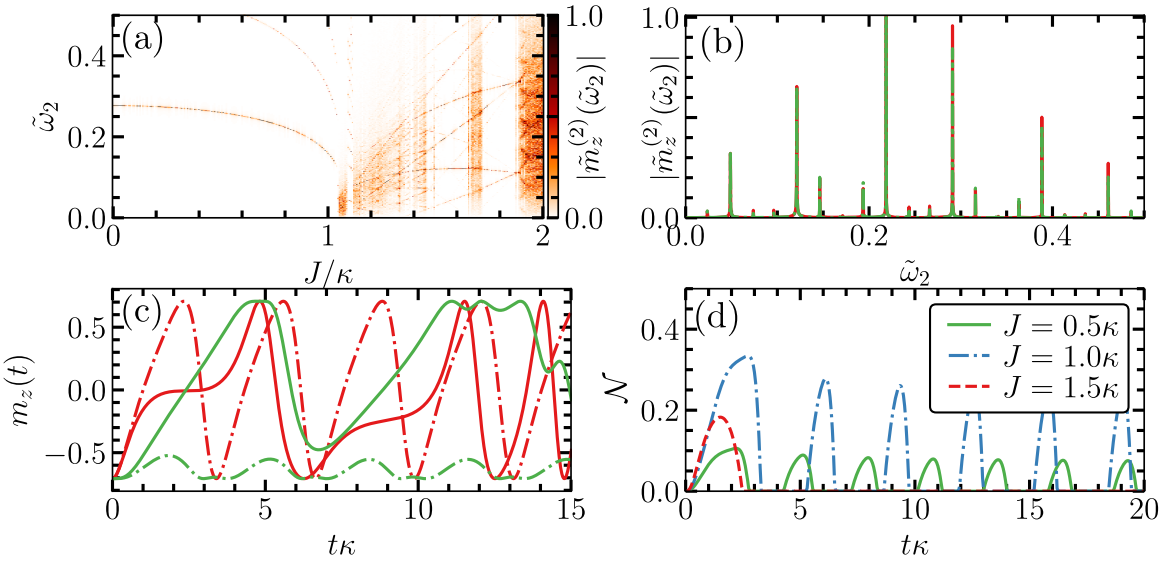

Figure E1. Fourier spectrum and trajectories of magnetization and entanglement. (a) Density plot of the Fourier spectrum of $|\tilde{m}_z^{(2)}(\tilde{\omega}_2)|$ as function of J/κ for the configuration in the setup two. In (b), we plot a section of the spectrum in (a) with $J = 1.6\kappa$ for the battery (red solid line) and the charger (green dot dashed line). In (c) we compared the behaviour of $m_z(t)$ for the battery (green lines) and the charger (red lines). The solid lines refer to a solution with $J = 1.5\kappa$, while the dot dashed lines to a solution with $J = \kappa$, for $\Omega = 2.5\kappa$. (d) Negativity for different values of J, as indicated in the legend. Here, $\Omega = 2.5\kappa$.

Fig. E1(a). In this figure, we observe the difference between the limit-cycle phase, displaying few well-resolved spectral peaks, and the quasi-periodic phase, in which the spectrum displays many nearby peaks. Also, we observe that as J varies, the Fourier spectrum in the quasi-periodic region varies in a non-trivial way, exhibiting sudden changes in the density of peaks. In Fig. E1(b) we show the Fourier spectrum for one case in the quasi-periodic phase. Notice that both atomic ensembles always display the same Fourier peaks, since their dynamics is synchronized. We remark that this behavior is not chaotic given that, due to the existence of conserved quantities, the effective manifold of dynamical equations has effectively only two dimensions.

Moreover, in Fig. E1(c) we plot the mean-field magnetisation $m_z(t)$ for the charger and for the battery. Our results show that for a small J, the battery undergoes a limit cycle having an average amplitude close to the ground state, thereby not being able to store much energy. However, when the system operates in the quasi-periodic phase, it oscillates between the minimum and the maximum of energy stored. Furthermore, in Fig. E1(d), we show trajectories for the entanglement negativity for different J. We see that the entanglement increases from $J = 0.5\kappa$ to $J = \kappa$, but it becomes zero in the quasi-periodic phase.

Finally, we investigate the presence of multistability for the parameters considered in Fig. 4(a), when allowing for different initial conditions. In Fig. E2(a), we show

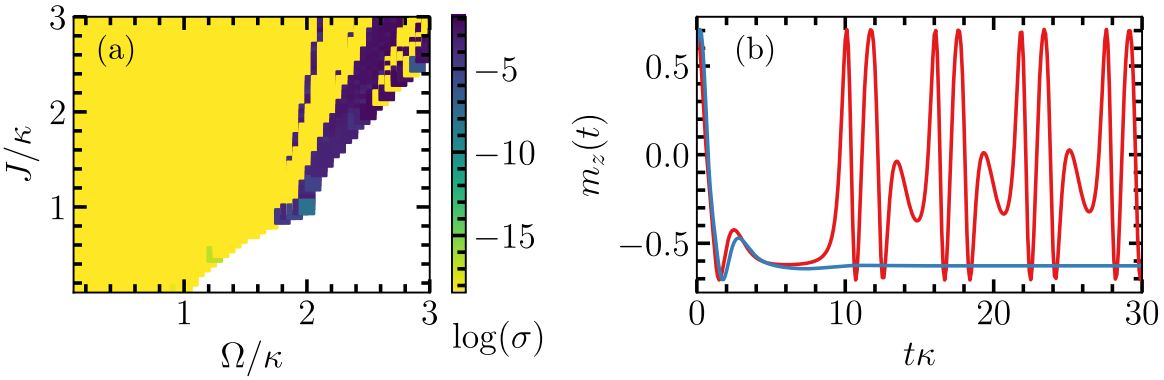

Figure E2. Multistability (a) Multistability in the stationary phase. In order to obtain this color plot, for each parameter value, we have time evolved 20 different trajectories of $m_z^{(2)}$ with random initial conditions. For each of these trajectories, we compute the time-average of $m_z^{(2)}$ between times $t\kappa = 180$ and $t\kappa = 200$. The color scale corresponds to the variance over trajectories of this time-averaged magnetization, σ. If there is a unique stationary solution, this variance is zero, otherwise there are multiple solutions. In (b) two trajectories of the magnetization of system two, obtained from two different initial conditions. For the time-crystal solution we use $m_x^{(1)}(0) = m_y^{(2)}(0) = 0$ and $m_z^{(1)}(0) = m_z^{(2)}(0) = 1/\sqrt{2}$. For the stationary solution, we set $m_x^{(1)}(0) = 0$, $m_z^{(1)}(0) = 1/\sqrt{2}$, $m_x^{(2)}(0) = \sin(\pi/2)/\sqrt{2}$, and $m_z^{(2)}(0) = \cos(\pi/2)\sqrt{2}$. Here, we consider $\Omega = 2.5\kappa$ and $J = 2.1\kappa$.

that within the stationary region, there are regions where oscillatory solutions are also possible. Dark regions correspond to regions where there is coexistence between oscillatory and stationary solutions. In Fig. E2(b) we exemplify the presence of multistability by considering two initial conditions for the same parameter choice, and observing that in one case the system relaxes to a stationary point (blue line) while in the other it goes to a limit-cycle solution (red line).

References

[1] Wilczek F 2012 *Phys. Rev. Lett.* **109**(16) 160401 URL https://link.aps.org/doi/10.1103/PhysRevLett.109.160401

[2] Else D V, Bauer B and Nayak C 2016 *Phys. Rev. Lett.* **117**(9) 090402 URL https://link.aps.org/doi/10.1103/PhysRevLett.117.090402

[3] Iemini F, Russomanno A, Keeling J, Schirò M, Dalmonte M and Fazio R 2018 *Phys. Rev. Lett.* **121**(3) 035301 URL https://link.aps.org/doi/10.1103/PhysRevLett.121.035301

[4] Gong Z, Hamazaki R and Ueda M 2018 *Phys. Rev. Lett.* **120**(4) 040404 URL https://link.aps.org/doi/10.1103/PhysRevLett.120.040404

[5] Watanabe H and Oshikawa M 2015 *Phys. Rev. Lett.* **114**(25) 251603 URL https://link.aps.org/doi/10.1103/PhysRevLett.114.251603

[6] Bruno P 2013 *Phys. Rev. Lett.* **110**(11) 118901 URL https://link.aps.org/doi/10.1103/PhysRevLett.110.118901

[7] Carmichael H J 1980 *J. Phys. B* **13** 3551 URL https://dx.doi.org/10.1088/0022-3700/13/18/009

[8] Carollo F and Lesanovsky I 2022 *Phys. Rev. A* **105**(4) L040202 URL https://link.aps.org/doi/10.1103/PhysRevA.105.L040202

[9] Riera-Campeny A, Moreno-Cardoner M and Sanpera A 2020 *Quantum* **4** 270 URL https://doi.org/10.22331/q-2020-05-25-270

[10] Tucker K, Zhu B, Lewis-Swan R J, Marino J, Jimenez F, Restrepo J G and Rey A M 2018 *New J. Phys.* **20** 123003 URL https://iopscience.iop.org/article/10.1088/1367-2630/aaf18b

[11] Buča B, Tindall J and Jaksch D 2019 *Nat. Commun.* **10** 1–6 URL https://doi.org/10.1038/s41467-019-09757-y

[12] Gambetta F M, Carollo F, Marcuzzi M, Garrahan J P and Lesanovsky I 2019 *Phys. Rev. Lett.* **122**(1) 015701 URL https://link.aps.org/doi/10.1103/PhysRevLett.122.015701

[13] Lazarides A, Roy S, Piazza F and Moessner R 2020 *Phys. Rev. Research* **2**(2) 022002 URL https://link.aps.org/doi/10.1103/PhysRevResearch.2.022002

[14] Seibold K, Rota R and Savona V 2020 *Phys. Rev. A* **101**(3) 033839 URL https://link.aps.org/doi/10.1103/PhysRevA.101.033839

[15] Lledó C, Mavrogordatos T K and Szymańska M H 2019 *Phys. Rev. B* **100**(5) 054303 URL https://link.aps.org/doi/10.1103/PhysRevB.100.054303

[16] Mattes R, Lesanovsky I and Carollo F 2023 *Phys. Rev. A* **108**(6) 062216 URL https://link.aps.org/doi/10.1103/PhysRevA.108.062216

[17] Prazeres L F d, Souza L d S and Iemini F 2021 *Phys. Rev. B* **103**(18) 184308 URL https://link.aps.org/doi/10.1103/PhysRevB.103.184308

[18] Cabot A, Muhle L S, Carollo F and Lesanovsky I 2023 *Phys. Rev. A* **108**(4) L041303 URL https://link.aps.org/doi/10.1103/PhysRevA.108.L041303

[19] Krishna M, Solanki P, Hajdušek M and Vinjanampathy S 2023 *Phys. Rev. Lett.* **130**(15) 150401 URL https://link.aps.org/doi/10.1103/PhysRevLett.130.150401

[20] Cabot A, Giorgi G L and Zambrini R 2024 *PRX Quantum* **5**(3) 030325 URL https://link.aps.org/doi/10.1103/PRXQuantum.5.030325

[21] Paulino P J, Lesanovsky I and Carollo F 2023 *Phys. Rev. A* **108**(2) 023516 URL https://link.aps.org/doi/10.1103/PhysRevA.108.023516

[22] Keßler H, Kongkhambut P, Georges C, Mathey L, Cosme J G and Hemmerich A 2021 *Phys. Rev. Lett.* **127**(4) 043602 URL https://link.aps.org/doi/10.1103/PhysRevLett.127.043602

[23] Kongkhambut P, Skulte J, Mathey L, Cosme J G, Hemmerich A and Keßler H 2022 *Science* **377** 670–673 URL https://www.science.org/doi/abs/10.1126/science.abo3382

[24] Wu X, Wang Z, Yang F, Gao R, Liang C, Tey M K, Li X, Pohl T and You L 2024 *Nat. Phys.* 1–6 URL https://doi.org/10.1038/s41567-024-02542-9

[25] Kongkhambut P, Cosme J G, Skulte J, Moreno Armijos M A, Mathey L, Hemmerich A and Keßler H 2024 *Rep. Prog. Phys.* **87** 080502 ISSN 1361-6633 URL http://dx.doi.org/10.1088/1361-6633/ad6585

[26] Skulte J, Kongkhambut P, Keßler H, Hemmerich A, Mathey L and Cosme J G 2024 *Phys. Rev. A* **109**(6) 063317 URL https://link.aps.org/doi/10.1103/PhysRevA.109.063317

[27] Montenegro V, Genoni M G, Bayat A and Paris M G 2023 *Commun. Phys.* **6** 304 URL https://doi.org/10.1038/s42005-023-01423-6

[28] Cabot A, Carollo F and Lesanovsky I 2024 *Phys. Rev. Lett.* **132**(5) 050801 URL https://link.aps.org/doi/10.1103/PhysRevLett.132.050801

[29] Iemini F, Fazio R and Sanpera A 2024 *Phys. Rev. A* **109**(5) L050203 URL https://link.aps.org/doi/10.1103/PhysRevA.109.L050203

[30] Yousefjani R, Sacha K and Bayat A 2024 *arXiv preprint arXiv:2405.00328* URL https://arxiv.org/abs/2405.00328

[31] Carollo F, Brandner K and Lesanovsky I 2020 *Phys. Rev. Lett.* **125**(24) 240602 URL https://link.aps.org/doi/10.1103/PhysRevLett.125.240602

[32] Levy A and Kosloff R 2014 *Europhys. Lett.* **107** 20004 URL https://dx.doi.org/10.1209/0295-5075/107/20004

[33] Deffner S and Campbell S 2019 *Quantum Thermodynamics: An introduction to the thermodynamics of quantum information* (Morgan & Claypool Publishers)

[34] Carollo F, Lesanovsky I, Antezza M and De Chiara G 2024 *Quantum Sci. Technol.* **9** 035024 URL https://dx.doi.org/10.1088/2058-9565/ad3f42

[35] Cusumano S 2022 *Entropy* **24** 1258 URL https://doi.org/10.3390/e24091258

[36] De Chiara G, Landi G, Hewgill A, Reid B, Ferraro A, Roncaglia A J and Antezza M 2018 *New J. Phys.* **20** 113024 URL https://doi.org/10.1088/1367-2630/aaecee

[37] Cattaneo M, De Chiara G, Maniscalco S, Zambrini R and Giorgi G L 2021 *Phys. Rev. Lett.* **126**(13) 130403 URL https://link.aps.org/doi/10.1103/PhysRevLett.126.130403

[38] Lorenzo S, Ciccarello F and Palma G M 2017 *Phys. Rev. A* **96**(3) 032107 URL https://link.aps.org/doi/10.1103/PhysRevA.96.032107

[39] Ciccarello F, Lorenzo S, Giovannetti V and Palma G M 2022 *Phys. Rep.* **954** 1–70 URL https://doi.org/10.1016/j.physrep.2022.01.001

[40] Strasberg P, Schaller G, Brandes T and Esposito M 2017 *Phys. Rev. X* **7**(2) 021003 URL https://link.aps.org/doi/10.1103/PhysRevX.7.021003

[41] De Chiara G and Imparato A 2022 *Phys. Rev. Res.* **4**(2) 023230 URL https://link.aps.org/doi/10.1103/PhysRevResearch.4.023230

[42] Hewgill A, De Chiara G and Imparato A 2021 *Phys. Rev. Res.* **3**(1) 013165 URL https://link.aps.org/doi/10.1103/PhysRevResearch.3.013165

[43] Alicki R and Fannes M 2013 *Phys. Rev. E* **87**(4) 042123 URL https://link.aps.org/doi/10.1103/PhysRevE.87.042123

[44] Gyhm J Y, Šafránek D and Rosa D 2022 *Phys. Rev. Lett.* **128**(14) 140501 URL https://link.aps.org/doi/10.1103/PhysRevLett.128.140501

[45] Ahmadi B, Mazurek P, Horodecki P and Barzanjeh S 2024 *Phys. Rev. Lett.* **132**(21) 210402 URL https://link.aps.org/doi/10.1103/PhysRevLett.132.210402

[46] Campaioli F, Gherardini S, Quach J Q, Polini M and Andolina G M 2024 *Rev. Mod. Phys.* **96**(3) 031001 URL https://link.aps.org/doi/10.1103/RevModPhys.96.031001

[47] Chen P, Yin T S, Jiang Z Q and Jin G R 2022 *Phys. Rev. E* **106**(5) 054119 URL https://link.aps.org/doi/10.1103/PhysRevE.106.054119

[48] Le T P, Levinsen J, Modi K, Parish M M and Pollock F A 2018 *Phys. Rev. A* **97**(2) 022106 URL https://link.aps.org/doi/10.1103/PhysRevA.97.022106

[49] Andolina G M, Keck M, Mari A, Giovannetti V and Polini M 2019 *Phys. Rev. B* **99**(20) 205437 URL https://link.aps.org/doi/10.1103/PhysRevB.99.205437

[50] Santos A C, Çakmak B i e i f m c, Campbell S and Zinner N T 2019 *Phys. Rev. E* **100**(3) 032107 URL https://link.aps.org/doi/10.1103/PhysRevE.100.032107

[51] Rossini D, Andolina G M and Polini M 2019 *Phys. Rev. B* **100**(11) 115142 URL https://link.aps.org/doi/10.1103/PhysRevB.100.115142

[52] Santos A C 2021 *Phys. Rev. E* **103**(4) 042118 URL https://link.aps.org/doi/10.1103/PhysRevE.103.042118

[53] Mitchison M T, Goold J and Prior J 2021 *Quantum* **5** 500 ISSN 2521-327X URL https://doi.org/10.22331/q-2021-07-13-500

[54] Alicki R 2019 *J. Chem. Phys.* **150** 214110 ISSN 0021-9606 URL https://doi.org/10.1063/1.5096772

[55] Farina D, Andolina G M, Mari A, Polini M and Giovannetti V 2019 *Phys. Rev. B* **99**(3) 035421 URL https://link.aps.org/doi/10.1103/PhysRevB.99.035421

[56] Barra F 2019 *Phys. Rev. Lett.* **122**(21) 210601 URL https://link.aps.org/doi/10.1103/PhysRevLett.122.210601

[57] Hovhannisyan K V, Barra F and Imparato A 2020 *Phys. Rev. Res.* **2**(3) 033413 URL https://link.aps.org/doi/10.1103/PhysRevResearch.2.033413

[58] Martins W S, Carollo F, Li W, Brandner K and Lesanovsky I 2023 *Phys. Rev. A* **108**(5) L050201 URL https://link.aps.org/doi/10.1103/PhysRevA.108.L050201

[59] Rodríguez R R, Ahmadi B, Mazurek P, Barzanjeh S, Alicki R and Horodecki P 2023 *Phys. Rev. A* **107**(4) 042419 URL https://link.aps.org/doi/10.1103/PhysRevA.107.042419

[60] Chang W, Yang T R, Dong H, Fu L, Wang X and Zhang Y Y 2021 *New J. Phys.* **23** 103026 URL https://dx.doi.org/10.1088/1367-2630/ac2a5b

[61] Catalano A, Giampaolo S, Morsch O, Giovannetti V and Franchini F 2024 *PRX Quantum* **5**(3) 030319 URL https://link.aps.org/doi/10.1103/PRXQuantum.5.030319

[62] Hu C K, Qiu J, Souza P J P, Yuan J, Zhou Y, Zhang L, Chu J, Pan X, Hu L, Li J, Xu Y, Zhong Y, Liu S, Yan F, Tan D, Bachelard R, Villas-Boas C J, Santos A C and Yu D 2022 *Quantum Sci. Technol.* **7** 045018 URL https://dx.doi.org/10.1088/2058-9565/ac8444

[63] Maillette de Buy Wenniger I, Thomas S E, Maffei M, Wein S C, Pont M, Belabas N, Prasad S, Harouri A, Lemaître A, Sagnes I, Somaschi N, Auffèves A and Senellart P 2023 *Phys. Rev. Lett.* **131**(26) 260401 URL https://link.aps.org/doi/10.1103/PhysRevLett.131.260401

[64] Gemme G, Grossi M, Ferraro D, Vallecorsa S and Sassetti M 2022 *Batteries* **8** ISSN 2313-0105 URL https://www.mdpi.com/2313-0105/8/5/43

[65] Joshi J and Mahesh T S 2022 *Phys. Rev. A* **106**(4) 042601 URL https://link.aps.org/doi/10.1103/PhysRevA.106.042601

[66] Morrone D, Rossi M A and Genoni M G 2023 *Phys. Rev. Appl.* **20**(4) 044073 URL https://link.aps.org/doi/10.1103/PhysRevApplied.20.044073

[67] Beleño Z, Santos M F and Barra F 2024 *New J. Phys.* **26** 073049 URL https://dx.doi.org/10.1088/1367-2630/ad6348

[68] Ferraro D, Campisi M, Andolina G M, Pellegrini V and Polini M 2018 *Phys. Rev. Lett.* **120**(11) 117702 URL https://link.aps.org/doi/10.1103/PhysRevLett.120.117702

[69] Kamin F H, Tabesh F T, Salimi S and Santos A C 2020 *Phys. Rev. E* **102**(5) 052109 URL https://link.aps.org/doi/10.1103/PhysRevE.102.052109

[70] Hajdušek M, Solanki P, Fazio R and Vinjanampathy S 2022 *Phys. Rev. Lett.* **128**(8) 080603 URL https://link.aps.org/doi/10.1103/PhysRevLett.128.080603

[71] Hepp K and Lieb E H 1973 *Phys. Rev. A* **8**(5) 2517–2525 URL https://link.aps.org/doi/10.1103/PhysRevA.8.2517

[72] Breuer H P, Petruccione F *et al.* 2002 *The theory of open quantum systems* (Oxford University Press on Demand)

[73] Carmichael H J and Walls D F 1973 *J. Phys. A* **6** 1552 URL https://dx.doi.org/10.1088/0305-4470/6/10/014

[74] Hofer P P, Perarnau-Llobet M, Miranda L D M, Haack G, Silva R, Brask J B and Brunner N 2017 *New J. Phys.* **19** 123037 URL https://dx.doi.org/10.1088/1367-2630/aa964f

[75] Brennecke F, Donner T, Ritter S, Bourdel T, Köhl M and Esslinger T 2007 *Nature* **450** 268–271 URL https://doi.org/10.1038/nature06120

[76] Brennecke F, Ritter S, Donner T and Esslinger T 2008 *Science* **322** 235–238 URL https://www.science.org/doi/abs/10.1126/science.1163218

[77] Purdy T P, Brooks D W C, Botter T, Brahms N, Ma Z Y and Stamper-Kurn D M 2010 *Phys. Rev. Lett.* **105**(13) 133602 URL https://link.aps.org/doi/10.1103/PhysRevLett.105.133602

[78] Keßler H, Kongkhambut P, Georges C, Mathey L, Cosme J G and Hemmerich A 2021 *Phys. Rev. Lett.* **127**(4) 043602 URL https://link.aps.org/doi/10.1103/PhysRevLett.127.043602

[79] Ritsch H, Domokos P, Brennecke F and Esslinger T 2013 *Rev. Mod. Phys.* **85**(2) 553–601 URL https://link.aps.org/doi/10.1103/RevModPhys.85.553

[80] Spohn H 1978 *J. Math. Phys.* **19** 1227–1230 ISSN 0022-2488 URL https://doi.org/10.1063/1.523789

[81] Alicki R 1979 *J. Phys. A* **12** L103 URL https://dx.doi.org/10.1088/0305-4470/12/5/007

[82] Carollo F and Lesanovsky I 2021 *Phys. Rev. Lett.* **126**(23) 230601 URL https://link.aps.org/doi/10.1103/PhysRevLett.126.230601

[83] Carollo F and Lesanovsky I 2024 *Phys. Rev. Lett.* **133**(15) 150401 URL https://link.aps.org/doi/10.1103/PhysRevLett.133.150401

[84] Drummond P and Carmichael H 1978 *Opt. Commun.* **27** 160–164 ISSN 0030-4018 URL https://www.sciencedirect.com/science/article/pii/0030401878901980

[85] Souza L d S, Manzano G, Fazio R and Iemini F 2022 *Phys. Rev. E* **106**(1) 014143 URL https://link.aps.org/doi/10.1103/PhysRevE.106.014143

[86] Benatti F, Carollo F and Floreanini R 2015 *Ann. Phys. (Berlin)* **527** 639–655 URL https://doi.org/10.1002/andp.201500165

[87] Goderis D, Verbeure A and Vets P 1990 *Commun. Math. Phys.* **128** 533–549 ISSN 1432-0916 URL https://doi.org/10.1007/BF02096872

[88] Benatti F, Carollo F, Floreanini R and Narnhofer H 2018 *J. Phys. A* **51** 325001 URL https://dx.doi.org/10.1088/1751-8121/aacbdb

[89] Pirandola S, Serafini A and Lloyd S 2009 *Phys. Rev. A* **79**(5) 052327 URL https://link.aps.org/doi/10.1103/PhysRevA.79.052327

[90] Boneberg M, Lesanovsky I and Carollo F 2022 *Phys. Rev. A* **106**(1) 012212 URL https://link.aps.org/doi/10.1103/PhysRevA.106.012212

[91] Lami L, Regula B, Wang X, Nichols R, Winter A and Adesso G 2018 *Phys. Rev. A* **98**(2) 022335 URL https://link.aps.org/doi/10.1103/PhysRevA.98.022335

[92] Giorda P and Paris M G A 2010 *Phys. Rev. Lett.* **105**(2) 020503 URL https://link.aps.org/doi/10.1103/PhysRevLett.105.020503

[93] Adesso G and Datta A 2010 *Phys. Rev. Lett.* **105**(3) 030501 URL https://link.aps.org/doi/10.1103/PhysRevLett.105.030501

[94] Lörch N, Nigg S E, Nunnenkamp A, Tiwari R P and Bruder C 2017 *Phys. Rev. Lett.* **118**(24) 243602 URL https://link.aps.org/doi/10.1103/PhysRevLett.118.243602

[95] Solanki P, Mehdi F M, Hajdušek M and Vinjanampathy S 2023 *Phys. Rev. A* **108**(2) 022216 URL https://link.aps.org/doi/10.1103/PhysRevA.108.022216

[96] Nigg S E 2018 *Phys. Rev. A* **97**(1) 013811 URL https://link.aps.org/doi/10.1103/PhysRevA.97.013811

[97] Allahverdyan A E, Balian R and Nieuwenhuizen T M 2004 *Europhys. Lett.* **67** 565 URL https://dx.doi.org/10.1209/epl/i2004-10101-2

[98] Andolina G M, Keck M, Mari A, Campisi M, Giovannetti V and Polini M 2019 *Phys. Rev. Lett.* **122**(4) 047702 URL https://link.aps.org/doi/10.1103/PhysRevLett.122.047702

[99] Sparaciari C, Jennings D and Oppenheim J 2017 *Nat. Commun.* **8** 1895 ISSN 2041-1723 URL https://doi.org/10.1038/s41467-017-01505-4

[100] Brown E G, Friis N and Huber M 2016 *New J. Phys.* **18** 113028 URL https://dx.doi.org/10.1088/1367-2630/18/11/113028

[101] Pavlov V P, Porras D and Ivanov P A 2023 *Phys. Scr.* **98** 095103 URL https://dx.doi.org/10.1088/1402-4896/ace99f

[102] Ma J, Wang X, Sun C and Nori F 2011 *Phys. Rep.* **509** 89–165 ISSN 0370-1573 URL https://www.sciencedirect.com/science/article/pii/S0370157311002201

[103] Paulo J Paulino, Albert Cabot, Igor Lesanovsky, Mauro Antezza, Gabriele De Chiara and Federico Carollo 2024 Github repository supporting the paper "Thermodynamics of coupled time crystals with an application to energy storage" URL https://github.com/PauloJPS/Coupled-Time-Crystals

[104] Landi G T and Paternostro M 2021 *Rev. Mod. Phys.* **93**(3) 035008 URL https://link.aps.org/doi/10.1103/RevModPhys.93.035008

[105] Simon R, Chaturvedi S and Srinivasan V 1999 *J. Math. Phys.* **40** 3632–3642 ISSN 0022-2488 URL https://doi.org/10.1063/1.532913

[106] Chan C K, Lee T E and Gopalakrishnan S 2015 *Phys. Rev. A* **91**(5) 051601 URL https://link.aps.org/doi/10.1103/PhysRevA.91.051601

Bibliography

[1] H. B. Callen, *Thermodynamics and an Introduction to Thermostatistics*. John wiley & sons, 1991.

[2] G. T. Landi and M. Paternostro, "Irreversible entropy production: From classical to quantum," *Rev. Mod. Phys.*, vol. 93, p. 035008, Sep 2021.

[3] J. Goold, M. Huber, A. Riera, L. d. Rio, and P. Skrzypczyk, "The role of quantum information in thermodynamics—a topical review," *Journal of Physics A: Mathematical and Theoretical*, vol. 49, p. 143001, feb 2016.

[4] D. J. Griffiths, *Introduction to electrodynamics*. Cambridge University Press, 2023.

[5] F. Bacon, *True Suggestions for the Interpretation of Nature*. BoD–Books on Demand, 2019.

[6] F. Reif, *Fundamentals of statistical and thermal physics*. Waveland Press, 2009.

[7] D. L. Goodstein, *States of matter*. Courier Corporation, 1985.

[8] J. Casas-Vázquez and D. Jou, "Temperature in non-equilibrium states: a review of open problems and current proposals," *Reports on Progress in Physics*, vol. 66, p. 1937, oct 2003.

[9] T. Tomé, *Dinâmica Estocástica e Irreversibilidade Vol. 35*. Edusp, 2001.

[10] S. Gherardini, S. Marcantoni, and F. Caruso, "Irreversibility mitigation in unital non-markovian quantum evolutions," *Phys. Rev. Res.*, vol. 2, p. 033250, Aug 2020.

[11] E. M. Sevick, R. Prabhakar, S. R. Williams, and D. J. Searles, "Fluctuation theorems," *Annual Review of Physical Chemistry*, vol. 59, pp. 603–633, 2008.

[12] M. A. Nielsen and I. Chuang, "Quantum computation and quantum information," 2002.

[13] S. Deffner and S. Campbell, *Quantum Thermodynamics: An introduction to the thermodynamics of quantum information*. Morgan & Claypool Publishers, 2019.

[14] W. Thomson, "Kinetic theory of the dissipation of energy," *Nature*, vol. 9, no. 232, pp. 441–444, 1874.

[15] R. Landauer, "Irreversibility and heat generation in the computing process," *IBM Journal of Research and Development*, vol. 5, no. 3, pp. 183–191, 1961.

[16] A. Bérut, A. Arakelyan, A. Petrosyan, S. Ciliberto, R. Dillenschneider, and E. Lutz, "Experimental verification of landauer's principle linking information and thermodynamics," *Nature*, vol. 483, no. 7388, pp. 187–189, 2012.

[17] K. Proesmans, J. Ehrich, and J. Bechhoefer, "Finite-time landauer principle," *Phys. Rev. Lett.*, vol. 125, p. 100602, Sep 2020.

[18] S. Milz and K. Modi, "Quantum stochastic processes and quantum non-markovian phenomena," *PRX Quantum*, vol. 2, p. 030201, Jul 2021.

[19] G. T. Landi, M. J. Kewming, M. T. Mitchison, and P. P. Potts, "Current fluctuations in open quantum systems: Bridging the gap between quantum continuous measurements and full counting statistics," *PRX Quantum*, vol. 5, p. 020201, Apr 2024.

[20] K. Micadei, J. P. S. Peterson, A. M. Souza, R. S. Sarthour, I. S. Oliveira, G. T. Landi, T. B. Batalhão, R. M. Serra, and E. Lutz, "Reversing the direction of heat flow using quantum correlations," *Nature Communications*, vol. 10, p. 2456, June 2019.

[21] A. Levy and R. Kosloff, "The local approach to quantum transport may violate the second law of thermodynamics," *Europhys. Lett.*, vol. 107, p. 20004, jul 2014.

[22] G. De Chiara, G. Landi, A. Hewgill, B. Reid, A. Ferraro, A. J. Roncaglia, and M. Antezza, "Reconciliation of quantum local master equations with thermodynamics," *New J. Phys.*, vol. 20, no. 11, p. 113024, 2018.

[23] A. Hewgill, G. De Chiara, and A. Imparato, "Quantum thermodynamically consistent local master equations," *Phys. Rev. Res.*, vol. 3, p. 013165, Feb 2021.

[24] K. Kuroiwa, R. Takagi, G. Adesso, and H. Yamasaki, "Every quantum helps: Operational advantage of quantum resources beyond convexity," *Phys. Rev. Lett.*, vol. 132, p. 150201, Apr 2024.

[25] G. Manzano, F. Galve, R. Zambrini, and J. M. R. Parrondo, "Entropy production and thermodynamic power of the squeezed thermal reservoir," *Phys. Rev. E*, vol. 93, p. 052120, May 2016.

[26] J. Roßnagel, O. Abah, F. Schmidt-Kaler, K. Singer, and E. Lutz, "Nanoscale heat engine beyond the carnot limit," *Phys. Rev. Lett.*, vol. 112, p. 030602, Jan 2014.

[27] J. Klaers, S. Faelt, A. Imamoglu, and E. Togan, "Squeezed thermal reservoirs as a resource for a nanomechanical engine beyond the carnot limit," *Phys. Rev. X*, vol. 7, p. 031044, Sep 2017.

[28] L. Pezzè, A. Smerzi, M. K. Oberthaler, R. Schmied, and P. Treutlein, "Quantum metrology with nonclassical states of atomic ensembles," *Rev. Mod. Phys.*, vol. 90, p. 035005, Sep 2018.

[29] G. Francica, F. C. Binder, G. Guarnieri, M. T. Mitchison, J. Goold, and F. Plastina, "Quantum coherence and ergotropy," *Phys. Rev. Lett.*, vol. 125, p. 180603, Oct 2020.

[30] R. Salvia, M. Perarnau-Llobet, G. Haack, N. Brunner, and S. Nimmrichter, "Quantum advantage in charging cavity and spin batteries by repeated interactions," *Phys. Rev. Res.*, vol. 5, p. 013155, Feb 2023.

[31] J.-Y. Gyhm and U. R. Fischer, "Beneficial and detrimental entanglement for quantum battery charging," *AVS Quantum Science*, vol. 6, p. 012001, 01 2024.

[32] A. Auffèves, "Quantum technologies need a quantum energy initiative," *PRX Quantum*, vol. 3, p. 020101, Jun 2022.

[33] N. A. Lemos, *Analytical mechanics*. Cambridge University Press, 2018.

[34] F. Strocchi, *Symmetry breaking*, vol. 643. Springer, 2005.

[35] F. Wilczek, "Quantum time crystals," *Phys. Rev. Lett.*, vol. 109, p. 160401, Oct 2012.

[36] P. Bruno, "Impossibility of spontaneously rotating time crystals: A no-go theorem," *Phys. Rev. Lett.*, vol. 111, p. 070402, Aug 2013.

[37] P. Bruno, "Comment on "quantum time crystals"," *Phys. Rev. Lett.*, vol. 110, p. 118901, Mar 2013.

[38] H. Watanabe and M. Oshikawa, "Absence of quantum time crystals," *Phys. Rev. Lett.*, vol. 114, p. 251603, Jun 2015.

[39] F. Iemini, A. Russomanno, J. Keeling, M. Schirò, M. Dalmonte, and R. Fazio, "Boundary time crystals," *Phys. Rev. Lett.*, vol. 121, p. 035301, Jul 2018.

[40] K. Sacha and J. Zakrzewski, "Time crystals: a review," *Reports on Progress in Physics*, vol. 81, p. 016401, nov 2017.

[41] M. P. Zaletel, M. Lukin, C. Monroe, C. Nayak, F. Wilczek, and N. Y. Yao, "Colloquium: Quantum and classical discrete time crystals," *Rev. Mod. Phys.*, vol. 95, p. 031001, Jul 2023.

[42] Z. Gong, R. Hamazaki, and M. Ueda, "Discrete time-crystalline order in cavity and circuit qed systems," *Phys. Rev. Lett.*, vol. 120, p. 040404, Jan 2018.

[43] K. Tucker, B. Zhu, R. J. Lewis-Swan, J. Marino, F. Jimenez, J. G. Restrepo, and A. M. Rey, "Shattered time: can a dissipative time crystal survive many-body correlations?," *New J. Phys.*, vol. 20, no. 12, p. 123003, 2018.

[44] B. Buča, J. Tindall, and D. Jaksch, "Non-stationary coherent quantum many-body dynamics through dissipation," *Nat. Commun.*, vol. 10, no. 1, pp. 1–6, 2019.

[45] F. M. Gambetta, F. Carollo, M. Marcuzzi, J. P. Garrahan, and I. Lesanovsky, "Discrete time crystals in the absence of manifest symmetries or disorder in open quantum systems," *Phys. Rev. Lett.*, vol. 122, p. 015701, Jan 2019.

[46] A. Lazarides, S. Roy, F. Piazza, and R. Moessner, "Time crystallinity in dissipative floquet systems," *Phys. Rev. Research*, vol. 2, p. 022002, Apr 2020.

[47] K. Seibold, R. Rota, and V. Savona, "Dissipative time crystal in an asymmetric nonlinear photonic dimer," *Phys. Rev. A*, vol. 101, p. 033839, Mar 2020.

[48] C. Lledó, T. K. Mavrogordatos, and M. H. Szymańska, "Driven bose-hubbard dimer under nonlocal dissipation: A bistable time crystal," *Phys. Rev. B*, vol. 100, p. 054303, Aug 2019.

[49] R. Mattes, I. Lesanovsky, and F. Carollo, "Entangled time-crystal phase in an open quantum light-matter system," *Phys. Rev. A*, vol. 108, p. 062216, Dec 2023.

[50] L. F. d. Prazeres, L. d. S. Souza, and F. Iemini, "Boundary time crystals in collective d-level systems," *Phys. Rev. B*, vol. 103, p. 184308, May 2021.

[51] A. Cabot, L. S. Muhle, F. Carollo, and I. Lesanovsky, "Quantum trajectories of dissipative time crystals," *Phys. Rev. A*, vol. 108, p. L041303, Oct 2023.

[52] M. Krishna, P. Solanki, M. Hajdušek, and S. Vinjanampathy, "Measurement-induced continuous time crystals," *Phys. Rev. Lett.*, vol. 130, p. 150401, Apr 2023.

[53] A. Cabot, G. L. Giorgi, and R. Zambrini, "Nonequilibrium transition between dissipative time crystals," *PRX Quantum*, vol. 5, p. 030325, Aug 2024.

[54] P. J. Paulino, I. Lesanovsky, and F. Carollo, "Nonequilibrium thermodynamics and power generation in open quantum optomechanical systems," *Phys. Rev. A*, vol. 108, p. 023516, Aug 2023.

[55] H. Keßler, P. Kongkhambut, C. Georges, L. Mathey, J. G. Cosme, and A. Hemmerich, "Observation of a dissipative time crystal," *Phys. Rev. Lett.*, vol. 127, p. 043602, Jul 2021.

[56] P. Kongkhambut, J. Skulte, L. Mathey, J. G. Cosme, A. Hemmerich, and H. Keßler, "Observation of a continuous time crystal," *Science*, vol. 377, no. 6606, pp. 670–673, 2022.

[57] X. Wu, Z. Wang, F. Yang, R. Gao, C. Liang, M. K. Tey, X. Li, T. Pohl, and L. You, "Dissipative time crystal in a strongly interacting rydberg gas," *Nat. Phys.*, pp. 1–6, 2024.

[58] P. Kongkhambut, J. G. Cosme, J. Skulte, M. A. Moreno Armijos, L. Mathey, A. Hemmerich, and H. Keßler, "Observation of a phase transition from a continuous to a discrete time crystal," *Rep. Prog. Phys.*, vol. 87, p. 080502, July 2024.

[59] J. Skulte, P. Kongkhambut, H. Keßler, A. Hemmerich, L. Mathey, and J. G. Cosme, "Realizing limit cycles in dissipative bosonic systems," *Phys. Rev. A*, vol. 109, p. 063317, Jun 2024.

[60] D. Dreon, A. Baumgärtner, X. Li, S. Hertlein, T. Esslinger, and T. Donner, "Self-oscillating pump in a topological dissipative atom–cavity system," *Nature*, vol. 608, no. 7923, pp. 494–498, 2022.

[61] A. Greilich, N. E. Kopteva, A. N. Kamenskii, P. S. Sokolov, V. L. Korenev, and M. Bayer, "Robust continuous time crystal in an electron–nuclear spin system," *Nature Physics*, vol. 20, pp. 631–636, April 2024.

[62] V. Montenegro, M. G. Genoni, A. Bayat, and M. G. Paris, "Quantum metrology with boundary time crystals," *Commun. Phys.*, vol. 6, no. 1, p. 304, 2023.

[63] A. Cabot, F. Carollo, and I. Lesanovsky, "Continuous sensing and parameter estimation with the boundary time crystal," *Phys. Rev. Lett.*, vol. 132, p. 050801, Jan 2024.

[64] F. Iemini, R. Fazio, and A. Sanpera, "Floquet time crystals as quantum sensors of ac fields," *Phys. Rev. A*, vol. 109, p. L050203, May 2024.

[65] R. Yousefjani, K. Sacha, and A. Bayat, "Discrete time crystal phase as a resource for quantum enhanced sensing," *arXiv preprint arXiv:2405.00328*, 2024.

[66] F. Carollo, K. Brandner, and I. Lesanovsky, "Nonequilibrium many-body quantum engine driven by time-translation symmetry breaking," *Phys. Rev. Lett.*, vol. 125, p. 240602, Dec 2020.

[67] P. J. Paulino, A. Cabot, G. De Chiara, M. Antezza, I. Lesanovsky, and F. Carollo, "Thermodynamics of coupled time crystals with an application to energy storage," *arXiv preprint arXiv:2411.04836*, 2024.

[68] W. S. Martins, F. Carollo, W. Li, K. Brandner, and I. Lesanovsky, "Rydberg-ion flywheel for quantum work storage," *Phys. Rev. A*, vol. 108, p. L050201, Nov 2023.

[69] H. J. Carmichael and D. F. Walls, "Master equation for strongly interacting systems," *J. Phys. A*, vol. 6, p. 1552, oct 1973.

[70] P. P. Hofer, M. Perarnau-Llobet, L. D. M. Miranda, G. Haack, R. Silva, J. B. Brask, and N. Brunner, "Markovian master equations for quantum thermal machines: local versus global approach," *New J. Phys.*, vol. 19, p. 123037, dec 2017.

[71] A. Soret, V. Cavina, and M. Esposito, "Thermodynamic consistency of quantum master equations," *Phys. Rev. A*, vol. 106, p. 062209, Dec 2022.

[72] J. O. González, L. A. Correa, G. Nocerino, J. P. Palao, D. Alonso, and G. Adesso, "Testing the validity of the 'local' and 'global' gkls master equations on an exactly solvable model," *Open Systems & Information Dynamics*, vol. 24, no. 04, p. 1740010, 2017.

[73] F. Brennecke, T. Donner, S. Ritter, T. Bourdel, M. Köhl, and T. Esslinger, "Cavity qed with a bose–einstein condensate," *Nature*, vol. 450, no. 7167, pp. 268–271, 2007.

[74] F. Brennecke, S. Ritter, T. Donner, and T. Esslinger, "Cavity optomechanics with a bose-einstein condensate," *Science*, vol. 322, no. 5899, pp. 235–238, 2008.

[75] T. P. Purdy, D. W. C. Brooks, T. Botter, N. Brahms, Z.-Y. Ma, and D. M. Stamper-Kurn, "Tunable cavity optomechanics with ultracold atoms," *Phys. Rev. Lett.*, vol. 105, p. 133602, Sep 2010.

[76] H. Keßler, P. Kongkhambut, C. Georges, L. Mathey, J. G. Cosme, and A. Hemmerich, "Observation of a dissipative time crystal," *Phys. Rev. Lett.*, vol. 127, p. 043602, Jul 2021.

[77] H. Ritsch, P. Domokos, F. Brennecke, and T. Esslinger, "Cold atoms in cavity-generated dynamical optical potentials," *Rev. Mod. Phys.*, vol. 85, pp. 553–601, Apr 2013.

[78] S. Lorenzo, F. Ciccarello, and G. M. Palma, "Composite quantum collision models," *Phys. Rev. A*, vol. 96, p. 032107, Sep 2017.

[79] F. Ciccarello, S. Lorenzo, V. Giovannetti, and G. M. Palma, "Quantum collision models: Open system dynamics from repeated interactions," *Phys. Rep.*, vol. 954, pp. 1–70, 2022.

[80] M. Cattaneo, G. De Chiara, S. Maniscalco, R. Zambrini, and G. L. Giorgi, "Collision models can efficiently simulate any multipartite markovian quantum dynamics," *Phys. Rev. Lett.*, vol. 126, p. 130403, Apr 2021.

[81] S. Cusumano, "Quantum collision models: A beginner guide," *Entropy*, vol. 24, no. 9, p. 1258, 2022.

[82] J. Jin and C.-s. Yu, "Non-markovianity in the collision model with environmental block," *New Journal of Physics*, vol. 20, p. 053026, may 2018.

[83] V. Giovannetti and G. M. Palma, "Master equations for correlated quantum channels," *Phys. Rev. Lett.*, vol. 108, p. 040401, Jan 2012.

[84] P. Strasberg, G. Schaller, T. Brandes, and M. Esposito, "Quantum and information thermodynamics: A unifying framework based on repeated interactions," *Phys. Rev. X*, vol. 7, p. 021003, Apr 2017.

[85] J. Dalibard, Y. Castin, and K. Mølmer, "Wave-function approach to dissipative processes in quantum optics," *Phys. Rev. Lett.*, vol. 68, pp. 580–583, Feb 1992.

[86] K. Mølmer, Y. Castin, and J. Dalibard, "Monte carlo wave-function method in quantum optics," *J. Opt. Soc. Am. B*, vol. 10, pp. 524–538, Mar 1993.

[87] H. M. Wiseman and G. J. Milburn, *Quantum measurement and control*. Cambridge university press, 2009.

[88] M. B. Plenio and P. L. Knight, "The quantum-jump approach to dissipative dynamics in quantum optics," *Rev. Mod. Phys.*, vol. 70, pp. 101–144, Jan 1998.

[89] S. Gleyzes, S. Kuhr, C. Guerlin, J. Bernu, S. Deléglise, U. Busk Hoff, M. Brune, J.-M. Raimond, and S. Haroche, "Quantum jumps of light recording the birth and death of a photon in a cavity," *Nature*, vol. 446, no. 7133, pp. 297–300, 2007.

[90] F. Minganti, A. Biella, N. Bartolo, and C. Ciuti, "Spectral theory of liouvillians for dissipative phase transitions," *Phys. Rev. A*, vol. 98, p. 042118, Oct 2018.

[91] C. Guerlin, J. Bernu, S. Deléglise, and et al., "Progressive field-state collapse and quantum non-demolition photon counting," *Nature*, vol. 448, no. 7156, pp. 889–893, 2007.

[92] K. W. Yip, T. Albash, and D. A. Lidar, "Quantum trajectories for time-dependent adiabatic master equations," *Phys. Rev. A*, vol. 97, p. 022116, Feb 2018.

[93] P. Menczel, C. Flindt, and K. Brandner, "Quantum jump approach to microscopic heat engines," *Phys. Rev. Res.*, vol. 2, p. 033449, Sep 2020.

[94] G. Manzano and R. Zambrini, "Quantum thermodynamics under continuous monitoring: a general framework," *AVS Quantum Sci.*, vol. 4, no. 2, p. 025302, 2022.

[95] K. Brandner and K. Saito, "Thermodynamic geometry of microscopic heat engines," *Phys. Rev. Lett.*, vol. 124, p. 040602, Jan 2020.

[96] M. Esposito, U. Harbola, and S. Mukamel, "Nonequilibrium fluctuations, fluctuation theorems, and counting statistics in quantum systems," *Rev. Mod. Phys.*, vol. 81, pp. 1665–1702, Dec 2009.

[97] G. Manzano, J. M. Horowitz, and J. M. R. Parrondo, "Quantum fluctuation theorems for arbitrary environments: Adiabatic and nonadiabatic entropy production," *Phys. Rev. X*, vol. 8, p. 031037, Aug 2018.

[98] V. Lecomte, C. Appert-Rolland, and F. van Wijland, "Thermodynamic formalism for systems with markov dynamics," *J. Stat. Phys.*, vol. 127, no. 1, pp. 51–106, 2007.

[99] G. Falasco and M. Esposito, "Macroscopic stochastic thermodynamics," *Rev. Mod. Phys.*, vol. 97, p. 015002, Jan 2025.

[100] F. Avanzini, M. Bilancioni, V. Cavina, S. D. Cengio, M. Esposito, G. Falasco, D. Forastiere, N. Freitas, A. Garilli, P. E. Harunari, V. Lecomte, A. Lazarescu, S. G. M. Srinivas, C. Moslonka, I. Neri, E. Penocchio, W. D. Piñeros, M. Polettini, A. Raghu, P. Raux, K. Sekimoto, and A. Soret, "Methods and conversations in (post)modern thermodynamics," *SciPost Phys. Lect. Notes*, p. 80, 2024.

[101] H. Touchette, "The large deviation approach to statistical mechanics," *Phys. Rep.*, vol. 478, no. 1, pp. 1–69, 2009.

[102] J. P. Garrahan and I. Lesanovsky, "Thermodynamics of quantum jump trajectories," *Phys. Rev. Lett.*, vol. 104, p. 160601, Apr 2010.

[103] F. Carollo, R. L. Jack, and J. P. Garrahan, "Unraveling the large deviation statistics of markovian open quantum systems," *Phys. Rev. Lett.*, vol. 122, p. 130605, Apr 2019.

[104] R. S. Ellis, "The theory of large deviations: from boltzmann's 1877 calculation to equilibrium macrostates in 2d turbulence," *Physica D: Nonlinear Phenomena*, vol. 133, no. 1-4, pp. 106–136, 1999.

[105] F. Carollo, J. P. Garrahan, I. Lesanovsky, and C. Pérez-Espigares, "Making rare events typical in markovian open quantum systems," *Phys. Rev. A*, vol. 98, p. 010103, Jul 2018.

[106] J. P. Garrahan and M. u. u. u. u. Guţă, "Catching and reversing quantum jumps and thermodynamics of quantum trajectories," *Phys. Rev. A*, vol. 98, p. 052137, Nov 2018.

[107] Z. K. Minev, S. O. Mundhada, S. Shankar, P. Reinhold, R. Gutiérrez-Jáuregui, R. J. Schoelkopf, M. Mirrahimi, H. J. Carmichael, and M. H. Devoret, "To catch and reverse a quantum jump mid-flight," *Nature*, vol. 570, no. 7760, pp. 200–204, 2019.

[108] H. Touchette, "Introduction to dynamical large deviations of markov processes," *Physica A: Statistical Mechanics and its Applications*, vol. 504, pp. 5–19, 2018. Lecture Notes of the 14th International Summer School on Fundamental Problems in Statistical Physics.

[109] E. Gillman, D. C. Rose, and J. P. Garrahan, "Combining reinforcement learning and tensor networks, with an application to dynamical large deviations," *Phys. Rev. Lett.*, vol. 132, p. 197301, May 2024.

[110] L. Causer, M. C. Bañuls, and J. P. Garrahan, "Optimal sampling of dynamical large deviations in two dimensions via tensor networks," *Phys. Rev. Lett.*, vol. 130, p. 147401, Apr 2023.

[111] P. J. Paulino, I. Lesanovsky, and F. Carollo, "Large deviation full counting statistics in adiabatic open quantum dynamics," *Phys. Rev. Lett.*, vol. 132, p. 260402, Jun 2024.

[112] M. S. Sarandy and D. A. Lidar, "Adiabatic approximation in open quantum systems," *Phys. Rev. A*, vol. 71, p. 012331, Jan 2005.

[113] H.-P. Breuer, F. Petruccione, *et al.*, *The theory of open quantum systems*. Oxford University Press on Demand, 2002.

[114] B. Vacchini, *Open Quantum Systems: Foundations and Theory*. Springer Nature, 2024.

[115] D. A. Lidar, "Lecture notes on the theory of open quantum systems," *arXiv preprint arXiv:1902.00967*, 2020.

[116] R. Alicki, "The quantum open system as a model of the heat engine," *J. Phys. A*, vol. 12, p. L103, may 1979.

[117] L. E. Ballentine, *Quantum mechanics: a modern development*. World Scientific Publishing Company, 2014.

[118] H. J. Carmichael, *Statistical methods in quantum optics 1: master equations and Fokker-Planck equations*. Springer Science & Business Media, 2013.

[119] A. P. Babu, S. Alipour, A. T. Rezakhani, and T. Ala-Nissila, "Unfolding system-environment correlation in open quantum systems: Revisiting master equations and the born approximation," *Phys. Rev. Res.*, vol. 6, p. 013243, Mar 2024.

[120] G. Adesso and A. Datta, "Quantum versus classical correlations in gaussian states," *Phys. Rev. Lett.*, vol. 105, p. 030501, Jul 2010.

[121] A. G. Redfield, "On the theory of relaxation processes," *IBM Journal of Research and Development*, vol. 1, no. 1, pp. 19–31, 1957.

[122] R. Hartmann and W. T. Strunz, "Accuracy assessment of perturbative master equations: Embracing nonpositivity," *Phys. Rev. A*, vol. 101, p. 012103, Jan 2020.

[123] D. E. Evans, "Irreducible quantum dynamical semigroups," *Communications in Mathematical Physics*, vol. 54, no. 3, pp. 293–297, 1977.

[124] M. O. Scully and M. S. Zubairy, *Quantum optics*. Cambridge university press, 1997.

[125] M. Cattaneo, G. L. Giorgi, S. Maniscalco, and R. Zambrini, "Local versus global master equation with common and separate baths: superiority of the global approach in partial secular approximation," *New Journal of Physics*, vol. 21, p. 113045, nov 2019.

[126] P. Strasberg and A. Winter, "First and second law of quantum thermodynamics: A consistent derivation based on a microscopic definition of entropy," *PRX Quantum*, vol. 2, p. 030202, Aug 2021.

[127] B. Gardas and S. Deffner, "Thermodynamic universality of quantum carnot engines," *Phys. Rev. E*, vol. 92, p. 042126, Oct 2015.

[128] T. Albash, S. Boixo, D. A. Lidar, and P. Zanardi, "Quantum adiabatic markovian master equations," *New Journal of Physics*, vol. 14, no. 12, p. 123016, 2012.

[129] W. Pusz and S. L. Woronowicz, "Passive states and kms states for general quantum systems," *Communications in Mathematical Physics*, vol. 58, no. 3, pp. 273–290, 1978.

[130] M. Perarnau-Llobet, K. V. Hovhannisyan, M. Huber, P. Skrzypczyk, J. Tura, and A. Acín, "Most energetic passive states," *Phys. Rev. E*, vol. 92, p. 042147, Oct 2015.

[131] A. E. Allahverdyan, R. Balian, and T. M. Nieuwenhuizen, "Maximal work extraction from finite quantum systems," *Europhys. Lett.*, vol. 67, p. 565, aug 2004.

[132] F. Campaioli, S. Gherardini, J. Q. Quach, M. Polini, and G. M. Andolina, "Colloquium: Quantum batteries," *Rev. Mod. Phys.*, vol. 96, p. 031001, Jul 2024.

[133] H. E. D. Scovil and E. O. Schulz-DuBois, "Three-level masers as heat engines," *Phys. Rev. Lett.*, vol. 2, pp. 262–263, Mar 1959.

[134] H. T. Quan, Y.-x. Liu, C. P. Sun, and F. Nori, "Quantum thermodynamic cycles and quantum heat engines," *Phys. Rev. E*, vol. 76, p. 031105, Sep 2007.

[135] D. A. Wharam, T. J. Thornton, R. Newbury, M. Pepper, H. Ahmed, J. E. F. Frost, D. G. Hasko, D. C. Peacock, D. A. Ritchie, and G. A. C. Jones, "One-dimensional transport and the quantisation of the ballistic resistance," *Journal of Physics C: Solid State Physics*, vol. 21, p. L209, mar 1988.

[136] K. Brandner and K. Saito, "Thermodynamic uncertainty relations for coherent transport," *arXiv preprint arXiv:2502.07917*, 2025.

[137] H. Spohn, "Entropy production for quantum dynamical semigroups," *J. Math. Phys.*, vol. 19, pp. 1227–1230, 05 1978.

[138] C. Elouard, D. Herrera-Martí, M. Esposito, and A. Auffèves, "Thermodynamics of optical bloch equations," *New Journal of Physics*, vol. 22, p. 103039, oct 2020.

[139] H. Walther, B. T. H. Varcoe, B.-G. Englert, and T. Becker, "Cavity quantum electrodynamics," *Reports on Progress in Physics*, vol. 69, p. 1325, apr 2006.

[140] F. Beaudoin, J. M. Gambetta, and A. Blais, "Dissipation and ultrastrong coupling in circuit qed," *Phys. Rev. A*, vol. 84, p. 043832, Oct 2011.

[141] C. Nill, K. Brandner, B. Olmos, F. Carollo, and I. Lesanovsky, "Many-body radiative decay in strongly interacting rydberg ensembles," *Phys. Rev. Lett.*, vol. 129, p. 243202, Dec 2022.

[142] G. Lindblad, "On the generators of quantum dynamical semigroups," *Communications in mathematical physics*, vol. 48, pp. 119–130, 1976.

[143] B. Debecker, J. Martin, and F. m. c. Damanet, "Spectral theory of non-markovian dissipative phase transitions," *Phys. Rev. A*, vol. 110, p. 042201, Oct 2024.

[144] F. Carollo, A. Lasanta, and I. Lesanovsky, "Exponentially accelerated approach to stationarity in markovian open quantum systems through the mpemba effect," *Phys. Rev. Lett.*, vol. 127, p. 060401, Aug 2021.

[145] M. Moroder, O. Culhane, K. Zawadzki, and J. Goold, "Thermodynamics of the quantum mpemba effect," *Phys. Rev. Lett.*, vol. 133, p. 140404, Oct 2024.

[146] J. Bechhoefer, A. Kumar, and R. Chétrite, "A fresh understanding of the mpemba effect," *Nature Reviews Physics*, vol. 3, no. 8, pp. 534–535, 2021.

[147] K. Macieszczak, D. C. Rose, I. Lesanovsky, and J. P. Garrahan, "Theory of classical metastability in open quantum systems," *Phys. Rev. Res.*, vol. 3, p. 033047, Jul 2021.

[148] A. Cabot, G. L. Giorgi, and R. Zambrini, "Metastable quantum entrainment," *New Journal of Physics*, vol. 23, p. 103017, oct 2021.

[149] F. Barra, "The thermodynamic cost of driving quantum systems by their boundaries," *Scientific Reports*, vol. 5, no. 1, p. 14873, 2015.

[150] F. Carollo, I. Lesanovsky, M. Antezza, and G. De Chiara, "Quantum thermodynamics of boundary time-crystals," *Quantum Sci. Technol.*, vol. 9, p. 035024, may 2024.

[151] M. Esposito, K. Lindenberg, and C. Van den Broeck, "Entropy production as correlation between system and reservoir," *New Journal of Physics*, vol. 12, p. 013013, jan 2010.

[152] A. Cabot, F. Carollo, and I. Lesanovsky, "Exploiting nonequilibrium phase transitions and strong symmetries for continuous measurement of collective observables," *arXiv preprint arXiv:2407.13352*, 2024.

[153] D. Nagy, G. Kónya, G. Szirmai, and P. Domokos, "Dicke-model phase transition in the quantum motion of a bose-einstein condensate in an optical cavity," *Phys. Rev. Lett.*, vol. 104, p. 130401, Apr 2010.

[154] F. Carollo and I. Lesanovsky, "Exact solution of a boundary time-crystal phase transition: Time-translation symmetry breaking and non-markovian dynamics of correlations," *Phys. Rev. A*, vol. 105, p. L040202, Apr 2022.

[155] P. Solanki and F. Minganti, "Chaos in time: A dissipative continuous quasi time crystals," *arXiv preprint arXiv:2411.07297*, 2024.

[156] F. Carollo and I. Lesanovsky, "Exactness of Mean-Field Equations for Open Dicke Models with an Application to Pattern Retrieval Dynamics," *Phys. Rev. Lett.*, vol. 126, p. 230601, Jun 2021.

[157] F. Carollo and I. Lesanovsky, "Applicability of mean-field theory for time-dependent open quantum systems with infinite-range interactions," *Phys. Rev. Lett.*, vol. 133, p. 150401, Oct 2024.

[158] S. H. Strogatz, *Nonlinear dynamics and chaos: with applications to physics, biology, chemistry, and engineering*. CRC press, 2018.

[159] H. J. Carmichael, *Statistical methods in quantum optics 2: Non-classical fields*. Springer Science & Business Media, 2007.

[160] H. Touchette, "Ensemble equivalence for general many-body systems," *Europhysics Letters*, vol. 96, p. 50010, nov 2011.

[161] J. P. Garrahan, "Classical stochastic dynamics and continuous matrix product states: gauge transformations, conditioned and driven processes, and equivalence of trajectory ensembles," *J. Stat. Mech.*, vol. 2016, no. 7, p. 073208, 2016.

[162] R. Chetrite and H. Touchette, "Nonequilibrium microcanonical and canonical ensembles and their equivalence," *Phys. Rev. Lett.*, vol. 111, p. 120601, Sep 2013.

[163] R. K. P. Zia, E. F. Redish, and S. R. McKay, "Making sense of the legendre transform," *Am. J. Phys.*, vol. 77, no. 7, pp. 614–622, 2009.

[164] M. Ferri-Cortés, J. A. Almanza-Marrero, R. López, R. Zambrini, and G. Manzano, "Entropy production and fluctuation theorems for monitored quantum systems under imperfect detection," *arXiv preprint arXiv:2308.08491*, 2023.

[165] M. A. Finn, G. W. Greenlees, J. Kumar, and D. A. Lewis, "Poisson, sub-poisson, and bose-einstein statistics in three-level atoms," *Phys. Rev. A*, vol. 38, pp. 773–777, Jul 1988.

[166] R. Gutiérrez, A. Canella-Ortiz, and C. Pérez-Espigares, "Finding the effective dynamics to make rare events typical in chaotic maps," *Phys. Rev. Lett.*, vol. 131, p. 227201, Nov 2023.

[167] R. Chetrite and H. Touchette, "Nonequilibrium markov processes conditioned on large deviations," *Annales Henri Poincaré*, vol. 16, no. 9, pp. 2005–2057, 2015.

[168] R. L. Jack and P. Sollich, "Large deviations and ensembles of trajectories in stochastic models," *Progress of Theoretical Physics Supplement*, vol. 184, pp. 304–317, 03 2010.

[169] M. Aspelmeyer, T. J. Kippenberg, and F. Marquardt, "Cavity optomechanics," *Rev. Mod. Phys.*, vol. 86, pp. 1391–1452, Dec 2014.

[170] J. M. Horowitz and T. R. Gingrich, "Thermodynamic uncertainty relations constrain non-equilibrium fluctuations," *Nature Physics*, vol. 16, no. 1, pp. 15–20, 2020.

[171] Y. Hasegawa, "Thermodynamic uncertainty relation for general open quantum systems," *Phys. Rev. Lett.*, vol. 126, p. 010602, Jan 2021.

[172] P. Talkner, E. Lutz, and P. Hänggi, "Fluctuation theorems: Work is not an observable," *Phys. Rev. E*, vol. 75, p. 050102, May 2007.

[173] C.-K. Hu, A. C. Santos, J.-M. Cui, Y.-F. Huang, D. O. Soares-Pinto, M. S. Sarandy, C.-F. Li, and G.-C. Guo, "Quantum thermodynamics in adiabatic open systems and its trapped-ion experimental realization," *npj Quantum Information*, vol. 6, no. 1, p. 73, 2020.

[174] F. Benatti, F. Carollo, and R. Floreanini, "Dissipative dynamics of quantum fluctuations," *Ann. Phys. (Berlin)*, vol. 527, no. 9-10, pp. 639–655, 2015.

[175] T. c. v. Prosen, "Open xxz spin chain: Nonequilibrium steady state and a strict bound on ballistic transport," *Phys. Rev. Lett.*, vol. 106, p. 217206, May 2011.

[176] S. Walter, A. Nunnenkamp, and C. Bruder, "Quantum synchronization of a driven self-sustained oscillator," *Phys. Rev. Lett.*, vol. 112, p. 094102, Mar 2014.

[177] T. Murtadho, S. Vinjanampathy, and J. Thingna, "Cooperation and competition in synchronous open quantum systems," *Phys. Rev. Lett.*, vol. 131, p. 030401, Jul 2023.